

Identification and Recovery of Objects in GEO and GTO to Maintain a Catalogue of Orbits

Inauguraldissertation
der Philosophisch-naturwissenschaftlichen Fakultät
der Universität Bern

vorgelegt von

Reto Musci

von Dielsdorf ZH

Leiter der Arbeit:
PD Dr. Thomas Schildknecht
Astronomisches Institut der Universität Bern

Identification and Recovery of Objects in GEO and GTO to Maintain a Catalogue of Orbits

Inauguraldissertation
der Philosophisch-naturwissenschaftlichen Fakultät
der Universität Bern

vorgelegt von

Reto Musci

von Dielsdorf ZH

Leiter der Arbeit:
PD Dr. Thomas Schildknecht
Astronomisches Institut der Universität Bern

Von der Philosophisch-naturwissenschaftlichen Fakultät angenommen.

Der Dekan

Bern, den 22. Juni 2006

Prof. P. Messerli

Contents

| | |
|-----------------------------------------------------|-----------|
| List of Figures | v |
| List of Tables | xi |
| Frequently Used Acronyms | xv |
| | |
| 1. Introduction | 1 |
| | |
| 2. General Information | 5 |
| 2.1 Space Surveillance Systems | 5 |
| 2.1.1 U.S. Space Surveillance Network | 5 |
| 2.1.2 Russian Space Surveillance System | 9 |
| 2.1.3 European Space Surveillance System | 9 |
| 2.2 Catalogues | 11 |
| 2.2.1 GEO | 12 |
| 2.2.2 GTO | 17 |
| 2.3 Instruments | 19 |
| 2.3.1 ZIMLAT | 19 |
| 2.3.2 ESASDT | 20 |
| | |
| 3. Search Surveys for Debris | 23 |
| 3.1 GEO Survey | 24 |
| 3.1.1 Contamination by Elliptical Orbits | 28 |
| 3.2 GTO Survey | 30 |
| 3.2.1 Objects With Follow-up Observations | 33 |
| | |
| 4. Identification of Multiple Detections | 37 |
| 4.1 The CAMRES Tool | 38 |
| 4.2 The CAMCOR Tool | 40 |
| 4.3 Results | 43 |
| 4.4 Conclusion | 45 |

| | |
|----------------------------------------------------------|------------|
| 5. Acquisition of a “Secured” Orbit | 47 |
| 5.1 GEO | 48 |
| 5.1.1 Simulated Orbits | 48 |
| 5.1.2 Discovery Observations | 49 |
| 5.1.3 Wide Field of View (2°) | 50 |
| 5.1.4 Narrow Field of View (0.4°) | 54 |
| 5.1.5 Without Near Real Time Orbit Improvement | 57 |
| 5.1.6 Observations Based on Surveys | 57 |
| 5.1.7 Examples of Real Observations | 62 |
| 5.1.8 Summary | 63 |
| 5.2 GTO | 64 |
| 5.2.1 Simulated Orbits | 64 |
| 5.2.2 Discovery Observations | 65 |
| 5.2.3 Wide Field of View (2°) | 67 |
| 5.2.4 Narrow Field of View (0.4°) | 72 |
| 5.2.5 Without Near Real Time Orbit Improvement | 76 |
| 5.2.6 Observations Based on Surveys | 77 |
| 5.2.7 Examples of Real Observations | 77 |
| 5.2.8 Summary | 78 |
| 5.3 Multiple Sites | 80 |
| 5.3.1 GEO | 80 |
| 5.3.2 GTO | 93 |
| 5.3.3 Examples of Real Observations | 104 |
| 5.4 Impact of the Observation Accuracy | 107 |
| | |
| 6. Concept for Catalogue Maintenance | 109 |
| 6.1 Maintenance Observations | 109 |
| 6.1.1 GEO | 109 |
| 6.1.2 GTO | 114 |
| 6.1.3 Influence of A/M Modeling Errors | 120 |
| 6.2 Planning | 123 |
| 6.2.1 Maintenance Observations | 124 |
| 6.3 Correlation | 124 |
| 6.3.1 Recommendations | 127 |
| | |
| 7. Summary and Outlook | 131 |
| | |
| A. The Program System CelMech | 137 |
| A.1 ORBDET | 137 |
| A.2 SATORB | 138 |

| | | |
|-------|---------------------------------|------------|
| A.2.1 | Satellite Ephemerides | 138 |
| A.2.2 | Orbit Improvement | 138 |
| | Bibliography | 141 |

List of Figures

| | | |
|------|-----------------------------------------------------------------------------------------------------------------------------------------------------|----|
| 2.1 | Measurement regions and sensitivity of some instruments. | 6 |
| 2.2 | The U.S. Space Surveillance Network. | 6 |
| 2.3 | The Haystack and the Eglin radar sensors. | 7 |
| 2.4 | The three GEODSS sites: Diego Garcia, Socorro, and Maui. | 8 |
| 2.5 | Artistic view of the MSX satellite. The SBV components are indicated by arrows. | 8 |
| 2.6 | The Russian Space Surveillance System. | 9 |
| 2.7 | The proposed European Space Surveillance System. | 10 |
| 2.8 | The GRAVES radar sensor. | 10 |
| 2.9 | Design of the proposed 0.5 m telescope. | 11 |
| 2.10 | Precession of the orbits of GEO objects. | 13 |
| 2.11 | Distribution of the semi-major axis of GEO objects (from DISCOS, status Dec. 2004). | 14 |
| 2.12 | Distribution of the eccentricity of GEO objects (from DISCOS, status Dec. 2004). | 14 |
| 2.13 | Distribution of the inclination of GEO objects (from DISCOS, status Dec. 2004). | 15 |
| 2.14 | Inclination versus right ascension of ascending node for GEO objects (from DISCOS, status Dec. 2004). | 15 |
| 2.15 | Visibilities of drifting GEO objects as a function of the distance Δa to the GEO radius for Tenerife (min. elevation: 20°). | 16 |
| 2.16 | The Geostationary Transfer Orbit (GTO). | 17 |
| 2.17 | Eccentricity versus semi-major axis for GTO objects (from DISCOS, status Dec. 2004). | 18 |
| 2.18 | Distributions of the perigee altitude (left) and the apogee altitude (right) of GTO objects (from DISCOS, status Dec. 2004). | 18 |
| 2.19 | Distribution of the inclination of GTO objects (from DISCOS, status Dec. 2004). | 19 |
| 2.20 | The Zimmerwald observatory. | 20 |
| 2.21 | The Zimmerwald Laser and Astrometry Telescope (ZIMLAT). | 20 |
| 2.22 | The optical ground station (OGS) on Tenerife. | 21 |
| 2.23 | The ESA Space Debris Telescope (ESASDT), front view. | 21 |
| 2.24 | The ESA Space Debris Telescope (ESASDT), side view. | 22 |
| 3.1 | Distributions for different ranges of semi-major axis for the detections of the 2002 GEO surveys. | 25 |
| 3.2 | Distribution of inclination for the detections of the 2002 GEO surveys. | 25 |
| 3.3 | Inclination versus right ascension of ascending node for the correlated (left) and uncorrelated (right) detections of the 2002 GEO surveys. | 26 |
| 3.4 | Comparison of the detections with modeled fragmentations of known breakup events. | 26 |
| 3.5 | Distribution of magnitude for the detections of the 2002 GEO surveys. | 27 |

| | | |
|------|-----------------------------------------------------------------------------------------------------------------------------------------------------------------------------------|----|
| 3.6 | Distribution of magnitude for different inclination ranges for the detections of the 2002 GEO surveys. | 28 |
| 3.7 | Distribution of semi-major axis for detections of GTO objects assuming circular orbits. | 29 |
| 3.8 | Inclination versus right ascension of ascending node for detections of GTO objects assuming circular orbits. | 29 |
| 3.9 | Inclination versus right ascension of ascending node for simulated detections with different observation epochs of a GTO object (97066C). | 30 |
| 3.10 | Distributions for different ranges of semi-major axis for the detections of the 2002 GEO surveys. | 31 |
| 3.11 | Distribution of inclination for the detections of the 2002 GTO surveys. | 31 |
| 3.12 | Inclination versus right ascension of ascending node for the correlated (left) and uncorrelated (right) detections of the 2002 GTO surveys. | 32 |
| 3.13 | Distribution of magnitude for the detections of the 2002 GTO surveys. | 32 |
| 3.14 | Distribution of magnitude for different inclination ranges for the detections of the 2002 GTO surveys. | 33 |
| 3.15 | Distribution of arc length for objects, which were observed multiple times. | 34 |
| 3.16 | Eccentricity versus semi-major axis for objects from the DISCOS database (left) and for objects, which were observed multiple times (right). | 34 |
| 3.17 | Inclination versus semi-major axis for objects, which were observed multiple times (Δ), compared to the objects from the DISCOS database (\times). | 35 |
| 3.18 | Inclination versus right ascension of ascending node for observed high A/M GEO objects (\diamond) compared to the objects from the DISCOS database (\times). | 35 |
| 4.1 | Flowchart of the CAMRES tool. | 39 |
| 4.2 | Flowchart of the CAMCOR tool. | 42 |
| 5.1 | GEO population from the DISCOS catalogue compared with the function given in equation 5.1. | 48 |
| 5.2 | Difference Δ between “true” and determined circular orbit representing three discovery observations of a GEO object spanning one minute of time. | 49 |
| 5.3 | Difference Δ between “true” and determined elliptical orbit representing the discovery track of a GEO object and the first follow-up track after 2 h. | 51 |
| 5.4 | Difference Δ between “true” and determined elliptical orbit representing the discovery track of a GEO object and the first follow-up track after 1 h. | 51 |
| 5.5 | Difference Δ between “true” and determined elliptical orbit representing the discovery track of a GEO object and the follow-up tracks after 1 h and 2 h. | 52 |
| 5.6 | Difference Δ between “true” and determined elliptical orbit representing the discovery track of a GEO object and the follow-up tracks after 1 h, 2 h, and one day. | 53 |
| 5.7 | Daily periodical errors in the difference Δ between “true” and determined elliptical orbit of a GEO object. | 53 |
| 5.8 | Formal error of the right ascension of ascending node Ω as a function of the inclination i | 54 |
| 5.9 | Difference Δ between “true” and determined elliptical orbit representing the discovery track of a GEO object and the follow-up tracks after 1 h, 2 h, and 3 h. | 55 |

| | | |
|------|---------------------------------------------------------------------------------------------------------------------------------------------------------------------------------------------------------------------------------------------------|----|
| 5.10 | Difference Δ between “true” and determined elliptical orbit representing the discovery track of a GEO object and the follow-up tracks after 1 h, 2 h, 3 h, and one day. | 56 |
| 5.11 | Difference Δ between “true” and determined elliptical orbit representing the discovery track of a GEO object and an additional survey track after 3 h. | 58 |
| 5.12 | Difference Δ between “true” and determined elliptical orbit representing the discovery track of a GEO object and additional survey tracks after 1.5 h and 3 h. | 59 |
| 5.13 | Difference Δ between “true” and determined elliptical orbit representing the discovery track of a GEO object and additional survey tracks after 1.5 h, 3 h, and one day. | 60 |
| 5.14 | Difference Δ between “true” and determined elliptical orbit representing the discovery track of a GEO object and an additional survey track after 20 h. | 60 |
| 5.15 | Difference Δ between “true” and determined elliptical orbit representing the discovery track of a GEO object and additional survey tracks after 20 h and 26 h. | 61 |
| 5.16 | Comparison of the simulated elements a and e (left) with part of the DISCOS catalogue (right). | 65 |
| 5.17 | Difference Δ between “true” and determined circular orbit representing three discovery observations of a GTO object spanning one minute of time. | 66 |
| 5.18 | Difference Δ between “true” and determined circular orbit of a GTO object after one hour as a function of the observation time. | 66 |
| 5.19 | Difference Δ between “true” and determined elliptical orbit representing the discovery track of a GTO object and the first follow-up track after 0.5 h. | 67 |
| 5.20 | Difference Δ between “true” and determined elliptical orbit representing the discovery track of a GTO object and the follow-up tracks after 0.5 h and 2 h. | 68 |
| 5.21 | Difference Δ between “true” and determined elliptical orbit for one simulated GTO object extrapolated for five days. | 69 |
| 5.22 | Difference Δ between “true” and determined elliptical orbit of a GTO object at the apogee. | 69 |
| 5.23 | Difference Δ between “true” and determined elliptical orbit representing the discovery track of a GTO object and the follow-up tracks after 0.5 h, 2 h, and the first apogee during the following night. | 70 |
| 5.24 | Difference Δ between “true” and determined elliptical orbit representing the discovery track of a GTO object and the follow-up tracks after 0.5 h, 2 h, the first apogee during the first and the fifth night after the discovery. | 71 |
| 5.25 | Difference Δ at apogee and perigee of orbits representing the discovery track of a GTO object and the follow-up tracks after 0.5 h, 2 h, the first apogee during the first and the fifth night after the discovery. | 71 |
| 5.26 | Difference Δ between “true” and determined elliptical orbit representing the discovery track of a GTO object and the follow-up tracks after 0.25 h and 0.5 h. | 73 |
| 5.27 | Difference Δ between “true” and determined elliptical orbit representing the discovery track of a GTO object and the follow-up tracks after 0.25 h, 0.5 h, and 2 h. | 74 |
| 5.28 | Difference Δ between “true” and determined elliptical orbit representing the discovery track of a GTO object and the follow-up tracks after 0.25 h, 0.5 h, 2 h and the first apogee during the following night. | 74 |

| | | |
|------|-------------------------------------------------------------------------------------------------------------------------------------------------------------------------------------------------------------------------------------------------------------------------|----|
| 5.29 | Difference Δ between “true” and determined elliptical orbit representing the discovery track of a GTO object and the follow-up tracks after 0.25 h, 0.5 h, 2 h, the first apogee during the first and the fifth night after the discovery. | 75 |
| 5.30 | Difference Δ between “true” and determined circular orbit of a GEO object representing one track observed from a virtual site. | 81 |
| 5.31 | Difference Δ between “true” and determined elliptical orbit of a GEO object representing two tracks observed simultaneously from two virtual sites with identical latitude and different longitudes. | 82 |
| 5.32 | Difference Δ between “true” and determined elliptical orbit of a GEO object representing two tracks observed simultaneously from two virtual sites with identical longitude and different latitudes. | 83 |
| 5.33 | Difference Δ between “true” and determined elliptical orbit of a GEO object representing two tracks separated by 1 h observed from a virtual site. | 84 |
| 5.34 | Difference Δ between “true” and determined elliptical orbit of a GEO object representing one track observed from the main site and one follow-up track after 1 h observed from virtual sites with identical latitude and different longitudes. | 85 |
| 5.35 | Difference Δ between “true” and determined elliptical orbit of a GEO object representing one track observed from the main site and one follow-up track after 1 h observed from virtual sites with identical longitude and different latitudes. | 86 |
| 5.36 | Mean formal errors σ for the elliptical orbit determination representing two tracks of a GEO object separated by Δt observed from virtual sites. | 88 |
| 5.37 | Mean formal errors σ for the semi-major axis of the elliptical orbit determination representing two tracks of a GEO object separated by 0 h, 1 h, 2 h, and 6 h observed from two virtual sites plotted against the longitude λ_o of the objects. | 91 |
| 5.38 | Mean formal errors σ for the semi-major axis of the elliptical orbit determination representing two tracks of a GEO object observed at the same epoch from two virtual sites with $\beta = 0^\circ$ and $\Delta\lambda = 40^\circ$ | 92 |
| 5.39 | Longitude λ_o of a GEO satellite S that is seen in the same direction from two observers O_1 and O_2 | 92 |
| 5.40 | Difference Δ between “true” and determined circular orbit of a GTO object representing one track observed from a virtual site. | 93 |
| 5.41 | Difference Δ between “true” and determined elliptical orbit of a GTO object representing two tracks observed simultaneously from two virtual sites with identical latitude and different longitudes. | 94 |
| 5.42 | Difference Δ between “true” and determined elliptical orbit of a GTO object representing two tracks observed simultaneously from two virtual sites with identical longitude and different latitudes. | 95 |
| 5.43 | Difference Δ between “true” and determined elliptical orbit of a GTO object representing two tracks separated by 0.25 h observed from a virtual site. | 96 |
| 5.44 | Difference Δ between “true” and determined elliptical orbit of a GEO object representing one track observed from the main site and one follow-up track after 0.25 h observed from virtual sites with identical latitude and different longitudes. | 97 |
| 5.45 | Difference Δ between “true” and determined elliptical orbit of a GEO object representing one track observed from the main site and one follow-up track after 0.25 h observed from virtual sites with identical longitude and different latitudes. | 98 |

| | | |
|------|--------------------------------------------------------------------------------------------------------------------------------------------------------------------------------------------------------------------------------------------------------------------------------|-----|
| 5.46 | Mean formal errors σ for the elliptical orbit determination representing two tracks of a GTO object separated by Δt observed from virtual sites. | 100 |
| 5.47 | Mean formal errors σ for the semi-major axis of the elliptical orbit determination representing two tracks of a GTO object separated by 0 h, 0.25 h, 0.5 h, and 1.5 h observed from two virtual sites plotted against the longitude λ_o of the objects. | 102 |
| 5.48 | Mean formal errors σ for the semi-major axis of the elliptical orbit determination representing two tracks of a GTO object observed at the same epoch from two virtual sites with $\beta = 0^\circ$ and $\Delta\lambda = 40^\circ$ | 103 |
| 5.49 | Mean formal errors σ for the semi-major axis of the elliptical orbit determination representing two tracks separated by 0.25 h of a GEO object observed from two virtual sites with $\beta = 0^\circ$ and $\Delta\lambda = 40^\circ$ | 103 |
| 5.50 | Formal errors σ for the elliptical orbit determination representing two tracks of 250 GEO objects separated by Δt observed from virtual sites. | 105 |
| 5.51 | Difference between “true” and determined elliptical orbit as a function of the arc length. The six lines represent simulations with different observation errors. | 107 |
| 6.1 | Difference Δ between “true” and determined elliptical orbit representing the discovery track of a GEO object and the follow-up tracks after 1 h, 2 h, 3 h, 1 day, and 30 days. . . | 110 |
| 6.2 | Difference Δ between “true” and determined elliptical orbit representing the discovery track of a GEO object and the follow-up tracks after 1 h, 2 h, 3 h, 1 day, 30 days and 60 days. | 111 |
| 6.3 | Difference Δ between “true” and determined elliptical orbit representing 6 maintenance tracks of a GEO object separated by 30 days. | 112 |
| 6.4 | Difference Δ between “true” and determined elliptical orbit representing the discovery track of a GEO object and the follow-up tracks after 1 h, 2 h, 3 h, one day, and 180 days. . . | 113 |
| 6.5 | [Difference Δ between “true” and determined elliptical orbit representing the discovery track of a GTO object and the follow-up tracks after 0.5 h, 2 h, at first apogee during the first and the fifth night after the discovery, and after 30 days. | 115 |
| 6.6 | Difference Δ between “true” and determined elliptical orbit representing 4 maintenance tracks of a GTO object separated by 30 days. | 116 |
| 6.7 | Difference Δ between “true” and determined elliptical orbit representing 4 maintenance tracks of a GTO object separated by 15 days. | 117 |
| 6.8 | Difference Δ between “true” and determined elliptical orbit representing 4 maintenance tracks of a GTO object separated by 30 days and two additional tracks one hour after the second and third maintenance track. | 118 |
| 6.9 | Difference Δ between “true” and determined elliptical orbit representing the discovery track of two GEO objects with $A/M = 0.02 \text{ m}^2/\text{kg}$ and $A/M = 20.48 \text{ m}^2/\text{kg}$ | 121 |
| 6.10 | Difference Δ between “true” and determined elliptical orbit representing the discovery track of two GTO objects with $A/M = 0.02 \text{ m}^2/\text{kg}$ and $A/M = 20.48 \text{ m}^2/\text{kg}$ | 122 |
| 6.11 | Comparison of the error ellipsoid with observed positions. | 126 |

List of Tables

| | | |
|------|----------------------------------------------------------------------------------------------------------------------------------------------------------------------|----|
| 2.1 | Classification of geostationary objects in drift orbits. | 15 |
| 2.2 | Return intervals and visibility windows for drifting GEO objects ($i = 0^\circ$) with a semi-major axis differing by Δa from a_0 | 16 |
| 3.1 | The ESA debris test campaign. | 24 |
| 3.2 | The ESA debris campaigns. | 24 |
| 4.1 | Delta-values used for the comparison within the tool CAMRES. | 38 |
| 4.2 | Successful follow-up observations for the campaigns from February 2001 to December 2004 resulting from the tool CAMCOR. | 44 |
| 4.3 | Identified multiple observations for the campaigns from February 2001 to December 2004 resulting from the tool CAMCOR. | 46 |
| 5.1 | Range of the orbital elements used for the simulation of 250 GEO orbits. | 48 |
| 5.2 | Mean formal errors for the elliptical orbit determination representing the discovery track of a GEO object and different numbers of follow-up tracks. | 53 |
| 5.3 | Mean formal errors for the elliptical orbit determination representing the discovery track of a GEO object and different numbers of follow-up tracks. | 56 |
| 5.4 | Mean formal errors for the elliptical orbit determination representing the discovery track of a GEO object and an additional survey track after 3 h. | 58 |
| 5.5 | Mean formal errors for the elliptical orbit determination representing the discovery track of a GEO object and additional survey tracks after 1.5 h and 3 h. | 59 |
| 5.6 | Mean formal errors for the elliptical orbit determination representing the discovery track of a GEO object and an additional survey track after 20 h. | 61 |
| 5.7 | Mean formal errors for the elliptical orbit determination representing the discovery track of a GEO object and additional survey tracks after 20 h and 26 h. | 61 |
| 5.8 | Difference Δp between the determined and the observed position for GEO objects observed with the ESASDT. | 62 |
| 5.9 | Difference Δp between the determined and the observed position for GEO objects observed with the ZIMLAT. | 63 |
| 5.10 | Range of the orbital elements used for the simulation of 250 GTO orbits. | 64 |
| 5.11 | Mean formal errors for the elliptical orbit determination representing the discovery track of a GTO object and different numbers of follow-up tracks. | 72 |
| 5.12 | Mean formal errors for the elliptical orbit determination representing the discovery track of a GTO object and different numbers of follow-up tracks. | 75 |

| | | |
|------|------------------------------------------------------------------------------------------------------------------------------------------------------------------------------------------------------------|-----|
| 5.13 | Difference Δp between the determined and the observed position for GTO objects observed with the ESASDT. | 77 |
| 5.14 | Difference Δp between the determined and the observed position for GTO objects observed with the ZIMLAT. | 78 |
| 5.15 | Mean formal errors for the elliptical orbit determination representing two tracks of a GEO object observed simultaneously from two virtual sites with identical latitude and different longitudes. | 82 |
| 5.16 | Mean formal errors for the elliptical orbit determination representing two tracks of a GEO object observed simultaneously from two virtual sites with identical longitude and different latitudes. | 83 |
| 5.17 | Mean formal errors for the elliptical orbit determination representing three tracks of a GEO object observed simultaneously from three virtual sites with different longitudes and latitudes. | 84 |
| 5.18 | Mean formal errors representing the discovery track of a GEO object and the follow-up after 1 h for virtual sites with identical latitude and different longitudes. | 85 |
| 5.19 | Mean formal errors representing the discovery track of a GEO object and the follow-up after 1 h for virtual sites with identical longitude and different latitudes. | 86 |
| 5.20 | Mean formal errors for the elliptical orbit determination representing two tracks of a GTO object observed simultaneously from two virtual sites with identical latitude and different longitudes. | 94 |
| 5.21 | Mean formal errors for the elliptical orbit determination representing two tracks of a GTO object observed simultaneously from two virtual sites with identical longitude and different latitudes. | 95 |
| 5.22 | Mean formal errors for the elliptical orbit determination representing three tracks of a GTO object observed simultaneously from three virtual sites with different longitudes and latitudes. | 96 |
| 5.23 | Mean formal errors representing the discovery track of a GTO object and the follow-up after 0.25 h for virtual sites with identical latitude and different longitudes. | 97 |
| 5.24 | Mean formal errors representing the discovery track of a GTO object and the follow-up after 0.25 h for virtual sites with identical longitude and different latitudes. | 98 |
| 5.25 | Separations in longitude λ and latitude β between the three sites of Nauchny (CRAO), Zimmerwald (ZIMLAT), and Tenerife (ESASDT). | 104 |
| 5.26 | Formal errors for the elliptical orbit determination of object GEO_M1 representing two tracks observed with the CRAO (top) and two tracks observed with the CRAO and the ZIMLAT (bottom). | 105 |
| 5.27 | Formal errors for the elliptical orbit determination of object GEO_M2 representing two tracks observed with the CRAO (top) and two tracks observed with the CRAO and the ESASDT (bottom). | 106 |
| 5.28 | Formal errors for the elliptical orbit determination of object GEO_M3 representing two tracks observed with the ZIMLAT (top) and two tracks observed with the ZIMLAT and the ESASDT (bottom). | 106 |
| 5.29 | Mean formal errors for the elliptical orbit determination assuming different observation errors. | 108 |

| | | |
|------|------------------------------------------------------------------------------------------------------------------------------------------------------------------------------------------------------------------------------------------------------------|-----|
| 6.1 | Mean formal errors for the elliptical orbit determination representing the discovery track of a GEO object and the follow-up tracks after 1 h, 2 h, 3 h, 1 day, and 30 days. | 110 |
| 6.2 | Mean formal errors for the elliptical orbit determination representing the discovery track of a GEO object and the follow-up tracks after 1 h, 2 h, 3 h, 1 day, 30 days, and 60 days. | 111 |
| 6.3 | Mean formal errors for the elliptical orbit determination representing 6 maintenance tracks of a GEO object separated by 30 days. | 112 |
| 6.4 | Mean formal errors for the elliptical orbit determination representing the discovery track of a GEO object and the follow-up tracks after 1 h, 2 h, 3 h, one day, and 180 days. | 113 |
| 6.5 | Difference Δp between the determined and the observed position for GEO objects observed with the ESASDT. | 114 |
| 6.6 | Difference Δp between the determined and the observed position for GEO objects observed with the ZIMLAT. | 114 |
| 6.7 | Mean formal errors for the elliptical orbit determination representing the discovery track of a GTO object and the follow-up tracks after 0.5 h, 2 h, at first apogee during the first and the fifth night after the discovery, and after 30 days. | 115 |
| 6.8 | Mean formal errors for the elliptical orbit determination representing 4 maintenance tracks of a GTO object separated by 30 days. | 116 |
| 6.9 | Mean formal errors for the elliptical orbit determination representing 4 maintenance tracks of a GTO object separated by 15 days. | 117 |
| 6.10 | Mean formal errors for the elliptical orbit determination representing 4 maintenance tracks of a GTO object separated by 30 days and two additional tracks one hour after the second and the third maintenance track. | 118 |
| 6.11 | Difference Δp between the determined and the observed position for GTO objects observed with the ESASDT. | 118 |
| 6.12 | Difference Δp between the determined and the observed position for GTO objects observed with the ZIMLAT. | 119 |
| 6.13 | Mean formal errors for the elliptical orbit determination of GEO objects with various A/M. The orbit determination does not include an estimation of A/M. | 120 |
| 6.14 | Mean formal errors for the elliptical orbit determination of GEO objects with various A/M. The orbit determination does include an estimation of A/M. | 121 |
| 6.15 | Mean formal errors for the elliptical orbit determination of GTO objects with various A/M. The orbit determination does not include an estimation of A/M. | 122 |
| 6.16 | Mean formal errors for the elliptical orbit determination of GTO objects with various A/M. The orbit determination does include an estimation of A/M. | 123 |

Frequently Used Acronyms

| | |
|------------|------------------------------------------------------------------------------|
| A/M | Area-to-Mass ratio |
| AIUB | Astronomical Institute of the University of Bern, Switzerland |
| CCD | Charge Coupled Device |
| CelMech | Celestial Mechanics program system |
| CRAO | CRimean Astrophysical Observatory |
| DRP | Direct Radiation Pressure |
| DISCOS | Database and Information System for the Characterization of Objects in Space |
| ESA | European Space Agency |
| ESASDT | ESA Space Debris Telescope |
| ESOC | European Space Operations Center |
| FOV | Field Of View |
| GEO | Geostationary Earth Orbit |
| GEODSS | Ground-based Electro-Optical Deep Space Surveillance |
| GTO | Geostationary Transfer Orbit |
| IAC | Instituto de Astrofisica de Canarias |
| IADC | Inter-Agency space Debris coordination Committee |
| LEO | Low Earth Orbit |
| NASA | National Aeronautics and Space Administration |
| OGS | Optical Ground Station |
| RMS | Root-Mean-Square (error) |
| RSSS | Russian Space Surveillance System |
| SBV | Space Based Visible |
| SSN | Space Surveillance Network |
| TLE | Two Line Elements |
| USSTRATCOM | United States STRATegic COMmand |
| ZIMLAT | ZIMmerwald Laser and Astrometry Telescope |

1. Introduction

Since the launch of Sputnik 1 on 4 October 1957 about 5 000 man-made satellites have been placed in orbits around the Earth. More than 4 000 launches have been recorded, i.e., about 100 launches per year have been performed.

Currently, about 10 000 objects are regularly tracked and catalogued by military space surveillance systems. Only about 7% (600-700) of these objects are operationally used for science, commercial, and other applications. The other part of the catalogued objects have no more purpose and are therefore denoted as space debris. Such space debris can be spent satellites, upper stages, mission-related objects, or fragments from satellites and rocket stages. The size of space debris objects ranges from micrometer to a few meters. The number of space debris is steadily increasing.

Space debris is a threat to operational satellites and manned missions, as the International Space Station. Already particles as small as a few micrometers can lead to visible pits. Such pits were inspected on the solar panels of the Hubble Space Telescope and also on the NASA Space Shuttle. Larger particles can cause severe damage and can endanger a mission when they collide with such a particle. The number of space debris is also increasing due to collisions between objects. Very large objects can cause damage on ground when they survive the reentry and impact on ground.

To reduce the risk of collisions an operated object can perform a collision avoidance manoeuvre. To do this, the positions of the other objects in space, at least the larger ones, have to be known. The positions can be determined from the orbital elements of the objects. This information has to be provided by catalogues containing the orbits of the objects. The orbits have to be updated regularly to guarantee a high accuracy. Therefore, regular observations of the objects have to be acquired. In addition, new objects have to be included into the catalogue. This is done by systematical surveys of the sky. Both tasks, regular observations and sky surveys are covered by space surveillance.

Routine space surveillance is performed by the United States Strategic Command's (USSTRATCOM) Space Surveillance Network (SSN). Radar and optical sensors are used to track objects in space. The sensors are well distributed on the Earth. The resulting catalogue of orbits is available in the TLE (Two Line Elements) format, but with restricted access only. The catalogue is limited to objects larger than about 10 cm in low Earth orbits (LEO; altitude $< 2\,000$ km) and about 1 m in the geostationary Earth orbit (GEO; altitude $33\,786$ km – $37\,786$ km). The Russian military service is also maintaining a catalogue but with less objects due to the worse distribution of the tracking sensors. This catalogue is not publicly available. Currently, no civilian institution provides a catalogue containing the orbits of objects in space. The European Space Agency (ESA) has recently investigated the feasibility of a European Space Surveillance System ([Donath *et al.*, 2004] and [Donath *et al.*, 2005a]). A major requirement for the system is that all objects larger than 1 m have to be contained in the resulting catalogue. The Astronomical Institute of the University of Bern (AIUB) was also contributing to these studies ([Flohner *et al.*, 2005b]). The work of AIUB was focused on optical observations of objects above LEO, e.g., GEO

objects.

The GEO region is of special interest for commercial applications. Objects in GEO have the same angular velocity as the Earth. The objects appear to remain at fixed longitudes and latitudes in the sky for an observer on Earth. This characteristic makes the GEO region important for telecommunication and Earth observation satellites. The first satellite inserted into a GEO was Syncom-3 in 1964. Over 900 large objects have since been inserted. Due to the characteristics of the orbit objects in GEO remain almost forever in this region.

Geostationary transfer orbits (GTO) are used to transport satellites from a circular orbit at low altitude to the GEO region. GTO objects therefore have a low perigee altitude and a high apogee altitude reaching the GEO. The spent upper stages of the used rockets often remain in the GTO region. The lifetime of objects in GTO is from a few months to several decades ([Sharma *et al.*, 2004]).

Objects in GEO and GTO can be observed using optical telescopes. The AIUB has been performing search campaigns (surveys) for satellites and space debris in the GEO region since 1999. Not only a unexpected large number of faint and small objects (between 10 cm and 1 m) have been detected but also a previously unknown population of GEO objects with large eccentricities has been discovered during the GEO surveys. The surveys for debris objects in GTO started in 2002. The results from both, GEO and GTO surveys, are regularly published, e.g., in [Schildknecht *et al.*, 2001], [Schildknecht *et al.*, 2003], or [Schildknecht *et al.*, 2004b]. The observations are acquired with the ESA space debris telescope (ESASDT) on Tenerife.

The objects are detected on a short series of frames. The resulting series of observations (also called “track”) are spanning a few minutes only. Because of the short arc length only circular orbits are normally determined. Some of the detected objects, however, have elliptical orbits. The assumption of circular orbits leads to wrong orbital elements determined for these objects. Follow-up observations during the night of the discovery and the following nights are therefore necessary to determine elliptical orbits.

Some of the GEO surveys are designed such that the detected objects have a good chance to be re-observed during the next night. Furthermore, observations of the same object spaced by a few days can be hidden in the acquired data. The identification of multiple detections of objects can also help to determine elliptical orbits.

The goal of this work is to develop a concept to efficiently maintain a catalogue of orbits for GEO and GTO objects. Such a concept strongly depends on the instrument, mainly on the field of view (FOV) of the telescope and the accuracy of the single observations of the positions. Concerning the position accuracy, this work will focus on the ESASDT. For the FOV, however, a more general solution will be presented.

Simulations are used to determine the number of tracks needed to determine “secured” orbits. Orbits are denoted as “secured” if they guarantee a safe recovery of the object after a few weeks. For a safe recovery the propagation error has to be smaller than half of the FOV. A follow-up strategy to achieve “secured” orbits is developed. The strategy provides an observation scheme, i.e., the number of observation tracks and the temporal spacing between the tracks. The presented observation scheme will guarantee, under certain assumptions, that the object is always within the FOV.

Catalogued orbits have to be maintained, i.e., the objects must be regularly re-observed. Again, simulations are used to determine the maximum time span for a safe recovery. The quality of the orbits determined from so-called “long arcs” is dominated by the modeling errors. The influence of errors on the prediction error is also investigated.

All results from the simulations are tested using real observations from the ESASDT and the Zimmerwald Laser and Astrometry Telescope (ZIMLAT). The later is owned by AIUB and located in Zimmerwald near Bern. Some objects have been observed by both instruments, some of them even during the same night. These observations are used to study the improvement of the orbit accuracy by using quasi-simultaneous observations from multiple sites.

Newly detected objects have to be correlated with the catalogue. A procedure for the correlation is presented. The procedure is slightly different for observations stemming from surveys and observations stemming from tasked observation, e.g., follow-up observations.

The follow-up observations have to be planned. Parameters, which have an influence on the planning, are the visibility of the object from the observing site and the accuracy of the orbit. These parameters have to be considered in a concept for the planning.

In Chapter 2, *General Information*, the US Space Surveillance Network used to produce the most important catalogue and other space surveillance systems are described. Some results from the studies for a European Space Surveillance System are presented. A description of the GEO and GTO populations from the catalogue is also given. At the end, the instruments used to acquire the observations presented in this work are introduced.

Chapter 3, *Search Surveys for Debris*, gives a short summary of the results from survey campaigns dedicated to the search for space debris in GEO and GTO.

In Chapter 4, *Identification of Multiple Detections*, the algorithms and programs used to identify multiple detections of an object within the surveys are presented. The identification is performed in two steps. First, potential detections of the same object are identifies. Then, the hypothesis from the first step is tested using orbit improvement techniques.

In Chapter 5, *Acquisition of a “Secured” Orbit*, concepts to achieve “secured” orbits for GEO and GTO objects are developed. The concepts include the number of necessary observation tracks, the temporal spacing between the tracks, and the needed total arc length. Observations from multiple sites are also considered. Simulations are used to achieve the concepts. The concepts are tested using real observations from the ESASDT and the ZIMLAT.

A concept to maintain the “secured” orbits is presented in Chapter 6, *Concept for Catalogue Maintenance*. The maximal temporal spacing for a save recovery as well as the procedures for the correlation and the planning of the observations are discussed. The influence of modeling errors on the prediction error is investigated.

Chapter 7, *Summary and Outlook*, summarizes the results. Further, a short conclusion on the results is given. An outlook shows future applications of this work.

Annex A, *The Program System CelMech*, describes the programs contained in CelMech used to perform the orbit determination and improvement as well as the orbit propagation.

2. General Information

Objects in space can be tracked and observed using radar and optical telescopes. Most instruments are ground-based. Only one space-based optical sensor is currently operating.

Radars are mainly used to observe objects in low altitudes, while optical telescopes are mostly used to observe objects in high altitudes. Figure 2.1 shows the measurement regions and sensitivity for some instruments (from [Krag, 2003]). The sensitivities of some radars are indicated with black lines. The Goldstone and the Haystack (HAYS) radars are located in the USA. TIRA is a German radar operated by FGAN (Forschungsgesellschaft für Angewandte Naturwissenschaften). The measurement ranges of radars are a few thousand kilometers. Objects in the size of a few millimeters can be detected.

From the optical sensors only the Liquid Mirror telescope (LMT) was used to observe objects in low altitudes. The CCD Debris Telescope (CDT) could observe objects in high altitudes, e.g., the GEO belt. Both telescopes, the LMT and the CDT, were part of the NASA space debris program and are both decommissioned now. The sensitivity of the ESASDT is also included in the figure. The sensitivity of the ZIMLAT is somewhere between the CDT and the ESASDT.

The sensitivity of the catalogue provided by USSTRATCOM, formerly called U.S. Space Command, is also included in Figure 2.1. Some of the instruments contributing to this catalogue are presented in the following section.

2.1 Space Surveillance Systems

Currently, only two countries maintain a space surveillance system: the United States of America and the Russian Federation. Both systems are under military control. Only the U.S. Space Surveillance Network has full coverage in longitude. China has also plans to build up its own space surveillance system, but probably only with limited coverage in longitude. A first feasibility study for a European Space Surveillance System has been carried out lately. The proposed system would have almost full coverage in longitude.

2.1.1 U.S. Space Surveillance Network

The responsibility for the U.S. Space Surveillance Network (SSN) is at the USSTRATCOM. The command is one of nine commands under the Department of Defense. The SSN started to track space objects in 1957, right after the launch of the Russian Sputnik I. More than 20 000 objects have since been tracked. Currently, the SSN tracks over 8 700 catalogued and 1 000 uncatalogued objects, mainly larger than 10 cm ([Johnson, 2001]).

The SSN is a worldwide network of 21 ground-based optical and radar sensors and one space-based

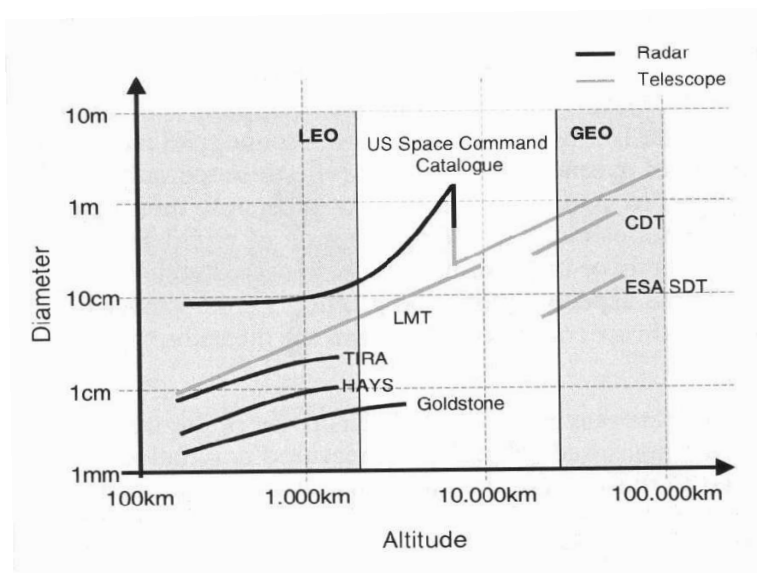


Figure 2.1: Measurement regions and sensitivity of some instruments (from [Krag, 2003]).

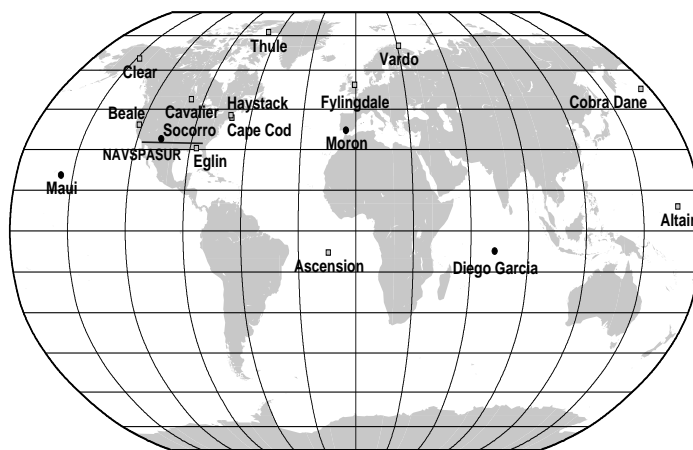


Figure 2.2: The U.S. Space Surveillance Network. ●: optical sensor, □: radar sensor.

sensor ([STRATCOM, 2004]). The distribution of the sensors is shown in Figure 2.2. The ground-based optical sensors are marked with ●, while the radar sensors are marked with □. A description of the sensors can be found at [NSSRM, 2006].

The radar sensors are concentrated along the border of the continental USA. The line across the USA indicates the Naval Space Surveillance System (NAVSPASUR). A few radar sensors are also distributed worldwide. Two typical types of radar sensors are shown in Figure 2.3. The Haystack radar is a conventional radar using a movable tracking antenna. The Eglin radar is a phased-array radar, which can scan large areas of space in a fraction of a second. Radar sensors are mainly used to track objects in Low Earth Orbits (LEO).

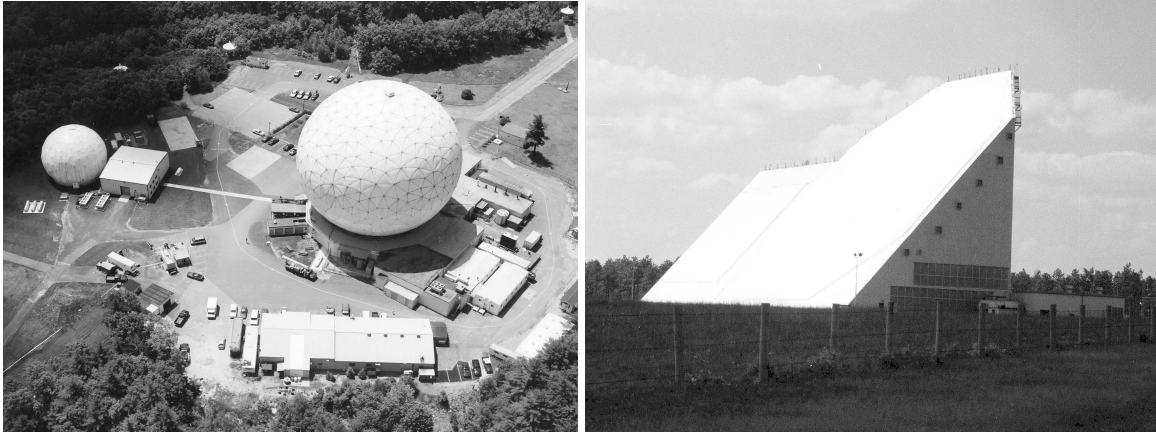


Figure 2.3: The Haystack and the Eglin radar sensors (images by NASA).

The sites with optical sensors are well distributed in longitude. They are located at Socorro, New Mexico; Maui, Hawaii; Diego Garcia, British Indian Ocean Territories; and Moron, Spain. The distribution guarantees a full coverage of the GEO belt. The first three sites are equipped with a Ground-based Electro-Optical Deep Space Surveillance (GEODSS) system. Images of the sites are shown in Figure 2.4. Each site has three telescopes. The telescopes have a 1-m aperture and a two-degree FOV.

The GEODSS telescopes scan the sky at the same rate as the stars appear to move. Several images of the same field are taken. The frames are overlaid on each other and the star images, which remain fixed, are electronically erased. The movement of artificial objects appear as streaks. These streaks are measured and the data used to determine the position of the objects.

The Moron Optical Space Surveillance (MOSS) system consists of one telescope with a 56 cm aperture. The only SSN sensor in space is the Space-Based Visible (SBV) sensor on board the Midcourse Space Experiment (MSX) satellite. Figure 2.5 shows an artistic view of the satellite. The SBV components are indicated with arrows. The MSX was launched in 1996 into an 898-km altitude, near sun-synchronous orbit. Since October 1997, the SBV has been a contributing sensor to the SSN. The SBV is primarily dedicated to track objects in GEO, but about 25 percent of the observations are non-GEO objects ([Sharma, 2000]). The SBV is the most productive sensor in the SSN for tracking GEO objects. A detailed description of the system can be found in [Stokes *et al.*, 1998], or in several articles published in [Schmidt, 2000].

Combined, the SSN sensors acquire over 100 000 observations each day. The data is transmitted to the Space Control Center (SSC) at Cheyenne Mountain Air Force Station in Colorado Springs. The SSC maintains a database of all identifiable objects in Earth orbit.



Figure 2.4: The three GEODSS sites: Diego Garcia (upper left; image courtesy of Bob Ralph and Thomas Lawson), Socorro (upper right; image by CelesTrak), and Maui (lower center; image by The Air Force Research Laboratory: Directed Energy Directorate). The lower image shows the whole Maui Space Surveillance Complex, which includes the MSSS (right building) and the GEODSS (three smaller domes on the left building).

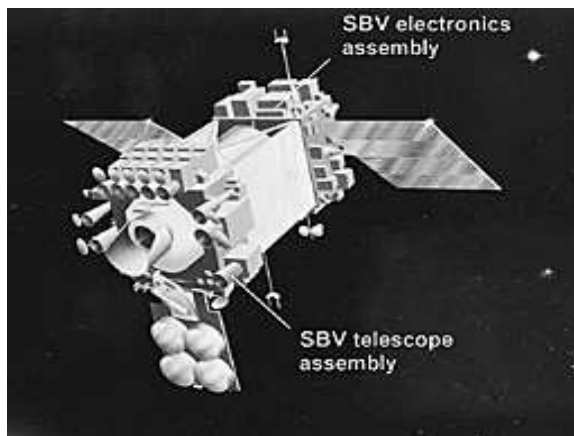


Figure 2.5: Artistic view of the MSX satellite. The SBV components are indicated by arrows (Figure courtesy of The John Hopkins University: Applied Physics Laboratory).

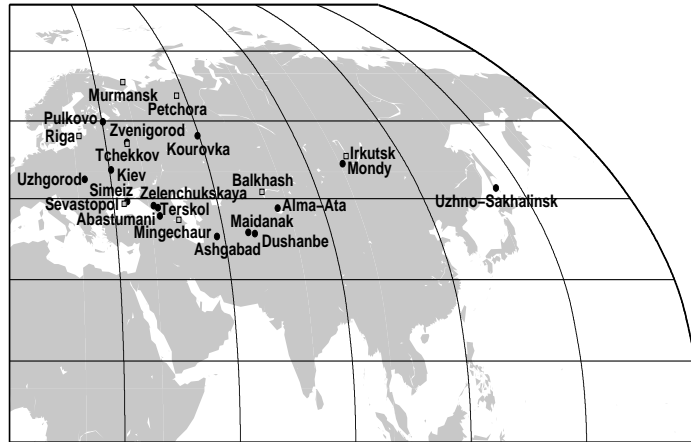


Figure 2.6: The Russian Space Surveillance System. ●: optical sensor, □: radar sensor.

2.1.2 Russian Space Surveillance System

The Russian Space Surveillance System (RSSS) started to track objects in 1962 using optical facilities of the Soviet Academy of Sciences and the Department of Defense ([Batyr *et al.*, 1993]). In 1969 the Space Surveillance Center was formed to coordinate the observations and to maintain a catalogue. According to [Aksenov *et al.*, 2003] the Russian catalogue contains about 6 000 objects.

The sensors of the RSSS are located on former USSR territories, only (Figure 2.6). Thus, the distribution is less optimized compared to the SSN. This leads to some “invisibility” zones, especially in GEO. A list of the locations of radar and optical sensors can be found in [Batyr *et al.*, 1993]. According to [Khutorovsky *et al.*, 2001], at least the optical sensors in that list were still used in 2001. [Agapov *et al.*, 2003] presents an updated list with five additional sensors. It is also stated that two of the facilities listed in [Batyr *et al.*, 1993] were dismantled and three facilities are not operational. The accuracy of a single observation of the sensors is within the range $1'' - 10''$.

No updated list of the radar sensors was found. Thus, the current status of the whole RSSS remains unclear.

2.1.3 European Space Surveillance System

Currently, no operating European space surveillance system exists, except for some limited systems under national control. A first feasibility study by ESA for a European Space Surveillance System was presented at the end of 2004 ([Donath *et al.*, 2004] and [Donath *et al.*, 2005b]). The study focused on a radar system to observe the LEO region and a system of optical sensors to observe the GEO region. A follow-on study including a system to observe the MEO region and improvements to the radar system was completed in 2005 ([Donath *et al.*, 2005a]).

Figure 2.7 shows the proposed locations for the radar and the optical sensors. The proposed radar sensor is based on the French GRAVES radar ([Michal *et al.*, 2005]). Figure 2.8 shows the transmitting antennas

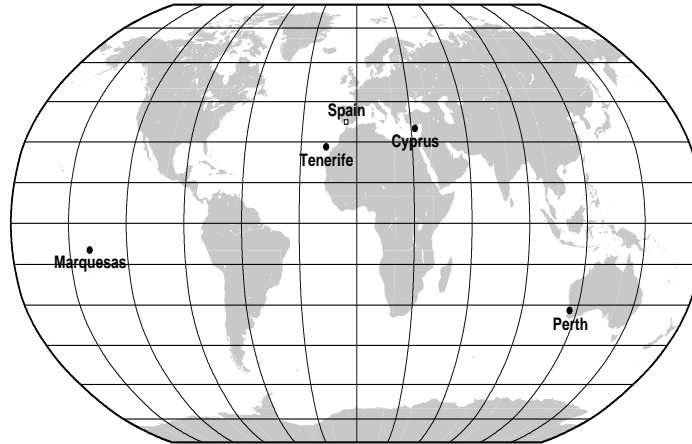


Figure 2.7: The proposed European Space Surveillance System. ●: optical sensor, □: radar sensor.



Figure 2.8: The GRAVES radar sensor. Left: transmitting antennas; right: receiving antennas (images by ONERA).

and the receiving antennas of the GRAVES radar. The radar is proposed to be extended to a UHF radar with a frequency of 435 MHz. The range of this radar would be between 1 500 and 1 700 km. The location is proposed to be in the south of Spain, with a distance between the transmitting and the receiving antennas of 200 km.

The sites for the optical sensors were chosen such that a large coverage ($\sim 95\%$) of the GEO objects in the DISCOS catalogue is guaranteed. Two 0.5 m $f/2$ telescopes per site with a FOV of $3 \times 3^\circ$ are proposed for the GEO surveillance. A design of the proposed telescope is shown in Figure 2.9. At each site, the telescopes are dedicated to perform surveys and to perform tasked observations, e.g., to perform follow-up observations. A description of the GEO system can be found in [Flohner *et al.*, 2005b]. Two additional 0.8 m telescopes located at two different sites are proposed for the MEO surveys and complete the network of ground-based optical sensors. The FOV of these fast $f/1$ instruments would be $4.7 \times 4.7^\circ$. The distance in longitude between the two sites should be around 90° . The Tenerife and the Marquesas site were therefore proposed.

Concerning space-based observations two studies for a European orbital telescope were carried out re-



Figure 2.9: Design of the proposed 0.5 m telescope [Donath *et al.*, 2004].

cently. The older one was presented in [Oswald *et al.*, 2004] and showed the feasibility in principle. The newer one was finalized in 2005 ([Valtonen *et al.*, 2006]) and presented a detailed system architecture, an operation concept, the system performance, and the lifetime and cost estimations. The key results of the study were presented in [Flohner *et al.*, 2005a] and [Wokke *et al.*, 2006]. The focus of both studies was on space debris surveys and not on space surveillance. Nevertheless, the study also showed that orbit determination would be possible for LEO and GEO objects and such an orbital telescope could therefore also contribute to a space surveillance system. But this needs further investigation.

2.2 Catalogues

The most important catalogue is the one published by USSTRATCOM, e.g., on [SPACE-TRACK, 2006]. It is not only the most complete catalogue but also most other available catalogues are based to a certain extent on this data. The USSTRATCOM catalogue contains orbital information on space objects. The orbital elements are updated several times per week. The format is the so-called 'Two-Line Elements' form. A description of the format can be found on [CELESTRAK, 2006]. The TLE are mean elements and must be used with one of the propagators SGP, SGP4, SDP4, SGP8, or SDP8. The models used by these propagators are described in [Hoots *et al.*, 1980]. This document is also available on [CELESTRAK, 2006].

Currently, no catalogue generated from the data gathered by the RSSS is available.

The European Space Operation Center (ESOC) maintains the 'Database and Information System for the Characterization of Objects in Space' (DISCOS). This database contains orbit and additional information on space objects. The basic source of information is the USSTRATCOM catalogue. Access to the DISCOS database is restricted.

Once per year, ESA publishes the ESA Classification of Geosynchronous Objects, e.g., ([Serraller and Jehn, 2005]). All GEO objects from the DISCOS database are included in this document. Furthermore, objects which are not available from the USSTRATCOM catalogue are included. The orbital information

of these objects is mainly provided by the Keldysh Institute of Applied Mathematics (KIAM), Moscow. Some of the orbits are a joint product of some Russian organizations led by KIAM, Observatory Sciences Ltd. (UK), and AIUB. First results from this joint work are presented in [Agapov *et al.*, 2005]. The total number of GEO objects listed in [Serraller and Jehn, 2005] is 1 124.

In the following, the catalogued GEO and GTO objects are characterized. The data is taken from the DISCOS database, status December 2004.

2.2.1 GEO

As the name indicates, geostationary objects appear to remain at fixed longitudes and latitudes in the sky for an observer on Earth. This is because a GEO objects performs nearly one revolution per sidereal day. For ideal GEO objects it is exactly one sidereal day. In addition, ideal orbits are circular and in the equatorial plane. According to [Soop, 1994], the radius of a perfect GEO orbit is 42 164.5 km.

In reality, operational objects have to be controlled due to various perturbations. The main forces causing these perturbations are the anomalies in the gravitational field of the Earth, the gravitational attraction of the Sun and the Moon, and the solar radiation pressure. Longitude-dependent spherical harmonics of the development of the gravitational potential of the Earth, in particular the term J_{22} , lead to resonance effects causing long-term perturbations of the semi-major axis. This leads to a libration motion of the objects around the stable points at 75° E or 105° W. Therefore, operational satellites have to be controlled in longitude. The combination of the perturbations due to the Earth's oblateness and the gravitational attractions of the Sun and the Moon causes the orbital plane of GEO objects to precess with a period of about 53 years around a stable plane, the so-called Laplace plane. The Laplace plane has an inclination of about 7.5° with respect to the equatorial plane and its nodal line coincides with the direction of the vernal equinox. Consequently, the normal to a geostationary orbital plane describes a cone with an opening angle of 15° (see Figure 2.10). The corresponding variation of the inclination i is about $\pm 15^\circ$. Figure 2.10 also shows that, as a consequence of the precession, the right ascension of the ascending node Ω is correlated with i . A control of the inclination is therefore also necessary for operational objects. The solar radiation pressure induces a small eccentricity, leading to variations in the geocentric distance of up to ± 75 km.

Catalogued Objects

The objects from the catalogue can be divided into three main classes:

- satellites (operational / non-operational),
- rocket bodies (fourth stages, apogee boost motors, small rocket bodies),
- fragments.

Issue 5 of the 'ESA classification' ([Hernández and Jehn, 2003]) identified 734 satellites, 187 rocket bodies, and 13 fragments. 323 satellites were controlled, but also some uncontrolled satellites were still active. The non-operational satellites, the rocket bodies, and the fragments can also be classified as space debris. This gives a few hundred debris objects in GEO.

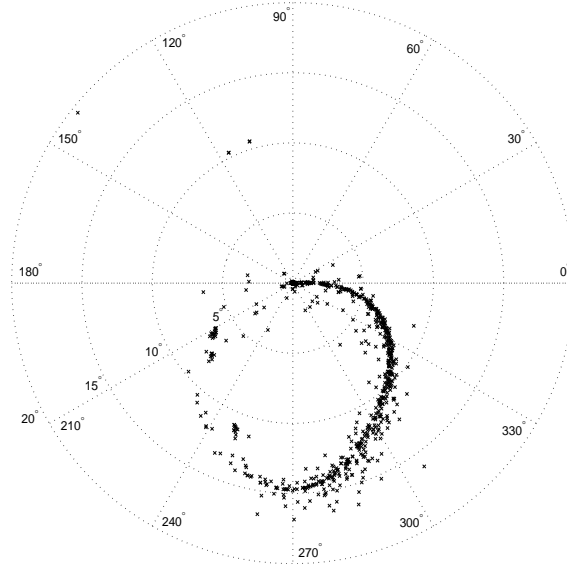


Figure 2.10: Precession of the orbits of GEO objects. The symbols give the location of the orbital poles corresponding to inclination i and right ascension of ascending node Ω (from DISCOS, status Dec. 2004). Coordinates are right ascension $\alpha = \Omega - 90^\circ$ and declination $\delta = i$.

The objects for the following analysis were selected from the DISCOS database (status Dec. 2004) using the following criteria:

- eccentricity smaller than 0.1,
- inclination smaller than 20° ,
- mean motion between 0.9 and 1.1 revolutions per day.

This range in the mean motion corresponds to semi-major axes of $42\,164 \pm 2\,800$ km.

The histogram in Figure 2.11 shows the distribution of the semi-major axes. A strong peak at the exact value of the GEO radius can be seen. There are also many objects with larger semi-major axes. Most of them are objects in so-called “graveyard orbits”. The semi-major axes of these objects were increased on purpose at the end of life of the satellite. This way, collisions with operational satellites are avoided. Figure 2.12 shows that the eccentricities of catalogued GEO objects are very small and the orbits therefore almost circular. Nevertheless, perturbations like the radiation pressure can force the eccentricities to increase ([Schildknecht *et al.*, 2005b]).

Most of the controlled GEO objects have inclinations close to 0° (Figure 2.13). As a consequence of the precession of GEO objects (see Figure 2.10) the histogram has a strong decrease at an inclination of 15° . This precession can also be seen in Figure 2.14, where the inclination is plotted against the right ascension of ascending node. The right ascension of ascending nodes of controlled objects are arbitrarily distributed over 360° , whereas the nodes are strongly correlated with the inclination for uncontrolled objects.

Controlled objects are only visible if their longitude is within the observable longitude range for a given station, e.g., 41° E – 74° W for Tenerife. Many uncontrolled objects, however, are drifting, i.e., the

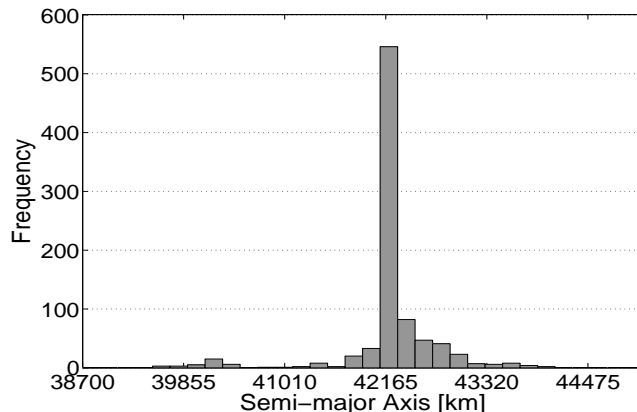


Figure 2.11: Distribution of the semi-major axis of GEO objects (from DISCOS, status Dec. 2004).

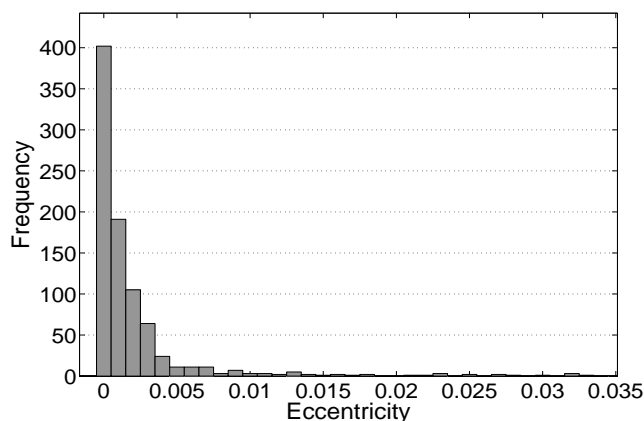


Figure 2.12: Distribution of the eccentricity of GEO objects (from DISCOS, status Dec. 2004).

longitude is changing with time. The drift rate may be computed from the difference Δa of the semi-major axis with respect to the geostationary radius $a_0 \approx 42\,164$ km using Kepler’s third law to first order by ([Hugentobler, 1998])

$$\Delta n [^\circ/\text{day}] \approx -0.0128 \Delta a [\text{km}]. \quad (2.1)$$

Objects in “super-synchronous” orbits (semi-major axis larger than a_0) have negative drift rates (in longitude), whereas objects below GEO exhibit positive drift rates. As an example, an object in a graveyard orbit 300 km above GEO has a drift rate of $\Delta n = -3.8^\circ$.

At the end of 2004, 416 of totally 1124 GEO objects from the DISCOS catalogue were classified as objects in drift orbits ([Serraller and Jehn, 2005]). A further classification of objects in drift orbits is provided by the ‘Catalogue of Geostationary Satellites’ ([Socholina et al., 1996]). The classification and the number of objects per class are given in Table 2.1. The table shows that about one third of the objects in drift orbits have drift rates smaller than $2.5^\circ/\text{day}$.

From a fixed location on earth objects in drift orbits are visible during certain time intervals (“visibility window”) only. The visibility windows for drifting objects with different orbital inclinations are shown in Figure 2.15 for an observer on Tenerife.

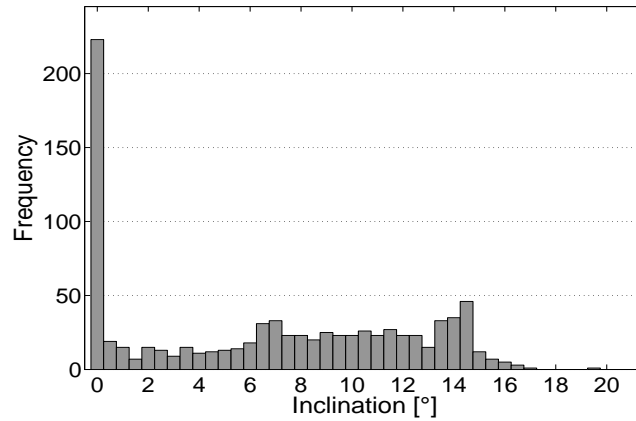


Figure 2.13: Distribution of the inclination of GEO objects (from DISCOS, status Dec. 2004).

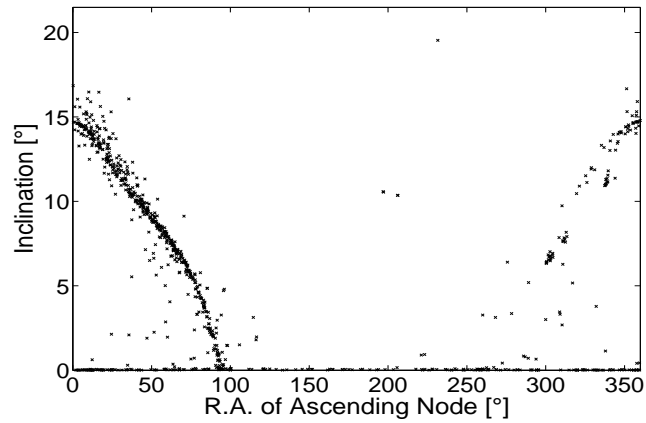


Figure 2.14: Inclination versus right ascension of ascending node for GEO objects (from DISCOS, status Dec. 2004).

Table 2.1: Classification of geostationary objects in drift orbits (from [Socholina *et al.*, 1996] and [Serraller and Jehn, 2005]).

| Orbital motion | 'Catalogue of Orbits', 1996 [Socholina <i>et al.</i> , 1996] | 'ESA Classification', 2005 [Serraller and Jehn, 2005] |
|------------------------------------------------------|-----------------------------------------------------------------|----------------------------------------------------------|
| Small drift rates $< 2.5^\circ/\text{day}$ | 102 | 145 |
| Large negative drift rates $< -2.5^\circ/\text{day}$ | 130 | 194 |
| Large positive drift rates $> 2.5^\circ/\text{day}$ | 78 | 77 |
| Total | 310 | 416 |

The visibility windows repeat with a period equal to the object's revolution period in an Earth fixed system. The drift rates and the corresponding Earth-fixed revolution time ("return time") as well as the visibility windows for an observer on Tenerife are listed in Table 2.2. The return time is longer for smaller drift rates. To determine the length of the time interval when the object is not visible, the visibility window has to be subtracted from the return time. An objects with a drift rate of $\pm 1.3^\circ/\text{day}$

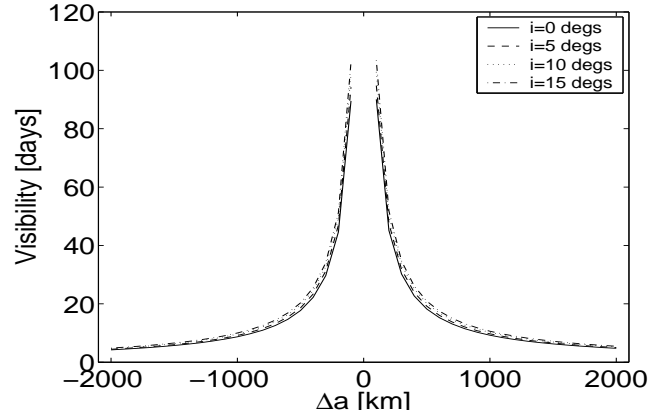


Figure 2.15: Visibilities of drifting GEO objects as a function of the distance Δa to the GEO radius for Tenerife (min. elevation: 20°).

Table 2.2: Return intervals (revolution period in the Earth-fixed system) and visibility windows for drifting GEO objects ($i = 0^\circ$) with a semi-major axis differing by Δa from a_0 (minimum elevation above horizon: 20°).

| Δa [km] | Drift rate [$^\circ$ /day] | Return time [days] | Visibility window [days] |
|--------------------|--------------------------------|-----------------------|-----------------------------|
| -2 000 | 27.2 | 13.2 | 4.2 |
| -1 500 | 20.1 | 17.0 | 5.7 |
| -1 000 | 13.2 | 27.3 | 8.7 |
| -500 | 6.5 | 55.4 | 17.7 |
| -200 | 2.6 | 139.7 | 44.6 |
| -100 | 1.3 | 280.3 | 89.5 |
| 0 | 0 | ∞ | ∞ |
| 100 | -1.3 | 281.9 | 90.1 |
| 200 | -2.5 | 141.4 | 45.2 |
| 500 | -6.3 | 57.1 | 18.2 |
| 1 000 | -12.4 | 28.9 | 9.2 |
| 1 500 | -18.4 | 19.6 | 6.3 |
| 2 000 | -24.2 | 14.9 | 4.8 |

would not be visible for about half a year, whereas objects with large drift rates are observable after a few days.

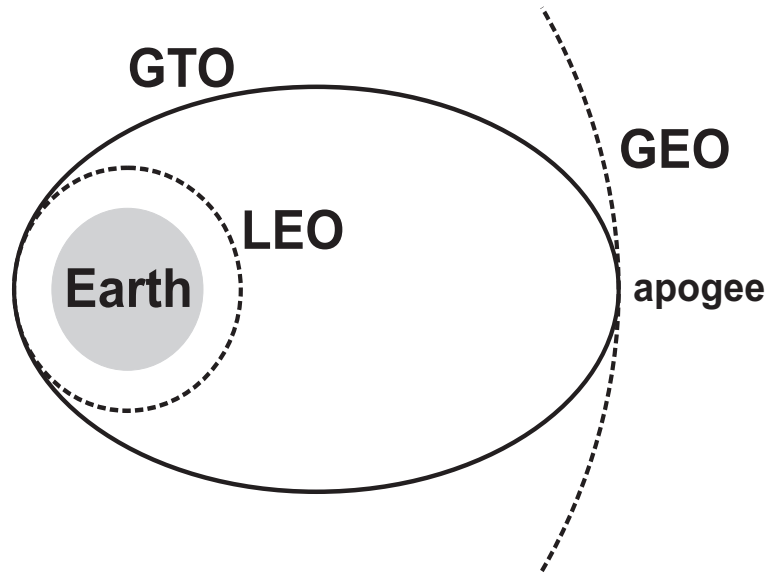


Figure 2.16: The Geostationary Transfer Orbit (GTO).

2.2.2 GTO

Geostationary transfer orbits (GTO) are used to transport satellites from a circular low Earth orbit (LEO) to the GEO. A GTO has therefore a low perigee altitude (180 – 650 km) and a high apogee altitude reaching the GEO (see Figure 2.16). The GTO are highly eccentric orbits. The spent upper stages of the used rockets often remain in the GTO region. The lifetime of objects in GTO is from a few month to several decades ([Sharma *et al.*, 2004]). It is influenced by the luni-solar perturbations, the atmospheric drag, and the launch time ([Flury *et al.*, 1992]). As the lifetime of GTO objects should be as short as possible it is recommended to launched the rockets within short launch windows. Unfortunately, the operational requirements do often not allow to follow this recommendation.

Catalogued Objects

The objects for the following analysis were selected from the DISCOS database (status Dec. 2004) using the following criteria:

- semi-major axis smaller than 30 000 km,
- eccentricity between 0.6 and 0.8,
- inclination smaller than 35°.

The inclination was limited to 35° to exclude the Molniya objects with inclinations of about 65°.

In Figure 2.17, the eccentricity is plotted against the semi-major axis. A clear correlation between the two elements can be seen. At the beginning of their lifetime, the objects in GTO have large eccentricities. Due to perturbations, the apogee altitudes, and consequently the semi-major axes and the eccentricities, decrease with time. Some theoretical discussions on the influence of perturbations on GTO objects can

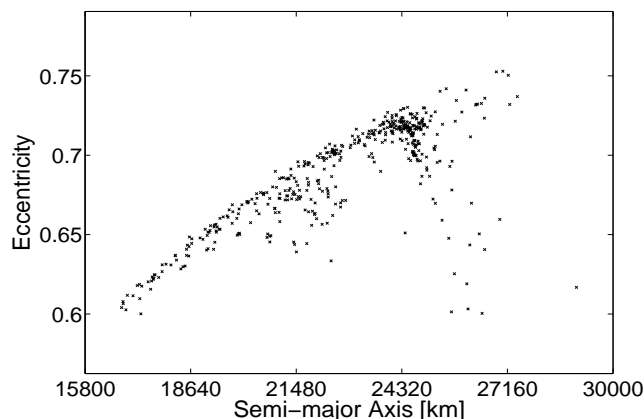


Figure 2.17: Eccentricity versus semi-major axis for GTO objects (from DISCOS, status Dec. 2004).

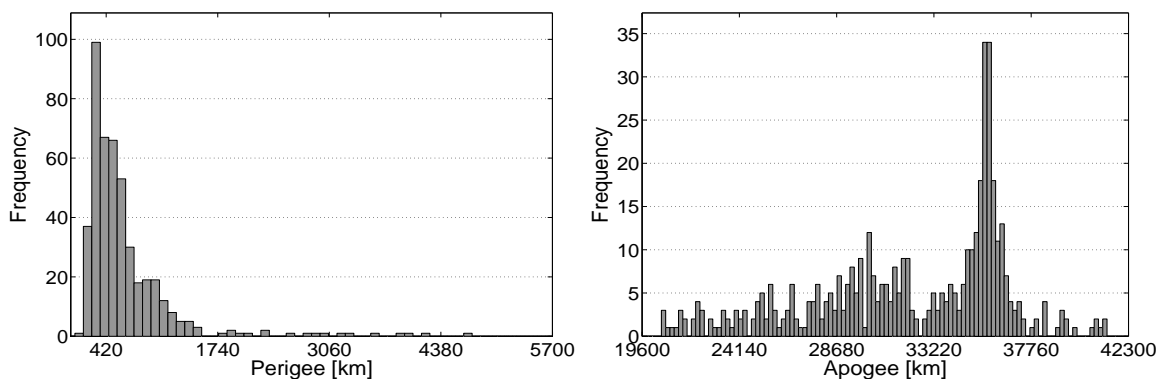


Figure 2.18: Distributions of the perigee altitude (left) and the apogee altitude (right) of GTO objects (from DISCOS, status Dec. 2004).

be found in [Siebold and Reynolds, 1995] and [Sharma et al., 2004]. The distribution in Figure 2.17 shows also a branch where the semi-major axes are increasing with decreasing eccentricities. Objects in this group have their apogee at the GEO altitude, but perigees at 6 900 to 10 500 km altitude.

The histograms in Figure 2.18 show the distribution of the perigee altitude (left) and the apogee altitude (right). The perigee altitude distribution is quite narrow. The left boundary is limited due to the Earth atmosphere. The peak is at an altitude of 300 km. Only a few objects have an altitude higher than 1 500 km. The apogee altitude is much wider. Its peak is at an altitude of 35 800 km, which is the altitude of the GEO. The decrease of the altitude with time can be clearly seen.

Figure 2.19 shows the distribution of the inclination. Two major peaks at an inclination of 7° and 27° can be seen. The inclination of GTO objects mainly depends on the site where they were launched. The peak at 7° results from Ariane rockets launched at Kourou, French Guiana (latitude: 5.2° N). Objects with inclinations between 15° and 30° mostly stem from rockets launched by the USA or the Russian Federation.

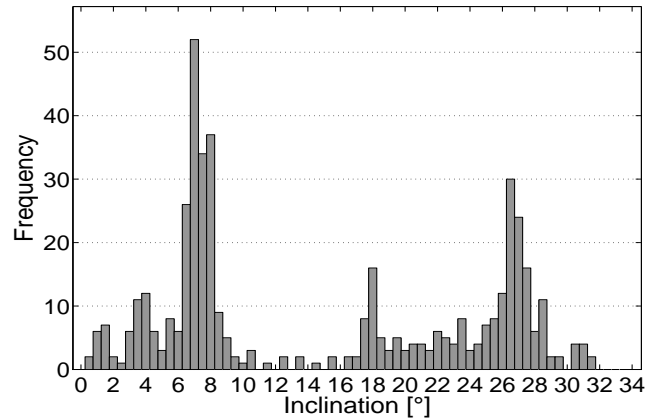


Figure 2.19: Distribution of the inclination of GTO objects (from DISCOS, status Dec. 2004).

2.3 Instruments

Observations from two different instruments were used within this work to test the theoretical results. One is the Zimmerwald Laser and Astrometry Telescope (ZIMLAT) near Bern owned by AIUB. The other is the ESA Space Debris Telescope (ESASDT) on Tenerife. A short description of the two instruments is given in the following.

2.3.1 ZIMLAT

The ZIMLAT is located at the Zimmerwald observatory, about 10 km south of the city of Bern at an altitude of 950 m. A location map and other information can be found on [AIUB, 2006]. The observatory consists of two buildings: the old dome building and the residential building including the new dome. An image of the observatory is shown in Figure 2.20. The old dome is visible on the left side. It contains a 40 cm Schmidt camera and a 60 cm Cassegrain telescope. The focus of the research with these instruments was on the search for supernovae, nova, variable stars, minor planets and comets. Lists of the detected objects can be found on [AIUB, 2006].

A Global Positioning System (GPS) antenna is installed on the top of the mast standing on the left to the residential building. It is the best determined point in Switzerland and contributes to the global network of the International GNSS Service (IGS).

The new dome is located on the right side of the residential building. It houses the ZIMLAT. A closer view of the ZIMLAT is shown in Figure 2.21. It is an alt-azimuth mounted Ritchey-Chrétien telescope with an aperture of 1 meter. It can be equipped with up to three CCD cameras. Currently, only one camera with 2048×2048 pixels is installed. The FOV for this camera is $0.39 \times 0.39^\circ$. Some of the observations used for this work were acquired with another camera, which has only 1024×1024 pixels and a FOV of $0.35 \times 0.35^\circ$. The limiting magnitude of the instrument is 18 – 19 magnitude for a 2 second exposure and under ideal conditions ([Flohner *et al.*, 2005b]). Satellite Laser Ranging (SLR) observations are also performed with the ZIMLAT. The system can automatically switch between CCD and SLR observations.



Figure 2.20: The Zimmerwald observatory.

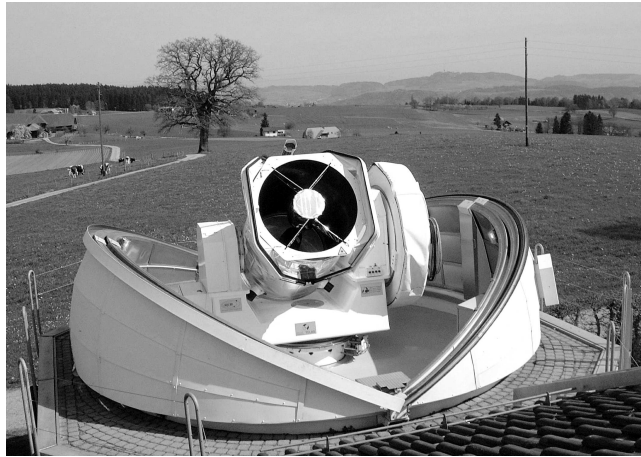


Figure 2.21: The Zimmerwald Laser and Astrometry Telescope (ZIMLAT).

2.3.2 ESASDT

The ESA Space Debris telescope is installed in the Optical Ground Station (OGS) at the Teide Observatory (OT) on Tenerife, Canary Islands. A description of the observatory can be found on [OT, 2006]. The observatory is located on the top of mount Izaña at an altitude of 2 393 m, about 20 km northeast from the Teide mountain. It consists of several solar and optical telescopes, and other instruments. An image of the OGS is shown in Figure 2.22. The mountain in the background is the Teide volcano, the highest mountain of Spain and the third largest volcano on Earth.

The ESASDT is a Ritchey-Chrétien telescope on an English mount with an aperture of 1 meter. Figure 2.23 shows a front view of the telescope. The telescope is owned by ESA and was originally established in the context of the Artemis spacecraft ([ARTEMIS, 2006]). Today, the observation time is shared between the Artemis project, the search for space debris, and other projects. Between 10 and 14 days are scheduled around every New Moon for the search for space debris. For optical observations, the



Figure 2.22: The optical ground station (OGS) on Tenerife. The Teide volcano is visible in the background.

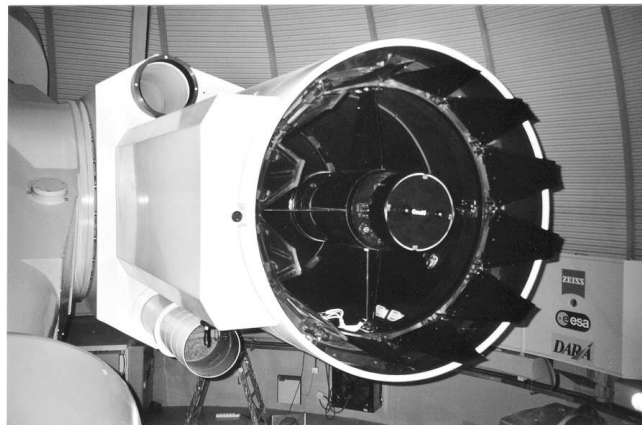


Figure 2.23: The ESA Space Debris Telescope (ESASDT), front view.

telescope is equipped with a CCD camera. The camera consists of a mosaic of four CCD chips with 2048×2048 pixels each. The FOV of the instrument is $0.71 \times 0.71^\circ$. The CCD camera can be seen at the rear end of the tube in Figure 2.24, showing a side view of the telescope. The limiting magnitude for a 2 second exposure is 19 – 20 magnitude.



Figure 2.24: The ESA Space Debris Telescope (ESASDT), side view.

3. Search Surveys for Debris

A first test campaign for the search of space debris in the GEO region was performed in 1999. Some statistics of this campaign are given in Table 3.1.

In the line “Obs. time”, the number of observation nights and the total observation time is given. The two rows below give the total scanned area and the number of acquired frames. The term “correlated” means that the detections or the objects could be identified, i.e., correlated, with an object from a catalogue. The DISCOS database was used for the correlation procedure. Thus, “uncorrelated” means that no identification was possible. “Detections” denotes an observation track of an object observed within a single observation series of frames of the same field on the sky. A single object could be detected several times during the surveys or even during one night. The number of observed “objects” is therefore smaller than the number of “detections”. All detections which were correlated with the same object belong to one object under the term “correlated objects”.

Several surveys of the GEO and GTO populations have been performed with the ESASDT. The search strategy is similar for the two types of surveys. In both cases, the telescope is tracking the objects during the exposure with its expected motion. For GEO objects, this simply means that the telescope tracking is stopped. The search strategy for GTO objects was optimized to detect them near the apogee. For GTO objects with low inclination the geocentric apparent apogee velocities are almost perfectly aligned along lines of constant declination. The difference to the GEO surveys is therefore a tracking in right ascension during the exposure. Two apparent velocities were selected for the surveys, one requiring a $7.5''/s$ tracking and one with $10.5''/s$ tracking.

Between 10 and 14 days were scheduled for a survey campaign. To get ideal observation conditions, the campaigns were scheduled around New Moon. During these campaigns, a multitude of debris objects have been detected (see [Schildknecht *et al.*, 2003] or [Schildknecht *et al.*, 2005b]). Table 3.2 gives some statistics of the surveys performed until December 2004.

The two lines “Optimized for GEO” and “Optimized for GTO” give the number of observation hours used for GEO or GTO surveys, while the row “Follow-ups” gives the observation time used for follow-up observations. Other than for the test campaign, the number of uncorrelated objects has not been determined for these campaigns.

The exposure time for each frame was 2 seconds. The time interval between two consecutive frames of the same field was 1 minute. An object normally appears on 2 – 4 consecutive frames, giving an arc length of 1 – 3 minutes. Because of the shortness of the observation arc only circular orbits could be determined. A circular orbit is a good approximation for most GEO objects. For elliptical orbits as the GTO, however, the fixed eccentricity will lead to large biases in the determined elements.

Statistical results for the GEO and the GTO surveys from 2002 are presented in the following two sections. Note that the “detections” and not the “objects” were analyzed. The GEO surveys until March 2002 are described in detail in [Schildknecht *et al.*, 2004a]. The results are biased as only part of the

Table 3.1: The ESA debris test campaign.

| | Aug-Sep 1999 |
|-------------------------|----------------------|
| Obs. time | 13 nights / 49 h |
| Scanned area | 895 deg ² |
| Frames | 5 400 |
| Correlated detections | 180 |
| Correlated objects | 56 |
| Uncorrelated detections | 348 |
| Uncorrelated objects | 150 |

Table 3.2: The ESA debris campaigns.

| | Jan-Jul 2001 | Jan-Dec 2002 | Jan-Dec 2003 | Jan-Dec 2004 |
|-------------------------|-------------------------|-------------------------|-------------------------|------------------------|
| Obs. time | 82 nights / 548 h | 96 nights / 691 h | 88 nights / 559 h | 70 nights / 417 h |
| Optimized for GEO | 548 h | 421 h | 211 h | 189 h |
| Optimized for GTO | | 200 h | 245 h | 145 h |
| Follow-ups | | 71 h | 103 h | 93 h |
| Scanned area | 11 200 deg ² | 13 700 deg ² | 10 600 deg ² | 7 800 deg ² |
| Frames | 65 000 | 81 800 | 66 000 | 49 500 |
| Correlated detections | 2 023 | 1 960 | 1 366 | 771 |
| Correlated objects | 364 | 404 | 374 | 311 |
| Uncorrelated detections | 1 300 | 2 394 | 2 350 | 1 814 |
| Uncorrelated objects | ? | ? | ? | ? |

populations could be observed and some parts more often than others.

3.1 GEO Survey

Figure 3.1 shows the distribution of the semi-major axes for the correlated and the uncorrelated detections for the results of the year 2002. Note that these are not the real semi-major axes of the orbits but the radii of the circular orbits determined from the detections. The range in the left plot is from 34 000 km to 50 000 km. The distribution of the correlated detections is very narrow and has its peak around 42 000 km, the radius of the GEO belt. The distribution is slightly asymmetric and broader for values larger than the GEO radius a_0 . Following the space debris mitigation guidelines of the Inter-Agency Space Debris Coordination Committee (IADC) some of the GEO satellites were manoeuvred to higher orbits at the end of their lifetime ([IADC, 2006]).

The distribution of the uncorrelated detections is much more expanded. The spreading is from 34 000 km to over 50 000 km. But it has to be kept in mind that this could be a result of the assumption of circular orbits, as will be shown in Section 3.1.1. Nevertheless, the peak is also around a_0 . The right plot of Figure 3.1 shows the distribution for the range between 46 000 km and 72 000 km. A semi-major axis larger than about 48 000 km was determined for only a few detections.

Figure 3.2 shows the distribution of the inclination. This figure clearly shows that the results are biased.

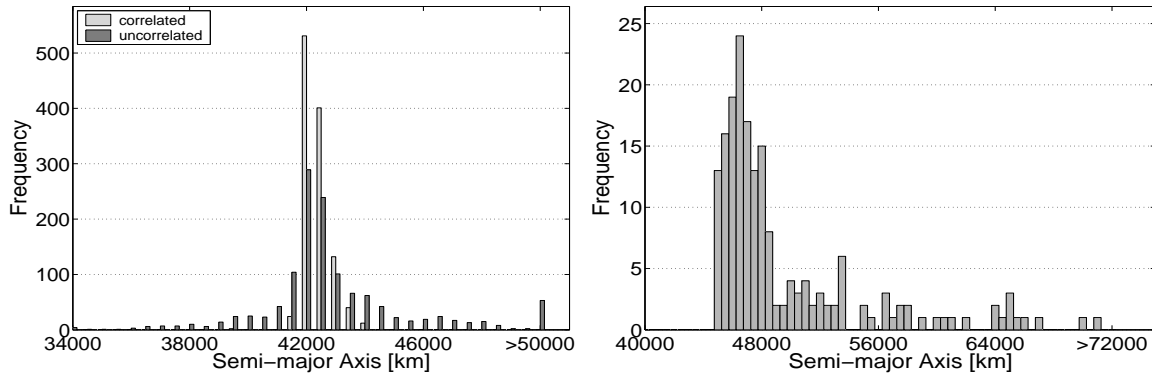


Figure 3.1: Distributions for different ranges of semi-major axis for the detections of the 2002 GEO surveys. The range is from 34 000 km to 50 000 km in the left plot, and from 46 000 km to 72 000 km in the right plot.

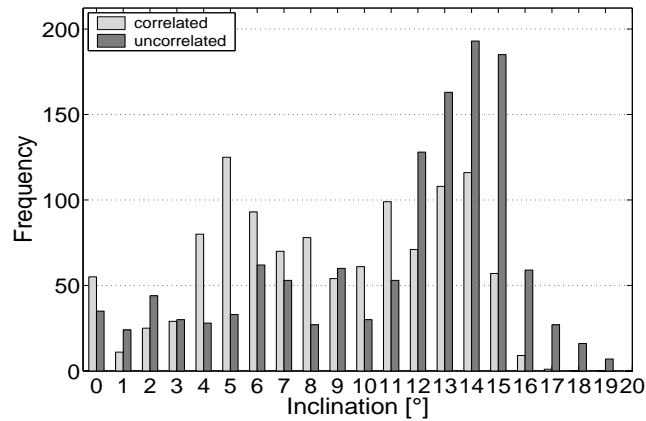


Figure 3.2: Distribution of inclination for the detections of the 2002 GEO surveys.

From Figure 2.13 we would expect a strong peak at 0° inclination. GEO objects with 0° inclination are detected in a field with 0° declination in geocentric coordinates. The declination of the fields observed during the 2002 surveys are mostly different from 0° . Nevertheless, for the correlated detections the distribution for larger inclinations mainly reflects the catalogue population.

The distribution of the uncorrelated detections is slightly different. The range is a little bit expanded compared to the correlated detections. Furthermore, the peak around $13^\circ - 15^\circ$ is larger than expected. The cause can be explained with Figure 3.3.

In Figure 3.3, the inclination i is plotted against the right ascension of the ascending node Ω . The left plot shows the correlated detections, while the uncorrelated detections are plotted on the right. The correlated detections nicely show the evolution of the orbital plane caused by the precession described in Section 2.2.1. This precession is also visible for the uncorrelated detections, but less prominent. The points for the uncorrelated detections are much more scattered than for the correlated. A possible explanation will be given in Section 3.1.1.

The right plot in Figure 3.3 also shows some unexpected concentrations of data points. Prominent are the

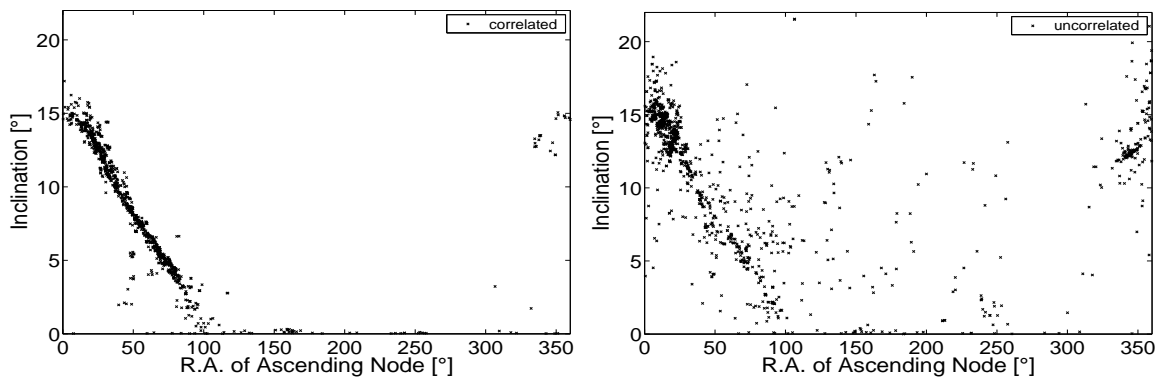


Figure 3.3: Inclination versus right ascension of ascending node for the correlated (left) and uncorrelated (right) detections of the 2002 GEO surveys.

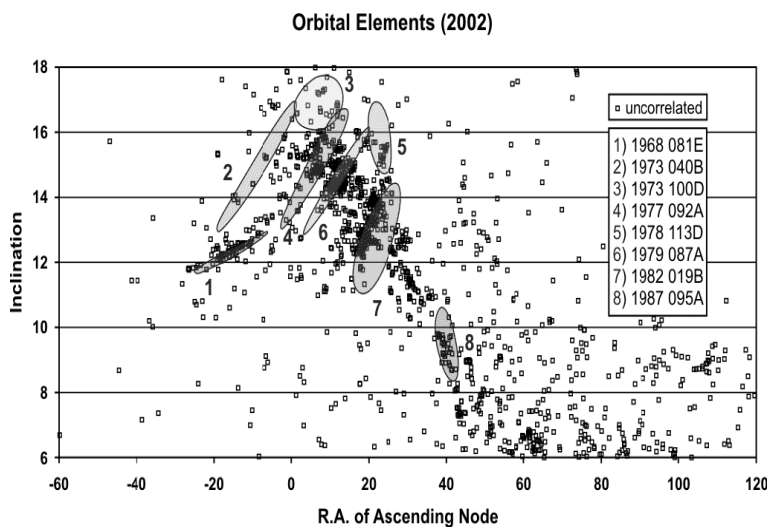


Figure 3.4: Comparison of the detections with modeled fragmentations of known breakup events (from [Grigoriev, 2005]).

concentrations, or “clouds”, at $(\Omega \approx 20^\circ, i \approx 13^\circ)$, $(\Omega \approx 15^\circ, i \approx 15^\circ)$, and $(\Omega \approx 345^\circ, i \approx 12.5^\circ)$, which explains the large peak in Figure 3.2. These “clouds” were analyzed in detail by [Musci, 2001] and also published in [Schildknecht et al., 2004a]. The analysis showed that at least some of the “clouds” are real and not an artefact of the assumption of circular orbits. Such “clouds” can result from explosions or other fragmentation events. [Grigoriev, 2005] showed that some of the “clouds” observed during the 2002 surveys might stem from known breakup events (see Figure 3.4). The plot shows the expected scattering in the (Ω, i) -diagram of the modeled fragmentation of 8 objects. Only two of these fragmentation events are confirmed, the other six are only suspected. Especially the correlation of the “cloud” at $(\Omega \approx 345^\circ, i \approx 12.5^\circ)$ with the modeled fragments of the confirmed fragmentation event of the Titan IIC Transtage (1968 081E) is remarkable. [Schildknecht et al., 2005b] also analyzed the evolution of the detected “clouds”. They follow the expected evolution in the (Ω, i) -diagram and change their shape.

The distribution of the magnitudes is shown in Figure 3.5. The distribution of the correlated detections

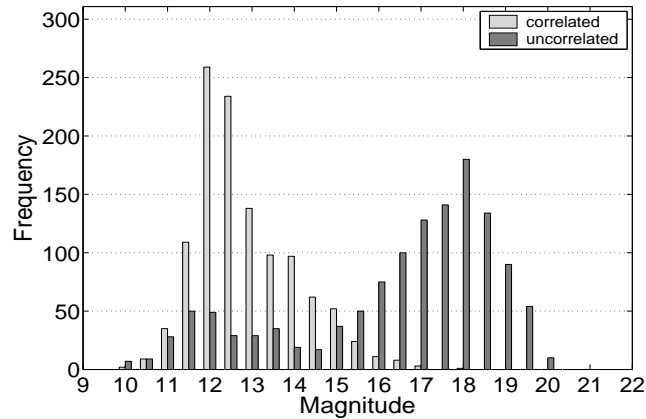


Figure 3.5: Distribution of magnitude for the detections of the 2002 GEO surveys.

has a prominent peak at about magnitude 12. The range is from magnitude 10 to 17. The main peak of the distribution of the uncorrelated detections is at about magnitude 18. A much smaller second peak is around magnitude 11.5 – 12. The range for the uncorrelated detections is from magnitude 10 to 20.

There are several reasons for uncorrelated bright detections. Some of the bright objects are classified and do not appear in the publicly available catalogues, like DISCOS. For some objects, the accuracies of the orbital elements in the catalogue are insufficient for a successful correlation. This is also the case if a maneuver took place after the catalogue was generated. In some cases, uncorrelated bright detections are observations of satellites from a clusters, e.g., the Astra satellites, which are located in the same 0.1° longitude slot. The result from the correlation procedure is that a detected object would correlate with several objects from the satellite cluster or that several detections from a group would correlate with the same object. In both cases the detection will remain “uncorrelated”, as no definite correlation could be made.

The magnitude of an objects is correlated with its size. Assuming a Lambertian sphere and a Bond albedo of 0.1, magnitude 16 corresponds to a diameter of 60 cm, while magnitude 20 corresponds to 10 cm. The detected bright objects have diameters of a few meters. It can be seen that many detections probably stem from objects smaller than 1 meter, the limiting size of the USSTRATCOM catalogue. This population of faint objects in GEO was unknown and unexpected when the search surveys with the ESASDT started in 1999.

The right boundary of the distribution does not reflect the real distribution of the faint objects but the sensitivity of the instrument. The sensitivity of the ESASDT was studied in [Musci, 2001]. The limiting magnitude for two second exposures with the ESASDT is around magnitude 19 – 20. The real distribution of objects fainter than about magnitude 18 therefore remains unknown.

The magnitude distribution depends on the inclination of the detected objects. This is shown in Figure 3.6, where the distribution of the magnitude is shown for different inclination ranges. Only very few faint objects with small inclinations were detected (upper left plot). This means that no recent fragmentation event of an object with a small inclination was discovered. The lower right plot shows that a large fraction of the detections from the “clouds” stem from faint and thus small objects. This is also an indication that these “clouds” are the result of fragmentation events.

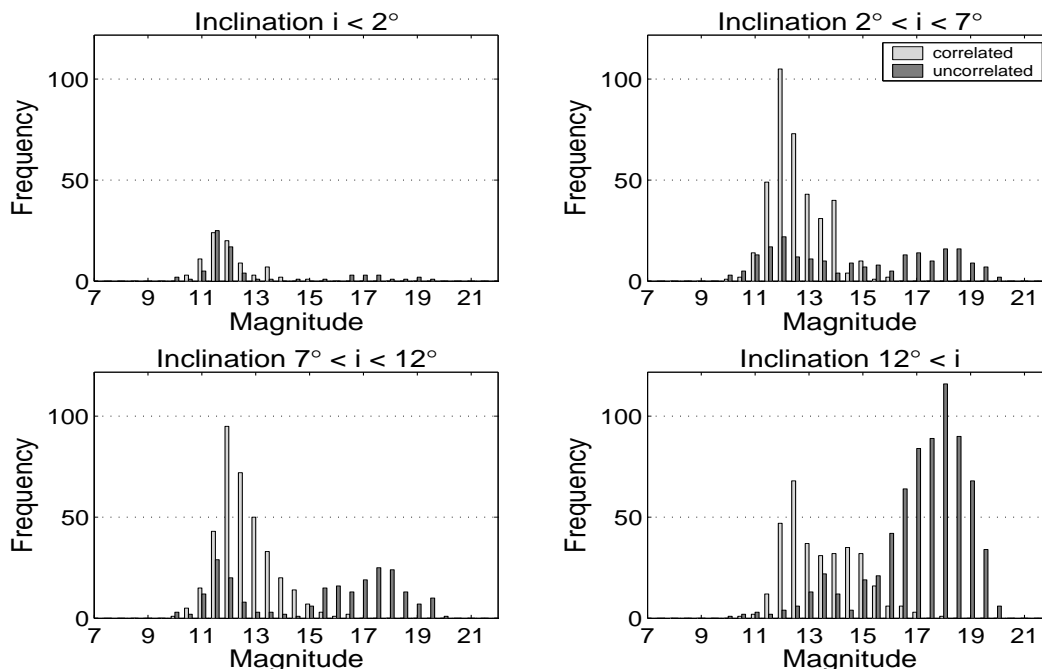


Figure 3.6: Distribution of magnitude for different inclination ranges for the detections of the 2002 GEO surveys.

3.1.1 Contamination by Elliptical Orbits

One limitation of the results emerges from the fact that circular orbits had to be inferred. This is a good approximation for GEO objects. But for objects with highly eccentric orbits we have to expect that the true orbital elements differ considerably from the inferred circular orbits. The “contamination” by elliptical orbits does in particular affect the distribution of semi-major axes and the orientation of the orbital planes, i.e., the inclination versus right ascension of ascending node distribution.

During a GEO survey objects with large eccentricities are normally detected when they are near the apogee. By inferring circular orbits for these detections we in fact interpret the change in the true anomaly near the apogee as the mean motion of a circular orbit ([Hugentobler, 1998]). The velocity of an object in an elliptical orbit at the apogee is slower than the corresponding velocity of an object on a circular orbit with a radius equal to the apogee radius of the former. This in turn means that the radius of the inferred circular orbit exceeds the apogee radius of the elliptical orbit. For an object observed at apogee in a geocentric system the semi-major axis a_{circ} of the inferred circular orbit is given by

$$a_{circ} = a \frac{1 + e}{(1 - e)^{1/3}}, \quad (3.1)$$

where a and e are the real semi-major axis and eccentricity ([Schildknecht *et al.*, 2005a]). For a GTO object with $a = 24\,500$ km and $e = 0.7$, i.e., with the apogee at the GEO belt, a radius of $a_{circ} \approx 62\,000$ km would result. If we take the parallax for the Tenerife site into account we get $a_{circ} \approx 63\,600$ km.

A dedicated survey of known GTO objects was performed in 2002. The objects were observed using the TLE from a catalogue. Not only the expected objects from the TLE catalogue were detected on the

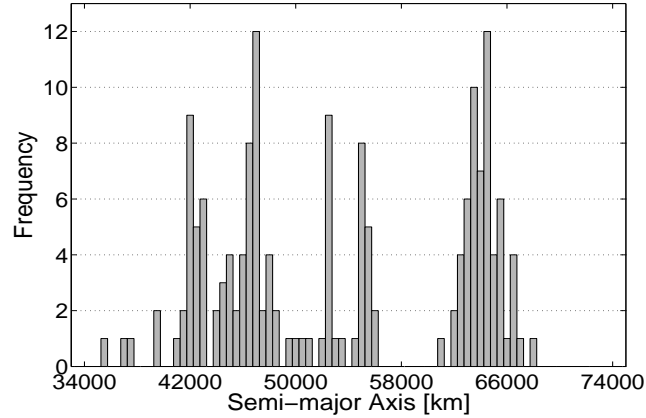


Figure 3.7: Distribution of semi-major axis for detections of GTO objects assuming circular orbits.

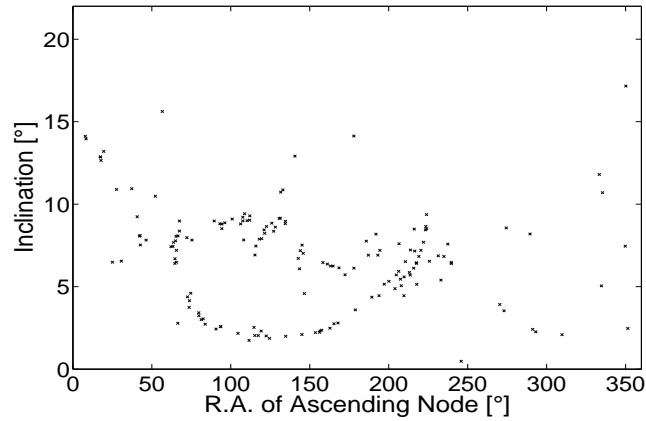


Figure 3.8: Inclination versus right ascension of ascending node for detections of GTO objects assuming circular orbits.

acquired series of frames, but also some other objects by coincidence. Circular orbits were determined for every detected object. Because the correlation with the catalogue was done on the basis of the position *and* the orbital elements the known GTO objects did not correlate. A histogram of the inferred semi-major axes, in fact radii of circular orbits, is shown in Figure 3.7.

Clearly visible are some peaks for the uncorrelated detections, e.g., at $a \approx 47\,000$ km and $a \approx 64\,000$ km. The latter are the values we expect for GTO objects observed close to the apogee. But also the other values greater than $a \approx 45\,000$ km may indicate that these orbits are elliptical in nature, as we do not expect many objects in circular orbits well above the GEO region.

If we plot the inclination i versus the right ascension of ascending node Ω some distinct structures are visible (Figure 3.8). Some of them stem from one object, which was observed multiple times. The one at inclination $5^\circ \leq i \leq 10^\circ$ and R.A. of ascending node $200^\circ \leq \Omega \leq 230^\circ$ stems from the object with the COSPAR number 97066C. The reason for these structures is that the objects were not always observed right at the apogee but in a range before and after the apogee.

This was tested with simulated observations of the GTO object 97066C. Observation tracks with an arc

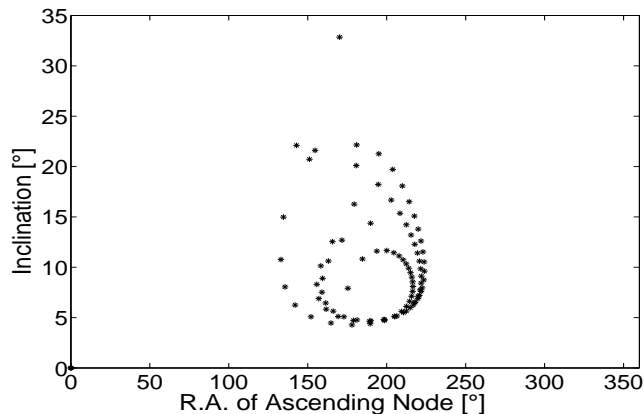


Figure 3.9: Inclination versus right ascension of ascending node for simulated detections with different observation epochs of a GTO object (97066C).

length of one minute were simulated for different epochs. In total, the simulated tracks span 3 orbital revolutions. Circular orbits were determined for each track. The (Ω, i) -diagram (Figure 3.9) shows a remarkable curved structure. The data points are closer together for observations near the apogee. The curved structures as they appear in Figure 3.8 can be sufficiently explained with this simulation.

The results from this dedicated survey illustrate how observations of objects with eccentric orbits may lead to biases in the semi-major axis distribution and the (Ω, i) -diagrams. The scattered data points in the right plot of Figure 3.3 might stem from detections of objects in elliptical orbits.

3.2 GTO Survey

Two survey scenarios were used to search for GTO objects, one with $7.5''/s$ tracking and one with $10.5''/s$ tracking. The merged results from the two scenarios are presented in this section. Figure 3.10 shows the distribution of the semi-major axes. The left diagram shows the range from 34 000 km to 50 000 km. The correlated detections are fairly dispersed around the GEO radius. But it has to be kept in mind that only objects with nearly circular orbits could be correlated as the elements of the determined circular orbits are parameters of the correlation procedure. Also the uncorrelated detections are concentrated around the GEO radius. But there are also many detections with large semi-major axes. The right plot in Figure 3.10 shows the distribution of the semi-major axes from 46 000 km to 72 000 km. The distribution is steadily decreasing with large semi-major axes. From Figure 3.7 we would expect a peak at $a \approx 64\,000$ km. The GTO objects used to produce that plot were observed close to the apogee. But the GTO objects observed within a survey do not have to be detected close to the apogee. When they are detected at a lower altitude, the inferred circular orbit is also smaller. Compared to the right plot of Figure 3.1 the fraction of large semi-major axes is clearly larger.

Many GEO objects have been detected during the GTO surveys. This is caused by the observation strategy, which was optimized to detect the GTO objects at their apogee. Thus, the distance to the object is approximately the same for GTO and GEO object.

The distribution of the inclinations (Figure 3.11) shows that many detections have very small inclina-

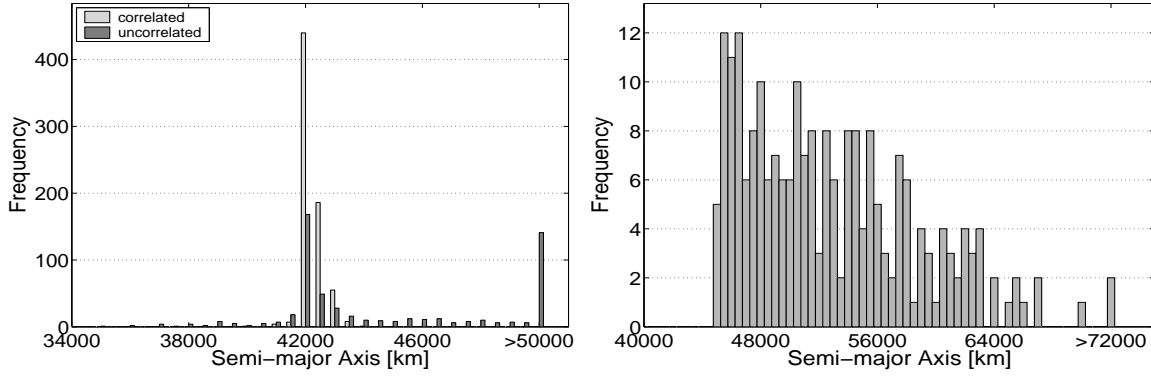


Figure 3.10: Distributions for different ranges of semi-major axis for the detections of the 2002 GTO surveys. The range is from 34 000 km to 50 000 km in the left plot, and from 46 000 km to 72 000 km in the right plot.

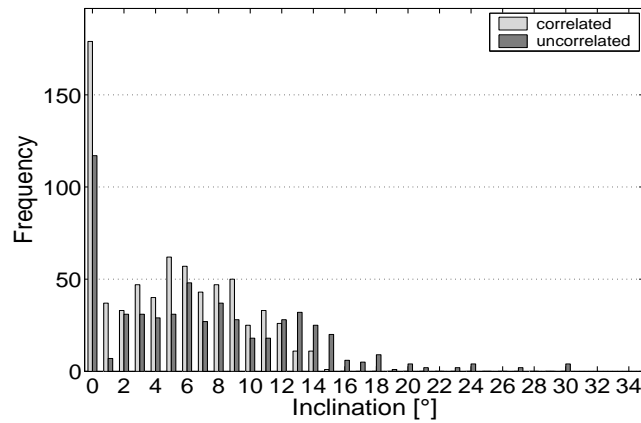


Figure 3.11: Distribution of inclination for the detections of the 2002 GTO surveys.

tions, i.e., these objects are most likely controlled. The reason is that more fields with a declination close to 0° were observed. Various detections of objects from satellite clusters led to a large number of uncorrelated detections of controlled objects. The distribution for higher inclinations seems to reflect more the distribution of the catalogued GEO objects (Figure 2.13) than the one of the GTO objects (Figure 2.19). Only a few objects with inclinations higher than 15° were detected. But the distribution is probably biased as only circular orbits were determined.

The (Ω, i) -diagrams for the correlated (left) and the uncorrelated (right) detections are shown in Figure 3.12. The left diagram looks very much the same as the left diagram in Figure 3.3. The major difference is that more objects with very small inclinations were detected during the GTO surveys. This is again due to the fact that more fields with declinations around 0° were observed.

The data points in the right diagram are very scattered, even more than in the right diagram in Figure 3.3. Only a few points follow the line from $(\Omega \approx 100^\circ, i = 0^\circ)$ to $(\Omega = 0^\circ, i \approx 15^\circ)$ caused by the precession. There are no such “clouds” visible as in Figure 3.3, but also no prominent curved lines as we would expect from multiple detections of the highly eccentric objects. However, we do not have to expect

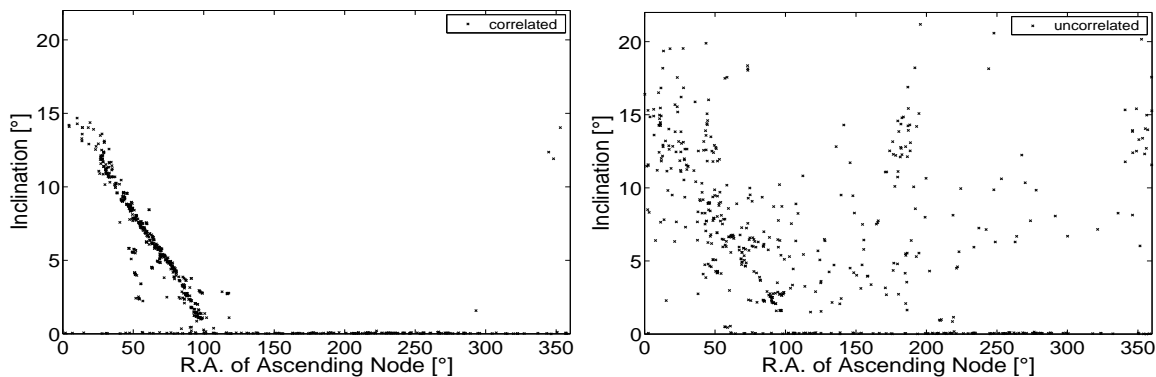


Figure 3.12: Inclination versus right ascension of ascending node for the correlated (left) and uncorrelated (right) detections of the 2002 GTO surveys.

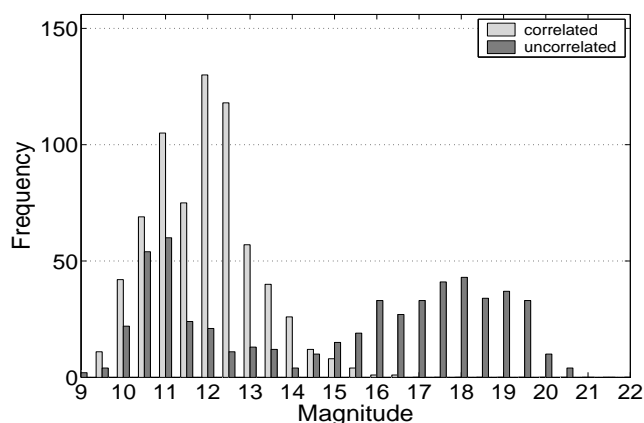


Figure 3.13: Distribution of magnitude for the detections of the 2002 GTO surveys.

multiple detections for many GTO objects as the variation of the revolution times of GTO objects is large and no survey strategy was applied that guarantees a re-observation of GTO objects within several nights.

The magnitude distribution in Figure 3.13 shows nearly the same bimodal distribution as in Figure 3.5. A large number of uncorrelated detections stem from bright objects. Most of them are controlled objects from satellite clusters. Many small objects have been detected, but the fraction of detections of faint objects is smaller than in the GEO survey. The reason is probably that no such “clouds” of faint objects have been observed.

This theory is underlined by comparing Figure 3.14 with Figure 3.6. The observed faint detections from the “clouds” reflect in a strong peak in the lower right plot in Figure 3.6. No such strong peak can be found for the faint detections from the GTO surveys. The upper left plot in Figure 3.14 confirms that many of the bright uncontrolled detections stem from controlled objects and probably from satellite clusters. Like in Figure 3.6 only very few faint objects with an inclination close to 0° have been detected during the GTO surveys.

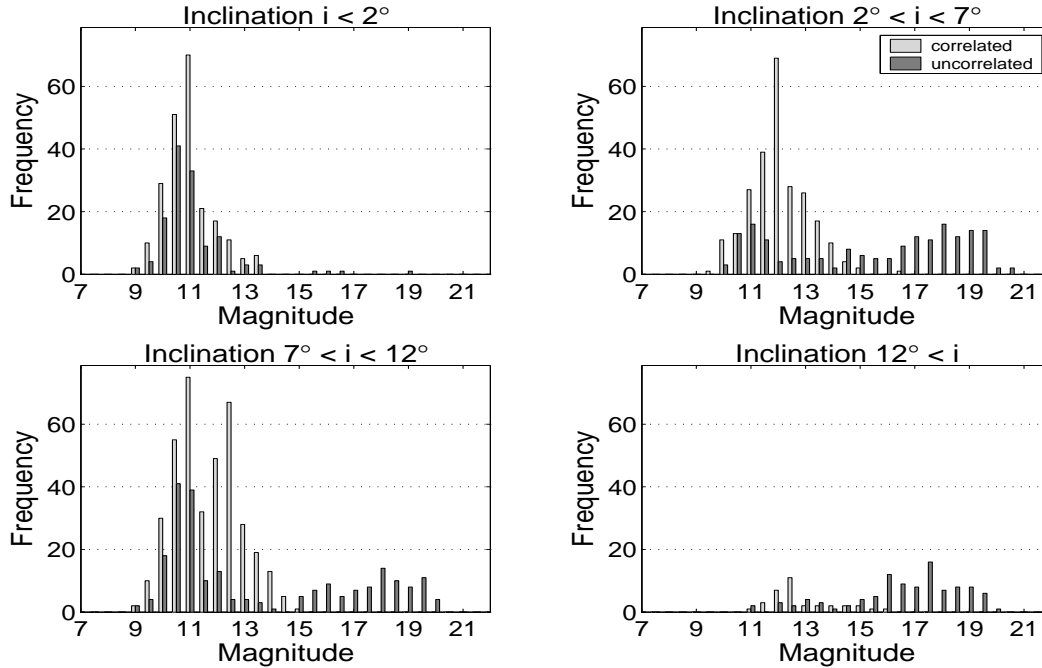


Figure 3.14: Distribution of magnitude for different inclination ranges for the detections of the 2002 GTO surveys.

3.2.1 Objects With Follow-up Observations

Follow-up observations (also just called “follow-ups”) were performed for part of the detected objects. Follow-up means that the orbit determined from the detection observations of an object was used to re-observe the object. During the GEO and GTO surveys, the determined circular orbits were used to acquire the follow-ups. As these orbits are not very accurate the follow-up observations had to be performed after a short time, i.e., after about 15 – 30 minutes. If the follow-up is successful the orbit determined from its observations can be used to acquire another follow-up of the object. This way, several follow-ups of a detected object can be acquired within an observation night.

The follow-up observations of an object from one night together with the observations of the first detection can be used to determine improved orbits, i.e., to determine all six orbital elements. This, of course, is of special interest for objects in eccentric orbits, like the GTO objects. If the new orbit is accurate enough it can even be used to perform a follow-up during the following night.

Elliptical orbits were determined for 387 objects until the end of the April 2005 survey. Figure 3.15 shows the distribution of the arc length for these objects. A strong peak is visible at 1 hour, i.e., the arc length for the majority of the objects is quite short. Only one or two follow-ups during the night of the first detection were acquired for these objects. The determined orbits for these objects are not very accurate. Nevertheless, the orbits are good enough to compare them with the orbits of the objects from a catalogue. Other group of objects are concentrated around 24 h and 48 h. No objects have an arc length around 12 h or 36 h. These gaps are of course caused by daytime, when no optical observations are possible. For a large number of objects an observation arc of more than 60 h is available. The orbits determined for these objects are very accurate.

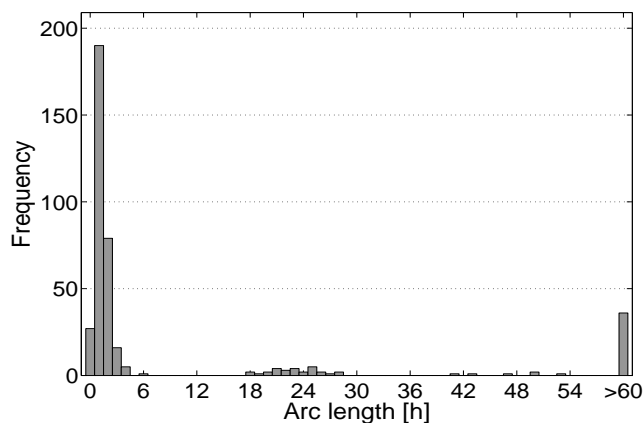


Figure 3.15: Distribution of arc length for objects, which were observed multiple times.

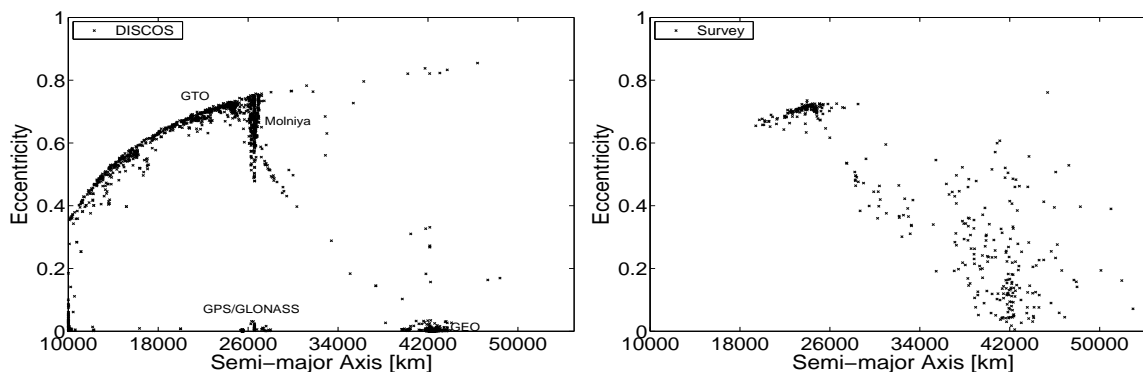


Figure 3.16: Eccentricity versus semi-major axis for objects from the DISCOS database (left) and for objects, which were observed multiple times (right).

A comparison of the elements from the 387 determined elliptical orbits with the elements of objects from the DISCOS database is shown in Figure 3.16 and Figure 3.17. In Figure 3.16, the eccentricity e is plotted against the semi-major axis a . The left plot shows the data points for the objects from the DISCOS database. The GEO and the GTO populations, as well as the navigation satellites (GPS/GLONASS) and Molniya type objects are labeled. The objects from the surveys are plotted in the right diagram. It can be seen that many GTO objects have been observed. They are concentrated around $a \approx 25\,000$ km and $e \approx 0.7$. Also some objects with the apogee at GEO but smaller eccentricities than nominal GTO objects have been detected (line from $(a \approx 25\,000$ km, $e \approx 0.7)$ to $(a \approx 29\,000$ km, $e \approx 0.4)$).

But there is also a previously unknown and unexpected group of objects visible with a semi-major axis close to the GEO radius and eccentricities up to 0.6! The existence of this type of objects was first published by [Schildknecht *et al.*, 2003]. Since then, several attempts to explain the large eccentricities have been made. [Liou and Weaver, 2004] first suggested that the large eccentricities are caused by perturbations due to the solar radiation pressure, which increase with increasing area-to-mass ratio (A/M). To reach an eccentricity of 0.6, the A/M has to be as high as $20\text{ m}^2/\text{kg}$. For comparison, a GPS satellite has a A/M of $\approx 0.02\text{ m}^2/\text{kg}$ and an ordinary writing paper $\approx 10\text{ m}^2/\text{kg}$. Thermal blankets, or Multi-Layer Insulations are materials with A/M of about $20\text{ m}^2/\text{kg}$. More detailed theoretical analyses of the orbital

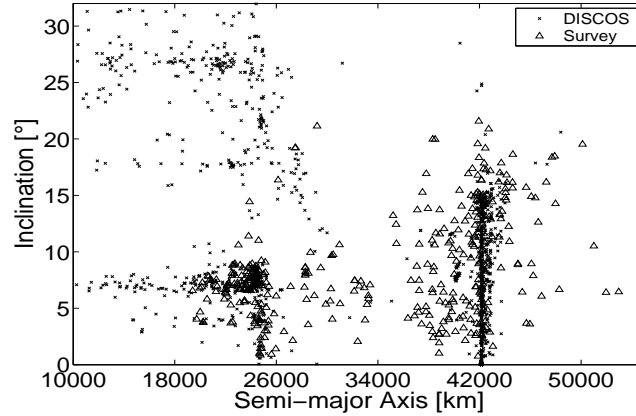


Figure 3.17: Inclination versus semi-major axis for objects, which were observed multiple times (Δ), compared to the objects from the DISCOS database (\times).

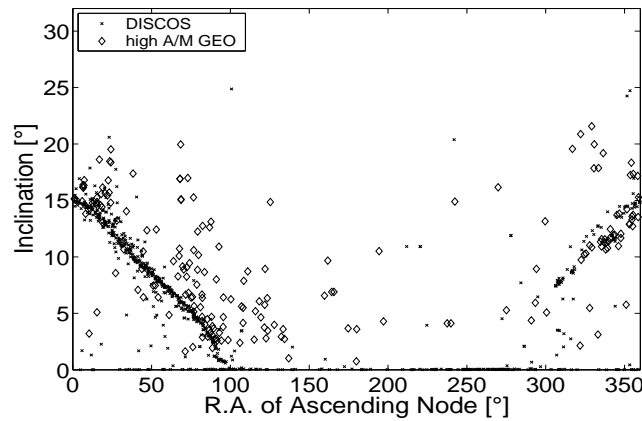


Figure 3.18: Inclination versus right ascension of ascending node for observed high A/M GEO objects (\diamond) compared to the objects from the DISCOS database (\times).

evolution of GEO objects with high A/M can be found in [Anselmo and Pardini, 2005] and [Liou and Weaver, 2005]. A first successful test of this theory was presented by [Schildknecht et al., 2005b], using observations from the ESASDT and the ZIMLAT.

In Figure 3.17, the inclination i of the determined elliptical orbits (Δ) and from the DISCOS database (\times) is plotted against the semi-major axis a . Most of the observed GTO objects have an inclination of about 7° , i.e., they stem from launches from Kourou, French Guiana. The inclinations of the high A/M GEO objects reach up to over 20° .

Figure 3.18 shows the (Ω, i) -diagram for the observed high A/M GEO objects compared to the GEO objects from the DISCOS database. The high A/M GEO objects show similar “clouds” like the detections of the GEO surveys (Figure 3.3). Two “clouds” also are located at $(\Omega \approx 15^\circ, i \approx 15^\circ)$ and $(\Omega \approx 345^\circ, i \approx 12^\circ)$. Assuming that these two “clouds” stem from fragmentation events we can conclude that fragmentation events can cause debris objects with high A/M. This aspect has to be considered in the modeling of the space debris population and also for the space debris mitigation guidelines.

4. Identification of Multiple Detections

A large amount of objects have been observed within the search surveys for GEO and GTO objects. As circular orbits were determined, only the detections of some of the GEO objects could be correlated with objects from the DISCOS catalogue. As a name is clearly defined for these detections it can be exactly determined how many different objects have been observed and how frequently they have been detected. For the other objects, however, multiple detections of the same object cannot so easily be identified as each detection has a different name. In this case, some other way has to be found to correlate the detections with each other. Again, detection denotes an observation track observed within a single observation series of frames of the same field.

The most promising way to identify multiple detections of an object, which could not be correlated with a catalogue, is to determine an orbit using the observations from each combination of detections. But this approach is very time consuming. It is therefore recommended to make a preselection of detections which might belong together. One possibility to do this is to compare the orbits. The differences between the orbital elements have to be within a given range to be accepted as candidates. But the problem with this type of preselection is, that only circular orbits could be determined from the observation tracks. This makes it almost impossible to find a pair of GTO detections that might belong together. The described method is only successful for detections of GEO objects. But also other methods, e.g., propagating the orbit of one track to the epoch of a second track, might fail for GTO detections because the accuracy of the orbits is not sufficient. Therefore, the method of comparing the orbits was followed to make a preselection. The method is implemented in the tool CAMRES (CAMpaign RESults), which was developed to extract the results from the survey campaigns. One result is a list of all detections that are possibly from an identical object. The tool is described in Section 4.1.

As mentioned in Chapter 3, follow-up observations of part of the detections have been performed. In this case it is predefined which detections might stem from an identical object. The result of a short series of follow-up observations is a small number of detections. Only this sample has to be tested for a correlation with the firstly detected object. The CAMRES tool also searches for follow-ups of previous detections and lists them in an output file. A detection, for which a follow-up is performed, is called “progenitor” of the follow-up detections within this work.

The two output lists, one for the possibly identical detections and one for the follow-ups, are used to determine orbits for each combination of the selected detections. It can be decided on the basis of the accuracy of the determined orbits if the detections belong to the same object or not. This correlation can be performed by the tool CAMCOR (CAMpaign CORrelation), which is described in Section 4.2.

Table 4.1: Delta-values used for the comparison within the tool CAMRES.

| | | |
|-----------------|-----|----------|
| Δa | $=$ | 1 000 km |
| Δi | $=$ | 0.10° |
| $\Delta \Omega$ | $=$ | 0.75° |

4.1 The CAMRES Tool

The CAMRES tool is used to extract the final results from the processing of the search surveys performed with the ESASDT. The tool was firstly described in [Musci, 2001]. A short description is repeated here, including the details that are important for this work.

The main functions of the tool are visualized in the flowchart in Figure 4.1. The observation nights that should be processed are selected in the first step. These are preferably all the nights from one survey campaign, usually about 10 – 14 nights (see Chapter 3). The observation nights are searched for detected objects, their orbits, positions, and magnitudes. Some files are created in the following (ELF-file, IDE-file, ELE-file, and FDS-file) that are used to statistically analyze the observed tracks and to generate plots like the ones in Chapter 3. These files will not be further described here.

The interesting part of the tool starts with the function “Compare orbital elements of detections”. As only circular orbits are determined, the elements e and ω are not compared. In addition, the perigee passing time T_0 is also not compared. The orbit of each detection is compared with the one of every other detection. If the difference between all three selected orbital elements is below the delta-values given in Table 4.1 the two detections are identified as possibly correlated. If one or both of the two detections has already been identified as possibly correlated to other detections, then all those detections are declared as possibly correlated. At the end several groups with various numbers of detections result and their names and orbital elements are written into the PIO-file. This file is used by the tool CAMCOR to perform a final correlation between the detections in the groups.

The next step is the search for identical object names. This applies only to the detections of those objects that could be correlated with an object from the DISCOS catalogue. The orbits of the detections that belong to the same object from the catalogue are compared and the differences written into the PCO-file.

Finally, it is checked for every detection if a series of follow-up observations was acquired within the same observation night. If this is the case, then the follow-up series is searched for detections and the name and the orbital elements of all detections, the progenitor and the detections from the follow-up, are stored in the FUP-file. This type of file can also be used as input for the CAMCOR tool. The tool is then used to determine if one of the follow-up detections belongs to the progenitor. During the observation campaigns, the observers also perform further follow-up observations of successful follow-ups. Between two and three follow-ups are normally performed for GEO objects, whereas up to six follow-ups are acquired for GTO objects during the night of the discovery. The CAMRES tool does not connect the whole series of follow-up detections but only a follow-up to its progenitor. This means that a progenitor can also be a follow-up from another detection.

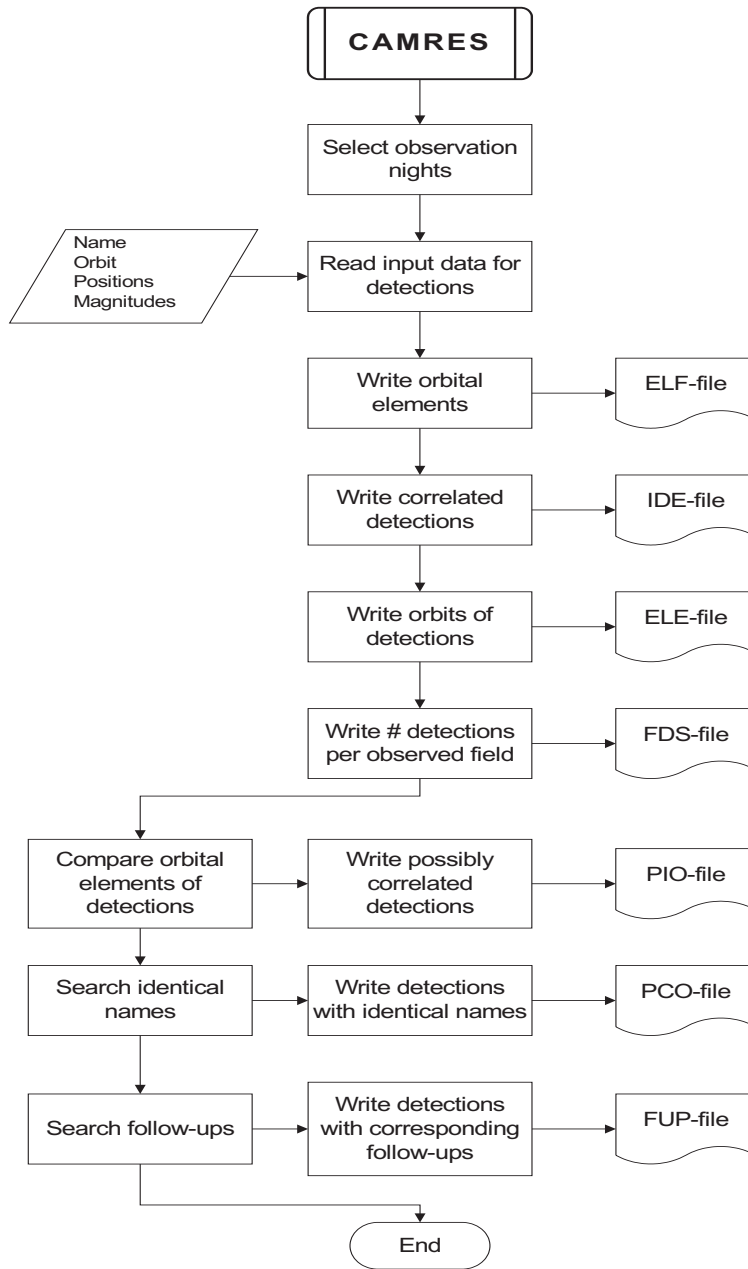


Figure 4.1: Flowchart of the CAMRES tool.

4.2 The CAMCOR Tool

The CAMCOR tool is used to make a final correlation between the detections. The correlation process is based on the comparison of the RMS of the residuals of the determined elliptical orbits. Either a PIO-file or a FUP-file can be used as input. Both files contain groups of detections that are somehow connected. In the case of the PIO-file, this connection is done by comparing three orbital elements of the circular orbits. For the FUP-file, the connection is defined by the observation sequence of the night. For both input files, the CAMCOR tool searches for correlations between the detections of a group. A flowchart of the tool is given in Figure 4.2.

First, the groups of detections are read from the input file. From these detections, only those that could not be correlated with an object from the catalogue are selected. This is not only done because the others could already be correlated to a known object, but also because the tool can currently not get the necessary data from other files for the correlated detections.

The next step is the big loop over all groups, i.d. each group of detections is treated separately in the main part of the tool. It follows another small loop where the necessary data (right ascension and declination of the observations, the corresponding epochs, and the station name of the instrument that performed the observation) for each detection is read from various files. This data is used to generate the observations file (OBS-file).

From this point on, the processing depends on the type of the input file. It is simpler for the FUP-file. For every follow-up detection in the group the OBS-file is merged with the OBS-file from the progenitor and stored in a new OBS-file. This new file is used to determine an elliptical orbit, i.e., all six orbital elements. After a new orbit is determined for every combination of follow-up detection and progenitor, the orbit with the smallest RMS of the residuals is searched. If this RMS is smaller than two arcseconds the follow-up detection is correlated with the progenitor. The corresponding elliptical orbit will be tried to correlate with the objects from the DISCOS catalogue. Finally, an entry summarizing the results is written to an output file and the next group is processed.

The processing for the PIO-file is similar, but extended compared to the processing of the FUP-file. The OBS-file of the first detection in the group is merged with the one of the second detection. An elliptical orbit is determined using the new OBS-file. If the RMS is smaller than $2''$ the second detection is correlated with the first. From here on the new OBS-file will be selected as the OBS-file of the first detection, i.e., the first detection is now a combination of the observations of the former first detection with those of the second detection. The second detection will not be used for further comparison with other detections. The new orbit is also correlated with the catalogue. Afterwards, the new OBS-file of the first detection is merged with the one from the third detection. For those combinations where the RMS is larger than $2''$ it is checked if it is at least smaller than $5''$. If this is true, the two detections are marked as possibly correlated. This procedure is continued until an orbit is determined for all possible combinations of detections. The detections are then searched for all detections that are possibly correlated to it. The result will be some groups of possibly correlated detections. For all those groups the OBS-files of the detections are merged and used to determine an improved orbit using a more sophisticated force model than before. This step is necessary as the total observation arc of the possibly correlated detections can be quite long, up to two weeks when a survey campaign is processed. The better force model can lead to an orbit that is accurate enough to accept the involved detections as the same object. An entry to the output file is written and the next group of possibly identical detections is processed.

All combinations of detections and the corresponding RMS resulting from the orbit determination are

listed in the output file. Further, it is noted which detections were correlated with another object and if the resulting orbit could also be correlated with an object from the catalogue. At the end, a short summary is written, which can be used for statistical analysis as in the following Section 4.3. The summary includes the number of processed groups, the total number of detections related to the groups, the number of detections that were correlated to another detection, the number of possible correlations ($\text{RMS} < 5''$) and the number of combined detections that could be correlated with the catalogue. For the follow-ups the percentage of the cases where one of the detected follow-ups could be correlated with the progenitor is also determined. Note that this will give no information on the percentage of successful follow-ups as those follow-up series where no object at all was detected are not included.

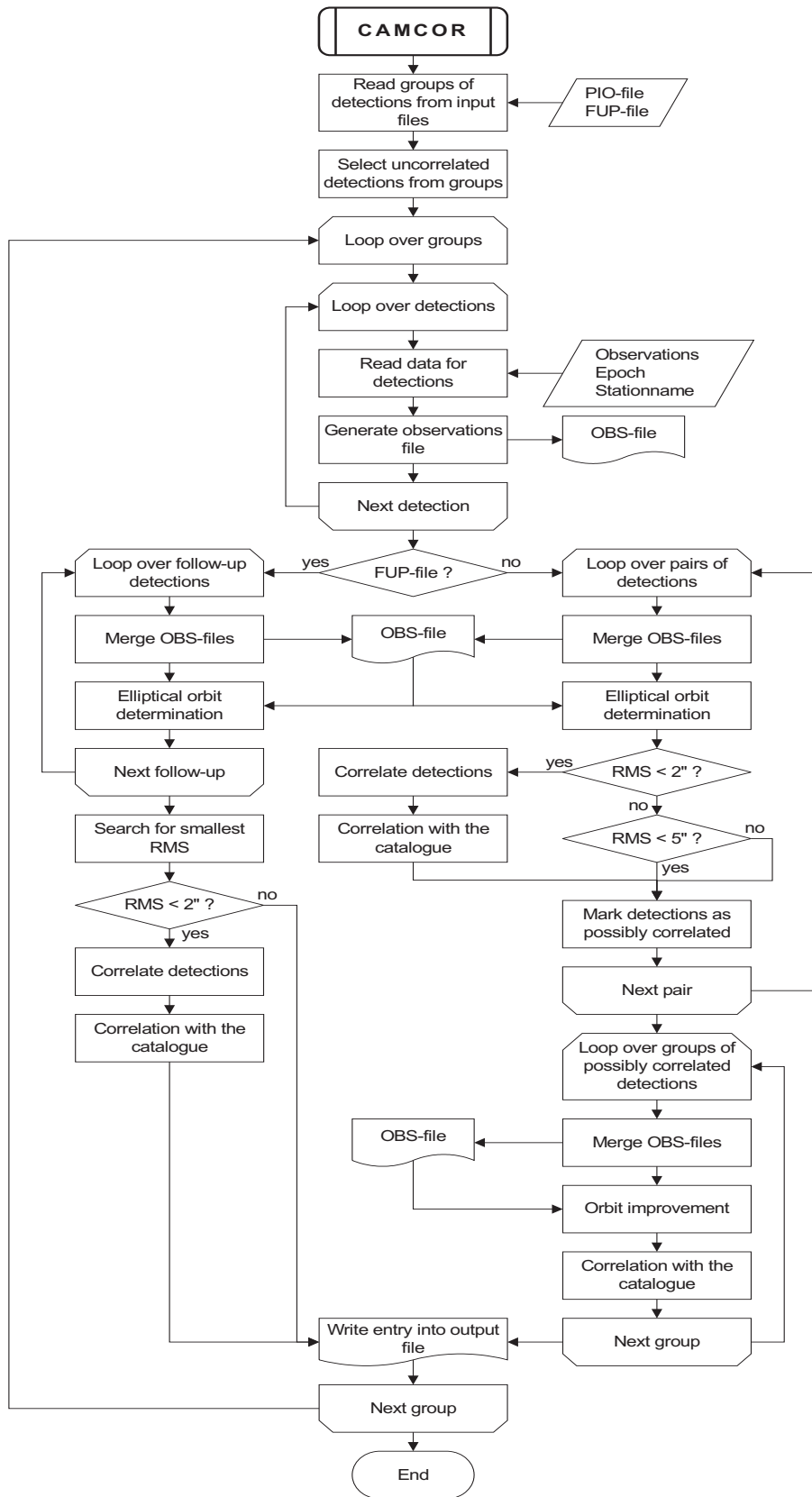


Figure 4.2: Flowchart of the CAMCOR tool.

4.3 Results

All observation campaigns from February 2001 to December 2004 were processed with the CAMRES and the CAMCOR tool. Both types of files, PIO-file and FUP-file, were used as input for the CAMCOR tool.

Let us first look at the results for the FUP-files. The results for the different monthly campaigns are shown in Table 4.2. Four campaigns are not listed (2001/02, 2001/02, 2003/02, and 2003/09) as no follow-ups of newly detected objects were acquired during these campaigns. The left most column shows the names of the campaigns. The name is generated from the year and the month during which the New Moon occurred. Two New Moons were visible in May 2003, that is why one of the campaigns is named 2003/05 b. The row at the bottom gives the totals of each of the other columns.

The column “Follow-ups” lists the number of follow-up observation series that were considered. “Detections” gives the number of detections within these series. It can be seen that this number is larger than the one in “Follow-ups”. This shows that more than one object was detected in some follow-up series. The number of detections that could be correlated with its progenitor is listed in “Correlations”. If this number is equal to the number in “Follow-ups”, then every performed follow-up was successful. Also given is the number of possibly correlated detections (“possible Cor.”) with the weaker correlation criteria of $RMS < 5$ ”. These numbers are clearly smaller as in “Correlations”. This was expected as observations of the same object from one night normally result in a very accurate orbit, i.e. the detections can be correlated with each other. The column “Catalogued” gives the number of combined detections, which could be correlated with the DISCOS catalogue. Most of these detections are associated with GTO objects. The reason that only few combined detections could be correlated with GEO objects is that they could already be correlated on the basis of the circular orbit determined from the on-line processing during the observation night and that there is no interest in follow-ups of known GEO objects within the search campaigns. The success rate of the follow-ups is listed in the last column. A follow-up is not successful if at least one object could be detected within the follow-up observation series but none of these detections could be correlated with the progenitor. This means that these rates do not tell how many of the totally performed follow-ups were successful as those follow-ups where no object at all was detected are not included in the calculation.

The table shows that many successful follow-ups have been performed. The number of objects detected within the follow-up observation series is about one third of the totally uncorrelated detections (see Table 3.2).

The results for the PIO-files are shown in Table 4.3. The table is a little bit different from the one for the FUP-files. The column “Total Det.” lists the number of the total uncorrelated detections for each monthly campaign. The next column “GEO Det.” shows the number of uncorrelated detections that seem to be the detection of a GEO object. These detections were selected by the size of the determined semi-major axis, in fact the radius of the determined circular orbit, using the filter $40\,164\text{ km} < a < 44\,164\text{ km}$. The column “GEO Det.” was inserted as we only expect possibly identical detections for this type of objects. For the detections of other objects, like GTO objects, the inferred circular orbits change too fast to meet the correlation criteria. The possibly identical detections are listed in “pos. ident. Det.”. Except for 2004/06 all values are smaller than in “GEO Det.”, which is consistent with the statement that the majority of the possibly identical detections are supposed to be GEO objects.

The most interesting result are the “Correlations”. The values are clearly smaller than in “pos. ident. Det.”. But nevertheless, a lot of detections could be correlated with another detection. As almost all

Table 4.2: Successful follow-up observations for the campaigns from February 2001 to December 2004 resulting from the tool CAMCOR.

| Campaign | Follow-ups | Detections | Correlations | possible Cor. | Catalogued | Success rate |
|-----------|------------|------------|--------------|---------------|------------|--------------|
| 2001/04 | 2 | 2 | 2 | 0 | 0 | 100% |
| 2001/05 | 2 | 2 | 2 | 0 | 0 | 100% |
| 2001/06 | 21 | 26 | 16 | 1 | 0 | 76% |
| 2001/07 | 84 | 106 | 81 | 0 | 3 | 96% |
| 2001/12 | 1 | 1 | 1 | 0 | 0 | 100% |
| 2002/01 | 8 | 9 | 7 | 0 | 0 | 87% |
| 2002/02 | 20 | 25 | 12 | 8 | 0 | 60% |
| 2002/03 | 15 | 19 | 9 | 6 | 0 | 60% |
| 2002/06 | 18 | 19 | 17 | 1 | 2 | 94% |
| 2002/08 | 40 | 47 | 36 | 2 | 5 | 90% |
| 2002/09 | 73 | 84 | 68 | 2 | 7 | 93% |
| 2002/10 | 66 | 88 | 62 | 0 | 0 | 93% |
| 2002/11 | 49 | 61 | 44 | 1 | 7 | 89% |
| 2002/12 | 20 | 20 | 20 | 0 | 0 | 100% |
| 2003/03 | 27 | 32 | 24 | 1 | 2 | 88% |
| 2003/04 | 9 | 11 | 9 | 0 | 0 | 100% |
| 2003/05 | 44 | 49 | 38 | 0 | 2 | 86% |
| 2003/05 b | 55 | 71 | 53 | 0 | 4 | 96% |
| 2003/06 | 105 | 122 | 101 | 2 | 18 | 96% |
| 2003/07 | 131 | 169 | 129 | 0 | 21 | 98% |
| 2003/08 | 134 | 182 | 129 | 0 | 5 | 96% |
| 2003/10 | 23 | 28 | 22 | 0 | 1 | 95% |
| 2003/11 | 77 | 106 | 73 | 0 | 14 | 94% |
| 2003/12 | 30 | 39 | 29 | 0 | 3 | 96% |
| 2004/01 | 132 | 180 | 126 | 0 | 1 | 95% |
| 2004/02 | 18 | 27 | 16 | 0 | 0 | 88% |
| 2004/03 | 62 | 74 | 56 | 3 | 1 | 90% |
| 2004/04 | 3 | 3 | 3 | 0 | 0 | 100% |
| 2004/05 | 6 | 6 | 6 | 0 | 0 | 100% |
| 2004/06 | 76 | 93 | 72 | 1 | 11 | 94% |
| 2004/07 | 42 | 47 | 40 | 0 | 0 | 95% |
| 2004/09 | 13 | 18 | 13 | 0 | 0 | 100% |
| 2004/10 | 29 | 30 | 29 | 0 | 7 | 100% |
| 2004/11 | 38 | 44 | 38 | 0 | 10 | 100% |
| 2004/12 | 28 | 33 | 25 | 1 | 1 | 89% |
| Total | 1501 | 1873 | 1388 | 29 | 115 | 92% |

detections in the column “Correlations” are from GEO objects, we can determine the number of uncorrelated GEO objects, i.e., objects not correlated with the catalogue, by subtracting the number of correlations (total of column “Correlations”) from the number of uncorrelated GEO detections (total of

column “GEO Det.”). The result is 2 654 objects. The factor between the number of uncorrelated GEO detections and the number of uncorrelated GEO objects is 1.59. From Table 3.2 we determine an average ratio of 4.09 between the correlated detections and the correlated objects. For the ESA debris test campaign, the factor between the correlated detections and the correlated objects is 3.21, and between the uncorrelated detections and the uncorrelated objects 2.32. Note that all correlated detections and correlated objects that resulted for the surveys are GEO objects. The factor resulting from the PIO-files is clearly smaller than the others. The reason is that only the uncorrelated detections of the monthly campaigns were processed with the two tools CAMRES and CAMCOR, whereas the yearly data was analyzed to generate Table 3.2. It has to be assumed that many objects have been detected during several campaigns. The tools are useful to identify multiple detections for at least part of the uncorrelated objects.

Much more possible correlated detections resulted for the PIO-files than for the FUP-files. This was expected as the considered observation arcs are much longer. As a consequence, the orbit determination can result in a larger RMS. Nevertheless, the possible correlated detections should not be accepted as identical without further investigations. The chance for a detection of another object that cannot be screened out with the orbit determination is also rising with a longer observation arcs. Only very few combined detections could be correlated with an object from the DISCOS catalogue.

4.4 Conclusion

The two presented tools CAMRES and CAMCOR can be used to identify multiple detections of an object and to correlate follow-up detections with its progenitor. The identification of multiple detections is limited to GEO objects because only circular orbits are compared. Follow-up observations of every detected object would be needed to correlate multiple detections of GTO objects from surveys, as no correlation between the detections can be guaranteed. Currently, only follow-up observations of newly detected objects are processed by the CAMRES tool. The tool could be extended to follow-ups of objects, which were detected during previous nights or even campaigns.

The results also showed the limits of the two tools. They are not efficient enough to build up a catalogue, even for GEO objects. Another concept has to be developed to build up and maintain a catalogue. This concept can e.g., be based on follow-up observations.

Table 4.3: Identified multiple observations for the campaigns from February 2001 to December 2004 resulting from the tool CAMCOR.

| Campaign | Total Det. | GEO Det. | pos. ident. Det. | Correlations | possible Cor. | Catalogued |
|-----------|------------|----------|------------------|--------------|---------------|------------|
| 2001/02 | 221 | 162 | 100 | 29 | 7 | 1 |
| 2001/03 | 114 | 80 | 47 | 19 | 0 | 0 |
| 2001/04 | 217 | 173 | 108 | 36 | 7 | 2 |
| 2001/05 | 76 | 62 | 18 | 4 | 1 | 0 |
| 2001/06 | 264 | 210 | 163 | 54 | 23 | 1 |
| 2001/07 | 299 | 180 | 256 | 137 | 26 | 3 |
| 2001/12 | 9 | 6 | 2 | 1 | 0 | 0 |
| 2002/01 | 273 | 219 | 156 | 48 | 24 | 0 |
| 2002/02 | 262 | 196 | 132 | 37 | 31 | 0 |
| 2002/03 | 244 | 190 | 114 | 25 | 18 | 0 |
| 2002/06 | 178 | 81 | 59 | 17 | 9 | 0 |
| 2002/08 | 268 | 93 | 90 | 38 | 2 | 1 |
| 2002/09 | 310 | 107 | 100 | 38 | 5 | 1 |
| 2002/10 | 313 | 119 | 97 | 41 | 7 | 3 |
| 2002/11 | 413 | 247 | 190 | 73 | 8 | 13 |
| 2002/12 | 133 | 61 | 58 | 16 | 4 | 0 |
| 2003/02 | 48 | 22 | 19 | 4 | 0 | 0 |
| 2003/03 | 145 | 72 | 63 | 27 | 0 | 0 |
| 2003/04 | 96 | 48 | 22 | 6 | 0 | 0 |
| 2003/05 | 169 | 112 | 90 | 57 | 7 | 2 |
| 2003/05 b | 204 | 147 | 87 | 54 | 9 | 3 |
| 2003/06 | 299 | 124 | 117 | 76 | 6 | 2 |
| 2003/07 | 390 | 138 | 121 | 72 | 11 | 0 |
| 2003/08 | 499 | 266 | 223 | 140 | 20 | 4 |
| 2003/09 | 29 | 13 | 4 | 2 | 0 | 0 |
| 2003/10 | 109 | 54 | 33 | 23 | 0 | 0 |
| 2003/11 | 269 | 134 | 87 | 55 | 2 | 1 |
| 2003/12 | 93 | 39 | 30 | 20 | 0 | 0 |
| 2004/01 | 482 | 268 | 236 | 134 | 17 | 0 |
| 2004/02 | 62 | 45 | 28 | 17 | 0 | 0 |
| 2004/03 | 306 | 175 | 141 | 80 | 12 | 1 |
| 2004/04 | 45 | 25 | 12 | 7 | 0 | 0 |
| 2004/05 | 34 | 18 | 13 | 10 | 0 | 0 |
| 2004/06 | 281 | 85 | 88 | 52 | 5 | 0 |
| 2004/07 | 174 | 83 | 65 | 51 | 1 | 0 |
| 2004/09 | 131 | 48 | 23 | 11 | 2 | 0 |
| 2004/10 | 84 | 31 | 23 | 16 | 0 | 2 |
| 2004/11 | 100 | 29 | 27 | 16 | 0 | 1 |
| 2004/12 | 115 | 52 | 48 | 27 | 2 | 0 |
| Total | 7758 | 4224 | 3290 | 1570 | 266 | 41 |

5. Acquisition of a “Secured” Orbit

Currently, only the USSTRATCOM catalogue is, with restricted access, publicly available. A disadvantage of this catalogue is that it is limited to objects larger than about 1 m in diameter at GEO altitudes. A large number of objects smaller than 1 m have been detected during the performed GEO and GTO surveys. But only circular orbits were determined for most of the detected objects. Only a few objects are regularly observed and their orbits maintained.

Of course, it would be nice to have a catalogue not only of the large and bright objects but also of part of the small debris pieces. Furthermore, it would be interesting to have a catalogue independent from the USSTRATCOM catalogue. Both tasks require a good concept for the observations. First of all, the concept should lead to very accurate orbits. These orbits should allow to recover the objects after a few weeks or even months. Such orbits are also called “secured” orbits.

A concept for the acquisition of a “secured” orbit for GEO and GTO objects is presented in the following. Simulations were used in order to study the number of observations, their temporal spacing and the total arc length required to generate “secured” GEO and GTO orbits. A modified version of the Celestial Mechanics software system (CelMech) developed by Prof. Gerhard Beutler (published together with [Beutler, 2005]) was used to simulate the observations and for the orbit determination. A short description of CelMech is given in Appendix A. The models used within this chapter do not include air drag and only include a simple model for the direct radiation pressure. For longer arcs, however, it is essential that these perturbations can be sufficiently modeled. Therefore, the presented concepts are “best cases”. Nevertheless, the experience gained from the observations from the ESASDT and the ZIMLAT shows that these perturbations are sufficiently modeled or can be estimated in CelMech for arcs of a few months. The influence of the perturbations is analyzed at the end of this chapter.

The concepts depend on the possibility to determine improved orbits in near real time, i.e., within a few minutes. In the following sections, concepts for GEO and GTO objects are discussed in detail assuming that orbit improvement in near real time is possible. The case where no orbit in near real time is possible was also analyzed, but only the final results are presented in this work, as the method to achieve the results is the same.

Concepts to acquire “secured” GEO and GTO orbits for the ESASDT were presented in [Musci *et al.*, 2004] and [Musci *et al.*, 2005b]. More general concepts are presented in this work. Two ranges for the FOV are considered, $0.4^\circ - 1^\circ$ for a narrow FOV and $2^\circ - 6^\circ$ for a wide FOV. The concepts are optimized for the smallest values of the two ranges. Nevertheless, the resulting concepts can be adapted to the whole range. It is assumed within this and also within the following chapter that all follow-up tracks can be successfully correlated with the corresponding object. Furthermore it is assumed that the Earth is transparent, i.e., the objects can be observed wherever their position is on the orbit. The presented results are only theoretical. Real observations from the ESASDT and the ZIMLAT are used to confirm the theoretical results.

Table 5.1: Range of the orbital elements used for the simulation of 250 GEO orbits.

| | |
|------------------------|-----------------------------------------------|
| Semi-major axis | $40\,164 \text{ km} < a < 44\,164 \text{ km}$ |
| Eccentricity | $0.00 < e < 0.05$ |
| Inclination | $0^\circ < i < 15^\circ$ |
| R.A. of ascending node | $0^\circ < \Omega < 360^\circ$ |
| Argument of perigee | $0^\circ < \omega < 360^\circ$ |
| Longitude | $-70^\circ < \lambda < 120^\circ$ |

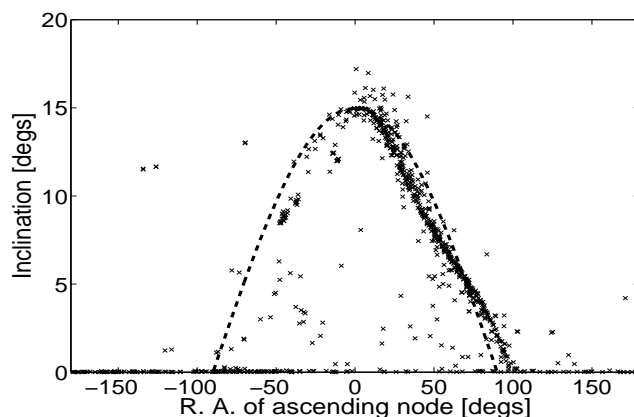


Figure 5.1: GEO population from the DISCOS catalogue compared with the function given in equation 5.1.

5.1 GEO

5.1.1 Simulated Orbits

The simulated elements were randomly varied within the ranges listed in Table 5.1. The semi-major axis was varied within 2 000 km below and above the GEO. The right ascension of the ascending node Ω of the majority of uncontrolled GEO objects is strongly correlated with the inclination. For inclinations $i > 0.5^\circ$ the right ascension of the ascending node Ω was approximated by the function ([Hugentobler, 1998]):

$$\cos \Omega = \cot 7.5^\circ \frac{1 - \cos i}{\sin i}. \quad (5.1)$$

How well this function fits the GEO population from the DISCOS database is shown in Figure 5.1. The GEO part visible from European sensors was selected as longitude range. In total 250 sets of orbital elements were simulated (from now on called “true” orbits).

The generated “true” orbits were used to simulate observations of the 250 objects for the ESASDT. An error of $\sigma = 0.5''$ was assumed for the accuracy of the single observations. This value is a typical error for observations from the ESASDT. The accuracy of the ZIMLAT is much better ($\sigma = 0.1 - 0.2''$). The time interval between the observations of a single track was set to 30 seconds for all tracks. Orbits were determined using these observations in order to study the accuracy of the orbit determination. The perturbations due to the Earth’s oblateness, the lunar and solar gravity were included in all simulations

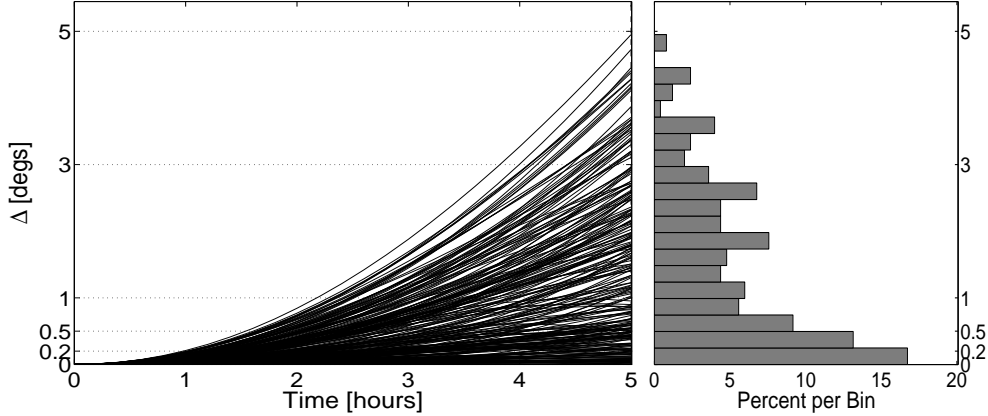


Figure 5.2: Left: difference Δ between “true” and determined circular orbit representing three discovery observations of a GEO object spanning one minute of time. Each line represents the result from one of 250 simulations. Right: distribution of the difference at the end of the shown time interval.

and orbit determinations performed for this section.

5.1.2 Discovery Observations

The discovery track of an object usually consists of a small number (two to ten) of observations. The track length is a few minutes. Three observations were simulated for the discovery tracks, giving an arc length of one minute. Circular orbits were determined using all three observations.

In order to recover an object after a few hours it is necessary that the determined orbit represents the “true” orbit rather accurately during this time interval. The differences between the positions of the determined circular orbits and the “true” orbits were determined with ([Bigalke, 1984]):

$$\Delta = \arccos(\sin \delta_t \sin \delta_d + \cos \delta_t \cos \delta_d \cos \Delta\alpha), \quad (5.2)$$

where

δ_t is the declination from the “true” orbit,

δ_d is the declination from the determined orbit,

$\Delta\alpha$ is the difference between the right ascension α of the “true” and the determined orbit.

The differences Δ as a function of time are shown on the left in Figure 5.2. Each line represents one of 250 simulations of a GEO object. The differences are smaller than 0.5° for more than one hour. To recover a detected object the difference between the determined orbit and the “true” orbit has to be less than half of the FOV of the sensor. Therefore, an object must be re-observed after a shorter time interval with an instrument with a narrow FOV than with a wide FOV. The ticks on the y-axis indicate the ranges for a narrow FOV ($0.2^\circ - 0.5^\circ$) and for a wide FOV ($1^\circ - 3^\circ$) where the objects can be recovered. Using an instrument with a narrow FOV of 1° the objects must be re-observed not later than about 1 hour after the discovery. With a wide FOV the objects can still be recovered after 2 hours. The distribution on the

right side shows that the differences are still small after 5 hours for a large fraction of the objects. Only a few objects have differences larger than 3° and all are within 5° .

The goal, however, is to recover the objects during the following night. Therefore, follow-up tracks are required to improve the orbits. The total arc length, including the observations from the discovery and the follow-up tracks, should be as short as possible, as this would guarantee a successful acquisition of a “secured” orbit for objects discovered close to the end of the observation night. The number of needed follow-up tracks and the minimal arc length, depending on the FOV, is studied in the following.

Follow-up observations with various numbers and temporal spacing of the observation tracks were simulated. Each simulated follow-up track consists of three observations. In this section it is assumed that online improvement is possible during the observation night. Elliptical orbits were determined using the discovery observations and the observations from every corresponding follow-up track.

5.1.3 Wide Field of View (2°)

The concept is developed for a wide FOV of 2° . But the presented concept can also be applied to a wider FOV.

First Follow-up Track

Figure 5.2 shows that the differences are smaller than 1° for more than two hours. For a wide FOV of 2° the first follow-up tracks can therefore be acquired after two hours. Elliptical orbits were determined using the observations from the discovery and the first follow-up track. The differences between the positions of the determined elliptical orbits and the “true” orbits as a function of time are shown in Figure 5.3. The objects are re-observable until about 6 hours after the discovery. Nevertheless, a large part of the objects cannot be recovered during the following night. Therefore, at least one additional follow-up track is needed. But as the total arc length should be short, it is recommended to acquire the first follow-up tracks earlier.

Another set of first follow-up tracks was therefore simulated one hour after the discovery observations. A gap of one hour was chosen as this would also allow to recover the objects with a narrow FOV and similar concepts for wide and narrow FOV might result (see Section 5.1.4). An arc length of one hour is long enough to determine all six orbital elements. This leads to the following concept:

- 1. follow-up 1 hour after the discovery,
- determination of elliptical orbits.

The differences Δ between the positions of the determined elliptical orbits and the “true” orbits as a function of time are shown in Figure 5.4. The initial epoch is the observation epoch of the first discovery observation. The differences are smaller than 1° within the first four hours. For about half of the objects the differences are still smaller than 0.5° after five hours.

Second Follow-up Track

Another follow-up track was simulated two hours after the discovery observations. There are two reasons why the second follow-up track should be acquired two hours after the discovery, although a recovery

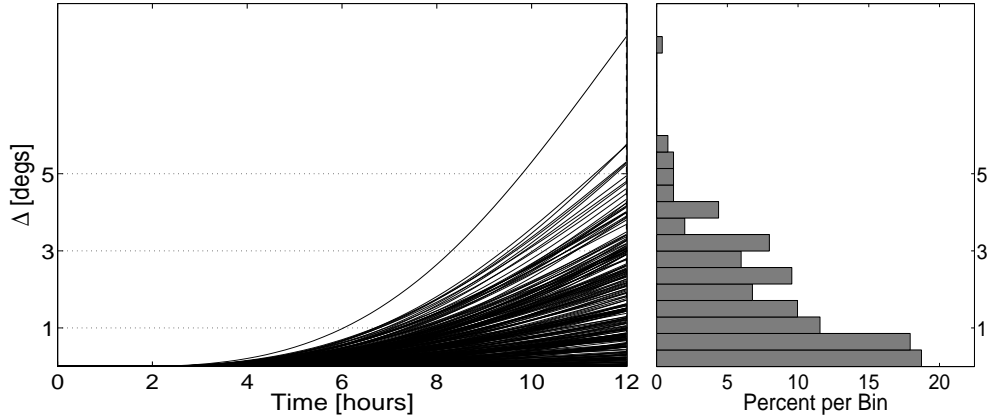


Figure 5.3: Left: difference Δ between “true” and determined elliptical orbit representing the discovery track of a GEO object and the first follow-up track after 2 h. Each line represents the result from one of 250 simulations. Right: distribution of the difference at the end of the shown time interval.

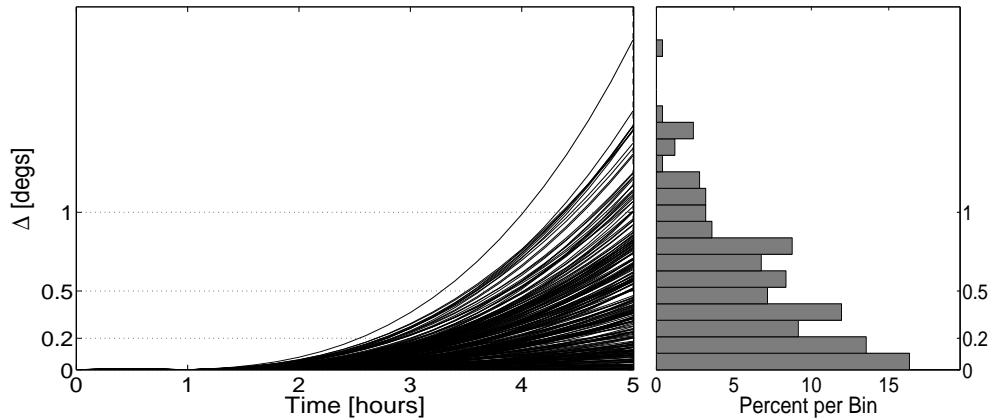


Figure 5.4: Left: difference Δ between “true” and determined elliptical orbit representing the discovery track of a GEO object and the first follow-up track after 1 h. Each line represents the result from one of 250 simulations. Right: distribution of the difference at the end of the shown time interval.

would be possible after four hours. The first is that the arc length should be short. The other reason is that no online orbit improvement using the discovery and the follow-up observations might be possible. In the case that no online orbit improvement is possible, the observations from the follow-up track can be used to determine a circular orbit, which will be used to plan the next follow-up. Figure 5.2 showed that a recovery is then possible one hour after the latest follow-up. The same concept may then result for the cases with or without the possibility of orbit improvement in near real time. The updated concept is:

- 1. follow-up 1 hour after the discovery,
- 2. follow-up 2 hours after the discovery,
- determination of elliptical orbits after each follow-up.

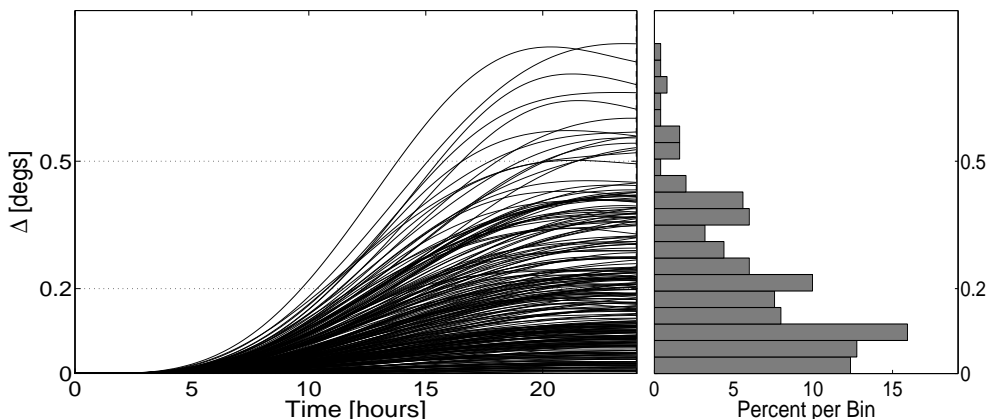


Figure 5.5: Left: difference Δ between “true” and determined elliptical orbit representing the discovery track of a GEO object and the follow-up tracks after 1 h and 2 h. Each line represents the result from one of 250 simulations. Right: distribution of the difference at the end of the shown time interval.

Figure 5.5 shows that the objects would be re-observable after one day, i.e., we have found a follow-up concept for the night of the discovery. Two follow-up tracks, one after one hour and one after two hours, are necessary to recover a GEO object during the following night with a wide FOV. This means that the objects have to be discovered at least two hours before astronomical dawn in order to acquire “secured” orbits.

Third Follow-up Track

A third follow-up track was simulated one day after the discovery observations. The updated concept is:

- 1. follow-up 1 hour after the discovery,
- 2. follow-up 2 hours after the discovery,
- 3. follow-up 1 day after the discovery,
- determination of elliptical orbits after each follow-up.

The differences Δ are shown in Figure 5.6. Daily periodical structures due to the errors in the eccentricity were eliminated by averaging the differences over one day. To analyze the size of the daily periodical errors, the first 30 days are plotted with these errors included and eliminated (Figure 5.7). The daily errors are negligible compared to the linear growth due to the errors in the mean motion that are dominating. Other periodical structures with a period of about half a month are also visible in Figure 5.6. Nevertheless, all objects would be re-observable with a wide FOV after one year. For a majority of the objects the difference is around 0.5° after one year.

Formal Errors

The averages of the formal errors of the determined elements (from now on called “mean formal errors”) are given in Table 5.2. The first column shows the number of available follow-up tracks. The second col-

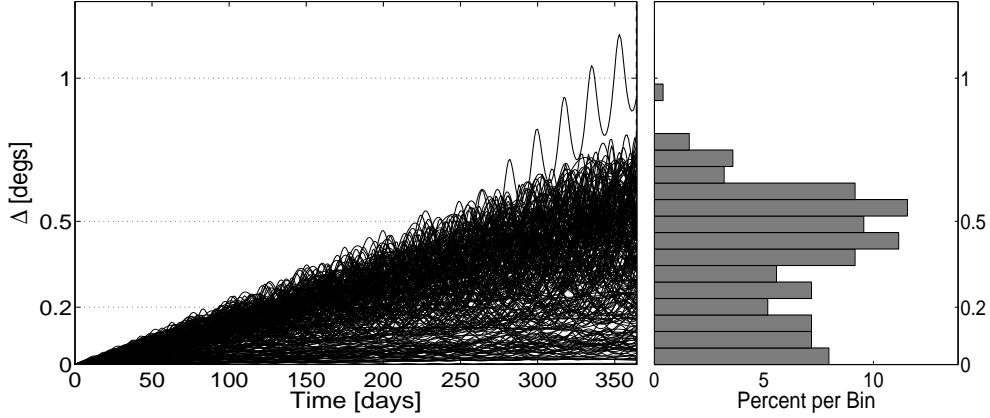


Figure 5.6: Left: difference Δ between “true” and determined elliptical orbit representing the discovery track of a GEO object and the follow-up tracks after 1 h, 2 h, and one day. Each line represents the result from one of 250 simulations. Right: distribution of the difference at the end of the shown time interval.

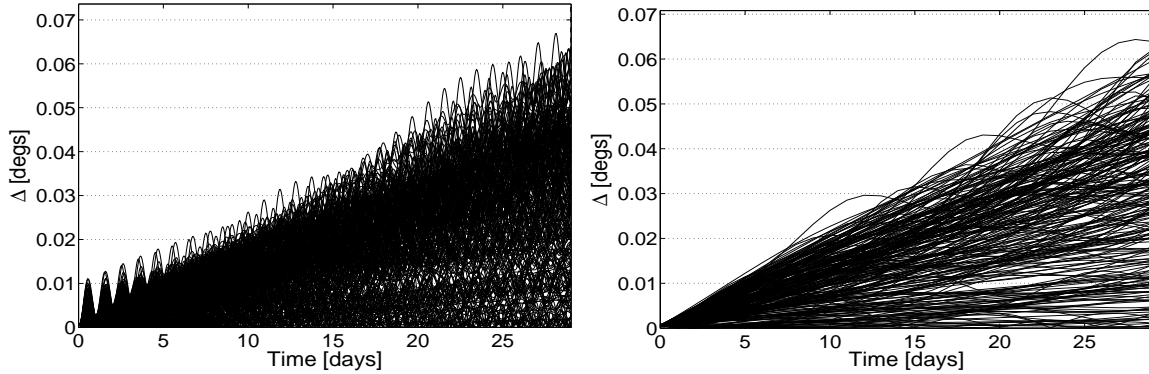


Figure 5.7: Daily periodical errors in the difference Δ between “true” and determined elliptical orbit of a GEO object. Left: including daily periodical errors, right: averaged over one day.

Table 5.2: Mean formal errors for the elliptical orbit determination representing the discovery track of a GEO object and different numbers of follow-up tracks.

| | arc | a [m] | e | i [°] | Ω [°] | ω [°] | T_0 [s] |
|---------|-----|------------------|---------------------|---------------------|--------------|--------------|------------------|
| 1. F-up | 1 h | $1.1 \cdot 10^6$ | $1.5 \cdot 10^{-2}$ | $2.1 \cdot 10^{-2}$ | 1.0 | 35 | $7.7 \cdot 10^3$ |
| 2. F-up | 2 h | $1.8 \cdot 10^4$ | $2.1 \cdot 10^{-4}$ | $3.6 \cdot 10^{-4}$ | 0.1 | 3.5 | $8.2 \cdot 10^2$ |
| 3. F-up | 1 d | 25 | $1.0 \cdot 10^{-5}$ | $8.6 \cdot 10^{-5}$ | 0.1 | 0.2 | 29 |

umn gives the total arc length and the other columns the mean formal errors for the six orbital elements. All observations up to the follow-up named in the row were used to determine elliptical orbits.

The orbital elements are not well determined after the first follow-up, especially the semi-major axis a . But the mean formal errors improve with the second follow-up track. The error in the semi-major axis is still large, but accurate enough for a successful recovery during the following night.

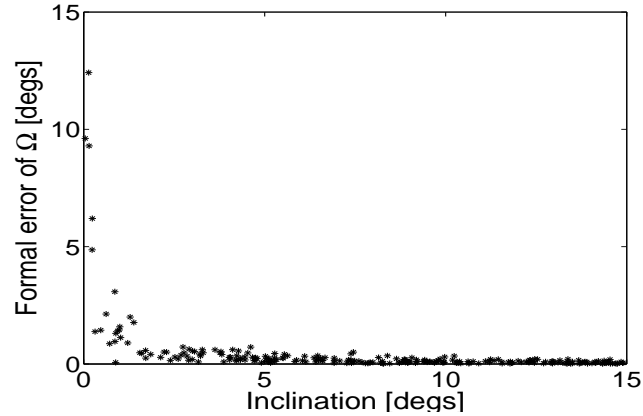


Figure 5.8: Formal error of the right ascension of ascending node Ω as a function of the inclination i .

The accuracy of the semi-major axis clearly improved after one day. The inclination i and the right ascension of ascending node Ω , however, did not improve much compared to the orbit after two follow-up tracks. This shows that the orbital plane was already well determined before. The orbits after one day can be considered as “secured” orbits.

The orbital plane is described by the inclination i and the accuracy of the right ascension of ascending node Ω . Therefore, we would expect that the formal errors of i and Ω are of the same magnitude. But in Table 5.2 we see that the mean formal error of Ω is by a factor of more than 50 larger than the one of i . This is because the accuracy of the right ascension of ascending node Ω depends on the inclination i (Figure 5.8). Ω is not well determined for very small i . Without the formal errors for small inclinations the average formal error for the 1. follow-up would be in the order of 0.1° . This does not mean that the orbital planes are not well determined for small inclinations. This is just a consequence of the selected elements. If we use other elements, e.g., so-called non-singular elements, we would see that all orbital planes are well determined.

The errors for T_0 are large for the 1.- and the 2. follow-up. This is because of the small eccentricities. The perigee, and therefore also the perigee passing time, is poorly defined for small eccentricities.

5.1.4 Narrow Field of View (0.4°)

The concept is developed for a narrow FOV of 0.4° . But it can also be applied to a narrow FOV up to about 1° . Of course, it can be also used for a wide FOV, but the concept presented in the previous section has a better performance as less observation time is needed.

First and Second Follow-up Track

In Section 5.1.3, the first two follow-ups were chosen such that the objects could also be recovered with a narrow FOV. Therefore, the beginning of the concept remains the same:

- 1. follow-up 1 hour after the discovery,
- 2. follow-up 2 hours after the discovery,

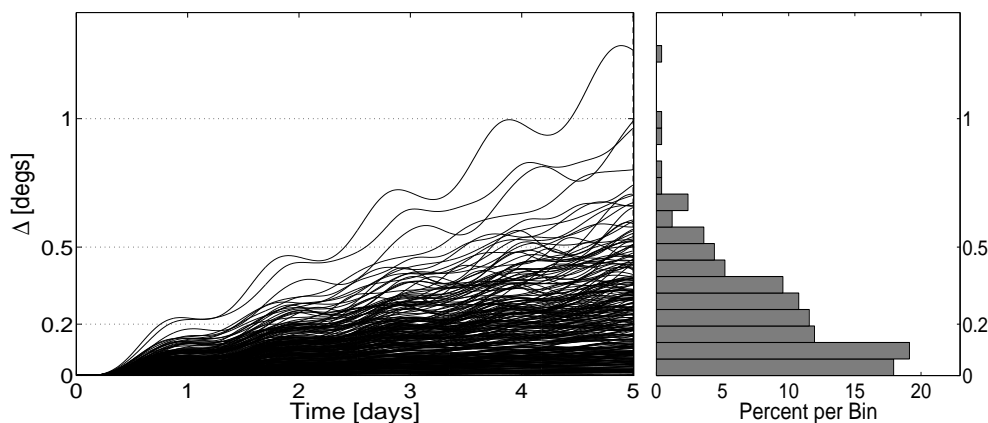


Figure 5.9: Left: difference Δ between “true” and determined elliptical orbit representing the discovery track of a GEO object and the follow-up tracks after 1 h, 2 h, and 3 h. Each line represents the result from one of 250 simulations. Right: distribution of the difference at the end of the shown time interval.

- determination of elliptical orbits after each follow-up.

But unlike to the wide FOV, two follow-up tracks are not sufficient to recover all objects during the following night with a narrow FOV (see Figure 5.5).

Third Follow-up Track

A third follow-up track was simulated three hours after the discovery. The concept has to be changed to:

- 1. follow-up 1 hour after the discovery,
- 2. follow-up 2 hours after the discovery,
- 3. follow-up 3 hours after the discovery,
- determination of elliptical orbits after each follow-up.

Figure 5.9 shows that almost all objects can be recovered after one day with three follow-up tracks. Only two objects are not re-observable with a very narrow FOV of about 0.4° . But already a FOV larger than 0.5° would be wide enough to recover these two objects. A large part of the objects can be recovered after five days. The daily periodical structures due to the errors in the eccentricity are clearly visible. But the linear growth of the differences due to the errors in the mean motion is already dominating.

Fourth Follow-up Track

The fourth follow-up tracks were simulated one day after the discovery. Therefore, the concept for a narrow FOV is as follows:

- 1. follow-up 1 hour after the discovery,

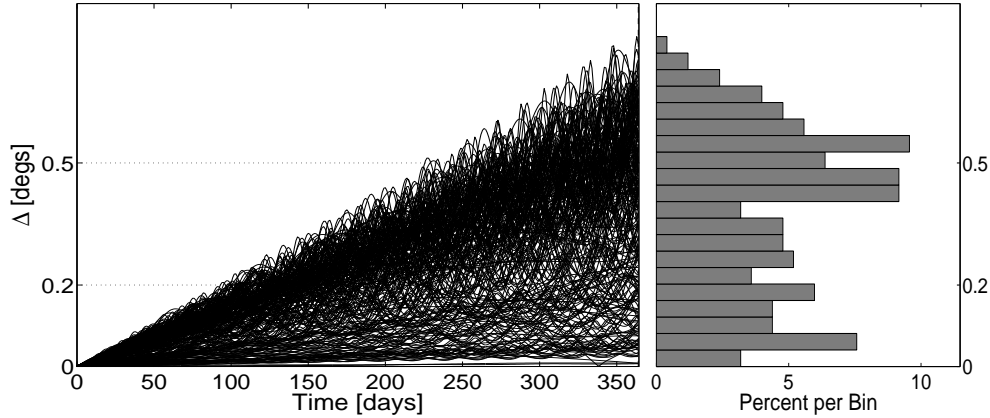


Figure 5.10: Left: difference Δ between “true” and determined elliptical orbit representing the discovery track of a GEO object and the follow-up tracks after 1 h, 2 h, 3 h, and one day. Each line represents the result from one of 250 simulations. Right: distribution of the difference at the end of the shown time interval.

Table 5.3: Mean formal errors for the elliptical orbit determination representing the discovery track of a GEO object and different numbers of follow-up tracks.

| | arc | a [m] | e | i [°] | Ω [°] | ω [°] | T_0 [s] |
|---------|-----|------------------|---------------------|---------------------|---------------------|---------------------|------------------|
| 1. F-up | 1 h | $1.1 \cdot 10^6$ | $1.5 \cdot 10^{-2}$ | $2.1 \cdot 10^{-2}$ | 1.0 | 35 | $7.7 \cdot 10^3$ |
| 2. F-up | 2 h | $1.8 \cdot 10^4$ | $2.1 \cdot 10^{-4}$ | $3.6 \cdot 10^{-4}$ | 0.1 | 3.5 | $8.2 \cdot 10^2$ |
| 3. F-up | 3 h | $4.7 \cdot 10^3$ | $5.6 \cdot 10^{-5}$ | $1.2 \cdot 10^{-4}$ | $5.3 \cdot 10^{-2}$ | 0.7 | $1.4 \cdot 10^2$ |
| 4. F-up | 1 d | 13 | $4.3 \cdot 10^{-6}$ | $5.4 \cdot 10^{-5}$ | $2.7 \cdot 10^{-2}$ | $7.6 \cdot 10^{-2}$ | 12 |

- 2. follow-up 2 hours after the discovery,
- 3. follow-up 3 hours after the discovery,
- 4. follow-up 1 day after the discovery,
- determination of elliptical orbits after each follow-up.

The differences Δ averaged over one day are shown in Figure 5.10. The disadvantage of a narrow FOV becomes clear by comparing this figure with Figure 5.6. While an object can be recovered after one year with a wide FOV, they have to be re-observed before about 100 days with a narrow FOV. For about half of the objects the differences are larger than 0.2° after half a year.

Formal Errors

The mean formal errors are given in Table 5.3. The first two rows (“1. F-up” and “2. F-up”) are identical with Table 5.2 as the concept until the 2. follow-up is the same.

The mean formal errors after the 4. follow-up are very small for all elements. Even an improvement compared to the last row in Table 5.2 can be seen, although the total arc length is the same. The reason for this improvement is the follow-up track after three hours. The accuracy of an orbit not only depends

on the length of the arc but also on a good distribution of the observations over one revolution. Of course, these orbits can also be considered as “secured”.

5.1.5 Without Near Real Time Orbit Improvement

The concepts for a wide FOV and a narrow FOV presented in the previous sections are based on the assumption that an orbit improvement in near real time is possible. Nevertheless, the chosen concepts are also valid if no orbit improvement during the observation night is possible. The only difference then is that an orbit improvement is not performed after each follow-up, but after the first observation night. The circular orbit determined for the follow-ups is used to perform the next follow-ups. Therefore, the concepts with or without online orbit improvement are almost the same.

Wide FOV (2°)

- 1. follow-up 1 hour after the discovery,
- 2. follow-up 2 hours after the discovery,
- determination of elliptical orbits.
- 3. follow-up 1 day after the discovery,
- determination of elliptical orbits.

Narrow FOV (0.4°)

- 1. follow-up 1 hour after the discovery,
- 2. follow-up 2 hours after the discovery,
- 3. follow-up 3 hours after the discovery,
- determination of elliptical orbits.
- 4. follow-up 1 day after the discovery,
- determination of elliptical orbits.

5.1.6 Observations Based on Surveys

Instead of performing tasked observations an object can also be recovered by performing an additional survey of the same part of the GEO ring after a certain time span. One critical issue using this attempt is the gap between the observation tracks. If the gap is too long the orbit determination could be problematic. Another problem are the drifting objects. The mean motion of these objects is not known a priori and therefore has to be computed from the first orbit determination of the discovery. But that is just what has to be done for the tasked observations. The problem of drifting objects can also be solved by using several telescopes, which are well distributed in longitude. An example of a survey strategy for such a system is presented in [Flohner *et al.*, 2005b].

Using only one telescope, the survey strategy is not ideal for every type of object in GEO. It is a feasible strategy for objects, which are at least controlled in longitude. The mean motion, especially its along

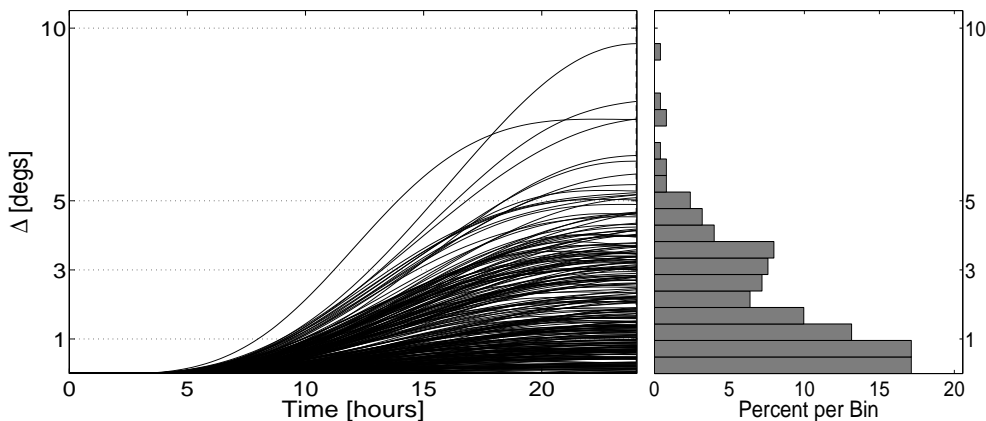


Figure 5.11: Left: difference Δ between “true” and determined elliptical orbit representing the discovery track of a GEO object and an additional survey track after 3 h. Each line represents the result from one of 250 simulations. Right: distribution of the difference at the end of the shown time interval.

Table 5.4: Mean formal errors for the elliptical orbit determination representing the discovery track of a GEO object and an additional survey track after 3 h.

| a [m] | e | i [°] | Ω [°] | ω [°] | T_0 [s] |
|------------------|---------------------|---------------------|--------------|--------------|------------------|
| $1.7 \cdot 10^5$ | $2.1 \cdot 10^{-3}$ | $4.2 \cdot 10^{-3}$ | 0.4 | 10.7 | $2.5 \cdot 10^3$ |

track part, of these objects is known a priori. An advantage of this strategy is that a group of objects can be observed at the same time. This would reduce the observation time needed to get “secured” orbits.

As we have shown in Section 5.1.4, an observation arc of three hours is long enough to determine an orbit that is sufficient to recover the object during the night following the discovery with a narrow FOV. A second observation track was therefore simulated three hours after the discovery.

The differences Δ between the positions of the determined elliptical orbits and the “true” orbits as a function of time are shown in Figure 5.11. Many objects would not be re-observable after one day, even with a wide FOV. A FOV of 20° would be needed to recover all objects. The result is clearly worse than in Figure 5.9.

The mean formal errors are given in Table 5.4. Comparing these values with the third line of Table 5.3, where more observations within the same arc were available, we note that the orbits from the surveys are much less accurate, although the arc length is the same.

We have already seen in Section 5.1.4 that four tracks distributed over an arc of three hours are enough to recover the objects during the following night. The next step is to look if three tracks would also be sufficient. Therefore, a second observation track was simulated one and a half hours and a third one three hours after the first survey.

The differences Δ in Figure 5.12 show that some objects cannot be recovered after one day with a FOV of 0.4° . Thus, more observations are needed in order to guarantee a safe recovery after one day. But this would lead to the same concept as with tasked follow-up tracks (see Section 5.1.4). For a wide FOV, the concept developed in Section 5.1.3 is also recommended for surveys, as the arc length resulting from the

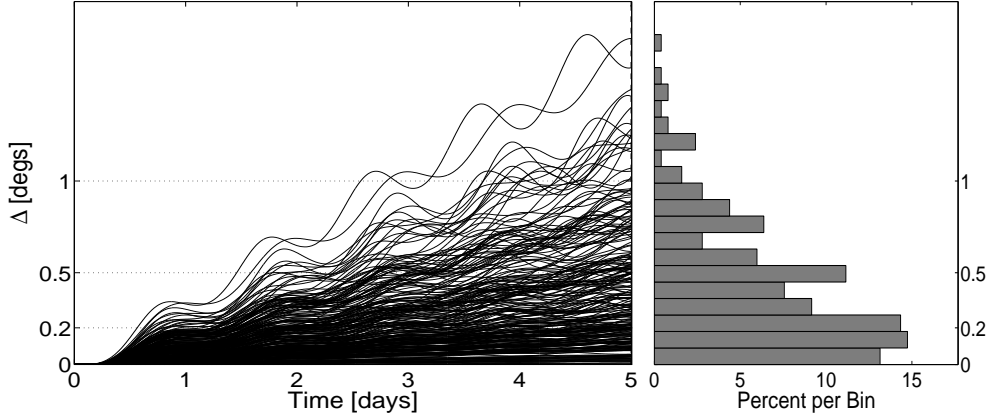


Figure 5.12: Left: difference Δ between “true” and determined elliptical orbit representing the discovery track of a GEO object and additional survey tracks after 1.5 h and 3 h. Each line represents the result from one of 250 simulations. Right: distribution of the difference at the end of the shown time interval.

Table 5.5: Mean formal errors for the elliptical orbit determination representing the discovery track of a GEO object and additional survey tracks after 1.5 h and 3 h.

| a [m] | e | i [°] | Ω [°] | ω [°] | T_0 [s] |
|------------------|---------------------|---------------------|--------------|--------------|------------------|
| $7.9 \cdot 10^3$ | $9.5 \cdot 10^{-5}$ | $1.7 \cdot 10^{-4}$ | 0.1 | 1.1 | $2.3 \cdot 10^2$ |

night of the discovery is shorter than the arc of three hours considered here.

The mean formal errors are given in Table 5.5. The errors are by factor of about two larger than the errors in the third row of Table 5.3, where the arc length is the same but more observations were available.

As mentioned above, for a single site the survey strategy is useful for controlled objects with small inclination. These objects move along a stripe of 0° declination. From the results above we can conclude that a field with a declination of about 0° should be observed for one and a half hours. Assuming a uniform distribution of the objects over the GEO ring about 6% of the controlled objects can be observed during such a survey. If we want to observe the same objects again, the right ascension of the selected field has to be changed by 22.5° . This new field should then be observed again for one and a half hours. A third field has to be selected and observed in the same manner. Of course, the first field has to be selected in a way that the objects are visible during the night for at least 4.5 hours after the survey starts.

To get “secured” orbits, one of the selected fields has to be observed at the same time during the following night. Therefore, a fourth survey track was simulated 24 hours after the discovery. The differences of the positions between the determined and the “true” orbits as a function of time are shown in Figure 5.13. The differences are averaged over one day. The results are very similar to Figure 5.6 and Figure 5.10. The mean formal errors are almost identical to the values in the last row of Table 5.3 and therefore not explicitly listed here.

The next question is if it is also sufficient just to observe the same part of the GEO ring again during the following night, without a second and a third survey during the first night. The problem is that for longer observation gaps the orbit determination becomes more and more difficult and sometimes fails. For an

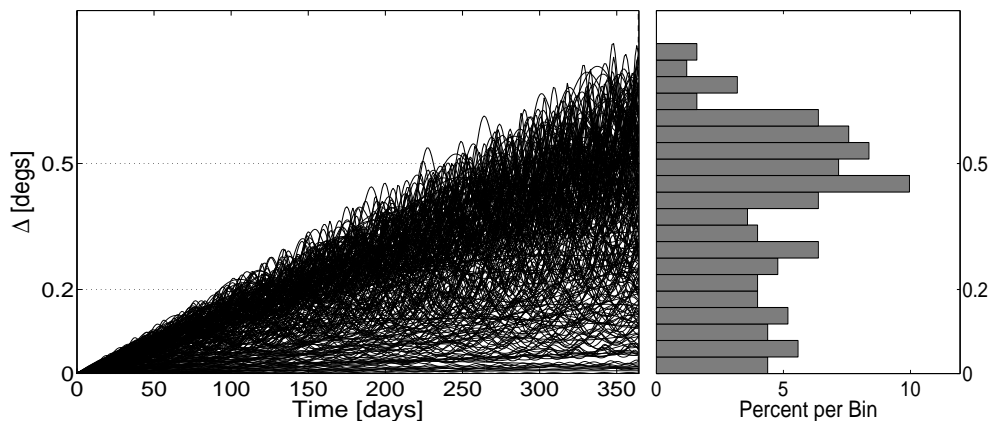


Figure 5.13: Left: difference Δ between “true” and determined elliptical orbit representing the discovery track of a GEO object and additional survey tracks after 1.5 h, 3 h, and one day. Each line represents the result from one of 250 simulations. Right: distribution of the difference at the end of the shown time interval.

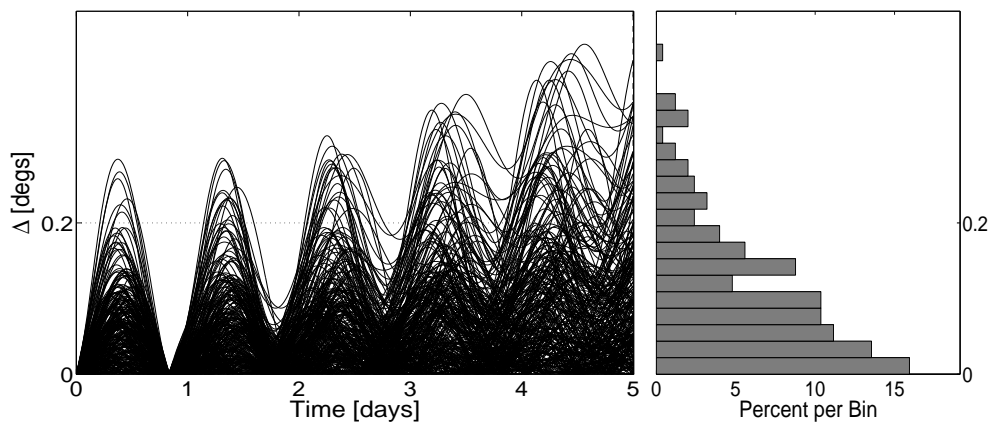


Figure 5.14: Left: difference Δ between “true” and determined elliptical orbit representing the discovery track of a GEO object and an additional survey track after 20 h.. Each line represents the result from one of 250 simulations. Right: distribution of the difference at the end of the shown time interval.

observation gap of exactly one day no orbit could be determined for more than one tenth of the simulated observations. This number increases for longer observation gaps. An orbit could be determined for only about half of the simulated observations with an observation gap of 15 days. The longest gap, which allowed determining an orbit for all 250 sets of observations, was 20 hours.

A second survey track was simulated 20 hours after the discovery. The differences of the positions between the determined and the “true” orbits as a function of time are shown in Figure 5.14. The result is much better than in Figure 5.11, but worse than in Figure 5.13. Due to the large gap between the tracks the differences get large within this time interval.

The mean formal errors are given in Table 5.6. Except of the semi-major axis all elements are less

Table 5.6: Mean formal errors for the elliptical orbit determination representing the discovery track of a GEO object and an additional survey track after 20 h.

| a [m] | e | i [°] | Ω [°] | ω [°] | T_0 [s] |
|------------------|---------------------|---------------------|--------------|--------------|------------------|
| $1.8 \cdot 10^3$ | $2.7 \cdot 10^{-4}$ | $1.2 \cdot 10^{-3}$ | 0.2 | 2.6 | $5.8 \cdot 10^2$ |

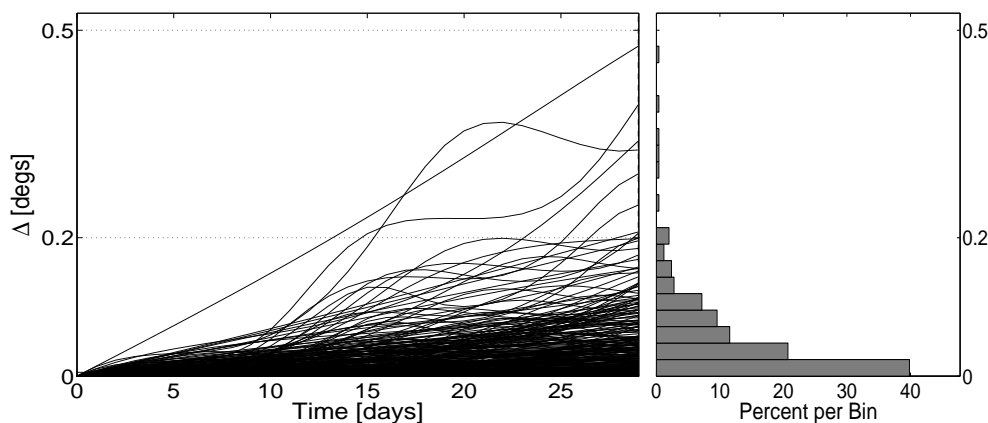


Figure 5.15: Left: difference Δ between “true” and determined elliptical orbit representing the discovery track of a GEO object and additional survey tracks after 20 h and 26 h. Each line represents the result from one of 250 simulations. Right: distribution of the difference at the end of the shown time interval.

Table 5.7: Mean formal errors for the elliptical orbit determination representing the discovery track of a GEO object and additional survey tracks after 20 h and 26 h.

| a [m] | e | i [°] | Ω [°] | ω [°] | T_0 [s] |
|------------------|---------------------|---------------------|--------------|--------------|------------------|
| $1.7 \cdot 10^2$ | $5.6 \cdot 10^{-5}$ | $2.3 \cdot 10^{-4}$ | 0.1 | 1.1 | $2.4 \cdot 10^2$ |

accurate than in Table 5.5. This shows once again that a good distribution of the observations is very important.

A third survey track was simulated 26 hours after the discovery. This time interval had been chosen to get a better distribution of the observations on the orbit. For an interval of 24 hours the position of the objects within their orbits would be nearly the same as for the first observation track. Several time intervals between 21 and 26 hours had been tested and an interval of 26 hours showed the best result. The differences Δ are shown in Figure 5.15. Again, only the averaged functions are plotted. The results are clearly worse than in Figure 5.13, although the arc length is a bit longer. The daily variations are much larger.

The mean formal errors are given in Table 5.7. Compared to the last row in Table 5.3, the values are worse by approximately a factor of ten. This shows the effect of a good distribution of the observations during the first night. A good distribution reduces the errors and thus the daily variations.

From the results of this section we conclude that the best survey concept is very similar to the follow-up concept. A few tracks during the night of the discovery and one track during the following night lead to “secured” orbits. The number of tracks during the first night can be reduced compared to the follow-up

Table 5.8: Difference Δp between the determined and the observed position for GEO objects observed with the ESASDT.

| Object | | 1. Follow-up | 2. Follow-up | 3. Follow-up | 4. Follow-up | 5. Follow-up |
|--------|--------------------------|--------------|--------------|--------------|--------------|--------------|
| GEO 1 | $\Delta T[\text{h}] / U$ | 0.96 / 1 | 2.08 / 1 | 3.08 / 1 | 26.37 / 2 | 52.28 / 3 |
| | $\Delta p[^\circ]$ | 0.0143 | 0.0147 | 0.0037 | 0.1505 | 0.0031 |
| GEO 2 | $\Delta T[\text{h}] / U$ | 0.77 / 1 | 1.35 / 1 | 2.44 / 1 | 30.53 / 2 | |
| | $\Delta p[^\circ]$ | 0.0019 | 0.0093 | 0.0719 | 0.0069 | |
| GEO 3 | $\Delta T[\text{h}] / U$ | 0.67 / 1 | 1.85 / 1 | 3.24 / 1 | 22.65 / 2 | 55.19 / 3 |
| | $\Delta p[^\circ]$ | 0.0028 | 0.0101 | 0.0113 | 0.0211 | 0.0039 |
| GEO 4 | $\Delta T[\text{h}] / U$ | 0.56 / 1 | 2.79 / 1 | 3.76 / 1 | 23.68 / 2 | 71.15 / 4 |
| | $\Delta p[^\circ]$ | 0.0019 | 0.0338 | 0.0147 | 0.1361 | 0.0018 |

concept for a FOV between 0.35° and 0.5° . For a narrower FOV and a wide FOV, however, the concept is identical to the follow-up concept. Other survey strategies are possible but the resulting orbits are less accurate.

It has to be noted that the survey strategy is only feasible for part of the GEO population and cannot fully replace the follow-up strategy when only one telescope is available. Only about one third of the GEO ring is visible from one site. All operational GEO satellites outside this sector can not be observed. And also some drifting objects might get lost when they move out of the visible sector. A system of several telescopes well distributed in longitude would be needed to get “secured” orbits for all GEO objects that are bright enough to be detected.

5.1.7 Examples of Real Observations

In the previous sections we showed on the basis of simulations that it is theoretically possible to recover a discovered GEO object after a few nights if follow-up observations from the first two nights are available. This result was tested with real observations from the ESASDT and the ZIMLAT.

ESASDT

Four examples of objects observed with the ESASDT are given in Table 5.8. All objects have been discovered during GEO surveys. Tasked observations have been performed during the night of the discovery and during the following nights. Object GEO 2 was identified with the object 93073B MOP 3 from the DISCOS catalogue (see [Serraller and Jehn, 2005]). The other three objects could not be correlated with the catalogue. They have magnitudes of about 18, 17, and 13.

In Table 5.8 ΔT is the time interval between the discovery and the follow-up observations. U is the revolution number during which the observations were acquired. The revolution number is 1 for the discovery. A circular orbit was determined representing the discovery observations. This orbit was used to determine the position for the first follow-up observation. Δp is the difference between this determined position and the observed position. Elliptical orbits were used to determine the positions of the other follow-up observations using all previous observations.

The examples confirm the results from the simulations. All objects were recovered with the determined

Table 5.9: Difference Δp between the determined and the observed position for GEO objects observed with the ZIMLAT.

| Object | | 1. Follow-up | 2. Follow-up | 3. Follow-up | 4. Follow-up |
|--------|---------------------------------|--------------|--------------|--------------|--------------|
| GEO 5 | $\Delta T[\text{h}] / \text{U}$ | 1.04 / 1 | 2.03 / 1 | 19.01 / 2 | 97.53 / 5 |
| | $\Delta p[^\circ]$ | 0.0078 | 0.0006 | 0.0176 | 0.0085 |
| GEO 6 | $\Delta T[\text{h}] / \text{U}$ | 0.35 / 1 | 2.55 / 1 | 20.35 / 2 | 192.74 / 9 |
| | $\Delta p[^\circ]$ | 0.0006 | 0.0378 | 0.1566 | 0.0060 |
| GEO 7 | $\Delta T[\text{h}] / \text{U}$ | 0.88 / 1 | 2.23 / 1 | 26.87 / 2 | 118.43 / 6 |
| | $\Delta p[^\circ]$ | 0.0033 | 0.0069 | 0.0925 | 0.0066 |

orbits. An arc length of about three hours from the night of the discovery was sufficient to recover the objects during the following night.

ZIMLAT

Three examples of objects observed with the ZIMLAT are given in Table 5.9. The three objects are 82044F (GEO 5), 91010F (GEO 6), and 92088A (GEO 7). Elements from the DISCOS catalogue were used to determine ephemerides for these objects. The ephemerides were then used to perform observations. As the observations were acquired arbitrarily and not based on a specific concept, the available observations were searched for a subset matching the concept described in Section 5.1.4.

Note that only two follow-up tracks were available from the first night. Nevertheless, the differences are smaller than half of the FOV of the ZIMLAT, i.e., smaller than 0.2° , after about one day. This is not contradictory to the results from Section 5.1.4. As we have seen in Figure 5.5, a large part of the objects can be recovered after one day with only two follow-up tracks.

5.1.8 Summary

The concept for the acquisition of a “secured” GEO orbit does not depend on the possibility to determine improved orbits in near real-time. The size of the FOV, the accuracy of the single observation, and the requirement of short arcs affect the concept the most.

Simulations were performed to assess the number of observations, their temporal spacing, and the total arc length required to determine “secured” orbits. An error of $\sigma = 0.5''$ was assumed for the single observations. Each simulated track consisted of three observations. A circular orbit was determined using the observations from the discovery track. This orbit is sufficient to recover a GEO object after one hour. The concepts for both, wide and narrow FOV, are based on this result.

The resulting concepts are:

Wide FOV (2°)

- 1. follow-up 1 hour after the discovery,
- 2. follow-up 2 hours after the discovery,
- 3. follow-up 1 day after the discovery,

Table 5.10: Range of the orbital elements used for the simulation of 250 GTO orbits.

| | |
|------------------------|---------------------------------------|
| Eccentricity | $0.60 < e < 0.75$ |
| Inclination | $0^\circ < i < 30^\circ$ |
| R.A. of ascending node | $0^\circ < \Omega < 360^\circ$ |
| Argument of perigee | $0^\circ < \omega < 360^\circ$ |
| Mean anomaly | $M(t_{osc}) = 180^\circ \pm 20^\circ$ |

- determination of elliptical orbits after each follow-up.

Narrow FOV (0.4°)

- 1. follow-up 1 hour after the discovery,
- 2. follow-up 2 hours after the discovery,
- 3. follow-up 3 hours after the discovery,
- 4. follow-up 1 day after the discovery,
- determination of elliptical orbits after each follow-up.

The concepts were tested with real observations from the ESASDT and the ZIMLAT. The tests showed a good correlation with the simulations.

A survey strategy was also analyzed. The same part of the GEO belt will be observed after certain time intervals. This strategy is only recommended for controlled GEO object or for a system with several instruments well distributed in longitude. Using only one telescope, two different concepts can lead to “secured” orbits. The first is very similar to the concepts using follow-up observations. Three surveys with a duration of 1.5 hours have to be performed one after another. The selected fields in right ascension and declination have to be selected such, that the same objects are observed within each survey. One of the fields has to be observed again after one day. With the second concept, only three surveys are needed. The gap between the first and the second survey has to be 20 hours, while the gap between the second and the third survey should be 6 hours.

5.2 GTO

5.2.1 Simulated Orbits

Orbital elements for 250 different GTO objects were simulated. The elements were varied randomly within the limits specified in Table 5.10. The semi-major axes a and the eccentricities e were selected such, that they fit approximately the GTO population of the DISCOS catalogue. A comparison of the simulated elements a and e with the catalogue is shown in Figure 5.16. Note that the objects in the right diagram with a semi-major axis of about 26 000 km are Molniya objects with inclinations of about 60°. They are not included in the simulation.

Using optical telescopes objects with highly eccentric orbits are best observed when they are close to the apogee. At the apogee, the mean anomaly at the osculating epoch is $M(t_{osc}) = 180^\circ$. A normal

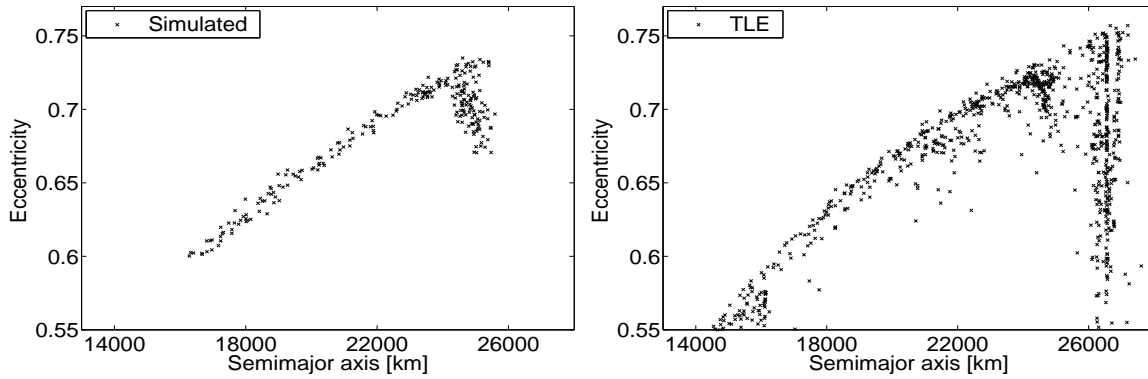


Figure 5.16: Comparison of the simulated elements a and e (left) with part of the DISCOS catalogue (right).

distribution with a mean value of 180° and a standard deviation of 20° was chosen for the values of the mean anomaly. For GTO objects a difference of 20° in the mean anomaly corresponds to a difference in time of about half an hour.

The generated “true” orbits were used to simulate observations of the 250 objects. An error of $\sigma = 0.5''$ was assumed for the accuracy of the single observations. The time interval between the observations was set to 30 seconds for all tracks. The simulated observations were used to study the accuracy of the orbit determination. The perturbations due to the Earth’s oblateness, the lunar and solar gravity were included in all orbit determinations performed for this section. But no model for the air drag was included.

5.2.2 Discovery Observations

Three observations were simulated for the discovery track. Circular orbits were determined using all three observations.

The differences Δ between the positions of the determined circular orbits and the “true” orbits as a function of time are shown in Figure 5.17. Each line represents one of 250 simulations of a GTO object. For all simulated orbits the differences are smaller than 0.5° within about the first twenty minutes after the discovery. With a wide FOV of 2° , all objects except one can be recovered after half an hour. The FOV has to be larger than 2.8° to recover all objects after 0.5 h. Using a narrow FOV of 0.4° , on the other side, the objects have to be re-observed after about 15 minutes. The right diagram in Figure 5.17 shows that the differences are small for the majority of the objects and can be recovered after the times mentioned before.

Comparing Figure 5.17 with the result for the GEO objects (Figure 5.2) it can be clearly seen that the result for the GTO objects is much worse. This is no surprise as a circular orbit is of course a better approximation for an almost circular GEO as for a very eccentric GTO. Nevertheless, the result shows that a circular orbit can be used to recover a GTO object after some minutes.

The accuracy of the circular orbits depends on where the object was detected in its elliptical orbit. The best accuracy results when the object is observed at the apogee. This can be seen in Figure 5.18, where the differences between the “true” and the determined circular orbit after one hour are plotted for different observation times with respect to the apogee passing time. The orbit of a typical GTO object was used to

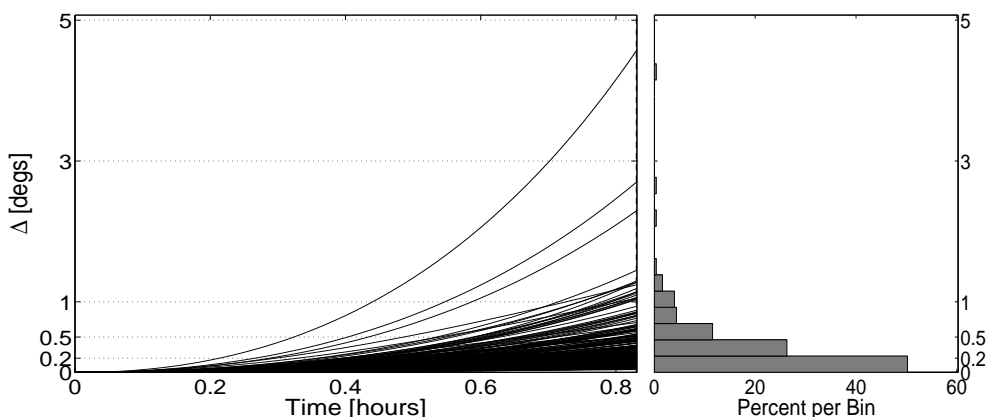


Figure 5.17: Left: difference Δ between “true” and determined circular orbit representing three discovery observations of a GTO object spanning one minute of time. Each line represents the result from one of 250 simulations. Right: distribution of the difference at the end of the shown time interval.

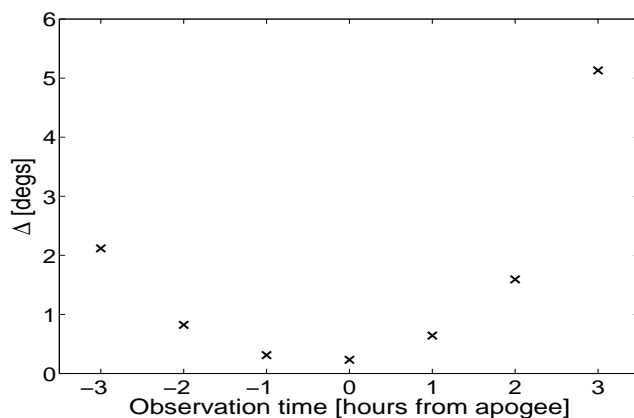


Figure 5.18: Difference Δ between “true” and determined circular orbit of a GTO object after one hour as a function of the observation time. The observation time is set to 0 at the apogee.

generate the plot. The difference is smallest at the apogee. Four hours after the apogee, when the object is close to the perigee, the difference would be more than 60° . This implies that the differences can be too large for a safe recovery after a very short time if the objects are not observed close to the apogee. Nevertheless, for most objects a gap of 15 minutes is sufficient with a narrow FOV of 0.4° , while a gap of 0.5 h is sufficient for a wide FOV of 2° .

As for the GEO objects, the number of follow-ups needed to recover the objects during the following night is studied in the following. Follow-up observations with various numbers and temporal spacing of the tracks were simulated. Each simulated follow-up track consists of three observations. Elliptical orbits were determined using the discovery observations and the observations from every corresponding follow-up track. Again, it is assumed that orbit improvement in near real time is possible.

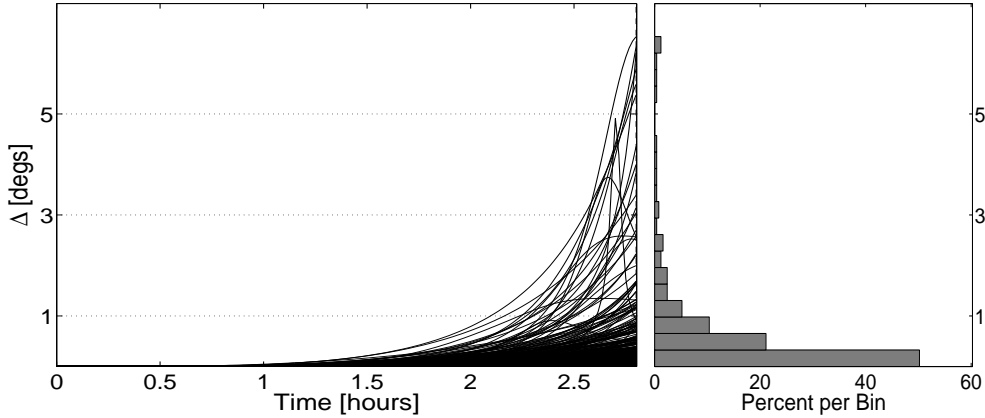


Figure 5.19: Left: difference Δ between “true” and determined elliptical orbit representing the discovery track of a GTO object and the first follow-up track after 0.5 h. Each line represents the result from one of 250 simulations. Right: distribution of the difference at the end of the shown time interval.

5.2.3 Wide Field of View (2°)

The presented concept is optimized for a FOV of 2° . Nevertheless, it can be also applied to instruments with a wider FOV.

First Follow-up Track

Taking the result from the previous section, the first follow-up track was simulated 30 minutes after the discovery. Only one of the simulated objects would then be missed. The resulting arc length of 30 minutes is long enough to determine all six orbital elements. The observations from the discovery track and the first follow-up track were used to determine elliptical orbits. This leads to the concept:

- 1. follow-up 0.5 hours after the discovery,
- determination of elliptical orbits.

The differences Δ between the positions of the determined and the “true” orbits as a function of time are shown in Figure 5.19. The differences are all smaller than 1° within the first two hours. A pronounced growth of the differences is observed for some objects after about 2.5 h. But for more than half of the objects the differences remain clearly below 1° within about the first three hours.

Second Follow-up Track

Figure 5.19 showed that the differences are getting to large for a safe recovery of an object after a few hours. A second follow-up track was therefore simulated after two hours. Elliptical orbits were determined using the observations from all tracks, including the discovery observations. The updated concept is:

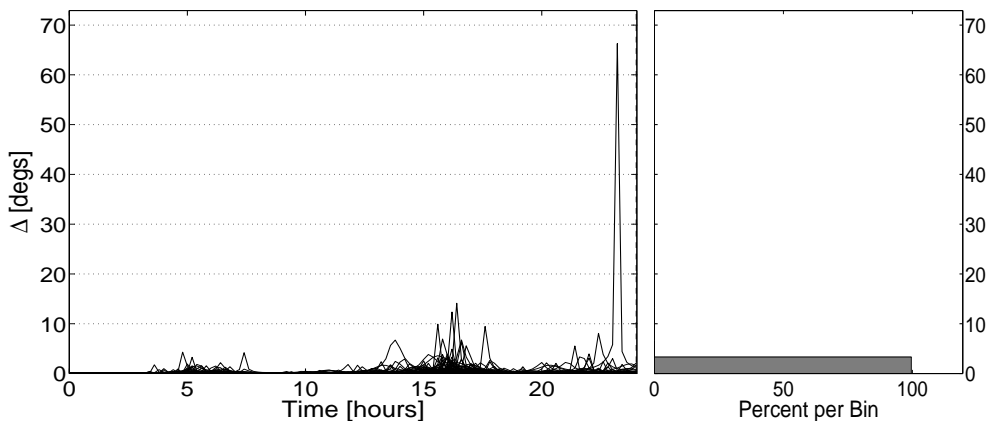


Figure 5.20: Left: difference Δ between “true” and determined elliptical orbit representing the discovery track of a GTO object and the follow-up tracks after 0.5 h and 2 h. Each line represents the result from one of 250 simulations. Right: distribution of the difference at the end of the shown time interval.

- 1. follow-up 0.5 hours after the discovery,
- 2. follow-up 2 hours after the discovery,
- determination of elliptical orbits after each follow-up.

The differences between the positions of the determined elliptical orbits and the “true” orbits as a function of time are shown in Figure 5.20. The extrapolation is performed over one day. The differences are small within the first few hours. The plot also shows several peaks with differences up to over 60° .

For a better understanding of these peaks, the differences for one object were extrapolated over five days (Figure 5.21). It can be clearly seen that the peaks appear periodically. The revolution period of the selected object is 10.94 hours. This is exactly the period seen in the figure. The peaks refer to the perigee. The explanation for this behavior is that the observations are performed close to the apogee and the orbit is therefore not well determined at the perigee. Furthermore, the objects are much faster near the perigee than near the apogee. Thus, an error in the perigee passing time also results in a larger difference near the perigee. In addition, the objects are much closer to the observer at the perigee than at the apogee. As topocentric positions are measured, the same error in distance leads to a larger error of the measured angle when it is closer to the observer.

From this result we conclude that the best chance to recover an object during the night following the discovery is when the object is close to the apogee. Figure 5.22 shows the differences at the apogee as a function of the number of revolutions. Note that the differences are not exactly at the apogee. The differences are taken from the table used to generate the left plot in Figure 5.20 and the values closest to the apogee were selected. Therefore, small sampling effects are possible. The result would only be slightly better if the differences were taken exactly at the apogee. Nevertheless, the differences are not much larger for about ± 2 hours from the apogee, as can be seen in Figure 5.21. The discoveries were made at the revolution number one. The number of revolutions per day for the simulated orbits is between two and four revolutions. The differences are all smaller than one degree at revolution number seven. This means that the recovery of those objects is guaranteed with a wide FOV during the following night.

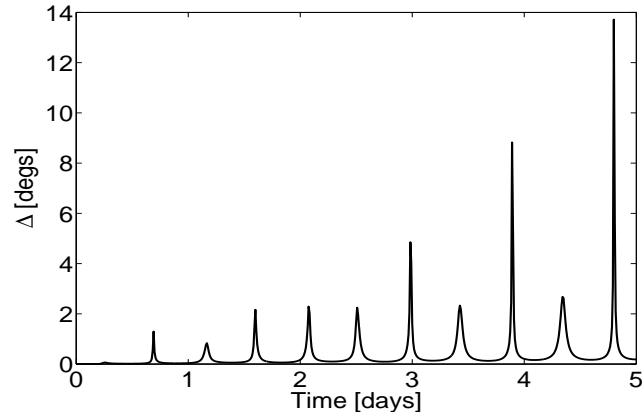


Figure 5.21: Difference Δ between “true” and determined elliptical orbit for one simulated GTO object extrapolated for five days.

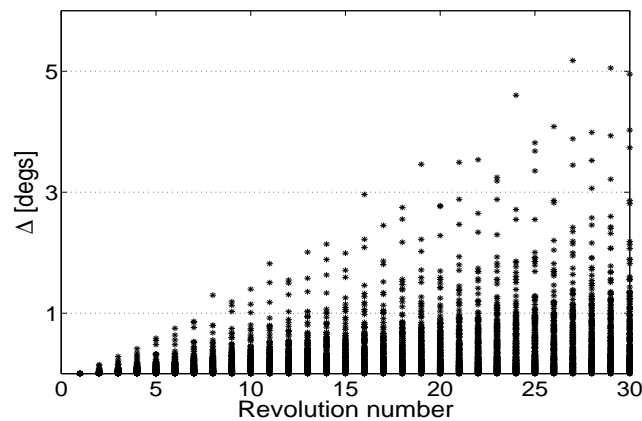


Figure 5.22: Difference Δ between “true” and determined elliptical orbit of a GTO object at the apogee as a function of the number of revolutions. The orbits represent the discovery and the follow-up tracks after 0.5 h and 2 h.

Follow-up During Following Night

As the best chance to recover the objects is when they are close to the apogee the third follow-up tracks were not all simulated after the same time but at the first apogee passage during the following night. A transparent Earth is assumed, i.e., the objects can be observed wherever they are. In reality, the objects can be observed up to about 2 hours before or after the apogee if the apogee itself is not visible, or they have to be observed during the first night when part of the 4 hour interval around the apogee is visible. The concept hitherto is:

- 1. follow-up 0.5 hours after the discovery,
- 2. follow-up 2 hours after the discovery,
- 3. follow-up at first apogee during the following night,
- determination of elliptical orbits after each follow-up.

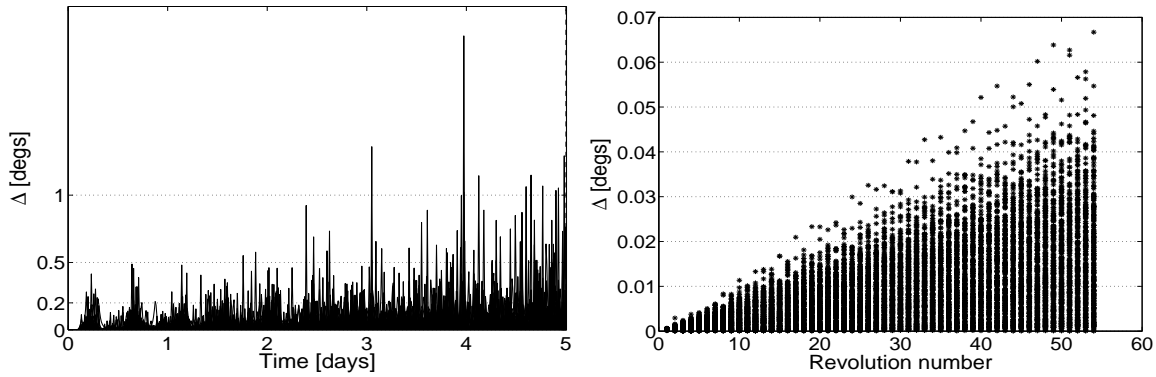


Figure 5.23: Difference Δ between “true” and determined elliptical orbit representing the discovery track of a GTO object and the follow-up tracks after 0.5 h, 2 h, and the first apogee during the following night. Each line represents the result from one of 250 simulations. Left: continuous, right: at apogee.

Figure 5.23 shows the differences Δ as a function of time. The continuous functions are plotted on the left hand side. The differences are smaller than 1° within the first 3 days, even at the perigee. Again, small sampling effects are possible as the peaks are not exactly at the perigee. The differences at the apogee are shown in the right plot. The differences are below 1° for more than 50 revolutions, corresponding to about 12 to 25 days. From this point of view, the orbits would fulfill the requirements for a “secured” orbit. Nevertheless, a “secured” orbit should also be accurate close to the perigee, although optical observations at the perigee are difficult to realize. Therefore, another follow-up track is needed.

Follow-up During Fifth Night After Discovery

The fourth follow-up tracks were simulated at the first apogee passage during the fifth night after the discovery. The concept is therefore:

- 1. follow-up 0.5 hours after the discovery,
- 2. follow-up 2 hours after the discovery,
- 3. follow-up at first apogee during the following night,
- 4. follow-up at first apogee during the fifth night after the discovery,
- determination of elliptical orbits after each follow-up.

The differences Δ between the “true” and the determined elliptical orbits as a function of time are shown in Figure 5.24. The differences are small over the entire interval shown in the figure. Also the peaks are not larger than about 0.4° . Figure 5.25 shows the differences at the apogee (left) and the perigee (right). The differences at the apogee are very small. This shows how accurate these orbits are. But also the differences at the perigee are mostly below 0.05° . The largest differences in this plot match well with the peaks in Figure 5.24. This again confirms that the peaks in Figure 5.24 stem from the perigee.

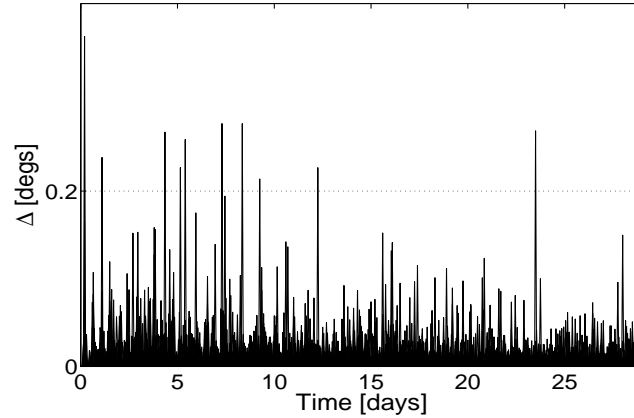


Figure 5.24: Difference Δ between “true” and determined elliptical orbit representing the discovery track of a GTO object and the follow-up tracks after 0.5 h, 2 h, the first apogee during the first and the fifth night after the discovery. Each line represents the result from one of 250 simulations.

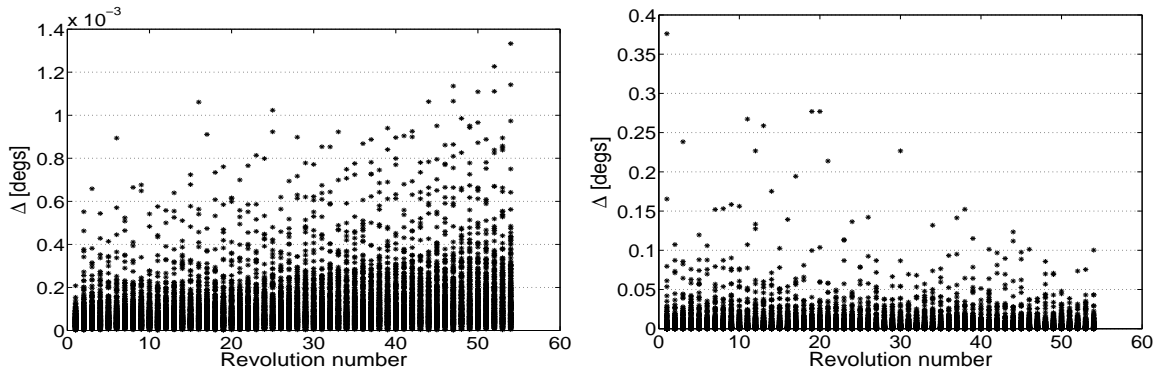


Figure 5.25: Difference Δ between “true” and determined elliptical orbit representing the discovery track of a GTO object and the follow-up tracks after 0.5 h, 2 h, the first apogee during the first and the fifth night after the discovery. Left: at apogee, right: at perigee.

Formal Errors

The mean formal errors are given in Table 5.11. For the third and the fourth follow-ups, the track was not observed after 1 day or 5 days respectively, but at the first apogee passage during that night. This is indicated by “apo” in the column “arc”.

The errors of a , ω , and T_0 are smaller than in the first row of Table 5.2, while the errors of the other elements are of the same magnitudes. This can be explained by the fact that a half hour arc near the apogee of a GTO is about the same portion of the orbit as a two hour arc of a GEO. A larger portion of the orbit was used to determine the GTO orbits after the first follow-up than for the GEO orbits, where the first follow-up tracks were observed after one hour.

The mean formal errors are getting much smaller after the 2. follow-up. The inclination i and the right ascension of ascending node Ω are already well determined and the accuracies do not improve much with

Table 5.11: Mean formal errors for the elliptical orbit determination representing the discovery track of a GTO object and different numbers of follow-up tracks.

| | arc | a [m] | e | i [°] | Ω [°] | ω [°] | T_0 [s] |
|---------|---------|------------------|---------------------|---------------------|---------------------|---------------------|------------------|
| 1. F-up | 0.5 h | $7.5 \cdot 10^5$ | $1.4 \cdot 10^{-2}$ | $5.0 \cdot 10^{-2}$ | 0.8 | 1.0 | $6.0 \cdot 10^2$ |
| 2. F-up | 2 h | $6.1 \cdot 10^3$ | $1.1 \cdot 10^{-4}$ | $5.0 \cdot 10^{-4}$ | $8.0 \cdot 10^{-3}$ | $1.1 \cdot 10^{-2}$ | 5.1 |
| 3. F-up | 1 d/apo | $3.1 \cdot 10^2$ | $9.6 \cdot 10^{-6}$ | $2.5 \cdot 10^{-4}$ | $2.7 \cdot 10^{-3}$ | $3.3 \cdot 10^{-3}$ | 0.6 |
| 4. F-up | 5 d/apo | 1.2 | $5.0 \cdot 10^{-6}$ | $1.4 \cdot 10^{-4}$ | $1.7 \cdot 10^{-3}$ | $1.9 \cdot 10^{-3}$ | 0.2 |

further observations. As expected, the largest improvement can be seen in the semi-major axis.

Compared to Table 5.2 and Table 5.3, the mean formal errors are larger after one day for GTO objects, although observations from more orbital revolutions were available. The reason is that the observations for the GTO objects were all simulated close to the apogee and the orbit can therefore not be well determined around the perigee. This makes the whole orbit determination less accurate.

The accuracies after five days are very small. These orbits can be declared as “secured” orbits.

5.2.4 Narrow Field of View (0.4°)

The presented concept, which is developed for a FOV of 0.4°, can also be applied for a narrow FOV up to about 2°. For a wider FOV, the concept resulting in the previous section is recommended.

First two Follow-up Tracks

We have seen in Section 5.2.2 that with a narrow FOV of 0.4° the objects have to be re-observed after about 15 minutes, assuming that the objects were discovered close to the apogee. The first follow-up track was therefore simulated 15 minutes after the discovery. The resulting arc length is still very short. The determination of an elliptical orbit from the discovery and the first follow-up track can be very inaccurate or even fail, e.g., the resulting perigee distance can be smaller than the Earth radius.

The observations from the follow-up track can be used to determine a circular orbit. This orbit allows to observe the object after another 15 minutes. Therefore, a second follow-up track was simulated 30 minutes after the discovery. Observation arcs of half an hour are long enough to reliably determine elliptical orbits. The concept for a narrow FOV hitherto is:

- 1. follow-up 15 minutes after the discovery,
- 2. follow-up 30 minutes after the discovery,
- determination of elliptical orbits.

Figure 5.26 shows that the differences Δ are all smaller than 0.2° within the first two hours. A pronounced growth of the differences after about three hours is visible for some objects. But the distribution on the right side shows that the differences remain small for more than three hours for the majority of the objects.

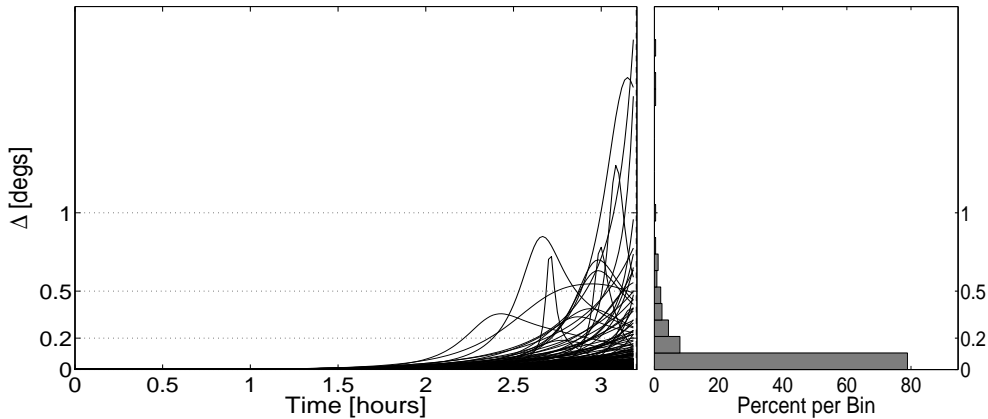


Figure 5.26: Left: difference Δ between “true” and determined elliptical orbit representing the discovery track of a GTO object and the follow-up tracks after 0.25 h and 0.5 h. Each line represents the result from one of 250 simulations. Right: distribution of the difference at the end of the shown time interval.

Third Follow-up Tracks

Another follow-up track was simulated two hours after the discovery. Therefore, the updated concept is:

- 1. follow-up 15 minutes after the discovery,
- 2. follow-up 30 minutes after the discovery,
- 3. follow-up 2 hours after the discovery,
- determination of elliptical orbits after the 2. and the 3. follow-up.

The differences Δ are shown in the left plot of Figure 5.27. Two groups of peaks are visible, whereas the right group is a little bit broader. This is expected as the peaks appear at the perigees and the revolution periods of the objects are different. It can also be seen that the differences are small at 10 hours and after 20 hours. The right plot shows the differences at the apogees. All objects can be recovered until revolution number 5, i.e., they can be recovered during the following night.

Follow-up During Following Night

As we have seen, three follow-ups are enough to recover a GTO object during the following night, if the observations are acquired when the object is close to its apogee. A fourth follow-up was therefore simulated at the first apogee during the first night after the discovery. Again, a transparent Earth is assumed. This leads to the following concept:

- 1. follow-up 15 minutes after the discovery,
- 2. follow-up 30 minutes after the discovery,
- 3. follow-up 2 hours after the discovery,
- 4. follow-up at first apogee during the following night,

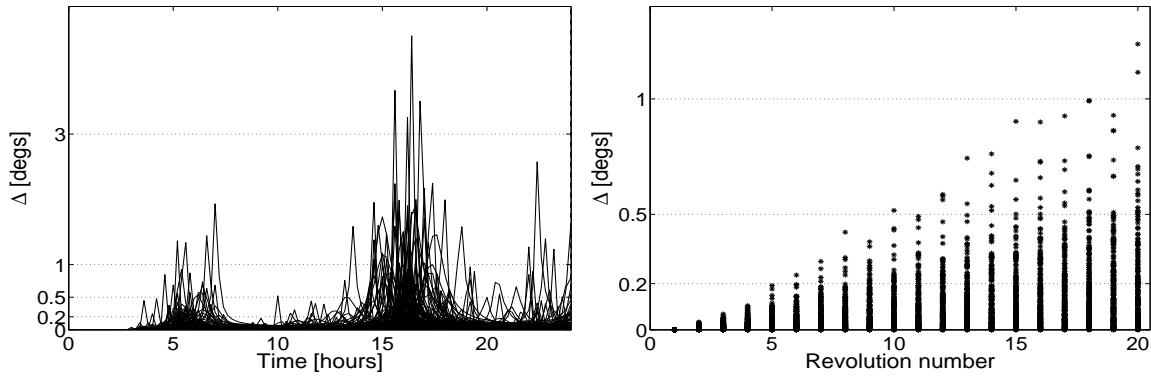


Figure 5.27: Difference Δ between “true” and determined elliptical orbit representing the discovery track of a GTO object and the follow-up tracks after 0.25 h, 0.5 h, and 2 h. Each line represents the result from one of 250 simulations. Left: continuous, right: at apogee.

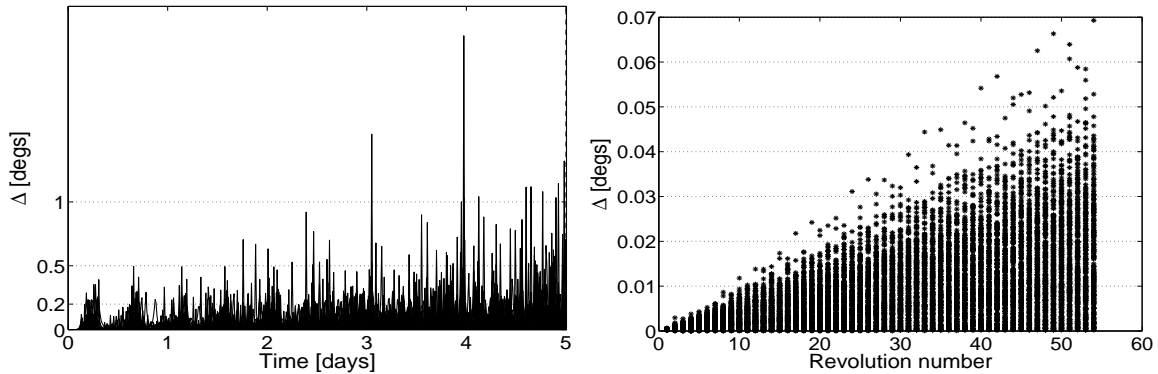


Figure 5.28: Difference Δ between “true” and determined elliptical orbit representing the discovery track of a GTO object and the follow-up tracks after 0.25 h, 0.5 h, 2 h, and the first apogee during the following night. Each line represents the result from one of 250 simulations. Left: continuous, right: at apogee.

- determination of elliptical orbits after each follow-up, except after the first.

The differences Δ in Figure 5.28 are very similar to the differences in Figure 5.23. This is no surprise as the concepts are nearly the same. The only difference is the follow-up track after 15 minutes, which does not affect the accuracy of the orbits much.

Follow-up During Fifth Night After Discovery

As for the wide FOV, an additional track during the fifth night after the discovery is added to the concept:

- 1. follow-up 15 minutes after the discovery,
- 2. follow-up 30 minutes after the discovery,
- 3. follow-up 2 hours after the discovery,

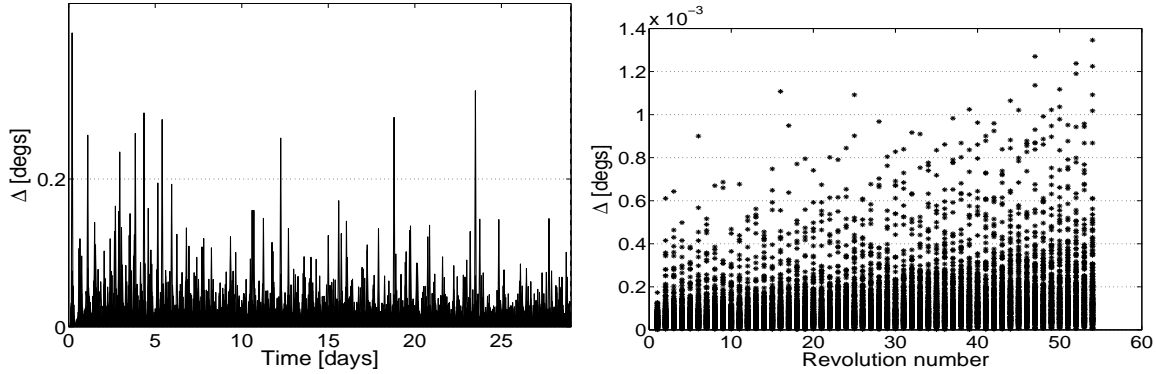


Figure 5.29: Difference Δ between “true” and determined elliptical orbit representing the discovery track of a GTO object and the follow-up tracks after 0.25 h, 0.5 h, 2 h, the first apogee during the first and the fifth night after the discovery. Each line represents the result from one of 250 simulations. Left: continuous, right: at apogee.

Table 5.12: Mean formal errors for the elliptical orbit determination representing the discovery track of a GTO object and different numbers of follow-up tracks.

| | arc | a [m] | e | i [°] | Ω [°] | ω [°] | T_0 [s] |
|---------|-----------|------------------|---------------------|---------------------|---------------------|---------------------|-----------|
| 2. F-up | 0.5 h | $7.9 \cdot 10^4$ | $1.4 \cdot 10^{-3}$ | $5.1 \cdot 10^{-3}$ | $9.3 \cdot 10^{-2}$ | 0.1 | 62.8 |
| 3. F-up | 2 h | $2.4 \cdot 10^3$ | $4.1 \cdot 10^{-5}$ | $2.4 \cdot 10^{-4}$ | $3.6 \cdot 10^{-3}$ | $5.0 \cdot 10^{-3}$ | 2.1 |
| 4. F-up | 1 d / apo | $3.0 \cdot 10^2$ | $9.3 \cdot 10^{-6}$ | $2.4 \cdot 10^{-4}$ | $2.7 \cdot 10^{-3}$ | $3.3 \cdot 10^{-3}$ | 0.6 |
| 5. F-up | 5 d / apo | 1.2 | $5.0 \cdot 10^{-6}$ | $1.4 \cdot 10^{-4}$ | $1.7 \cdot 10^{-3}$ | $2.0 \cdot 10^{-3}$ | 0.2 |

- 4. follow-up at first apogee during the following night,
- 5. follow-up at first apogee during the fifth night after the discovery,
- determination of elliptical orbits after each follow-up, except after the first.

Again, the differences Δ shown in Figure 5.29 are very similar to the ones in Figure 5.24. Especially the differences at the apogee look almost the same as in Figure 5.25.

The only difference between the concepts for wide and narrow FOV is an additional follow-up track needed for the narrow FOV of 0.4° 15 minutes after the discovery. But as we will see in the Section 5.2.5, the concepts for a wide and a narrow FOV are only similar if orbit improvement in near real time is possible. Without near real time orbit improvement much more follow-ups are necessary for a narrow FOV compared to a wide FOV.

Formal Errors

The mean formal errors are given in Table 5.12. The table starts with an entry for the 2. follow-up. The mean formal errors for the 1. follow-up are missing as no orbit has been determined using only the observations from the discovery and the first follow-up track.

The mean formal errors for the second follow-up are by a factor of about 10 smaller than the values in the first row of Table 5.11, although the arc length is the same. This is due to the additional track after

15 minutes, which improves the accuracy of the orbit. Also the mean formal errors after two hours are smaller in Table 5.12.

The mean formal errors after the first apogee during the night after the discovery are of the same magnitude as in Table 5.11, but slightly smaller. The last rows of the two tables, however, are almost identical.

5.2.5 Without Near Real Time Orbit Improvement

Contrary to the GEO, the concepts for GTO depend on the possibility of orbit improvement in near real time. If no orbit improvement in near real time can be performed, the latest observed observation track must be used to determine a circular orbit. As we have seen in Section 5.2.2, such an orbit allows to recover an object half an hour after the discovery with a wide FOV of 2° and 15 minutes after the discovery with a narrow FOV of 0.4° . The concepts without orbit improvement during the first observation night are:

Wide FOV (2°)

- 1. follow-up 0.5 hours after the discovery,
- 2. follow-up 1 hour after the discovery,
- 3. follow-up 1.5 hours after the discovery,
- determination of elliptical orbits.
- 4. follow-up at first apogee during the following night,
- determination of elliptical orbits.
- 5. follow-up at first apogee during the fifth night after the discovery,
- determination of elliptical orbits.

Narrow FOV (0.4°)

- 1.-8. follow-up every 15 minutes until 2 hours after the discovery,
- determination of elliptical orbits.
- 9. follow-up at first apogee during the following night,
- determination of elliptical orbits.
- 10. follow-up at first apogee during the fifth night after the discovery,
- determination of elliptical orbits.

It can be clearly seen that more follow-up tracks are needed, especially with a narrow FOV. Nevertheless, the concept for the wide FOV is interesting. Although more follow-up tracks are needed, the arc length resulting from the first night is shorter than for the concepts with orbit improvement in near real time. Therefore, this concept can be useful for object detected close to the end of the observation night.

Eight follow-up tracks during the first night are needed with a narrow FOV. But this assumes that the objects can be recovered 15 minutes after the last follow-up even two hours after the apogee. But Figure 5.18 showed that the differences rise with the time difference from the apogee. Thus, it is not guaranteed

Table 5.13: Difference Δp between the determined and the observed position for GTO objects observed with the ESASDT.

| Object | | 1. Follow-up | 2. Follow-up | 3. Follow-up | 4. Follow-up | 5. Follow-up |
|--------|---------------------------|--------------|--------------|--------------|--------------|--------------|
| GTO 1 | ΔT [h] / U | 0.56 / 1 | 1.29 / 1 | 22.57 / 2 | 42.09 / 4 | |
| | Δp [$^{\circ}$] | 0.0803 | 0.0085 | 0.1280 | 0.0032 | |
| GTO 2 | ΔT [h] / U | 0.47 / 1 | 1.11 / 1 | 1.89 / 1 | 24.80 / 2 | 100.00 / 8 |
| | Δp [$^{\circ}$] | 0.0365 | 0.0083 | 0.0042 | 0.4293 | 0.0027 |
| GTO 3 | ΔT [h] / U | 0.38 / 1 | 0.68 / 1 | 1.78 / 1 | 20.34 / 3 | 69.89 / 8 |
| | Δp [$^{\circ}$] | 0.0434 | 0.0013 | 0.0093 | 0.0495 | 0.0103 |
| GTO 4 | ΔT [h] / U | 0.48 / 1 | 1.13 / 1 | 1.81 / 1 | 23.86 / 2 | 68.03 / 6 |
| | Δp [$^{\circ}$] | 0.2010 | 0.3071 | 0.0024 | 0.0305 | 0.0407 |

that the presented concept for a narrow FOV will work for every discovered GTO object. When using a narrow FOV, orbit improvement in near real time is highly recommended.

5.2.6 Observations Based on Surveys

No survey strategy for GTO objects was studied in the frame of this work. The GTO population has a much larger variety of orbits than the GEO population. It is therefore not easy to develop a survey strategy which guarantees periodical observations of every GTO object.

5.2.7 Examples of Real Observations

In the previous section we showed on the basis of simulations that it is theoretically feasible to recover a newly detected GTO object after a few nights if follow-up observations from the first nights are available. This theoretical result was tested with real observations from the ESASDT and the ZIMLAT.

ESASDT

Four examples of GTO objects observed with the ESASDT are given in Table 5.13. The objects were detected during surveys and the follow-ups acquired from the determined orbits.

The first two objects are known. Object GTO 1 was identified with the debris object 88109L and object GTO 2 with the Russian rocket body 02023D from the DISCOS database. The other two objects are faint (magnitude 18 and 17) and could not be correlated with the catalogue. ΔT is the time interval between the discovery and the follow-up observations and U is the revolution number during which the observations were acquired. The discovery was made during revolution number 1. A circular orbit was determined representing the discovery observations. This orbit was used to determine the position for the first follow-up observation. Δp is the difference between this determined position and the observed position. Elliptical orbits were used to determine the positions of the other follow-up observations using all previous observations.

The examples confirm the results from the simulations. All objects were recovered with the determined orbits. For the object GTO 1, the orbit after two follow-ups was just good enough to recover the object

Table 5.14: Difference Δp between the determined and the observed position for GTO objects observed with the ZIMLAT.

| Object | | 1. Follow-up | 2. Follow-up | 3. Follow-up | 4. Follow-up |
|--------|---------------------------------|--------------|--------------|--------------|--------------|
| GTO 5 | $\Delta T[\text{h}] / \text{U}$ | 0.30 / 1 | 1.05 / 1 | 22.35 / 3 | 94.21 / 9 |
| | $\Delta p[^\circ]$ | 0.0020 | 0.0566 | 0.2425 | 0.0004 |
| GTO 6 | $\Delta T[\text{h}] / \text{U}$ | 2.01 / 1 | 4.32 / 1 | 26.12 / 3 | 50.49 / 5 |
| | $\Delta p[^\circ]$ | 1.7000 | 0.0076 | 0.0063 | 0.0005 |

during the next night. The resulting new orbit was a clear improvement and the object was successfully re-observed during the third night.

Object GTO 2 shows that the critical part of the acquisition of a “secured” orbit is the recovery during the night following the discovery. In the case of object GTO 2 the difference after one day would be too large for a successful recovery with the ESASDT due to the small FOV. The reason for this unexpected large difference is that the orbit determined after the 3. follow-up was not very accurate due to some bad observations. The resulting RMS was $0.89''$ instead of about $0.35''$ resulting for a good orbit. Nevertheless, the observation strategy used to perform the observations (see [Schildknecht et al., 2004a]) allows small errors in along-track and the object was recovered during the following night.

A circular orbit determined from the observations of the first follow-up track was used to determine the position of the second follow-up for object GTO 4. The results for object GTO 4 show that the orbit propagation can be inaccurate if the time span to the next follow-up track is too long. In this case, the orbit was just good enough to recover the object during the second follow-up.

The examples also show that the critical points are the recovering of the object with the first follow-up and during the night following the discovery. Nevertheless, the arcs from the night of the discovery were long enough for a successful recovery.

ZIMLAT

Two examples of objects observed with the ZIMLAT are given in Table 5.14. The observations of both objects were acquired on the basis of TLE. The two objects are the known Russian rocket bodies 92085D (GTO 5) and 00067D (GTO 6). Object GTO 5 shows that a very short arc can be sufficient to recover an object during the following night. Nevertheless, the difference for the third follow-up is clearly larger than for the other follow-ups. For object GTO 6 the orbit determined from the discovery observations would not have been accurate enough to recover the object after two hours. This nicely shows that the first follow-up has to be observed after a short time to guarantee a recovery.

5.2.8 Summary

The concept for the acquisition of a “secured” GTO orbit depends on the possibility to determine improved orbits in near real time. Furthermore, the concept is affected by the size of the FOV and the accuracy of the single observation.

Simulations were performed to assess the number of observations, their temporal spacing, and the total arc length required to determine “secured” orbits. An error of $\sigma = 0.5''$ was assumed for the single

observations. Each simulated track consisted of three observations. A circular orbit was determined using the observations from the discovery track. This orbit is sufficient to recover a GTO object after half an hour with a wide FOV, or 15 minutes with a narrow FOV. The concepts are based on this result.

The resulting concepts are:

Wide FOV, with Orbit Improvement in Near Real Time

- 1. follow-up 0.5 hours after the discovery,
- 2. follow-up 2 hours after the discovery,
- 3. follow-up at first apogee during the following night,
- 4. follow-up at first apogee during the fifth night after the discovery,
- determination of elliptical orbits after each follow-up.

Narrow FOV, with Orbit Improvement in Near Real Time

- 1. follow-up 15 minutes after the discovery,
- 2. follow-up 30 minutes after the discovery,
- 3. follow-up 2 hours after the discovery,
- 4. follow-up at first apogee during the following night,
- 5. follow-up at first apogee during the fifth night after the discovery,
- determination of elliptical orbits after each follow-up, except after the first.

Wide FOV, no Orbit Improvement in Near Real Time

- 1. follow-up 0.5 hours after the discovery,
- 2. follow-up 1 hour after the discovery,
- 3. follow-up 1.5 hours after the discovery,
- determination of elliptical orbits.
- 4. follow-up at first apogee during the following night,
- determination of elliptical orbits.
- 5. follow-up at first apogee during the fifth night after the discovery,
- determination of elliptical orbits.

Narrow FOV, no Orbit Improvement in Near Real Time

- 1.-8. follow-up every 15 minutes until 2 hours after the discovery,
- determination of elliptical orbits.
- 9. follow-up at first apogee during the following night,
- determination of elliptical orbits.

- 10. follow-up at first apogee during the fifth night after the discovery,
- determination of elliptical orbits.

For a narrow FOV, orbit improvement in near real time is highly recommended. Both concepts for a wide FOV have their advantages. Less follow-up tracks are needed to recover the object during the following night with orbit improvement, while a shorter arc length is sufficient without orbit improvement.

The concepts were tested with real observations from the ESASDT and the ZIMLAT. The tests showed a good correlation with the simulations.

No survey strategy was tested, as it is not so easy as for GEO to find a strategy, which guarantees periodical observations of every object in GTO.

5.3 Multiple Sites

Instead of improving the orbit by observing the object at different epochs, the orbit can also be improved by observing the object from different sites. Simultaneous observations from multiple sites allow to determine the distance of the object with a higher accuracy than from a short arc of observations from a single site due to the improved geometry. Generally, the accuracy of the orbit depends on the geometry of the observing sites during the observations. For two sites, the geometry is characterized with the differences in longitude λ and latitude β . As we will see later, a longer separation between the sites reduces the error of the orbit determination.

The orbit improvement resulting from observations from two and three sites are studied in the following. Virtual sites were simulated for this purpose. The main site was assumed to be located at longitude $\lambda = 0^\circ$ and latitude $\beta = 0^\circ$. For four other sites, the longitude was fixed to $\lambda = 0^\circ$ and the latitudes set to 10° , 20° , 30° , and 40° . The latitude was fixed to $\beta = 0^\circ$ and the longitude varied from 10° to 40° for four additional sites.

Again, each simulated observation track consists of three observations separated by 30 seconds. The error of the accuracy of the single observation was assumed to be $\sigma = 0.5''$.

5.3.1 GEO

The same 250 simulated orbits as in Section 5.1 were used.

Simultaneous Observations

First, the orbit accuracy for simultaneous observations from two sites was studied. For comparison, circular orbits were determined from single tracks observed from the main site. The differences Δ for this case are shown in Figure 5.30. The result is very similar to the one for the ESASDT in Figure 5.2. For almost all objects, the differences are smaller than 5° after 5 hours.

One observation track was simulated for each of the other eight sites for the same epoch as the track observed from the main site. Orbits were determined using the observations from the main site together with one of the other tracks. Although the observation arc is very short, it is possible to determine all six orbital elements.

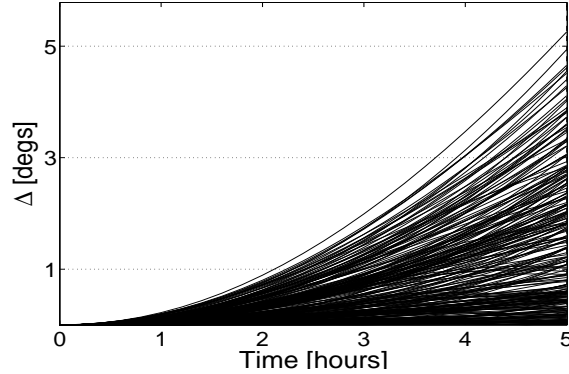


Figure 5.30: Difference Δ between “true” and determined circular orbit of a GEO object representing one track observed from a virtual site located at $\lambda = 0^\circ$ and $\beta = 0^\circ$.

Let us first look at the sites with the same latitude as the reference site but varied longitude. The differences Δ for the four cases are shown in Figure 5.31. Some objects with large differences (“outliers”) are visible in each of the four plots. They are the smallest for the site with $\lambda = 40^\circ$. An explanation for these large differences will be given later. Nevertheless, it can also be clearly seen that for a majority of the objects the differences are getting smaller for a larger separation between the sites. For a difference between the sites of 40° in longitude most of the differences are below 1° after 5 hours. This is by a factor of 5 better than for observations from one site only.

The mean formal errors resulting from the orbit determination are given in Table 5.15. The accuracy for all elements does improve with a longer separation in longitude between the sites, although the mean formal errors are affected by the outliers. The largest improvement results for the semi-major axis and the eccentricity.

The result is much better for the sites with identical longitude and different latitudes. In Figure 5.32, there are no such outliers with large differences visible as in Figure 5.31. Already for a separation between the sites of 10° in latitude, the differences are smaller than 1° after 5 hours. The results for separations larger than 30° are by a factor of about 50 better than when using one site only.

The mean formal errors for the sites with identical longitude and different latitudes in Table 5.16 are mostly smaller than in Table 5.15, except for i and Ω , which are slightly larger. Comparing only the results from the pairs including the sites with a separation of $\Delta\lambda = 40^\circ$ and $\Delta\beta = 40^\circ$ from the main site, the errors of a and e are by a factor of 3 smaller for the later. Also the accuracies of ω and T_0 are slightly better, but the improvement is not of the same magnitude.

Using simultaneous observations from two sites mainly allows a better determination of the shape of the orbit, while the improvement in the orbital plane is only small. The best result can be achieved with a large separation in latitude between the sites. But all results are much better than for the orbit determined from one track observed from one site. Nevertheless, additional observations are needed to recover all objects during the following night. Thus, additional follow-up observations are still needed.

It can be expected that the result is even better when three sites are observing an object simultaneously. The same virtual sites as before were used to simulate observations. From the 16 possible combinations of the sites, only those 4 where the sites have the same separation in longitude and latitude from the main site were analyzed.

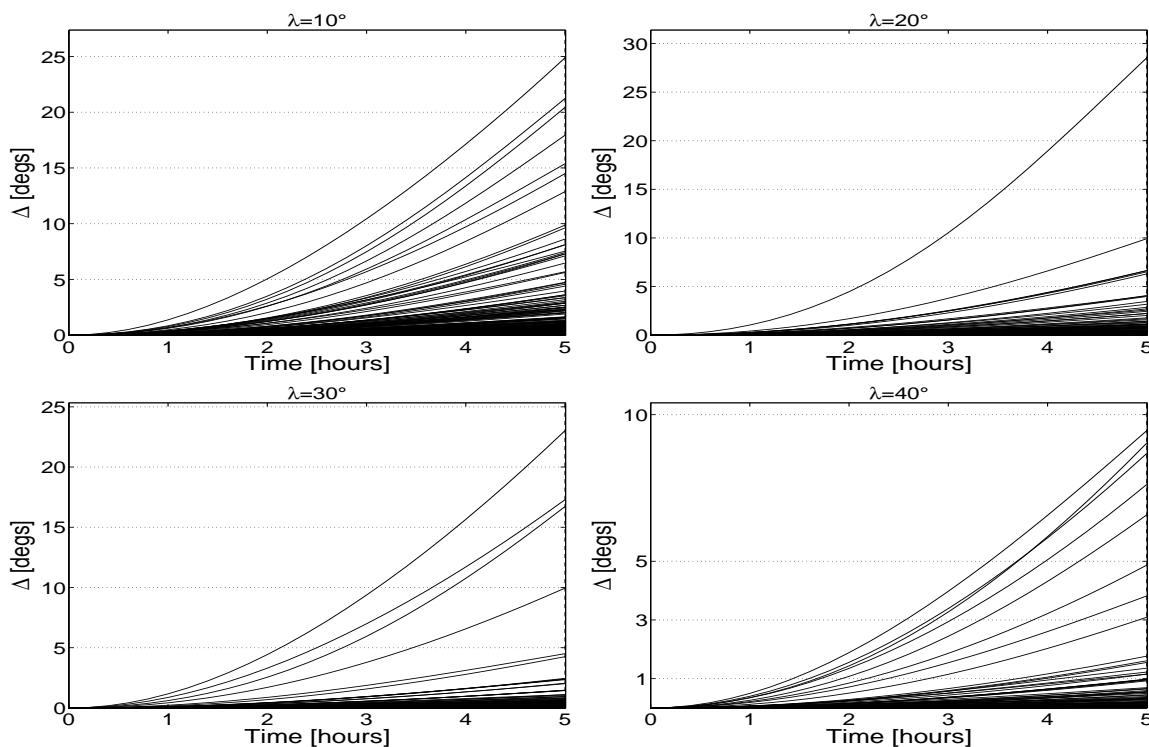


Figure 5.31: Difference Δ between “true” and determined elliptical orbit of a GEO object representing two tracks observed simultaneously from two virtual sites with identical latitude and different longitudes.

Table 5.15: Mean formal errors for the elliptical orbit determination representing two tracks of a GEO object observed simultaneously from two virtual sites with identical latitude and different longitudes.

| λ [°] | a [m] | e | i [°] | Ω [°] | ω [°] | T_0 [s] |
|---------------|-------------------|----------------------|----------------------|--------------|--------------|-------------------|
| 10 | $3.82 \cdot 10^5$ | $2.94 \cdot 10^{-2}$ | $2.27 \cdot 10^{-2}$ | 0.26 | 72.3 | $1.77 \cdot 10^4$ |
| 20 | $2.23 \cdot 10^5$ | $1.52 \cdot 10^{-2}$ | $1.54 \cdot 10^{-2}$ | 0.21 | 54.9 | $1.31 \cdot 10^4$ |
| 30 | $1.82 \cdot 10^5$ | $1.23 \cdot 10^{-2}$ | $1.35 \cdot 10^{-2}$ | 0.19 | 40.3 | $9.66 \cdot 10^3$ |
| 40 | $1.52 \cdot 10^5$ | $1.03 \cdot 10^{-2}$ | $1.27 \cdot 10^{-2}$ | 0.19 | 38.2 | $9.27 \cdot 10^3$ |

Table 5.17 gives the resulting mean formal errors. The errors from two sites separated by 40° in latitude are repeated in the last row for comparison. The results for three sites and separations of 40° in longitude and latitude are about 30% better than for two sites separated by 40° in latitude. The mean formal errors of a , e , ω , and T_0 for $\beta = 40^\circ$ are within the errors for three sites. The orbital plane, however, is better determined with observations from three sites.

We have seen that the improvement resulting from observing an object simultaneously from three sites is marginal compared to simultaneous observations from two sites separated by several ten degrees. It is therefore not recommended to use three telescopes for the acquisition of “secured” orbits. A third telescope could be used more reasonably for other tasks, e.g., follow-up observations of detected objects or perform a survey of another region.

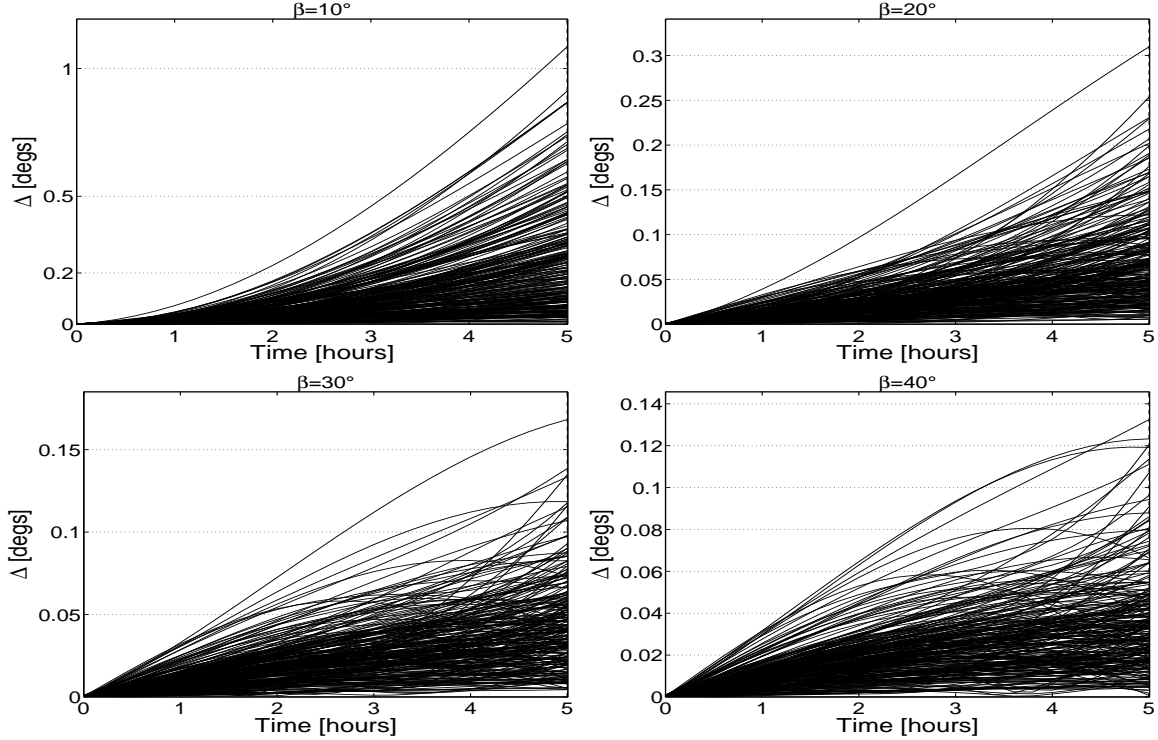


Figure 5.32: Difference Δ between “true” and determined elliptical orbit of a GEO object representing two tracks observed simultaneously from two virtual sites with identical longitude and different latitudes.

Table 5.16: Mean formal errors for the elliptical orbit determination representing two tracks of a GEO object observed simultaneously from two virtual sites with identical longitude and different latitudes.

| β [°] | a [m] | e | i [°] | Ω [°] | ω [°] | T_0 [s] |
|-------------|-------------------|----------------------|----------------------|--------------|--------------|-------------------|
| 10 | $1.59 \cdot 10^5$ | $1.17 \cdot 10^{-2}$ | $1.58 \cdot 10^{-2}$ | 0.27 | 54.3 | $1.31 \cdot 10^4$ |
| 20 | $8.20 \cdot 10^4$ | $5.93 \cdot 10^{-3}$ | $1.34 \cdot 10^{-2}$ | 0.26 | 36.2 | $8.74 \cdot 10^3$ |
| 30 | $5.67 \cdot 10^4$ | $4.08 \cdot 10^{-3}$ | $1.29 \cdot 10^{-2}$ | 0.26 | 26.1 | $6.30 \cdot 10^3$ |
| 40 | $4.46 \cdot 10^4$ | $3.20 \cdot 10^{-3}$ | $1.28 \cdot 10^{-2}$ | 0.25 | 20.5 | $4.92 \cdot 10^3$ |

Follow-up After 1 Hour

The task of observing an object simultaneously from two sites might not be easy to realize. An alternative is to perform the first follow-up observations from a second site. As in Section 5.1, the first follow-up tracks were simulated one hour after the discovery. For comparison, follow-up tracks were also simulated from the main site. The differences Δ between the “true” and the determined elliptical orbits for this case are shown in Figure 5.33. After 5 hours, the differences are still smaller than 3° for all objects.

Elliptical orbits were determined using the first track from the main site together with a follow-up track after one hour observed from one of the other sites. Some outliers still exist for the orbits including follow-up observations from the sites with different longitude (Figure 5.34). But they are less prominent as in Figure 5.31. In general, the differences seem to be smaller than for the simultaneous observations.

Table 5.17: Mean formal errors for the elliptical orbit determination representing three tracks of a GEO object observed simultaneously from three virtual sites with different longitudes and latitudes.

| λ, β [°] | a [m] | e | i [°] | Ω [°] | ω [°] | T_0 [s] |
|----------------------|-------------------|----------------------|----------------------|--------------|--------------|-------------------|
| 10 | $1.05 \cdot 10^5$ | $7.39 \cdot 10^{-3}$ | $9.76 \cdot 10^{-3}$ | 0.16 | 36.2 | $8.71 \cdot 10^3$ |
| 20 | $5.54 \cdot 10^4$ | $3.79 \cdot 10^{-3}$ | $8.11 \cdot 10^{-3}$ | 0.15 | 37.0 | $9.04 \cdot 10^3$ |
| 30 | $3.93 \cdot 10^4$ | $2.67 \cdot 10^{-3}$ | $7.84 \cdot 10^{-3}$ | 0.15 | 16.6 | $4.02 \cdot 10^3$ |
| 40 | $3.17 \cdot 10^4$ | $2.14 \cdot 10^{-3}$ | $7.88 \cdot 10^{-3}$ | 0.16 | 13.4 | $3.23 \cdot 10^3$ |
| $\beta = 40^\circ$ | $4.46 \cdot 10^4$ | $3.20 \cdot 10^{-3}$ | $1.28 \cdot 10^{-2}$ | 0.25 | 20.5 | $4.92 \cdot 10^3$ |

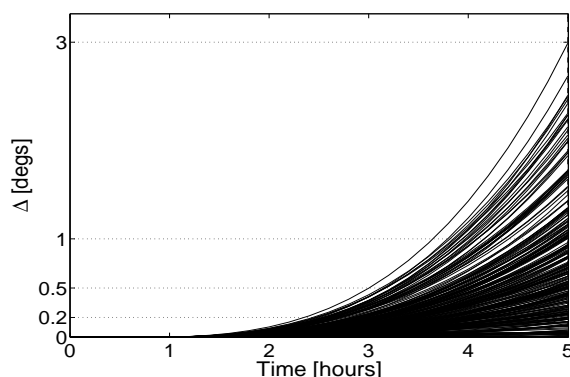


Figure 5.33: Difference Δ between “true” and determined elliptical orbit of a GEO object representing two tracks separated by 1 h observed from a virtual site located at $\lambda = 0^\circ$ and $\beta = 0^\circ$.

In Table 5.18, giving the mean formal errors, we see that the orbital planes are better determined than for the simultaneous observations in Table 5.15. Except for the semi-major axis, the errors are smaller for the follow-ups after 1 hour comparing the same separation between the sites. The inclination is by a factor of 3 better determined. As we have seen in Figure 5.34, the larger error in the semi-major axis is compensated by the improvement of the other elements.

Again, the results are different for the sites with identical longitude and different latitudes. The differences shown in Figure 5.35 are smaller than for the sites with different longitudes, and no outliers are visible. But the difference between the two cases is not as large as for the simultaneous observations. Interestingly, the differences are larger for an observation arc of one hour than for the simultaneous observations when comparing only the results for the sites with different latitude. This is an indication that the observation geometry is better for the simultaneous observations.

Table 5.19 shows that the orbital plane is not as well determined for two sites with different latitudes as for observations from one site (first row). Furthermore, the plane is not as well determined as for the sites with identical latitude and different longitudes. The other elements, however, are by a factor of about two better determined. Taking into account the results from the Figures 5.34 and 5.35 we can conclude that the difference between the “true” and the determined orbit is dominated by the accuracy of the orbital shape (a and e) together with T_0 rather than by the accuracy of the orbital plane. Comparing the mean formal errors for an observation arc of one hour with those for observations at the same epoch (Table 5.16) we see that the errors for Ω are larger, but the error for i are almost identical. I.e., the orbital plane

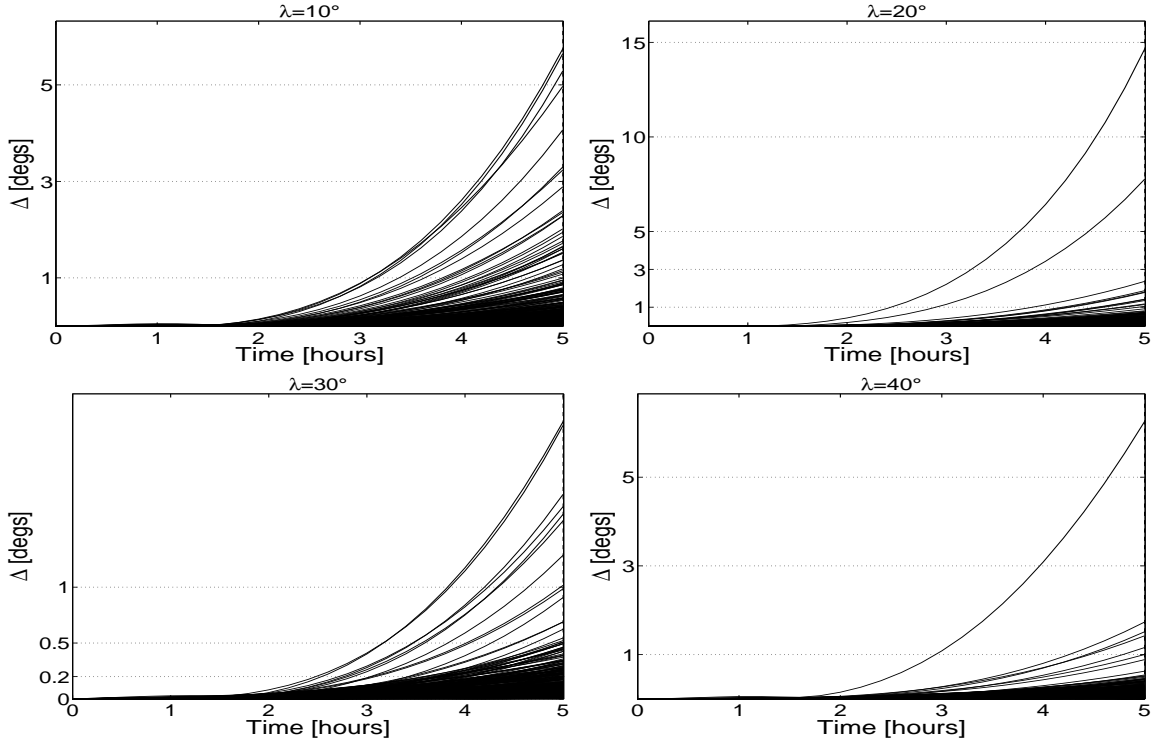


Figure 5.34: Difference Δ between “true” and determined elliptical orbit of a GEO object representing one track observed from the main site and one follow-up track after 1 h observed from virtual sites with identical latitude and different longitudes.

Table 5.18: Mean formal errors for the elliptical orbit determination representing the discovery track of a GEO object observed from the main site and the follow-up after 1 h. The follow-up observations were simulated for virtual sites with identical latitude and different longitudes.

| λ [°] | a [m] | e | i [°] | Ω [°] | ω [°] | T_0 [s] |
|---------------|-------------------|----------------------|----------------------|----------------------|--------------|-------------------|
| 0 | $1.64 \cdot 10^6$ | $2.28 \cdot 10^{-2}$ | $8.39 \cdot 10^{-3}$ | 0.17 | 43.8 | $9.96 \cdot 10^3$ |
| 10 | $1.39 \cdot 10^6$ | $2.00 \cdot 10^{-2}$ | $5.16 \cdot 10^{-3}$ | 0.12 | 37.2 | $8.56 \cdot 10^3$ |
| 20 | $7.12 \cdot 10^5$ | $9.88 \cdot 10^{-3}$ | $3.66 \cdot 10^{-3}$ | $9.96 \cdot 10^{-2}$ | 23.4 | $5.33 \cdot 10^3$ |
| 30 | $5.21 \cdot 10^5$ | $7.09 \cdot 10^{-3}$ | $3.25 \cdot 10^{-3}$ | $9.32 \cdot 10^{-2}$ | 21.8 | $5.02 \cdot 10^3$ |
| 40 | $3.68 \cdot 10^5$ | $4.66 \cdot 10^{-3}$ | $3.05 \cdot 10^{-3}$ | $8.23 \cdot 10^{-2}$ | 18.4 | $4.23 \cdot 10^3$ |

is slightly worse determined. The errors for the elements e , ω , and T_0 , on the other hand, are slightly smaller. The larger differences in Figure 5.35 compared to Figure 5.32 can mainly be explained by the larger errors in the semi-major axes.

When observing from two sites, the accuracies of the orbits depend on the separations in longitude and latitude between the two sites. A larger separation mostly reduces the errors. If the separation of the positions is mainly in longitude, follow-up observations after one hour lead to a better result than simultaneous observations. In the other case, a larger separation in latitude, a better result can be achieved with simultaneous observations.

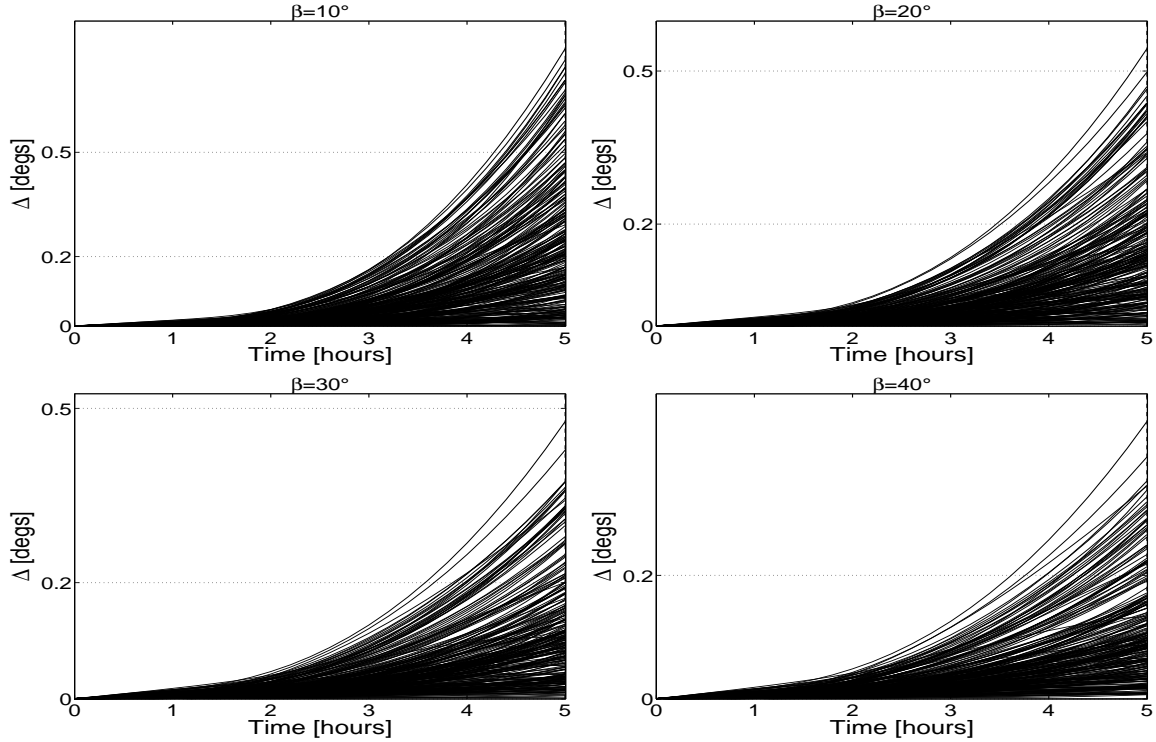


Figure 5.35: Difference Δ between “true” and determined elliptical orbit of a GEO object representing one track observed from the main site and one follow-up track after 1 h observed from virtual sites with identical longitude and different latitudes.

Table 5.19: Mean formal errors for the elliptical orbit determination representing the discovery track of a GEO object observed from the main site and the follow-up after 1 h. The follow-up observations were simulated for virtual sites with identical longitude and different latitudes.

| β [°] | a [m] | e | i [°] | Ω [°] | ω [°] | T_0 [s] |
|-------------|-------------------|----------------------|----------------------|--------------|--------------|-------------------|
| 0 | $1.64 \cdot 10^6$ | $2.28 \cdot 10^{-2}$ | $8.39 \cdot 10^{-3}$ | 0.17 | 43.8 | $9.96 \cdot 10^3$ |
| 10 | $5.22 \cdot 10^5$ | $6.60 \cdot 10^{-3}$ | $1.24 \cdot 10^{-2}$ | 0.86 | 21.5 | $4.80 \cdot 10^3$ |
| 20 | $2.73 \cdot 10^5$ | $3.46 \cdot 10^{-3}$ | $1.26 \cdot 10^{-2}$ | 0.49 | 15.4 | $3.53 \cdot 10^3$ |
| 30 | $1.86 \cdot 10^5$ | $2.47 \cdot 10^{-3}$ | $1.26 \cdot 10^{-2}$ | 0.42 | 11.6 | $2.89 \cdot 10^3$ |
| 40 | $1.43 \cdot 10^5$ | $2.01 \cdot 10^{-3}$ | $1.25 \cdot 10^{-2}$ | 0.38 | 9.7 | $2.25 \cdot 10^3$ |

Development of the Formal Errors

The previous section showed that the accuracy of the orbit does not necessarily improve with a longer observation arc. It does improve if the observations are performed from one site. Using two sites, the accuracy of the orbits can be worse when the observation tracks are separated by one hour compared to observations performed at the same epoch. The development of the mean formal errors with longer gaps between the observation tracks is studied in the following.

For this purpose, three of the virtual sites were selected, namely the main site with $\lambda = 0^\circ$, $\beta = 0^\circ$, one site with a large separation in longitude ($\lambda = 40^\circ$, $\beta = 0^\circ$), and one with a large separation in latitude

($\lambda = 0^\circ$, $\beta = 40^\circ$). The first observation tracks were in all cases assumed to be acquired from the main site. A second observation track was simulated for each of the three sites after different time gaps. Elliptical orbits were determined from the two tracks.

The mean formal errors σ for the six orbital elements plotted against the time gap Δt between the two tracks are shown in Figure 5.36. To avoid misleading structures due to outliers the mean formal errors were determined without the largest 5% and the smallest 5% of the formal errors. The errors for the case where both tracks were observed from the main site are marked with a circle connected with a solid line. They are from now on called “ Δ -errors”. There are no data points at $\Delta t = 0$ hours as no reasonable elliptical orbit can be determined from such a short observation arc observed from one site. Those mean formal errors where the second track was observed from the site with a large separation in latitude are marked with \times connected with a dotted line (“ $\Delta\beta$ -errors”). The + symbols connected with a dashed line mark the errors for the sites with different longitude (“ $\Delta\lambda$ -errors”). Note that the scale of the y-axis is logarithmic.

The plot on the top left shows the errors for the semi-major axis. As expected, the Δ -errors improve with longer observation arcs. The $\Delta\beta$ -errors and the $\Delta\lambda$ -errors get larger at the beginning and then improve after 2 hours and 1 hour respectively. Both converge to the Δ -errors after a few hours. The errors are almost identical for observation arcs longer than four hours. Interestingly, the $\Delta\beta$ -errors for $\Delta t = 0$ hours are almost as small as the Δ -errors for an arc of six hours.

The errors of the eccentricity show a similar development as the errors of the semi-major axis. The main difference is, that the errors for simultaneous observations are larger than for an observation arc of one hour. The $\Delta\beta$ -errors for $\Delta t = 0$ hours are of the same magnitude as the Δ -errors for an arc of three hours.

The accuracies of the orbital planes are shown in the two plots in the middle. The errors for the inclination are plotted on the left. The Δ -errors show again a steadily improvement. The $\Delta\lambda$ -errors are clearly smaller for an arc of one hour and slightly smaller for an arc of two hours compared to the Δ -errors. From there on, the accuracy is better for the Δ -errors. The $\Delta\beta$ -errors are always clearly larger than the others.

The plot for the errors in the right ascension of ascending node looks similar. The only difference is that the Δ -errors are already smaller than the $\Delta\lambda$ -errors after two hours.

The plots for ω and T_0 look very similar than the one for the eccentricity. The Δ -errors, however, are slightly larger than the others for an arc longer than three hours.

The above comparison showed that an arc of about 3 – 4 hours of observations from one single site is needed to get the same accuracy of the orbit as for simultaneous observations from two sites separated by 40° in latitude. A separation in longitude, which is normally realized in a space surveillance system, has about the same impact. From this, one can conclude that two instruments located at two different sites should be used to perform simultaneous observations during the acquisition of a “secured” orbit. A shorter observation arc would then be needed to be able to recover the object during the following night. But the loss of observation time has also to be considered as the second instrument cannot be used for other tasks. Another restriction is that the available observation time per night is shorter as the object has to be visible from both sites during the night. Three sites uniformly distributed in longitude would then not be enough to cover the whole GEO belt.

In general, the errors converge for longer observation arcs. This means that after a few hours the selection of the site has no big influence on the accuracy of the orbit. In that case, the site with the best observation

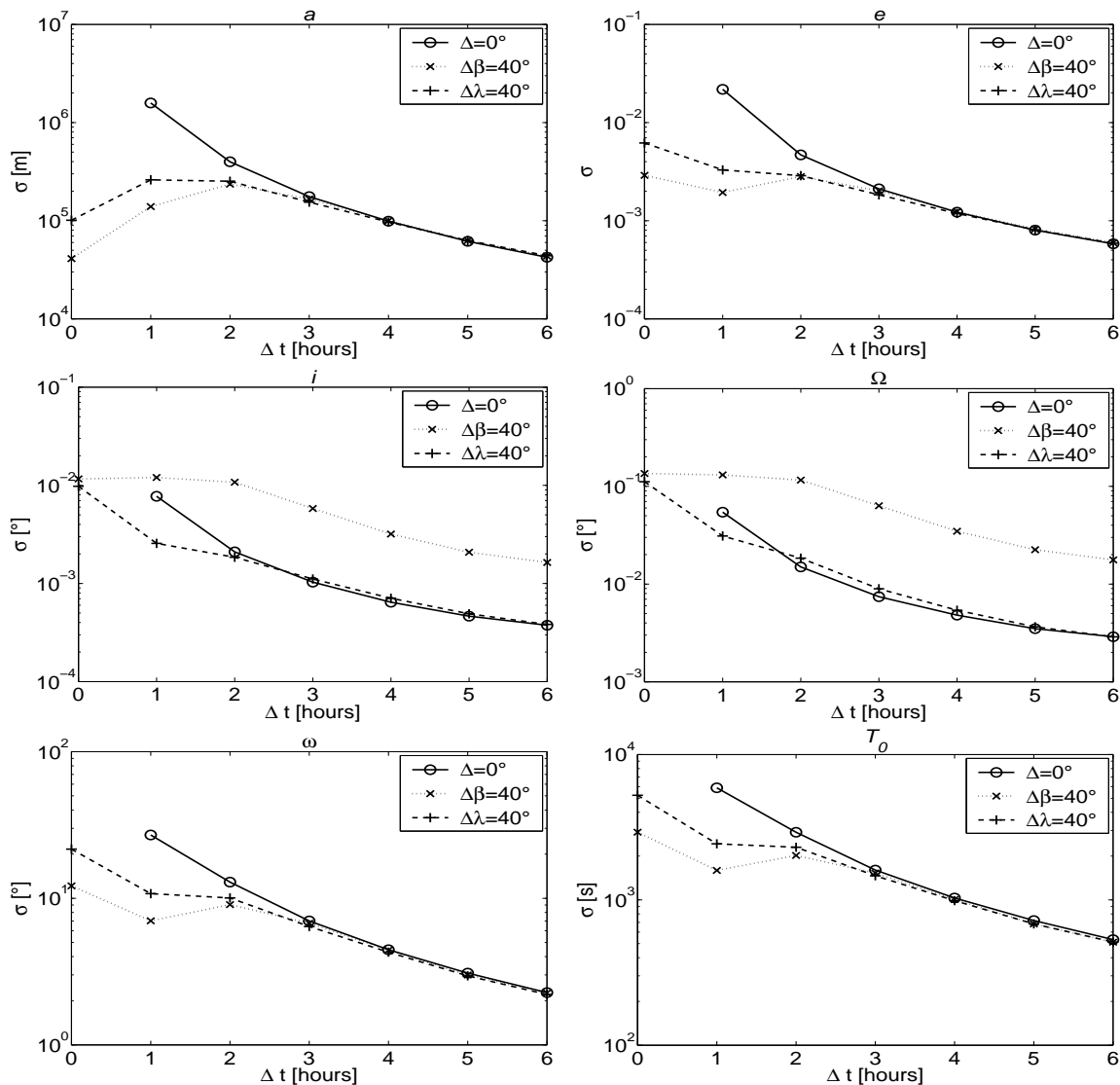


Figure 5.36: Mean formal errors σ for the elliptical orbit determination representing two tracks of a GEO object separated by Δt observed from one virtual site (\circ) or two virtual sites with identical longitude and different latitude (\times) and identical latitude and different longitude ($+$). The scale of the y-axis is logarithmic.

conditions, namely the best phase angle, should be selected if the objects is visible from more than one site.

Dependency on the Satellite Position

As we have seen in the previous sections, the orbits are better determined for two sites with different latitudes than with different longitudes. At first thought, this does not seem obvious, as the angle between the sites is the same. But the angle between the sites as seen from the objects does not have to be the

same. In our case, it is identical for objects with the same angle in longitude as in latitude, i.e., the positions fall in between the longitudes and latitudes of the selected sites. For debris populations that are uniformly distributed around the Earth, e.g., the LEO population, the situation is the same for the sites with different longitudes as for the sites with different latitudes and the errors should be of the same magnitude. The situation, however, is different for the GEO and the GTO populations. The GEO objects are distributed within a narrow band between $+17^\circ$ and -17° latitude. The average angle under which a site is seen from GEO objects is not the same for a site on the equator as for a site with a latitude different from 0° . In Section 5.2, only GTO objects with an inclination smaller than 30° were selected. This selection includes the majority of the GTO objects. The GTO objects are therefore distributed within a 60° -wide band around 0° latitude.

To demonstrate the impact of the object position on the orbital accuracy, the mean formal errors σ of the semi-major axis are plotted against the longitude λ_o of the object (Figure 5.37). The left column shows the plots for the $\Delta\lambda$ -errors, while the $\Delta\beta$ -errors are shown on the right. The length of the observation arc is the same for plots in the same row. The observations for the plots at the top were acquired simultaneously. The rows below are for observation arcs of 1 hour, 2 hours, and 6 hours.

Let us first look at the $\Delta\beta$ -errors on the right side. In the plot at the top, a minimum can be found close to $\lambda_o = 0^\circ$. The errors in this range are mostly below $\sigma = 50\,000$ m. The largest errors are around $\lambda_o = -70^\circ$, $\lambda_o = 70^\circ$, and $\lambda_o = 140^\circ$, where they reach almost $200\,000$ m. No clear minimum can be found in the three plots below. The distribution of the errors is uniform, with small peaks around $\lambda_o = 140^\circ$.

The first three plots for the $\Delta\lambda$ -errors look very different than those for the $\Delta\beta$ -errors. Two strong peaks, one for $\lambda_o > 100^\circ$ and one for $\lambda_o < -50^\circ$, are visible. In the plot for $\Delta t = 0$ hours, the peaks are located at $\lambda_o = -66.3^\circ$ and $\lambda_o = 106.5^\circ$. The errors are nearly symmetrically distributed around $\lambda_o = 20^\circ$. Objects with $\lambda_o = 20^\circ$ are located exactly in the middle between the two sites. One can easily see that the observation geometry is ideal for these objects. Therefore, we had to expect the smallest errors for $\lambda_o = 20^\circ$. Figure 5.38 shows that this is really the case. The same data points as in the top left plot in Figure 5.37 are plotted, but with a logarithmic scale for the y-axis. The minimum is clearly around $\lambda_o = 20^\circ$.

The distance between the peaks depends on the separation between the sites. It is larger for a larger separation in longitude between the sites. This is visualized with Figure 5.39, which shows the Earth and part of a GEO as seen from above. It is assumed that the two sites O_1 and O_2 as well as the orbit of the GEO object lie in the equator plane. The peaks result when an object is observed with the same direction from O_1 and O_2 (remember that a transparent Earth is assumed), i.e., when a singularity results. The longitude λ_o of such an object can then be determined with

$$\lambda_o = \frac{\Delta\lambda}{2} \pm \arccos\left(\frac{h}{r_{GEO}}\right), \quad (5.3)$$

$$\text{with } h = r_E \cdot \cos\frac{\Delta\lambda}{2}. \quad (5.4)$$

r_e and r_{GEO} are the radii of the Earth and of the GEO object respectively. For a separation of $\Delta\lambda = 40^\circ$ between the sites the resulting longitude is $\lambda_o = 20^\circ \pm 81.8^\circ$. This means that we expect the peaks at -61.8° and at 101.8° . This is approximately where the peaks are located in the plot.

In Figure 5.37, the distance is wider between the peaks for $\Delta t = 1$ h and $\Delta t = 2$ h. The cause are also singularities, but the situation is more complex than for simultaneous observations. Further, the errors

around $\lambda_o = 20^\circ$ are getting larger. This means that for an object that is positioned between or close to the two sites the orbit is better determined with simultaneous observations than with observations separated by a few hours.

The two plots at the bottom of Figure 5.37 are nearly identical. One has to look closely to see the small differences. This result had to be expected after consulting Figure 5.36. Both plots show neither a peak nor a minimum. The accuracies of these orbits are dominated by the length of the observation arc rather than by the location of the sites.

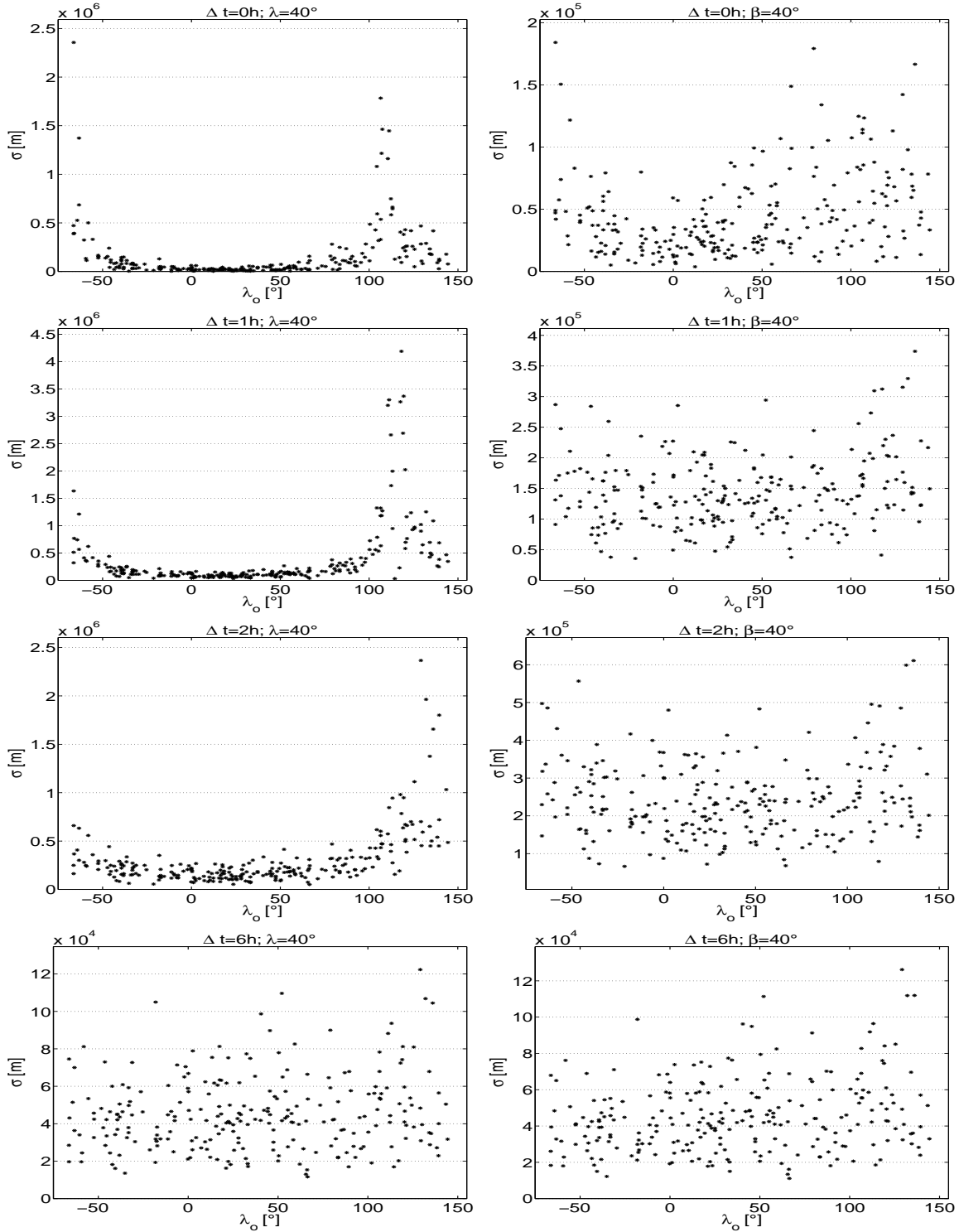


Figure 5.37: Mean formal errors σ for the semi-major axis of the elliptical orbit determination representing two tracks of a GEO object separated by 0 h, 1 h, 2 h, and 6 h observed from two virtual sites with identical latitude and different longitude (left) and identical longitude and different latitude (right) plotted against the longitude λ_o of the objects.

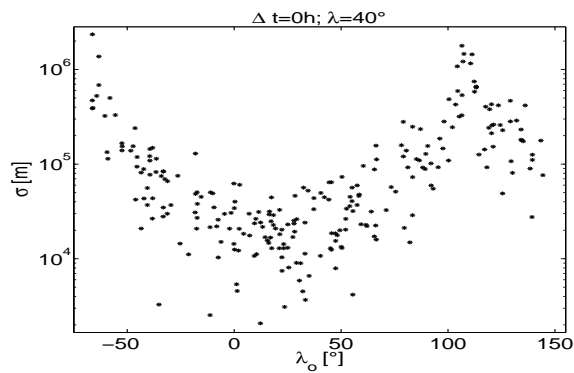


Figure 5.38: Mean formal errors σ for the semi-major axis of the elliptical orbit determination representing two tracks of a GEO object observed at the same epoch from two virtual sites with identical latitude $\beta = 0^\circ$ and a separation in longitude of $\Delta\lambda = 40^\circ$. The scale of the y-axis is logarithmic.

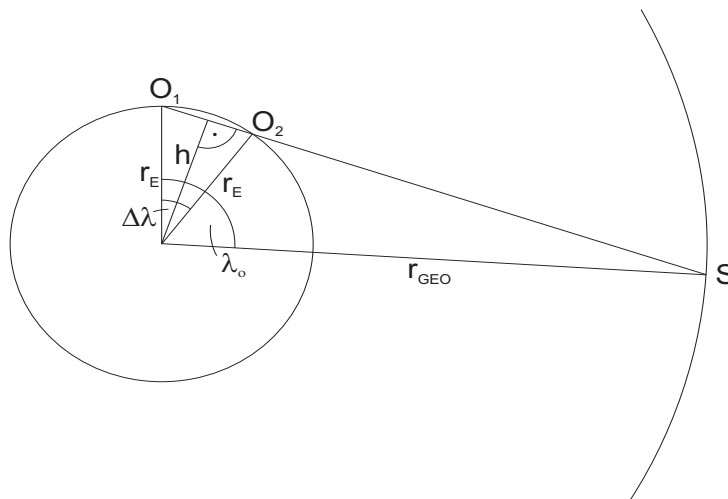


Figure 5.39: Longitude λ_o of a GEO satellite S that is seen in the same direction from two observers O_1 and O_2 .

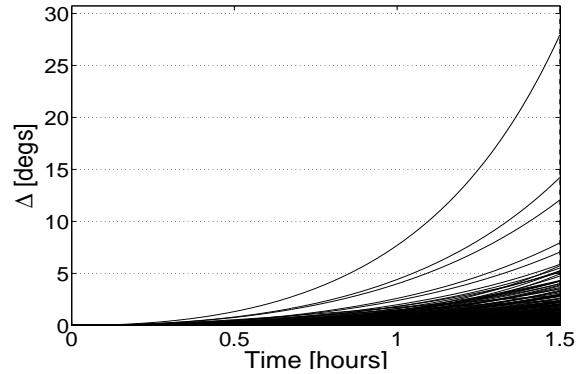


Figure 5.40: Difference Δ between “true” and determined circular orbit of a GTO object representing one track observed from a virtual site located at $\lambda = 0^\circ$ and $\beta = 0^\circ$.

5.3.2 GTO

The orbits simulated for Section 5.2 were used.

Simultaneous Observations

As for the GEO objects, simultaneous observations from two sites were studied in a first step. For comparison, circular orbits were determined from single tracks observed from the main site. Figure 5.40 shows the differences Δ between the “true” and the determined orbit for this case. For most objects, the differences are less than 5° after 1.5 hours. Nevertheless, some outliers have differences of up to 28° .

For each of the other sites, an observation track was simulated at the same epoch as the one observed from the main site. Elliptical orbits were determined using the track from the main site together with the observations from one of the other tracks.

First, we will look at the sites with identical latitude and different longitudes. Figure 5.41 shows the differences Δ for the four cases. As in Figure 5.40, some outliers can be seen in each of the four plots, but they are much smaller. In general, the differences in the plots in Figure 5.41 are smaller compared to the ones in Figure 5.40. But it is hard to tell in which of the four plots the differences are the smallest.

The outliers also reflect in the mean formal errors of the eccentricity (Table 5.20). The value resulting for a separation of 40° in latitude is slightly larger than the one for a separation of 30° , although an improvement would be expected. When we determine the mean formal errors without the 5% with the largest values then the errors are smaller for $\lambda = 40^\circ$. The shape of the orbit, i.e., a and e , is better determined compared to the GEO objects (Table 5.15), while the orbital plane is slightly worse determined.

Figure 5.42 shows that like for the GEO objects, the result is much better when the latitude is varied instead of the longitude. Only one outlier can be seen in the upper left plot and none in the others, i.e., the orbital elements for all objects could be well determined. Further, the three plots for $\beta = 20^\circ$, $\beta = 30^\circ$, and $\beta = 40^\circ$ look almost identical. The differences are by a factor of about 100 better than those resulting for observations from one site only.

The mean formal errors for the sites with different latitudes (Table 5.21) are much smaller than for the

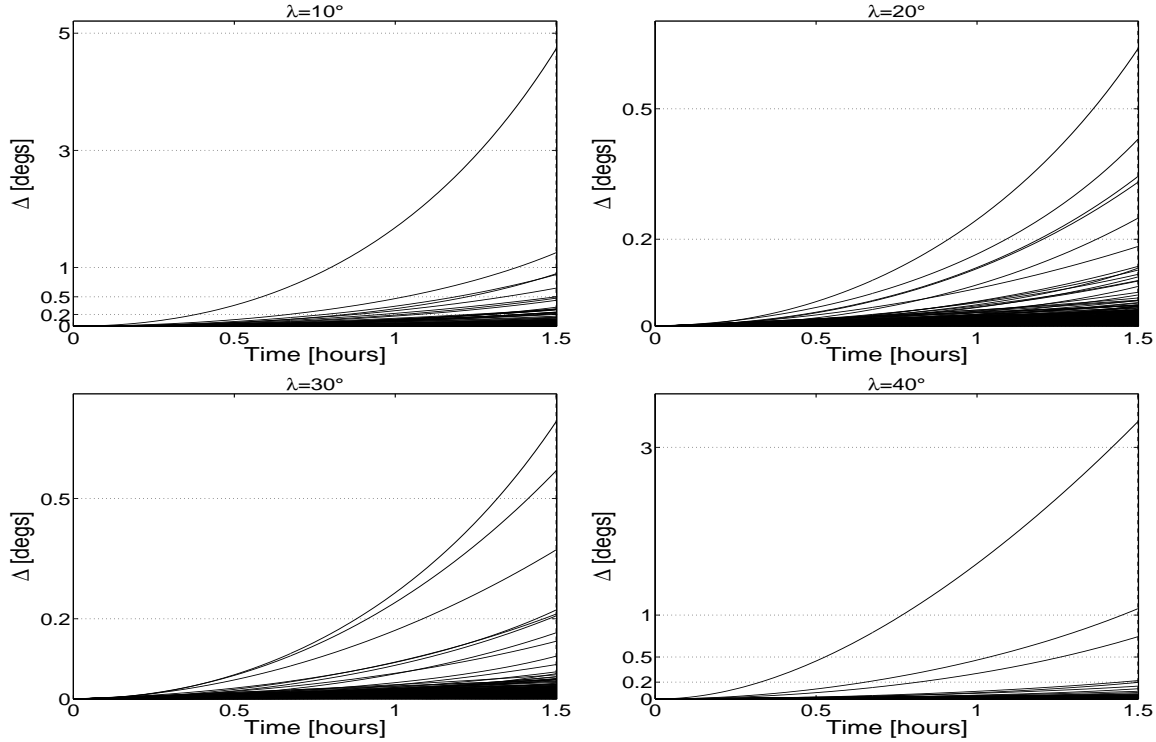


Figure 5.41: Difference Δ between “true” and determined elliptical orbit of a GTO object representing two tracks observed simultaneously from two virtual sites with identical latitude and different longitudes.

Table 5.20: Mean formal errors for the elliptical orbit determination representing two tracks of a GTO object observed simultaneously from two virtual sites with identical latitude and different longitudes.

| λ [°] | a [m] | e | i [°] | Ω [°] | ω [°] | T_0 [s] |
|---------------|-------------------|----------------------|----------------------|--------------|--------------|-------------------|
| 10 | $1.63 \cdot 10^5$ | $4.35 \cdot 10^{-3}$ | $4.94 \cdot 10^{-2}$ | 0.30 | 1.46 | $4.55 \cdot 10^2$ |
| 20 | $9.00 \cdot 10^4$ | $2.36 \cdot 10^{-3}$ | $3.04 \cdot 10^{-2}$ | 0.22 | 0.83 | $2.48 \cdot 10^2$ |
| 30 | $7.66 \cdot 10^4$ | $1.90 \cdot 10^{-3}$ | $2.51 \cdot 10^{-2}$ | 0.20 | 0.69 | $2.00 \cdot 10^2$ |
| 40 | $6.61 \cdot 10^4$ | $1.95 \cdot 10^{-3}$ | $2.24 \cdot 10^{-2}$ | 0.20 | 0.55 | $1.52 \cdot 10^2$ |

sites with different longitudes (Table 5.20). An exception is again the orbital plane. While the inclination is a little bit better determined for the sites with different latitudes, the right ascension of the ascending node is slightly worse determined.

As for the GEO objects, the best result for GTO objects could be achieved with simultaneous observations from two sites with a large separation in latitude. In Table 5.22, the result for a separation of 40° in latitude is compared with the mean formal errors for simultaneous observations from three sites. Again, the same separation from the main site in longitude as in latitude was assumed. Other than for the GEO objects, the inclination does not improve much with three sites. For Ω , however, a clear improvement can be seen. The errors of the other elements are of the same magnitude for the observations from three sites as for two sites with different latitudes. Again, simultaneous observations from three sites do not

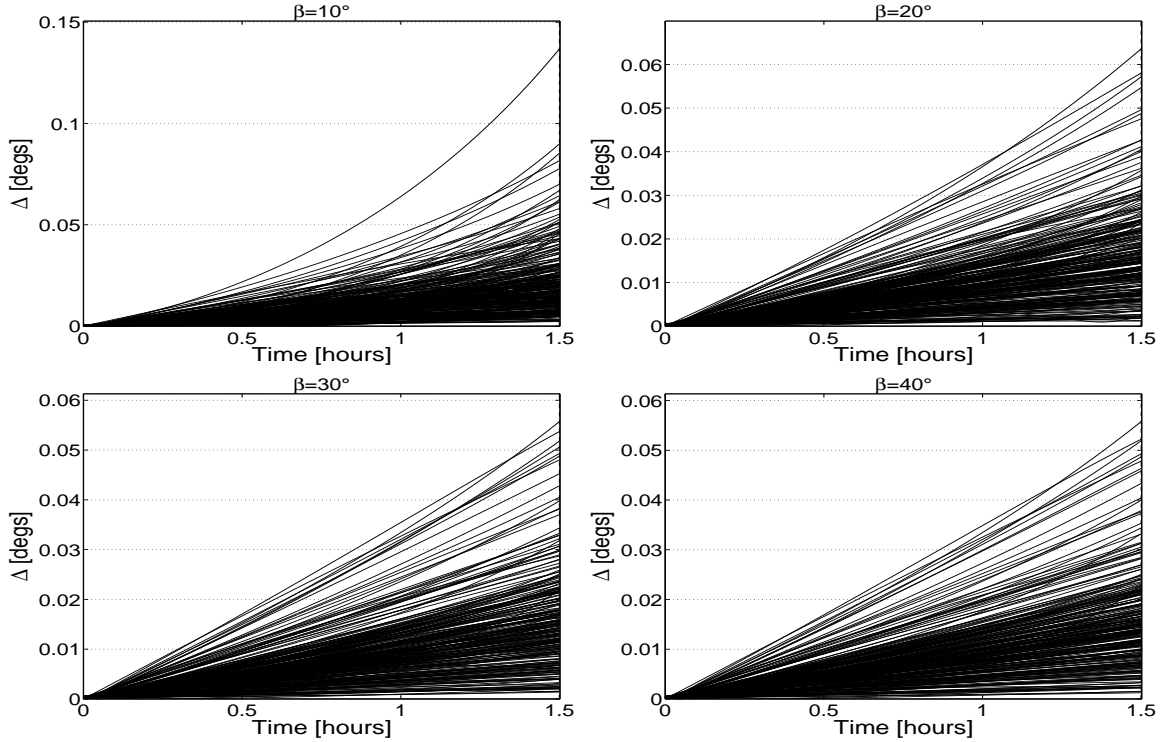


Figure 5.42: Difference Δ between “true” and determined elliptical orbit of a GTO object representing two tracks observed simultaneously from two virtual sites with identical longitude and different latitudes.

Table 5.21: Mean formal errors for the elliptical orbit determination representing two tracks of a GTO object observed simultaneously from two virtual sites with identical longitude and different latitudes.

| β [°] | a [m] | e | i [°] | Ω [°] | ω [°] | T_0 [s] |
|-------------|-------------------|----------------------|----------------------|--------------|--------------|-------------------|
| 10 | $7.42 \cdot 10^4$ | $2.00 \cdot 10^{-3}$ | $3.44 \cdot 10^{-2}$ | 0.29 | 0.89 | $2.56 \cdot 10^2$ |
| 20 | $3.80 \cdot 10^4$ | $1.02 \cdot 10^{-3}$ | $2.42 \cdot 10^{-2}$ | 0.25 | 0.51 | $1.30 \cdot 10^2$ |
| 30 | $2.61 \cdot 10^4$ | $7.04 \cdot 10^{-4}$ | $2.16 \cdot 10^{-2}$ | 0.25 | 0.41 | 88.10 |
| 40 | $2.04 \cdot 10^4$ | $5.50 \cdot 10^{-4}$ | $2.06 \cdot 10^{-2}$ | 0.24 | 0.36 | 67.92 |

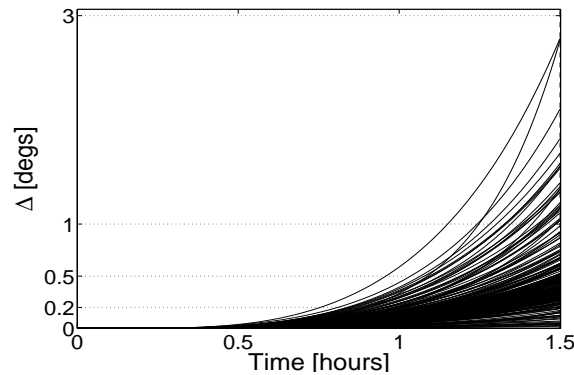
improve the orbits much compared to simultaneous observations from two sites.

Follow-up After 0.25 Hours

As discussed for the GEO objects, an instrument on a second site can also be used to perform the first follow-up observations instead of observing the objects simultaneously. We take the result from Section 5.2.2 for a narrow FOV and simulate the follow-up tracks 0.25 h after the discovery. The follow-up tracks were also simulated for the main site to compare the results. Figure 5.43 shows the differences Δ between the “true” and the determined elliptical orbits for the latter. The differences are smaller than 3° after 1.5 hours for all objects.

Table 5.22: Mean formal errors for the elliptical orbit determination representing three tracks of a GTO object observed simultaneously from three virtual sites with different longitudes and latitudes.

| λ, β [°] | a [m] | e | i [°] | Ω [°] | ω [°] | T_0 [s] |
|----------------------|-------------------|----------------------|----------------------|--------------|--------------|-------------------|
| 10 | $4.83 \cdot 10^4$ | $1.29 \cdot 10^{-3}$ | $2.11 \cdot 10^{-2}$ | 0.17 | 0.53 | $1.58 \cdot 10^2$ |
| 20 | $2.51 \cdot 10^4$ | $6.70 \cdot 10^{-4}$ | $1.48 \cdot 10^{-2}$ | 0.15 | 0.31 | 80.12 |
| 30 | $1.76 \cdot 10^4$ | $4.69 \cdot 10^{-4}$ | $1.31 \cdot 10^{-2}$ | 0.15 | 0.25 | 54.82 |
| 40 | $1.40 \cdot 10^4$ | $3.73 \cdot 10^{-4}$ | $1.52 \cdot 10^{-2}$ | 0.15 | 0.22 | 42.63 |
| $\beta = 40^\circ$ | $2.04 \cdot 10^4$ | $5.50 \cdot 10^{-4}$ | $2.06 \cdot 10^{-2}$ | 0.24 | 0.36 | 67.92 |


 Figure 5.43: Difference Δ between “true” and determined elliptical orbit of a GTO object representing two tracks separated by 0.25 h observed from a virtual site located at $\lambda = 0^\circ$ and $\beta = 0^\circ$.

The observation track from the main site together with the follow-up track from one of the other sites were used to determine elliptical orbits. The differences Δ for the sites with different longitudes are shown in Figure 5.44. The result for all four cases is clearly better than in Figure 5.43. Some outliers can be seen for $\lambda = 20^\circ$ and $\lambda = 30^\circ$. The outliers in these plots and the ones in Figure 5.41 make it difficult to compare the two figures.

As the outliers also have an influence on the mean formal errors, a comparison of the Tables 5.23 and 5.20 can only give some hints on which orbits are more accurate. The errors are a little bit smaller for a gap of 0.25 h between the observation tracks. This is also true for $\lambda = 20^\circ$ and $\lambda = 30^\circ$, although the differences for the outliers are smaller for the simultaneous observations. From this we can conclude that the orbits are better determined when the second track is observed after a short time interval.

Table 5.23 gives also the mean formal errors for follow-up observations from the main site ($\lambda = 0^\circ$). Except for the orbital plane, the errors are by a factor of about 10 larger than for different sites.

The results for the sites with identical longitude and different latitudes are shown in Figure 5.45. They are again better than for the sites with different longitudes, but less significant than for the simultaneous observations. When comparing the results for a gap of 0.25 h with the results for simultaneous observations in Figure 5.42 it seems that the orbits are better determined for the later case. But a closer look shows that the differences after half an hour are smaller for the first case. It is therefore hard to decide which orbits are better.

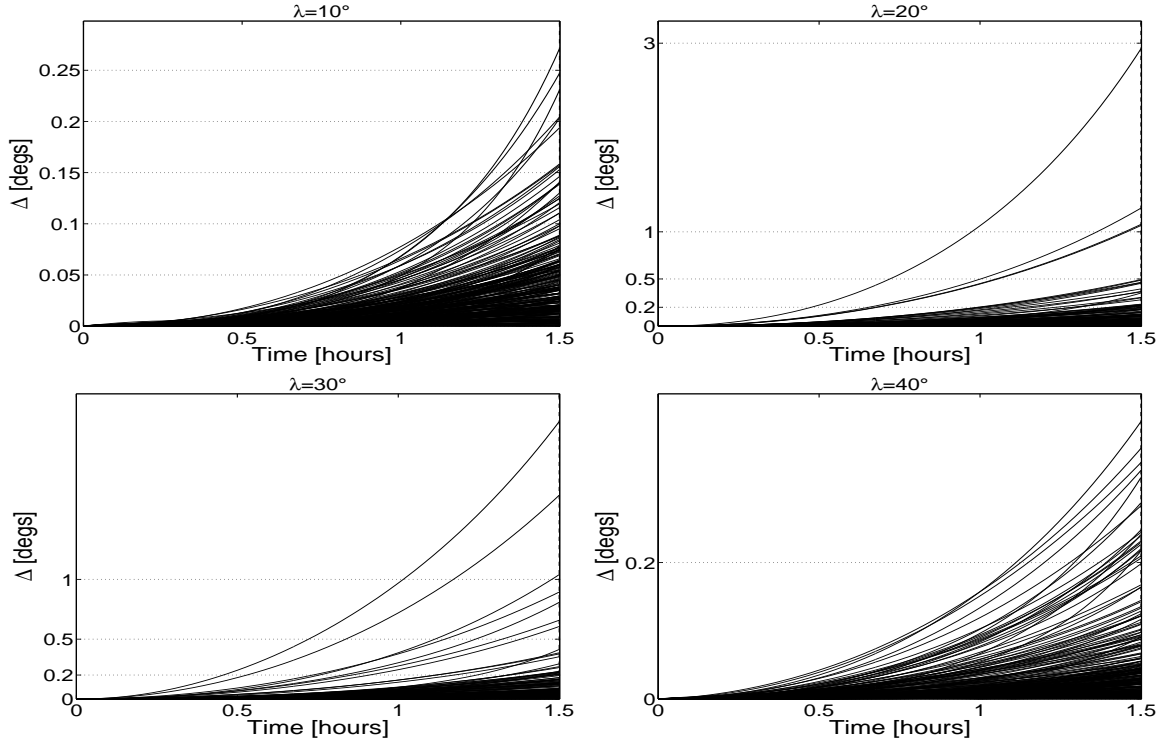


Figure 5.44: Difference Δ between “true” and determined elliptical orbit of a GEO object representing one track observed from the main site and one follow-up track after 0.25 h observed from virtual sites with identical latitude and different longitudes.

Table 5.23: Mean formal errors for the elliptical orbit determination representing the discovery track of a GTO object observed from the main site and the follow-up after 0.25 h. The follow-up observations were simulated for virtual sites with identical latitude and different longitudes.

| λ [°] | a [m] | e | i [°] | Ω [°] | ω [°] | T_0 [s] |
|---------------|-------------------|----------------------|----------------------|----------------------|--------------|-------------------|
| 0 | $6.75 \cdot 10^5$ | $2.79 \cdot 10^{-2}$ | $2.55 \cdot 10^{-2}$ | 0.15 | 6.37 | $2.95 \cdot 10^3$ |
| 10 | $8.47 \cdot 10^4$ | $1.80 \cdot 10^{-3}$ | $1.55 \cdot 10^{-2}$ | $8.52 \cdot 10^{-2}$ | 0.37 | $1.48 \cdot 10^2$ |
| 20 | $7.10 \cdot 10^4$ | $1.90 \cdot 10^{-3}$ | $1.97 \cdot 10^{-2}$ | 0.14 | 0.59 | $2.36 \cdot 10^2$ |
| 30 | $6.73 \cdot 10^4$ | $1.62 \cdot 10^{-3}$ | $1.64 \cdot 10^{-2}$ | 0.13 | 0.51 | $1.97 \cdot 10^2$ |
| 40 | $5.20 \cdot 10^4$ | $1.24 \cdot 10^{-3}$ | $1.38 \cdot 10^{-2}$ | $8.83 \cdot 10^{-2}$ | 0.35 | $1.30 \cdot 10^2$ |

This is underlined by the comparison of the mean formal errors. The errors in Table 5.24 are of the same magnitude as in Table 5.21. An exception is Ω , which is clearly better determined with simultaneous observations.

For GTO objects, observations from two sites do improve the accuracies of the orbits. A larger separation between the two sites leads to a better result, but the effect is not as large as for the GEO objects. For a separation in longitude, follow-up observations after a short time interval give a better result than simultaneous observations. Simultaneous observations lead to more accurate orbits if the separation between the two sites is mainly in latitude.

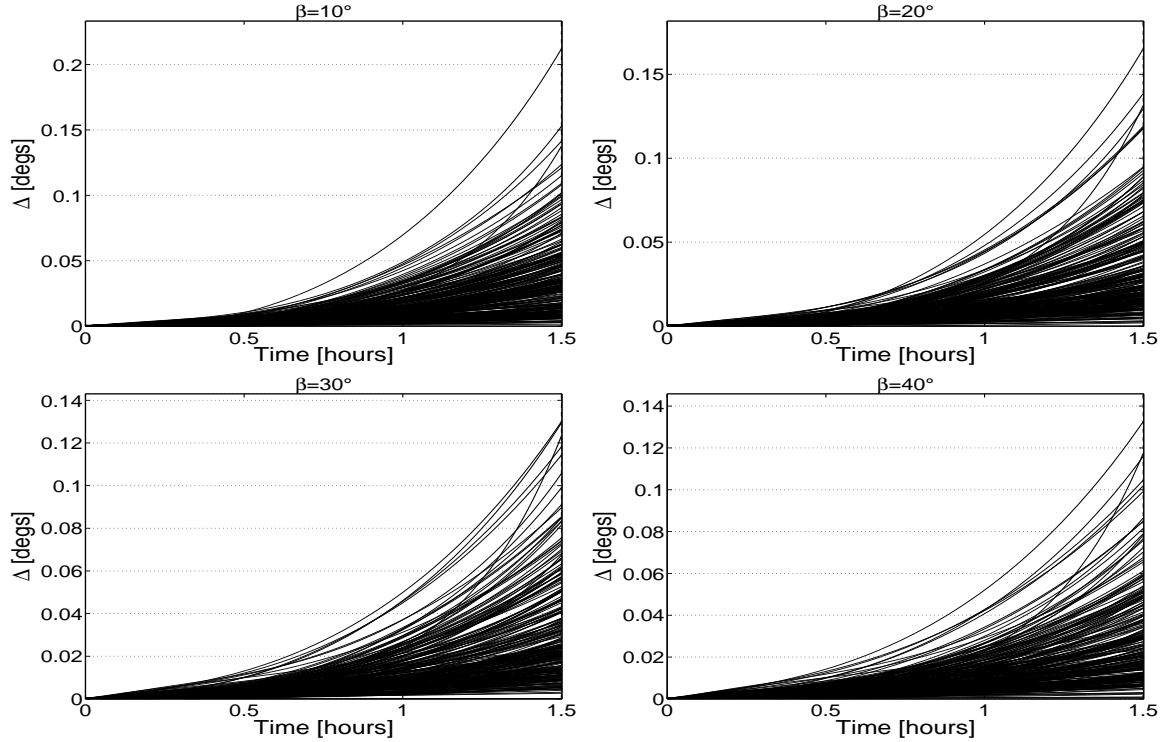


Figure 5.45: Difference Δ between “true” and determined elliptical orbit of a GEO object representing one track observed from the main site and one follow-up track after 0.25 h observed from virtual sites with identical longitude and different latitudes.

Table 5.24: Mean formal errors for the elliptical orbit determination representing the discovery track of a GTO object observed from the main site and the follow-up after 0.25 h. The follow-up observations were simulated for virtual sites with identical longitude and different latitudes.

| β [°] | a [m] | e | i [°] | Ω [°] | ω [°] | T_0 [s] |
|-------------|-------------------|----------------------|----------------------|--------------|--------------|-------------------|
| 0 | $6.75 \cdot 10^5$ | $2.79 \cdot 10^{-2}$ | $2.55 \cdot 10^{-2}$ | 0.15 | 6.37 | $2.95 \cdot 10^3$ |
| 10 | $5.23 \cdot 10^4$ | $1.16 \cdot 10^{-3}$ | $2.35 \cdot 10^{-2}$ | 0.37 | 0.58 | $1.16 \cdot 10^2$ |
| 20 | $3.51 \cdot 10^4$ | $8.49 \cdot 10^{-4}$ | $2.41 \cdot 10^{-2}$ | 0.38 | 0.56 | $1.00 \cdot 10^2$ |
| 30 | $2.75 \cdot 10^4$ | $6.90 \cdot 10^{-4}$ | $2.46 \cdot 10^{-2}$ | 0.34 | 0.49 | 86.06 |
| 40 | $2.24 \cdot 10^4$ | $5.74 \cdot 10^{-4}$ | $2.48 \cdot 10^{-2}$ | 0.31 | 0.43 | 74.73 |

Development of the Formal Errors

We have seen in the previous section that for GTO objects the orbit can either improve when using follow-up observations instead of simultaneous observations (different longitude) or it can get worse (different latitude). The further development of the mean formal errors is studied in the following, using the main site with $\lambda = 0^\circ$, $\beta = 0^\circ$ and the two sites with $\lambda = 40^\circ$, $\beta = 0^\circ$, and $\lambda = 0^\circ$, $\beta = 40^\circ$. The first track was assumed to be observed from the main site, while the second track was simulated for each of the three sites after various time gaps. Each pair of corresponding tracks was used to determine elliptical orbits.

Figure 5.46 shows the development of the mean formal errors σ against the time gap Δt between the two tracks. Again, the largest and the smallest 5% of the values of the formal errors were excluded. The same notation as in Figure 5.36 was used. Again, the scale of the y-axis is logarithmic.

In the top two plots, showing the errors for the semi-major axis and the eccentricity, the $\Delta\beta$ -errors are clearly the smallest. But other than for the GEO objects, the mean formal errors steadily increase with a longer gap between the tracks. This can also be seen for the $\Delta\lambda$ -errors, which are by a factor of about 3 – 4 larger than the $\Delta\beta$ -errors. An analysis of the orbit determinations showed that according to the covariance matrices the orbital elements exhibit a stronger correlation for the longer observation arcs. The consequence are larger formal errors. The cause could be that no observations other than the short series at the beginning and the end of the arc are available. This means that a better distribution of the observations is needed for GTO objects to improve the orbits.

Much larger errors can be found for the Δ -errors. Unexpectedly, the errors of the semi-major axis are smaller for $\Delta t = 0.25$ h than for $\Delta t = 0.5$ h and $\Delta t = 0.75$ h. But these numbers have to be taken with care. As the observation arc is very short for all three cases, the shape of the orbit, i.e., a and e , could not be reasonably determined for many of the objects. For some of them, even an almost circular orbit was determined. For an arc length of more than one hour, this problem in the orbit determination did not occur. Further, this was not a problem for the observation tracks from two different sites. Observations from two sites are therefore helpful to determine the shape of elliptical orbits with remarkable accuracy after a short time. No convergence between the three curves as it was the case for the GEO objects can be seen in the given time interval.

The orbital plane (see the two plots in the middle) is best determined for the $\Delta\lambda$ -errors, except for $\Delta t = 1.5$ h, where the Δ -errors are smaller. The $\Delta\beta$ -errors are much larger than the $\Delta\lambda$ -errors, especially for Ω . For the GEO objects, at least the $\Delta\lambda$ -errors were similar to the Δ -errors. For GTO objects, it looks completely different, even for $\Delta t > 1$ h. While the Δ -errors do improve with larger Δt , the $\Delta\lambda$ -errors get larger. The two curves even cross each other.

While the two plots for ω and T_0 are very similar for GEO objects, they do not look much the same for GTO objects. The Δ -errors for ω improve rapidly after three hours. The $\Delta\lambda$ -errors are clearly larger than the $\Delta\beta$ -errors at the beginning, but get smaller after three hours. After six hours, the two curves approach each other. The $\Delta\beta$ -errors have a small peak for $\Delta t = 1$ hour. The plot for T_0 looks similar than the one for e . The development of the Δ -errors is almost identical. But other than for e , the $\Delta\lambda$ -errors and the $\Delta\beta$ -errors for T_0 are larger at the beginning than for an arc of three hours.

Generally, to use two sites is much more recommendable for objects with elliptical orbits than for GEO objects, especially when the observation arc is short. But only the Δ -errors show a steadily improvement with longer arcs. Further studies are needed to decide which constellation really is more promising.

Dependency on the Satellite Position

The results from the previous section showed that the errors of the orbit determination are smaller for two sites with different latitudes compared to sites with different longitudes. The reason is, as for the GEO objects, the distribution of the GTO objects around the Earth, but also the filters for the orbital elements used to simulate the orbits. The inclination had been limited to $\pm 30^\circ$. This of course has an impact on the accuracy of the orbits determined from observations from two sites as the geometry is not the same for sites separated in longitude as for sites separated in latitude. Nevertheless, this selection reflects the majority of the GTO population.

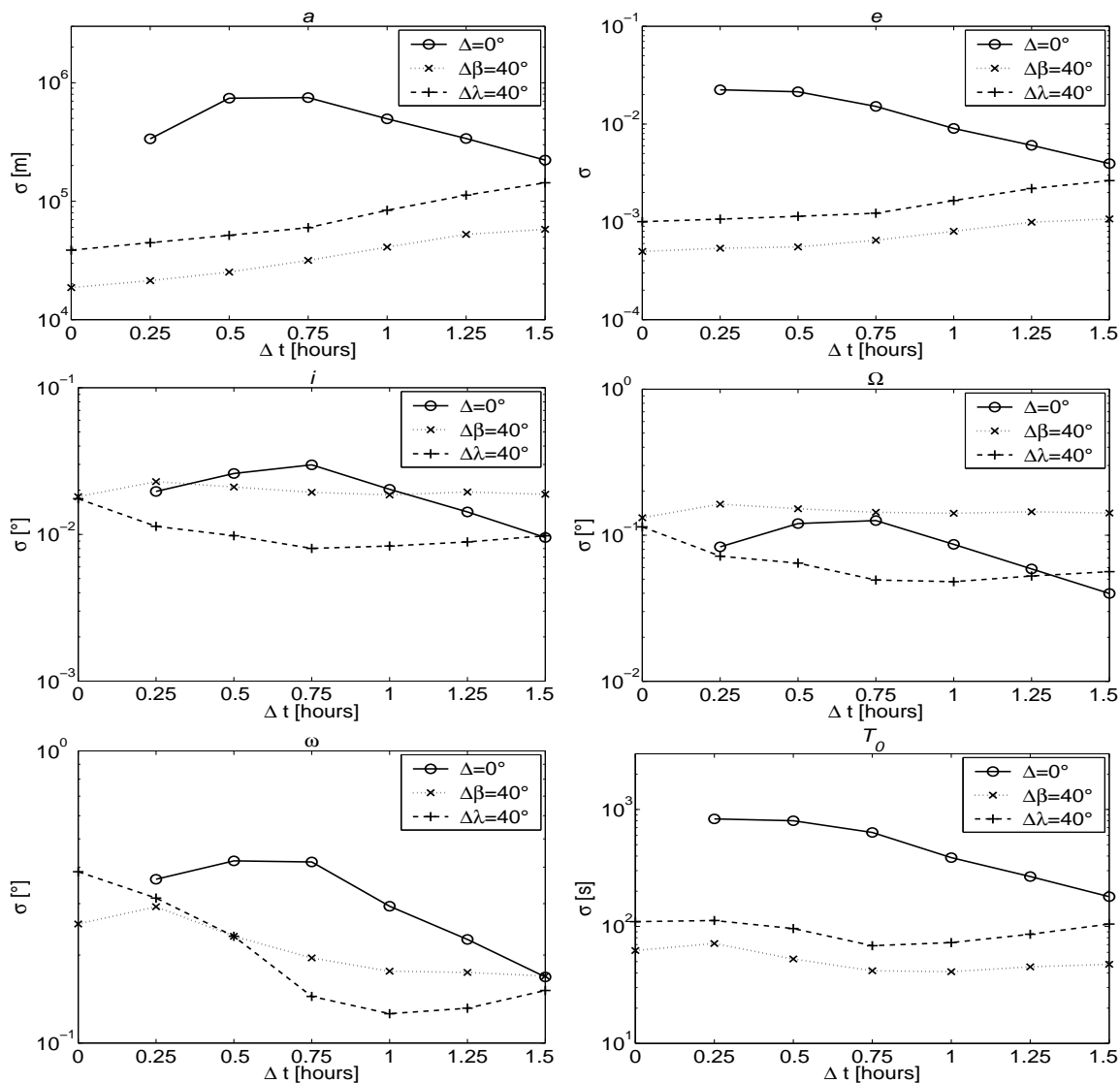


Figure 5.46: Mean formal errors σ for the elliptical orbit determination representing two tracks of a GTO object separated by Δt observed from one virtual site (\circ) or two virtual sites with identical longitude and different latitude (\times) and identical latitude and different longitude ($+$). The scale of the y-axis is logarithmic.

The effect of the selected distribution is shown in Figure 5.47, where the mean formal errors σ of the semi-major axes are plotted against the longitude λ_o of the object for the epoch of the first observation. The plots for the $\Delta\lambda$ -errors are on the left, while the ones for the $\Delta\beta$ -errors are on the right. The length of the observation arc is the same for each row. The errors for simultaneous observations are shown in the plots at the top, whereas the observation arcs of the rows below are 0.25 h, 0.5 h, and 1.5 h.

The four plots for the $\Delta\beta$ -errors on the right hand side all look very similar. The largest errors can be found at about $\lambda_o = 130^\circ - 140^\circ$. They are between $\sigma = 60\,000$ m and $\sigma = 80\,000$ m in the top three plots and larger than $\sigma = 150\,000$ m in the bottom plot. A minimum can only be found in the upper three

plots, where it is located at $\lambda_o = 0^\circ$. Generally, the plots are similar to the ones for the GEO objects in Figure 5.37, except that the errors in the upper three plots are by a factor of 4 – 5 smaller for the GTO objects.

This is not the case for plots of the $\Delta\lambda$ -errors. Only the plots for $\Delta t = 0$ h and $\Delta t = 0.5$ h look like the corresponding plots for the GEO objects, with two strong peaks at $\lambda_o = -70^\circ$ and $\lambda_o = 110^\circ$. That the minimum is also located at $\lambda_o = 20^\circ$ can be seen in Figure 5.48, where the top left plot is shown with a logarithmic y-axis.

The plot for $\Delta t = 0.25$ h looks different. A minimum is also located at $\Delta\lambda = 20^\circ$, but the peaks are closer to the minimum as in the plot above. No such structure is visible for the GEO objects in Figure 5.37. But there is a difference between the plots for the GEO and the GTO objects: the observation arcs. The arcs for the GTO plots are much shorter. Therefore, the errors have been also determined for GEO objects with an observation arc of 0.25 h. Figure 5.49 shows the plot for the site with a separation of 40° in longitude from the main site. The plot does not look exactly like the one for the GTO objects, but some similar structures are visible. A clear minimum can be seen at $\lambda_o = 20^\circ$. Two smaller peaks are close to this minimum, located at $\lambda_o = -10^\circ$ and $\lambda_o = 50^\circ$. But other than for the GTO objects, there are two further minima and two strong peaks visible for the GEO objects. Nevertheless, we can conclude that these structures are caused by the very short observation arcs.

The plot at the bottom left of Figure 5.47 is similar to the one at the top, with small errors around $\Delta\lambda = 20^\circ$ and a very strong peak at $\Delta\lambda = 120^\circ$. One of the outliers is located outside of the given ranges. It is marked with an arrow and the corresponding value is written on its side. In a scale large enough to include this data point none of the other structures would be visible.

The results for the GTO objects show, that the orbit determination of observations from multiple sites is more complex than for the GEO objects. A possible cause could be that the GTO objects move from west to east with an angular velocity of $4.5^\circ - 7.5^\circ$ in longitude when they are near the apogee. This is, of course, another situation as for GEO objects, which remain fixed. But further studies are needed to check the impact of this movement on the orbit determination.

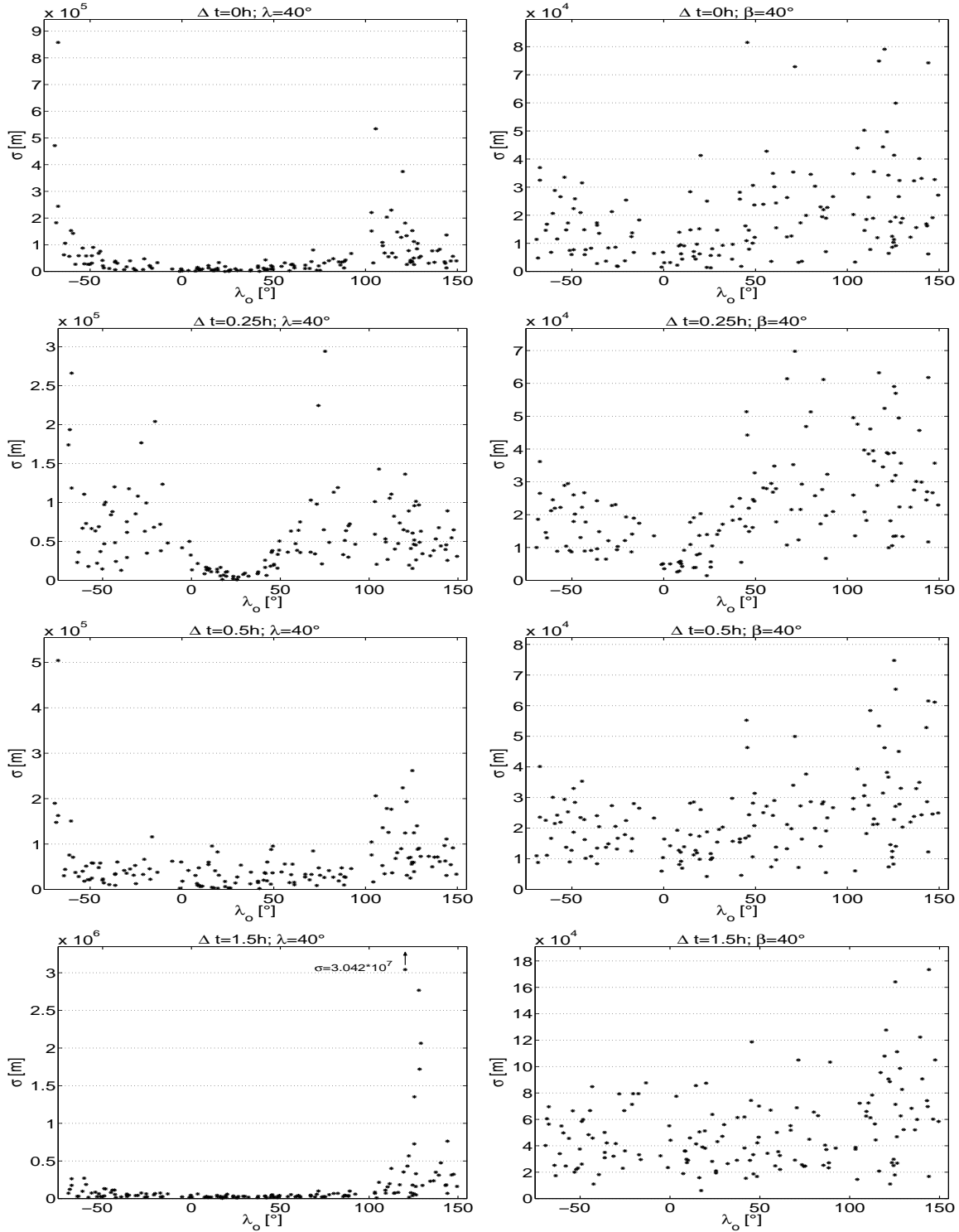


Figure 5.47: Mean formal errors σ for the semi-major axis of the elliptical orbit determination representing two tracks of a GTO object separated by 0 h, 0.25 h, 0.5 h, and 1.5 h observed from two virtual sites with identical latitude and different longitude (left) and identical longitude and different latitude (right) plotted against the longitude λ_o of the objects.

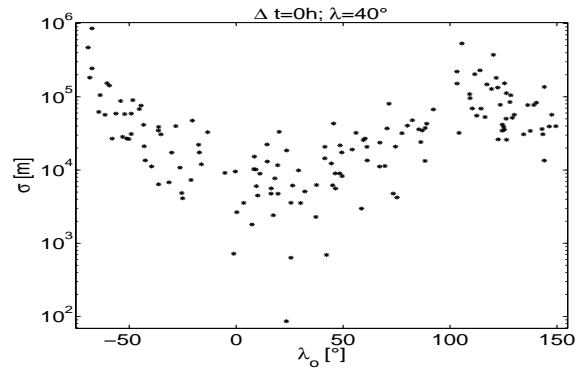


Figure 5.48: Mean formal errors σ for the semi-major axis of the elliptical orbit determination representing two tracks of a GTO object observed at the same epoch from two virtual sites with identical latitude $\beta = 0^\circ$ and a separation in longitude of $\Delta\lambda = 40^\circ$. The scale of the y-axis is logarithmic.

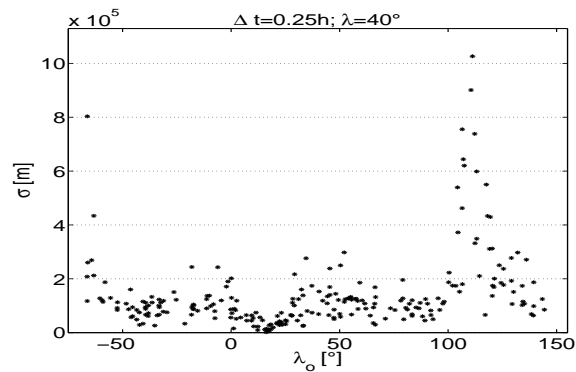


Figure 5.49: Mean formal errors σ for the semi-major axis of the elliptical orbit determination representing two tracks separated by 0.25 h of a GEO object observed from two virtual sites with identical latitude $\beta = 0^\circ$ and a separation in longitude of $\Delta\lambda = 40^\circ$.

Table 5.25: Separations in longitude λ and latitude β between the three sites of Nauchny (CRAO), Zimmerwald (ZIMLAT), and Tenerife (ESASDT).

| | $\Delta\lambda$ [°] | $\Delta\beta$ [°] |
|-----------------|---------------------|-------------------|
| ZIMLAT - ESASDT | 23.58 | 20.35 |
| CRAO - ZIMLAT | 26.73 | -2.09 |
| CRAO - ESASDT | 50.31 | 18.26 |

5.3.3 Examples of Real Observations

A large amount of observations has been gathered from the ESASDT and the ZIMLAT. These observations were searched for objects that were observed from both sites at the same day. In addition, some of the observations had to be acquired within half an hour from both sites and a few hours before that epoch from one of the two sites. Unfortunately, these requirements were not fulfilled very often.

In the framework of a joint GEO survey project ([Agapov *et al.*, 2005]) several GEO objects have been observed from Zimmerwald, Tenerife, and from other sites. Some observations from the Crimean Astrophysical Observatory (CRAO) in Nauchny were kindly provided by V. Agapov from the Keldysh Institute of Applied Mathematics (KIAM) for this work. The observations from the ESASDT, the ZIMLAT, and the CRAO were searched for objects meeting the requirements defined above. Also in this sample only very few object met the requirements. But nevertheless, some examples can be analyzed here.

As shown before, the separation between two sites has an impact on the accuracy of the determined orbit. The separations in longitude and latitude between the three sites of Nauchny (CRAO), Zimmerwald (ZIMLAT), and Tenerife (ESASDT) are given in Table 5.25. The separations were determined from East to West in longitude and from North to South in latitude. The sites of ZIMLAT and ESASDT have about the same separation in longitude as in latitude. Such a constellation was not used in the simulations in the section above. The two sites CRAO and ZIMLAT, however, are a good example as they are located nearly at the same latitude. For the sites CRAO and ESASDT the separation in longitude is much larger than in latitude.

A first example of a GEO object (GEO_M1) meeting the requirements is shown in Table 5.26. The table gives the formal errors resulting from the determination of elliptical orbits using two observation tracks. The time interval Δt between the two tracks is listed in the first column. The next six columns give the formal errors of the orbital elements. The RMS resulting from the orbit determination is given in the last column. The formal errors for the orbits determined from observations from CRAO only are shown in the upper part of the table, whereas the lower part shows the formal errors from observations from CRAO and ZIMLAT. In each case, the first observation track was observed with CRAO, while the second track was observed either from CRAO or ZIMLAT.

From the results in Figure 5.36 we expect that the formal error of the semi-major axis is larger for a gap of one hour between the tracks than for almost simultaneous observations. This is exactly what resulted for the object GEO_M1. It was unexpected, however, that the difference between the formal errors from one site compared to two sites is so small. But we have to consider that the separation between the two sites was 40° for Figure 5.36 and only about 25° for GEO_M1.

Let us first look at the formal errors for i and Ω before we look at those of the eccentricity. The formal errors are slightly smaller for the longer gap. In addition, the formal errors for one site are larger than for

Table 5.26: Formal errors for the elliptical orbit determination of object GEO_M1 representing two tracks observed with the CRAO (top) and two tracks observed with the CRAO and the ZIMLAT (bottom).

| CRAO | | | | | | | |
|-----------------|-------------------|----------------------|----------------------|--------------|--------------|-------------------|---------|
| Δt [h] | a [m] | e | i [°] | Ω [°] | ω [°] | T_0 [s] | RMS ["] |
| 1.21 | $3.14 \cdot 10^5$ | $5.49 \cdot 10^{-3}$ | $8.88 \cdot 10^{-3}$ | 0.32 | 17.66 | $4.26 \cdot 10^3$ | 0.46 |
| CRAO and ZIMLAT | | | | | | | |
| Δt [h] | a [m] | e | i [°] | Ω [°] | ω [°] | T_0 [s] | RMS ["] |
| 0.26 | $4.75 \cdot 10^4$ | $1.89 \cdot 10^{-3}$ | $1.02 \cdot 10^{-2}$ | 0.22 | 30.79 | $7.26 \cdot 10^3$ | 0.30 |
| 1.21 | $2.38 \cdot 10^5$ | $4.06 \cdot 10^{-3}$ | $7.52 \cdot 10^{-3}$ | 0.20 | 67.55 | $1.57 \cdot 10^4$ | 0.41 |

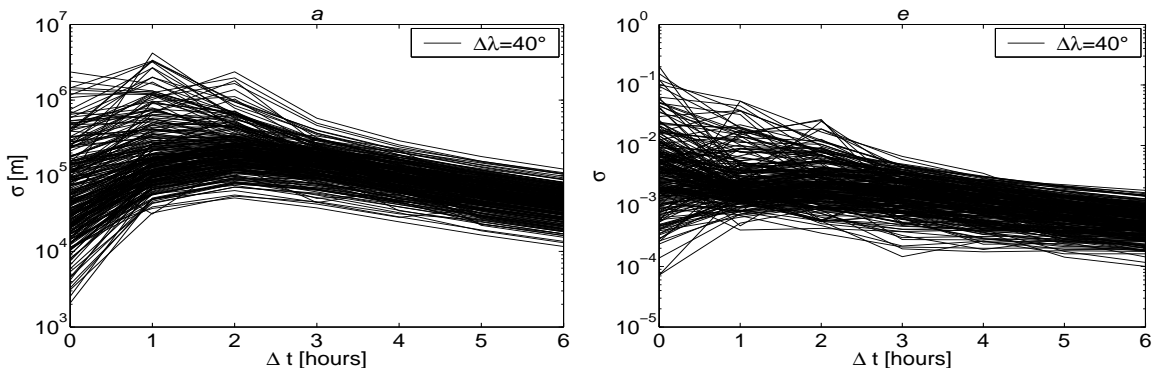


Figure 5.50: Formal errors σ of the semi-major axes (left) and the eccentricity (right) for the elliptical orbit determination representing two tracks of 250 GEO objects separated by Δt observed from two virtual sites with identical latitude and a separation of 40° in longitude. The scale of the y-axis is logarithmic.

two sites. This is more or less what could be expected.

For e , ω , and T_0 the formal errors are larger for the longer gap. From Figure 5.36 we expected smaller formal errors for all three cases. The question is now why the example from real observations does not match the results from the simulations. In Figure 5.36 we plotted the mean formal errors, i.e., we cannot see in that figure if all objects show the same development or not. Therefore, the formal errors for $\Delta\lambda = 40^\circ$ are plotted in Figure 5.50 for all 250 simulated objects. The left plot shows the formal errors of the semi-major axis, while the right plot shows those of the eccentricity. It can be seen that the main structure is correctly given by the mean formal errors in Figure 5.36. But both plots show that the development can be very different for Δt smaller than three hours. Looking at the formal errors of the eccentricity it can be seen that the simulations do match with the result for the example GEO_M1. For some simulated objects, the formal errors are also larger for a gap of one hour than for simultaneous observations. No plots for the formal errors of ω and T_0 for the 250 simulated objects are given as they look similar to the one for e .

A second example of a real object (GEO_M2) is given in Table 5.27. The upper part shows the formal errors resulting from the observations of the CRAO. Observation tracks observed from the CRAO and

Table 5.27: Formal errors for the elliptical orbit determination of object GEO_M2 representing two tracks observed with the CRAO (top) and two tracks observed with the CRAO and the ESASDT (bottom).

| CRAO | | | | | | | |
|-----------------|-------------------|----------------------|----------------------|----------------------|--------------|-------------------|---------|
| Δt [h] | a [m] | e | i [°] | Ω [°] | ω [°] | T_0 [s] | RMS [″] |
| 2.99 | $1.27 \cdot 10^5$ | $2.32 \cdot 10^{-3}$ | $2.52 \cdot 10^{-3}$ | $2.09 \cdot 10^{-2}$ | 12.84 | $3.06 \cdot 10^3$ | 0.47 |
| CRAO and ESASDT | | | | | | | |
| Δt [h] | a [m] | e | i [°] | Ω [°] | ω [°] | T_0 [s] | RMS [″] |
| 0.11 | $4.64 \cdot 10^4$ | $4.24 \cdot 10^{-3}$ | $1.92 \cdot 10^{-2}$ | 0.11 | 65.34 | $1.55 \cdot 10^4$ | 0.29 |
| 2.99 | $3.78 \cdot 10^5$ | $7.20 \cdot 10^{-3}$ | $4.67 \cdot 10^{-3}$ | $5.61 \cdot 10^{-2}$ | 7.78 | $2.10 \cdot 10^3$ | 0.60 |

Table 5.28: Formal errors for the elliptical orbit determination of object GEO_M3 representing two tracks observed with the ZIMLAT (top) and two tracks observed with the ZIMLAT and the ESASDT (bottom).

| ZIMLAT | | | | | | | |
|-------------------|-------------------|----------------------|----------------------|----------------------|----------------------|-------------------|---------|
| Δt [h] | a [m] | e | i [°] | Ω [°] | ω [°] | T_0 [s] | RMS [″] |
| 0.94 | $2.03 \cdot 10^6$ | $2.18 \cdot 10^{-2}$ | $3.06 \cdot 10^{-2}$ | 0.32 | 20.95 | $2.94 \cdot 10^3$ | 0.54 |
| 7.95 | $4.21 \cdot 10^4$ | $8.89 \cdot 10^{-4}$ | $2.00 \cdot 10^{-3}$ | $1.55 \cdot 10^{-2}$ | 0.26 | 64.92 | 0.51 |
| ZIMLAT and ESASDT | | | | | | | |
| Δt [h] | a [m] | e | i [°] | Ω [°] | ω [°] | T_0 [s] | RMS [″] |
| 0.08 | $2.10 \cdot 10^5$ | $1.53 \cdot 10^{-2}$ | $8.76 \cdot 10^{-2}$ | $4.73 \cdot 10^{-2}$ | 4.02 | $1.27 \cdot 10^3$ | 0.55 |
| 0.94 | $1.98 \cdot 10^5$ | $1.14 \cdot 10^{-3}$ | $7.65 \cdot 10^{-3}$ | $2.92 \cdot 10^{-2}$ | 2.62 | $4.86 \cdot 10^2$ | 0.18 |
| 7.95 | $1.06 \cdot 10^4$ | $2.39 \cdot 10^{-4}$ | $4.62 \cdot 10^{-4}$ | $6.27 \cdot 10^{-3}$ | $4.79 \cdot 10^{-2}$ | 19.11 | 0.09 |

from the ESASDT were used to determine the formal errors in the lower part. The time interval between the almost simultaneously observed tracks is shorter than in the previous example, whereas the longer gap is almost three hours.

For a gap of three hours, we would expect that the formal errors for the orbits determined from observations from one site and those from two sites have nearly the same value. For object GEO_M2, the formal errors for one site are clearly smaller than for two sites, except for ω and T_0 . But also the RMS is smaller. As the formal errors are proportional to the RMS, the value of the RMS has to be considered, too. This means for this example that it confirms the simulations anyhow.

Another nice example is object GEO_M3 (Table 5.28). For this object, there was not only a follow-up track after about one hour available from two sites, but also after almost eight hours. The object was observed with the ZIMLAT and the ESASDT.

For this object, the formal errors of a , e , and i show the expected rise or fall from the simultaneous observations to a gap of one hour. This is not the case for the other three elements, but as we have shown with Figure 5.50 this can also be accepted. A clear improvement of the accuracy for a gap of eight hours can be seen for all elements. When comparing the formal errors from two sites to those from one site we again have to consider the RMS values. The RMS is much smaller for the orbits determined from the observations from two sites than from one site. This also reflects in the formal errors for a gap of eight

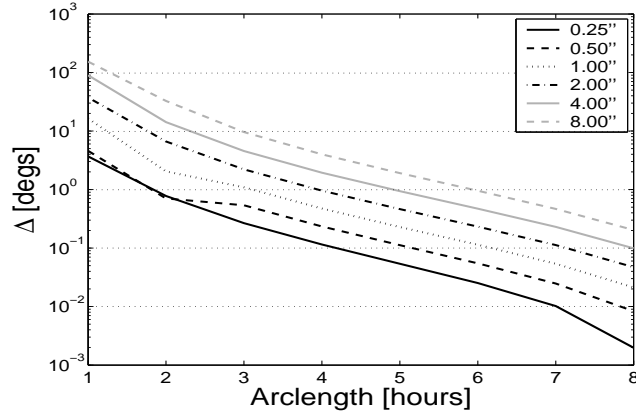


Figure 5.51: Difference after ten hours between “true” and determined elliptical orbit representing the discovery and one follow-up track as a function of the arc length. The six lines represent simulations with different observation errors.

hours. The formal errors from two sites are by factor of about 4 – 5 smaller than those from one site. This is more or less the factor between the RMS values.

5.4 Impact of the Observation Accuracy

It is obvious that the accuracy of the single observations affects the accuracy of the determined orbit. The influence of the accuracy was studied using the same set of simulated elements of a GEO object and assuming different errors for the simulated observations.

Three discovery observations and four follow-up observations were simulated. The time span between the discovery track and the follow-up track was varied from one hour to eight hours. Errors of 0.25'', 0.5'', 1'', 2'', 4'', and 8'' were assumed for the observations.

Figure 5.51 shows the difference after exactly ten hours between the position of the determined elliptical orbit and the “true” orbit as a function of the arc length. Note that the scale of the y-axis is logarithmic.

The figure shows that the differences are much smaller for longer arcs. Furthermore, the differences are larger for larger errors. The difference of the positions is proportional to the error of the observations. This means that the better the accuracy of the sensor, the shorter the observation arc has to be for a successful recovery.

The dependency is also noticeable in the formal errors of the elements. In order to study this dependency an error of $\sigma = 0.5''$, $\sigma = 1''$ and $\sigma = 5''$ was assumed for the observations of the discovery and the follow-up tracks. The follow-up tracks were simulated after 1 h, 2 h, 3 h, and 1 day. Elliptical orbits were determined using all observations from the discovery and the follow-up tracks. The mean formal errors are given in Table 5.29. The linear growth is significant for the elements a , e , and i , while the other elements seem to have something like a logarithmic growth.

Table 5.29: Mean formal errors for the elliptical orbit determination representing the discovery and the first follow-up observations assuming different observation errors. The arc length is one day.

| σ | a [m] | e | i [°] | Ω [°] | ω [°] | T_0 [s] |
|----------|---------|----------------------|----------------------|----------------------|----------------------|-----------|
| 0.5'' | 12.8 | $4.3 \cdot 10^{-6}$ | $5.4 \cdot 10^{-5}$ | $2.7 \cdot 10^{-2}$ | $7.6 \cdot 10^{-2}$ | 12.0 |
| 1.0'' | 25.6 | $8.6 \cdot 10^{-6}$ | $10.9 \cdot 10^{-5}$ | $4.8 \cdot 10^{-2}$ | $14.4 \cdot 10^{-2}$ | 23.3 |
| 5.0'' | 128.2 | $43.3 \cdot 10^{-6}$ | $55.9 \cdot 10^{-5}$ | $13.1 \cdot 10^{-2}$ | $51.9 \cdot 10^{-2}$ | 95.3 |

6. Concept for Catalogue Maintenance

The maintenance of a catalogue consists of three major steps. The first is to study the needed temporal spacing between the “maintenance” observations. The second step is the planning of the needed “maintenance” observations. The third step consists of updating the catalogue with newly detected objects and the associated improved orbits. This requires an efficient correlation procedure. A first concept for catalogue maintenance of GEO objects was presented in [Musci *et al.*, 2005a]. The concept presented here is based on this work. In addition, a concept for the maintenance of GTO objects is presented.

6.1 Maintenance Observations

As in Chapter 5, simulations were used to study the concept for the acquisition of “maintenance” observations for GEO and GTO objects. Again, the model used for the simulation of the observations and the orbit determination does not include air drag and only a simple model for the direct radiation pressure. Another restriction of the orbit determination are satellite manoeuvres, which were not studied in the scope of this work.

6.1.1 GEO

We have shown in Section 5.1 that four follow-up tracks with a total arc length of about one day are sufficient to determine a “secured” orbit. A save recovery is possible after much more than one month. In the following, the results for a narrow FOV of 0.4° were used for further simulations.

Follow-up Track After 30 Days

In order to study the behavior of the orbit determination for longer gaps between the tracks an additional follow-up track was simulated 30 days after the discovery observations.

The differences Δ between the positions of the determined elliptical orbits and the “true” orbits as a function of time are shown in Figure 6.1. The continuous functions including the daily periodical errors are plotted on the left hand side. The differences are very small. All objects would be re-observable after more than half a year with a narrow FOV. Two objects show a different behavior than the others, but no explanation can be given here. Nevertheless, also these two objects can be recovered. The same functions averaged over one day are shown on the right hand side of Figure 6.1. As expected, the orbits are well-determined 30 days after the discovery, at the time when the follow-up tracks were simulated.

The mean formal errors are given in Table 6.1. All elements are very well determined. As expected, the accuracy in the semi-major axis is getting much better for longer observation arcs.

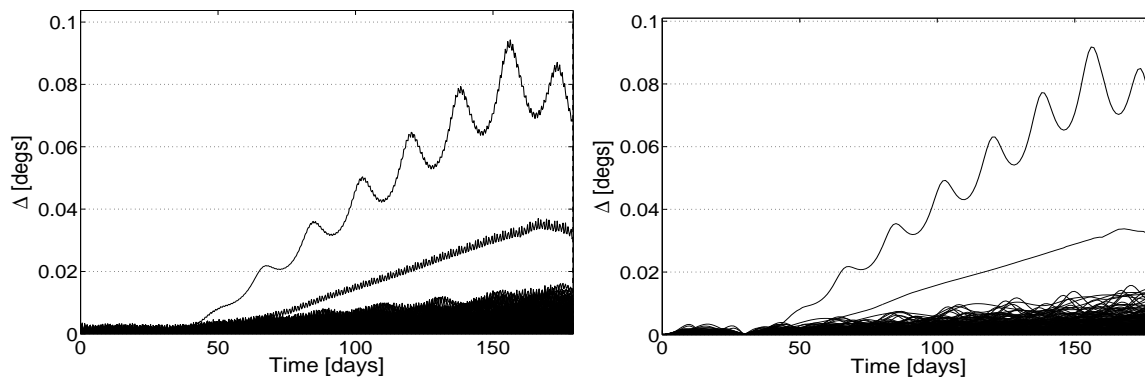


Figure 6.1: Difference Δ between “true” and determined elliptical orbit representing the discovery track of a GEO object and the follow-up tracks after 1 h, 2 h, 3 h, 1 day, and 30 days. Each line represents the result from one of 250 simulations. Left: continuous, right: averaged over one day.

Table 6.1: Mean formal errors for the elliptical orbit determination representing the discovery track of a GEO object and the follow-up tracks after 1 h, 2 h, 3 h, 1 day, and 30 days.

| a [m] | e | i [°] | Ω [°] | ω [°] | T_0 [s] |
|---------|---------------------|---------------------|---------------------|---------------------|-----------|
| 3.1 | $3.3 \cdot 10^{-6}$ | $4.3 \cdot 10^{-5}$ | $4.7 \cdot 10^{-3}$ | $4.4 \cdot 10^{-2}$ | 7.9 |

Follow-up Track After 60 Days

Another follow-up track was simulated 60 days after the discovery.

The differences Δ as a function of time are shown in Figure 6.2. The continuous functions on the left hand side show very small differences, but several objects show a strange behavior. One of these objects also shows larger daily variations. All objects, however, would be re-observable after much more than half a year. The right hand side shows again the averaged functions. The object with the large daily variations now shows quasi-periodic variations.

The mean formal errors are given in Table 6.2. An improvement compared to Table 6.1 is clearly visible, except for Ω .

Maintenance Tracks

The number of observations becomes very large and the observation arc very long for each object during several years of observing. Of course, it is not meaningful to use all observations for the orbit improvement, as this will extend the orbit determination process. Furthermore, a better force model is required for long observation arcs. Only the last portion of the observations from a few tracks and the latest determined orbit as a priori orbit should be used.

Six tracks separated by 30 days were simulated. The observations from the initial orbit determinations were not included. The initial orbits, i.e. the orbits resulting after four follow-up tracks spanning one day of time, were used as a priori orbits for the orbit improvement.

The continuous plots of the differences Δ on the left hand side in Figure 6.3 show large daily variations

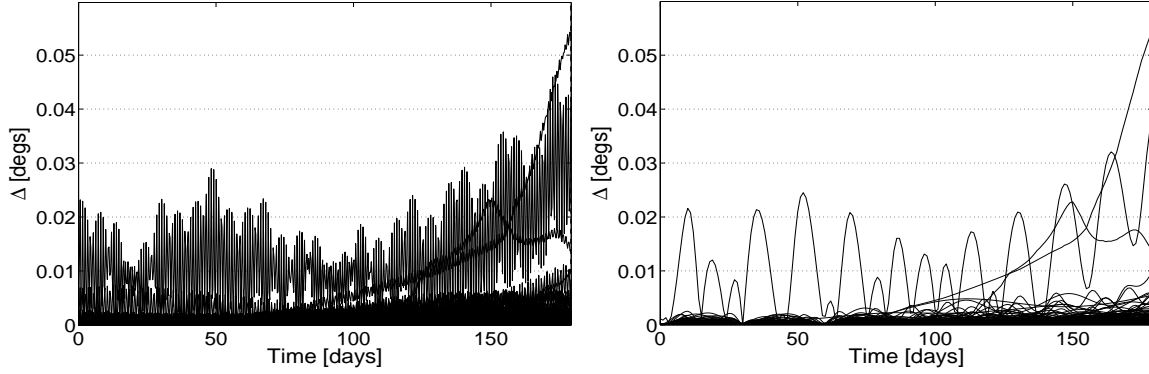


Figure 6.2: Difference Δ between “true” and determined elliptical orbit representing the discovery track of a GEO object and the follow-up tracks after 1 h, 2 h, 3 h, 1 day, 30 days, and 60 days. Each line represents the result from one of 250 simulations. Left: continuous, right: averaged over one day.

Table 6.2: Mean formal errors for the elliptical orbit determination representing the discovery track of a GEO object and the follow-up tracks after 1 h, 2 h, 3 h, 1 day, 30 days, and 60 days.

| a [m] | e | i [°] | Ω [°] | ω [°] | T_0 [s] |
|---------|---------------------|---------------------|---------------------|---------------------|-----------|
| 0.4 | $1.5 \cdot 10^{-6}$ | $3.6 \cdot 10^{-5}$ | $1.9 \cdot 10^{-2}$ | $4.2 \cdot 10^{-2}$ | 6.9 |

for some objects. For these objects, the orbit determination was not very good and the resulting RMS of the order of about $10''$ (instead of about $0.35''$ as for most of the objects). But for the majority of the objects the differences are clearly smaller than half of a narrow FOV of 0.4° . The averaged functions on the right hand side show that the large variations stem from two objects only. The variations for one of the objects have a period of about 30 days. This behavior is a potential consequence of the fact that the objects were observed exactly every 30 days. The variations of the other object have a period of about 14 days.

The mean formal errors are given in Table 6.3. Note that the errors for most elements are larger than in Table 6.1 and Table 6.2. One reason is most likely that a good distribution of the observations along the orbit is missing. In addition, the two objects with more inaccurate orbits make the result worse.

The results from this section show that it is possible to determine very accurate orbits without the observations from the initial orbit determination. This means that not all available observations of an object have to be included in the orbit improvement process, which simplifies the cataloging process considerably.

Survey

The results from the previous section can also be used to define a survey strategy. We have seen that the orbit determination is unproblematic for observation gaps of 30 days. Furthermore, the determined orbits are very accurate. Thus it is sufficient to observe the same part of the GEO ring every 30 days.

Theoretically, it might be also sufficient to observe the same part of the GEO ring only every two or even more month. But this is only true with the assumption that no manoeuvres are performed and only the

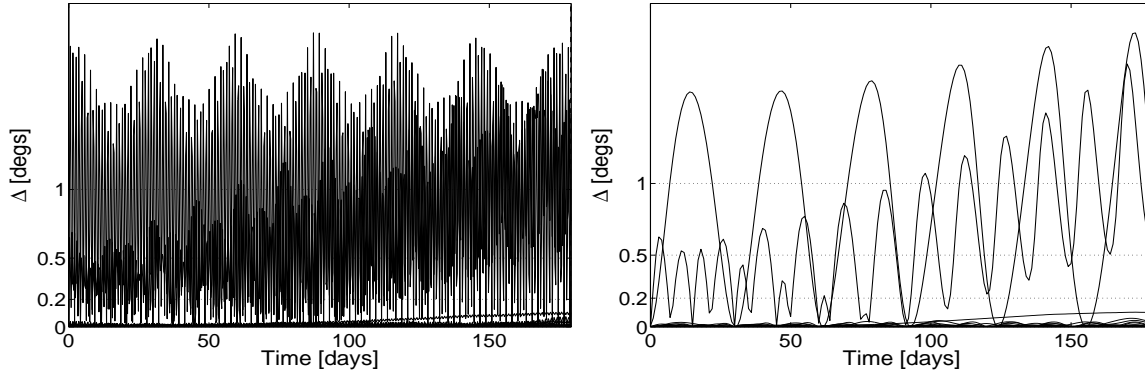


Figure 6.3: Difference Δ between “true” and determined elliptical orbit representing 6 maintenance tracks of a GEO object separated by 30 days. Each line represents the result from one of 250 simulations. Left: continuous, right: averaged over one day.

Table 6.3: Mean formal errors for the elliptical orbit determination representing 6 maintenance tracks of a GEO object separated by 30 days.

| a [m] | e | i [°] | Ω [°] | ω [°] | T_0 [s] |
|---------|---------------------|---------------------|---------------------|--------------|-----------|
| 0.3 | $4.3 \cdot 10^{-6}$ | $6.3 \cdot 10^{-5}$ | $8.6 \cdot 10^{-2}$ | 0.1 | 63.8 |

direct radiation pressure has to be considered. In reality, the situation is of course much more complex. In order to provide very accurate orbits all the time the observation gaps should therefore not be too long.

Objects in Drift Orbits

Not all objects in GEO are visible for an observer during the whole year. Controlled objects are only visible if their longitude is within the observable longitude range for a given station (e.g., $41^\circ \text{ E} - 74^\circ \text{ W}$ for Tenerife). Uncontrolled objects are drifting with drift rates up to $35^\circ/\text{day}$ (catalogued objects). For the catalogue maintenance, objects with small drift rates are the most critical. For a given site they may be outside the visible longitude range for several weeks to months. We have seen in Section 2.2.1 that an object with a drift rate of $\pm 1.3^\circ/\text{day}$ will not be visible for about half a year.

The question is now, if such an object can be recovered with an initial orbit. Figure 5.10 showed that the orbits determined from observations spanning an arc length of one day are very accurate. A FOV of about 1° would be needed to safely recover all objects after half a year. Using a wide FOV larger than 2° , the objects can be recovered after more than one year.

For all objects, a follow-up track was simulated half a year after the discovery. The differences Δ between the positions of the determined elliptical orbits and the “true” orbits as a function of time are shown in Figure 6.4. The functions are averaged over one day. Most of the orbits show very small differences. A few objects show larger periodical variations and some show no clear structure at all.

The mean formal errors are given in Table 6.4. The errors are of the same magnitude as in Table 6.1, except for the semi-major axis. This was expected because of the decreasing linear relationship between the error of the semi-major axis and the length of the observation arc.

The results show that a majority of the objects in drift orbits can be recovered when they return to

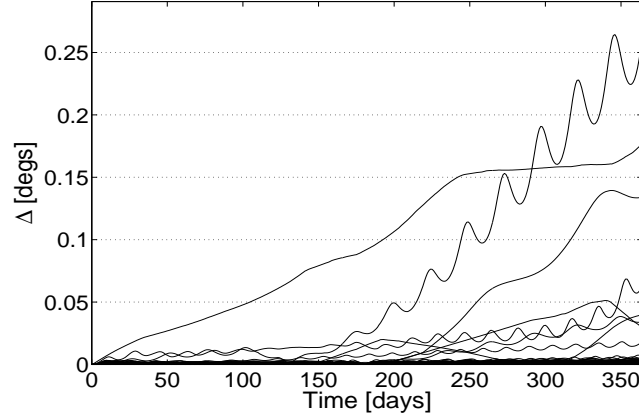


Figure 6.4: Difference Δ between “true” and determined elliptical orbit representing the discovery track of a GEO object and the follow-up tracks after 1 h, 2 h, 3 h, one day, and 180 days. Each line represents the result from one of 250 simulations. The functions are averaged over one day.

Table 6.4: Mean formal errors for the elliptical orbit determination representing the discovery track of a GEO object and the follow-up tracks after 1 h, 2 h, 3 h, one day, and 180 days.

| a [m] | e | i [°] | Ω [°] | ω [°] | T_0 [s] |
|---------|---------------------|---------------------|---------------------|---------------------|-----------|
| 0.3 | $3.2 \cdot 10^{-6}$ | $4.4 \cdot 10^{-5}$ | $7.5 \cdot 10^{-3}$ | $4.4 \cdot 10^{-2}$ | 8.3 |

the visible longitude range. Furthermore, a very accurate orbit can be determined despite the long gap between the tracks. Of course, some objects cannot be recovered because the return time is too long. This could be the case for objects with drift rates smaller than $1^\circ/\text{day}$, especially with a narrow FOV. In these cases, however, the very long visibility windows (> 100 days) may allow determining very accurate orbits before the long gap. Nevertheless, we again have to consider that the reality is more complex than the assumed force model and it therefore might not be possible to recover the objects after such a long time.

Examples of Real Observations

In Section 5.1.7 we showed that the results from the simulations to acquire “secured” orbits in the Sections 5.1.3 and 5.1.4 were confirmed by real observation. Simulations of longer observation arcs were discussed at the beginning of Section 6.1.1. These results were also tested with real observations from the ESASDT and the ZIMLAT. The same objects as in Section 5.1.7 were chosen.

ESASDT

Table 6.5 shows the results for the four GEO objects observed with the ESASDT. The last two columns from Table 5.8 are also included in Table 6.5 (4. Follow-up and 5. Follow-up) in order to show the development of the orbits. ΔT is the time interval between the discovery and the follow-up tracks. U is the revolution number during which the observations were acquired. Δp is the difference between the determined and the observed position. Elliptical orbits determined from all available observations were used to determine the positions of the follow-ups.

Table 6.5: Difference Δp between the determined and the observed position for GEO objects observed with the ESASDT.

| Object | | 4. Follow-up | 5. Follow-up | 6. Follow-up | 7. Follow-up |
|--------|---------------------------------|--------------|--------------|---------------|---------------|
| GEO 1 | $\Delta T[\text{h}] / \text{U}$ | 26.37 / 2 | 52.28 / 3 | 724.79 / 31 | 2715.13 / 114 |
| | $\Delta p[^\circ]$ | 0.1505 | 0.0031 | 0.0014 | 0.0093 |
| GEO 2 | $\Delta T[\text{h}] / \text{U}$ | 30.53 / 2 | 510.41 / 22 | | |
| | $\Delta p[^\circ]$ | 0.0069 | 0.1296 | | |
| GEO 3 | $\Delta T[\text{h}] / \text{U}$ | 22.65 / 2 | 55.19 / 3 | 483.44 / 21 | 4707 / 196 |
| | $\Delta p[^\circ]$ | 0.0211 | 0.0039 | 0.0224 | 0.0035 |
| GEO 4 | $\Delta T[\text{h}] / \text{U}$ | 23.68 / 2 | 71.15 / 4 | 2379.73 / 100 | |
| | $\Delta p[^\circ]$ | 0.1361 | 0.0018 | 0.0329 | |

Table 6.6: Difference Δp between the determined and the observed position for GEO objects observed with the ZIMLAT.

| Object | | 4. Follow-up | 5. Follow-up | 6. Follow-up | 7. Follow-up |
|--------|---------------------------------|--------------|--------------|--------------|--------------|
| GEO 5 | $\Delta T[\text{h}] / \text{U}$ | 97.53 / 5 | 600.35 / 25 | 1227.46 / 52 | 1657.90 / 70 |
| | $\Delta p[^\circ]$ | 0.0085 | 0.1134 | 0.0043 | 0.0277 |
| GEO 6 | $\Delta T[\text{h}] / \text{U}$ | 192.74 / 9 | 644.20 / 27 | 1874.75 / 79 | |
| | $\Delta p[^\circ]$ | 0.0060 | 0.1750 | 0.0156 | |
| GEO 7 | $\Delta T[\text{h}] / \text{U}$ | 118.43 / 6 | 454.10 / 19 | 1270.45 / 53 | 1685.24 / 71 |
| | $\Delta p[^\circ]$ | 0.0066 | 0.0344 | 0.0027 | 0.0160 |

For object GEO 2, only an observation arc of 21 days is available. For the other three objects, however, the available arc length is over 99 days. Note that for object GEO 4 the orbit determined from an arc length of three days was accurate enough to recover the object 96 days later. The results clearly confirm the simulations.

ZIMLAT

The three examples of objects observed with the ZIMLAT are shown in Table 6.6. The last column from Table 5.9 is also included (4. Follow-up).

Note that the differences are largest for the fifth follow-up. Nevertheless, all three objects could be recovered with a FOV larger than 0.4° . Object GEO 6, however, would probably not have been recovered with the ZIMLAT because of its small FOV (remember that these objects were acquired using the DISCOS elements).

6.1.2 GTO

In Section 5.2 we have shown that four or five follow-up tracks with a total arc length of about five days are sufficient to determine a “secured” orbit.

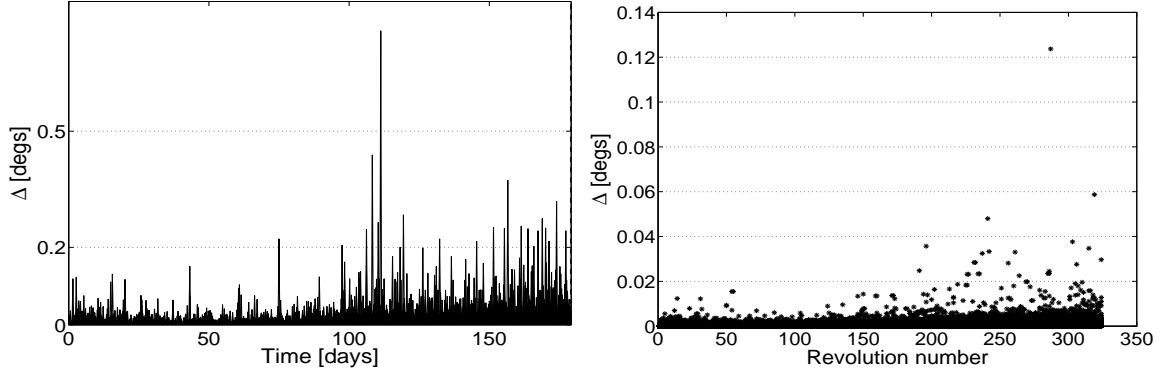


Figure 6.5: Difference Δ between “true” and determined elliptical orbit representing the discovery track of a GTO object and the follow-up tracks after 0.5 h, 2 h, at first apogee during the first and the fifth night after the discovery, and after 30 days. Each line represents the result from one of 250 simulations. Left: continuous, right: at apogee.

Table 6.7: Mean formal errors for the elliptical orbit determination representing the discovery track of a GTO object and the follow-up tracks after 0.5 h, 2 h, at first apogee during the first and the fifth night after the discovery, and after 30 days.

| a [m] | e | i [°] | Ω [°] | ω [°] | T_0 [s] |
|---------|---------------------|---------------------|---------------------|---------------------|-----------|
| 0.6 | $2.8 \cdot 10^{-6}$ | $8.5 \cdot 10^{-5}$ | $1.0 \cdot 10^{-3}$ | $1.2 \cdot 10^{-3}$ | 0.11 |

Follow-up After 30 Days

We have seen in Figure 5.24 that the determined “secured” orbits allow to recover the objects 30 days after the discovery. Another follow-up track was therefore simulated 30 days after the discovery observations. All follow-up tracks were simulated for the same epoch and not for the apogee passing time.

The differences Δ between the positions of the determined elliptical orbits and the “true” orbits as a function of time are shown in Figure 6.5. The continuous functions on the left side show that the differences are small within half a year. Some larger differences appear after a bit more than 100 days. The differences are very small at the apogees (Figure 6.5, right).

The mean formal errors are given in Table 6.7. The errors are clearly smaller than in Table 6.1. Especially the semi-major axis a and the perigee passing time T_0 are very well determined.

Maintenance Tracks

Four tracks separated by 30 days were simulated. It was assumed that the tracks were observed at midnight. The observations from the initial orbit determinations were not included. The initial orbits, i.e. ,the orbits resulting after five follow-up tracks spanning five days of time, were used as a priori orbits for the orbit improvement.

The differences Δ as a function of time are shown in Figure 6.6. The continuous functions on the left side show that the differences are very large. Many strong peaks are visible. For some objects the differences are also large at the apogees (Figure 6.6, right).

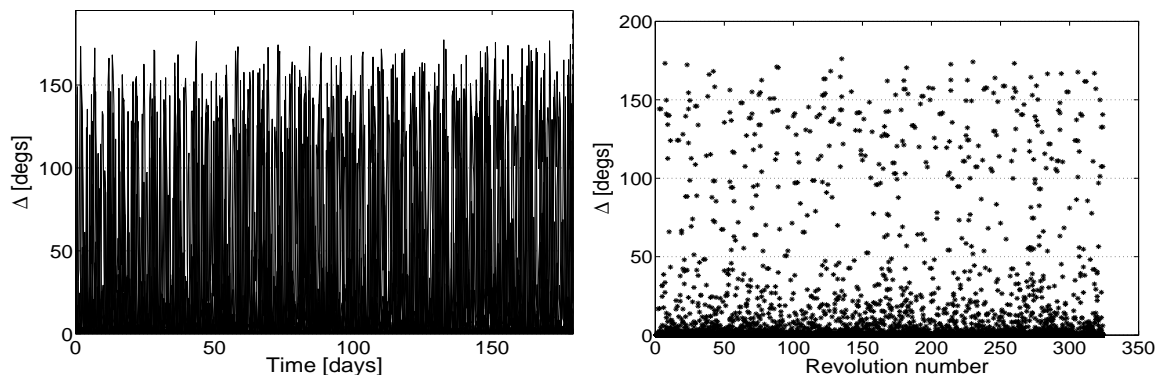


Figure 6.6: Difference Δ between “true” and determined elliptical orbit representing 4 maintenance tracks of a GTO object separated by 30 days. Each line represents the result from one of 250 simulations. Left: continuous, right: at apogee.

Table 6.8: Mean formal errors for the elliptical orbit determination representing 4 maintenance tracks of a GTO object separated by 30 days.

| a [m] | e | i [°] | Ω [°] | ω [°] | T_0 [s] |
|---------|---------------------|---------------------|---------------------|---------------------|-----------|
| 9.3 | $5.6 \cdot 10^{-5}$ | $3.7 \cdot 10^{-3}$ | $1.4 \cdot 10^{-2}$ | $6.4 \cdot 10^{-2}$ | 104.4 |

The mean formal errors shown in Table 6.8 are also much larger than in Table 6.7. Especially the perigee passing time T_0 is much worse determined. The average RMS of these determined orbits is $4.56''$, while it is $\sim 0.33''$ for all orbit determinations above.

A closer investigation showed that the determined RMS is very large for 10 out of the 250 simulated maintenance tracks, with values up to $576''$. For another 17 orbits not all available observations were included in the orbit determination. A screening procedure of the program SATORB automatically excludes observations with large residuals during the iteration process. This means that no good orbit could be determined for about 10% of the objects. As a consequence the mean formal errors are much larger than they would be without these objects. Also the results in Figure 6.6 are dominated by these critical objects.

One possible reason is that the gaps between the tracks are too long. Therefore, four tracks separated by 15 days were simulated.

The differences Δ between the determined elliptical orbits and the “true” orbits as a function of time are shown in Figure 6.7. Some large differences are still visible one the left and on the right plot. Nevertheless, it looks much better than in Figure 6.6.

The mean formal errors are given in Table 6.9. The errors are smaller than in Table 6.8 but still larger than in Table 6.7. The average RMS of these determined orbits is $0.43''$.

The RMS is large for 3 orbits determined for the simulated maintenance tracks. Not all observations were included in the orbit determination for 7 orbits. The result is better than with a gap of 30 days between the tracks, but still dominated by a few objects with large errors and therefore not good enough.

Another approach than to reduce the gap between the tracks is to increase the number of tracks in the same time interval. This allows a better determination of the eccentricity. Two additional tracks to the four separated by 30 days were simulated. They were placed one hour after the second and the third

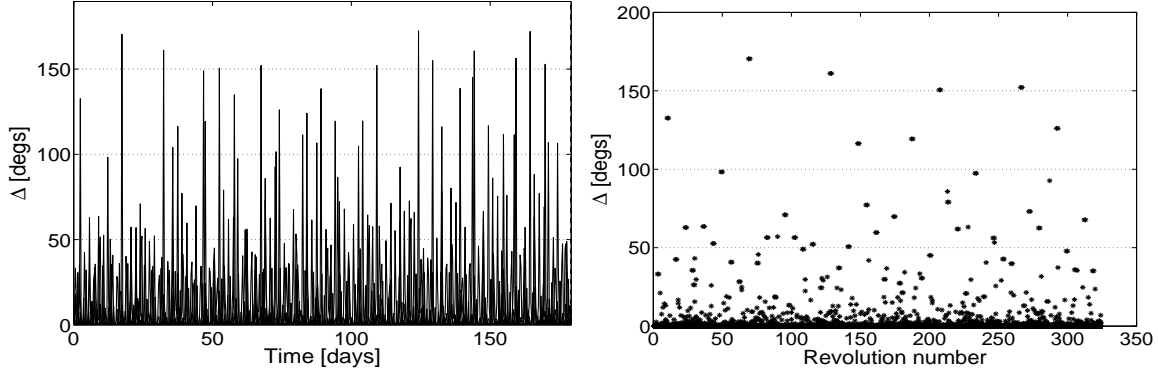


Figure 6.7: Difference Δ between “true” and determined elliptical orbit representing 4 maintenance tracks of a GTO object separated by 15 days. Each line represents the result from one of 250 simulations. Left: continuous, right: at apogee.

Table 6.9: Mean formal errors for the elliptical orbit determination representing 4 maintenance tracks of a GTO object separated by 15 days.

| a [m] | e | i [°] | Ω [°] | ω [°] | T_0 [s] |
|---------|---------------------|---------------------|---------------------|---------------------|-----------|
| 2.3 | $1.6 \cdot 10^{-5}$ | $3.3 \cdot 10^{-4}$ | $3.1 \cdot 10^{-3}$ | $1.1 \cdot 10^{-2}$ | 14.3 |

track.

Figure 6.8 shows the differences Δ as a function of time. The continuous functions on the left side show much fewer large peaks than in Figure 6.7. But still, some peaks are too large for a recovery. Nevertheless, the differences are very small at the apogee (Figure 6.8, right). This means that the maintenance observations are best observed close to the apogee. The observation arc should be about one hour, with a few observations at the beginning and at the end of the arc.

The mean formal errors are given in Table 6.10. They are much better than in Table 6.9 and even better than in Table 6.7. The average RMS is $0.32''$. All observations were included in the orbit determination for all objects. No large RMS resulted for any object.

Examples of Real Observations

Simulations of longer observation arcs were discussed at the beginning of Section 6.1.2. These results were also tested with real observations from the ESASDT and the ZIMLAT. The same objects as in Section 5.2.7 were chosen.

ESASDT

Table 6.11 shows the results for three GTO objects observed with the ESASDT. The last two columns from Table 5.13 are also included in Table 6.11 (4. Follow-up and 5. Follow-up) in order to show the development of the orbits. Object GTO 4 from Table 5.13 is not included in this table as no observations after a longer gap are available.

The object GTO 1 is an interesting case. The orbit determined from the first three nights was sufficiently

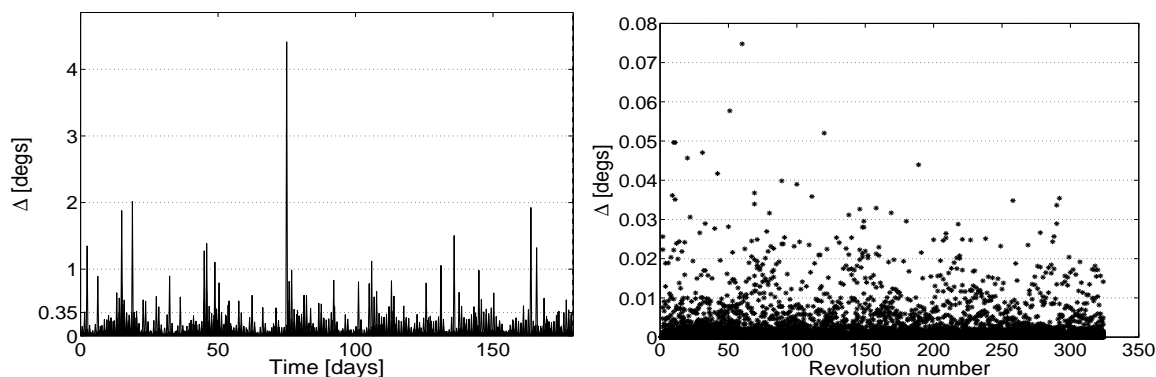


Figure 6.8: Difference Δ between “true” and determined elliptical orbit representing 4 maintenance tracks of a GTO object separated by 30 days and two additional tracks one hour after the second and third maintenance track. Each line represents the result from one of 250 simulations. Left: continuous, right: at apogee.

Table 6.10: Mean formal errors for the elliptical orbit determination representing 4 maintenance tracks of a GTO object separated by 30 days and two additional tracks one hour after the second and the third maintenance track.

| a [m] | e | i [°] | Ω [°] | ω [°] | T_0 [s] |
|---------|---------------------|---------------------|---------------------|---------------------|-----------|
| 0.1 | $9.8 \cdot 10^{-7}$ | $4.4 \cdot 10^{-5}$ | $5.5 \cdot 10^{-4}$ | $6.8 \cdot 10^{-4}$ | 0.2 |

Table 6.11: Difference Δp between the determined and the observed position for GTO objects observed with the ESASDT.

| Object | | 4. Follow-up | 5. Follow-up | 6. Follow-up | 7. Follow-up | 8. Follow-up |
|--------|--------------------|--------------|--------------|--------------|---------------|---------------|
| GTO 1 | ΔT [h] / U | 42.09 / 4 | 693.48 / 62 | | | |
| | Δp [°] | 0.0032 | 0.0483 | | | |
| GTO 2 | ΔT [h] / U | 24.80 / 2 | 100.00 / 8 | 553.10 / 44 | 1271.80 / 101 | 1939.87 / 155 |
| | Δp [°] | 0.4293 | 0.0027 | 0.0162 | 0.0075 | 0.0315 |
| GTO 3 | ΔT [h] / U | 20.34 / 3 | 69.89 / 8 | 572.14 / 59 | | |
| | Δp [°] | 0.0495 | 0.0103 | 0.2173 | | |

accurate such that the object was recovered about one month after the first detection. If we look at Figure 5.28 we see that we can expect orbits of this quality.

The differences for object GTO 2 are all very small, except for the 4. follow-up. The object could easily be recovered about 80 days or 155 revolutions after the discovery. Object GTO 3 has a larger difference after 59 revolutions although it was observed close to the apogee. The reason for this larger difference is a higher A/M of this object ($\approx 0.8 \text{ m}^2/\text{kg}$). The estimated A/M value was not applied to the orbit propagation. This example nicely shows that the gap between the observation tracks should be less than 30 days for GTO objects, especially for faint debris objects which orbits are sometimes more difficult to model.

Table 6.12: Difference Δp between the determined and the observed position for GTO objects observed with the ZIMLAT.

| Object | | 4. Follow-up | 5. Follow-up | 6. Follow-up | 7. Follow-up |
|--------|--------------------|--------------|---------------|---------------|---------------|
| GTO 5 | ΔT [h] / U | 94.21 / 9 | 383.05 / 34 | 1533.25 / 133 | |
| | Δp [°] | 0.0004 | 0.0712 | 0.3152 | |
| GTO 6 | ΔT [h] / U | 50.49 / 5 | 1316.68 / 107 | 2155.92 / 175 | 2803.46 / 227 |
| | Δp [°] | 0.0005 | 0.0747 | 0.0247 | 0.2185 |

ZIMLAT

The two examples of GTO objects observed with the ZIMLAT are shown in Table 6.12. The last two columns from Table 5.14 are also included (4. Follow-up and 5. Follow-up).

Both objects have larger differences for their last follow-up track. The reason is that the observations were acquired more than one hour (1.25 h for GTO 5 and 1.5 h for GTO 6) before the apogee. This leads to a larger difference, as explained in Section 5.2.2.

Table 6.13: Mean formal errors for the elliptical orbit determination of GEO objects with various A/M representing the discovery track and the follow-up tracks after 1 h, 2 h, 3 h, and 1 day. The orbit determination does not include an estimation of A/M.

| A/M [m ² /kg] | a [m] | e | i [°] | Ω [°] | ω [°] | rms ["] |
|--------------------------|---------|----------------------|----------------------|----------------------|----------------------|---------|
| 0.02 | 7.59 | $3.85 \cdot 10^{-6}$ | $4.87 \cdot 10^{-5}$ | $7.00 \cdot 10^{-3}$ | $4.65 \cdot 10^{-2}$ | 0.30 |
| 0.08 | 7.74 | $3.91 \cdot 10^{-6}$ | $4.97 \cdot 10^{-5}$ | $7.00 \cdot 10^{-3}$ | $5.82 \cdot 10^{-2}$ | 0.31 |
| 0.32 | 8.73 | $4.41 \cdot 10^{-6}$ | $5.61 \cdot 10^{-5}$ | $7.90 \cdot 10^{-3}$ | $6.26 \cdot 10^{-2}$ | 0.35 |
| 1.28 | 17.68 | $9.07 \cdot 10^{-6}$ | $1.16 \cdot 10^{-4}$ | $3.92 \cdot 10^{-2}$ | 0.13 | 0.71 |
| 5.12 | 63.90 | $3.30 \cdot 10^{-5}$ | $4.29 \cdot 10^{-4}$ | 0.13 | 0.36 | 2.57 |
| 20.48 | 252.53 | $1.31 \cdot 10^{-4}$ | $1.69 \cdot 10^{-3}$ | 0.28 | 1.00 | 10.27 |

6.1.3 Influence of A/M Modeling Errors

In Chapter 3 we have shown that GEO objects can have a very large A/M. For the orbit determination and the orbit propagation the A/M, i.e., the perturbations due to the radiation pressure, of such objects has to be sufficiently modeled. If it is not modeled at all the accuracy of the orbit will be rather poor.

In this section, we will study the impact of A/M modeling errors on the accuracy of the orbits for GEO and GTO objects. For this purpose, the 250 GEO and 250 GTO orbits from Chapter 5 were used to simulate observations with different A/M. The A/M value was assumed to vary from 0.02 m²/kg to 20.48 m²/kg with a factor of 4 between two consecutive values. A/M = 0.02 m²/kg is a typical value for a satellite.

GEO

For each GEO object, a discovery track and follow-up tracks after 1 h, 2 h, 3 h, and 1 day were simulated. Elliptical orbits were determined for all cases. No estimation of the A/M was included in the orbit determination. The mean formal errors and the mean of the RMS values (rms) are listed in Table 6.13. Unfortunately, the output of the used program does not include a formal error for T_0 , therefore it is missing in the table. The first column shows the assumed A/M values.

There is no big difference between the accuracies of the orbits for an A/M of 0.08 m²/kg compared to 0.02 m²/kg. Particularly, there is no linear dependency visible between the formal errors and A/M for small A/M. The cause is the assumed error of the single observations, which limits the rms to values larger than 0.3". But with higher A/M the dependency becomes more and more linear. The orbits are much worse determined for higher A/M. The table also shows the linear correlation between the RMS and the formal errors.

It is obvious that the inaccuracy of those orbits has also a huge impact on the orbit propagation. For a comparison, the determined orbits of the two extreme cases, A/M = 0.02 m²/kg and A/M = 20.48 m²/kg, were propagated over five days and compared with the corresponding "true" orbits. The differences between the positions of the determined orbits and the "true" orbits as a function of time are shown in Figure 6.9. The left plot shows the differences for A/M = 0.02 m²/kg. As expected, the differences are very small within the given range. The differences for A/M = 20.48 m²/kg are much larger. They can get even larger than 0.5° within the first day, the period where observations are available. A wide FOV telescope would be needed to recover the objects after a few days. This demonstrates how important it is

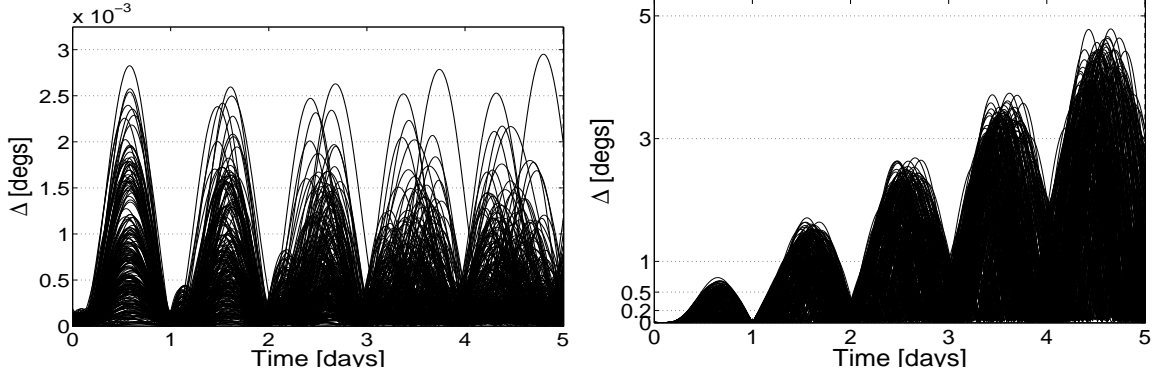


Figure 6.9: Difference Δ between “true” and determined elliptical orbit representing the discovery track of two GEO objects with $A/M = 0.02 \text{ m}^2/\text{kg}$ (left) and $A/M = 20.48 \text{ m}^2/\text{kg}$ (right). The orbits include the discovery observations and follow-up tracks after 1 h, 2 h, 3 h, and 1 day. The orbit determination does not include an estimation of A/M . Each line represents the result from one of 250 simulations.

Table 6.14: Mean formal errors for the elliptical orbit determination of GEO objects with various A/M representing the discovery track and the follow-up tracks after 1 h, 2 h, 3 h, and 1 day. The orbit determination does include an estimation of A/M .

| $A/M \text{ [m}^2/\text{kg]}$ | $a \text{ [m]}$ | e | $i \text{ [}^\circ\text{]}$ | $\Omega \text{ [}^\circ\text{]}$ | $\omega \text{ [}^\circ\text{]}$ | rms [$''$] |
|-------------------------------|-------------------|----------------------|-----------------------------|----------------------------------|----------------------------------|--------------|
| 0.02 | $4.48 \cdot 10^2$ | $7.73 \cdot 10^{-6}$ | $6.05 \cdot 10^{-5}$ | $7.43 \cdot 10^{-3}$ | 0.09 | 0.30 |
| 0.08 | $4.54 \cdot 10^2$ | $7.88 \cdot 10^{-6}$ | $6.14 \cdot 10^{-5}$ | $7.45 \cdot 10^{-3}$ | 0.11 | 0.31 |
| 0.32 | $4.50 \cdot 10^2$ | $7.84 \cdot 10^{-6}$ | $6.10 \cdot 10^{-5}$ | $7.44 \cdot 10^{-3}$ | 0.11 | 0.30 |
| 1.28 | $4.49 \cdot 10^2$ | $7.78 \cdot 10^{-6}$ | $6.09 \cdot 10^{-5}$ | $7.43 \cdot 10^{-3}$ | 0.09 | 0.30 |
| 5.12 | $4.52 \cdot 10^2$ | $7.80 \cdot 10^{-6}$ | $6.12 \cdot 10^{-5}$ | $7.17 \cdot 10^{-3}$ | 0.09 | 0.30 |
| 20.48 | $4.56 \cdot 10^2$ | $8.02 \cdot 10^{-6}$ | $6.14 \cdot 10^{-5}$ | $7.44 \cdot 10^{-3}$ | 0.11 | 0.31 |

that the A/M is well modeled.

The CelMech tool used at AIUB for the orbit improvement is capable to estimate the A/M . For all 250 objects, orbits were determined including an estimation of the A/M value. The error of the estimated A/M was less than 1% in average. The resulting mean formal errors are listed in Table 6.14. The mean formal errors and the rms for all A/M are nearly identical. Comparing Table 6.14 with Table 6.13 it can be noted that the mean formal errors for $A/M = 0.02 \text{ m}^2/\text{kg}$ are larger with an estimation of the A/M value than without. The reason is that more parameters have to be determined when estimating an A/M value which leads to larger formal errors.

GTO

For the GTO objects, the follow-up tracks were simulated after 0.25 h, 0.5 h, 2 h, and at the first apogee after one day. Again, no estimation of A/M was included in the determination of elliptical orbits. Table 6.15 shows the mean formal errors and the mean RMS.

As expected, the result is similar to the result for the GEO objects. The formal errors get larger for higher

Table 6.15: Mean formal errors for the elliptical orbit determination of GTO objects with various A/M representing the discovery track and the follow-up tracks after 0.25 h, 0.5 h, 2 h, and at the first apogee after one day. The orbit determination does not include an estimation of A/M.

| A/M [m ² /kg] | a [m] | e | i [°] | Ω [°] | ω [°] | rms ["] |
|--------------------------|---------|----------------------|----------------------|----------------------|----------------------|---------|
| 0.02 | 9.29 | $7.08 \cdot 10^{-6}$ | $1.85 \cdot 10^{-4}$ | $2.41 \cdot 10^{-3}$ | $2.78 \cdot 10^{-3}$ | 0.32 |
| 0.08 | 9.36 | $7.13 \cdot 10^{-6}$ | $1.86 \cdot 10^{-4}$ | $2.42 \cdot 10^{-3}$ | $2.97 \cdot 10^{-3}$ | 0.33 |
| 0.32 | 10.46 | $7.90 \cdot 10^{-6}$ | $2.05 \cdot 10^{-4}$ | $2.64 \cdot 10^{-3}$ | $3.05 \cdot 10^{-3}$ | 0.36 |
| 1.28 | 19.24 | $1.40 \cdot 10^{-5}$ | $3.67 \cdot 10^{-4}$ | $4.58 \cdot 10^{-3}$ | $5.26 \cdot 10^{-3}$ | 0.66 |
| 5.12 | 62.75 | $4.45 \cdot 10^{-5}$ | $1.19 \cdot 10^{-3}$ | $1.45 \cdot 10^{-2}$ | $1.66 \cdot 10^{-2}$ | 2.13 |
| 20.48 | 244.60 | $1.73 \cdot 10^{-4}$ | $4.63 \cdot 10^{-3}$ | $5.63 \cdot 10^{-2}$ | $6.46 \cdot 10^{-2}$ | 8.29 |

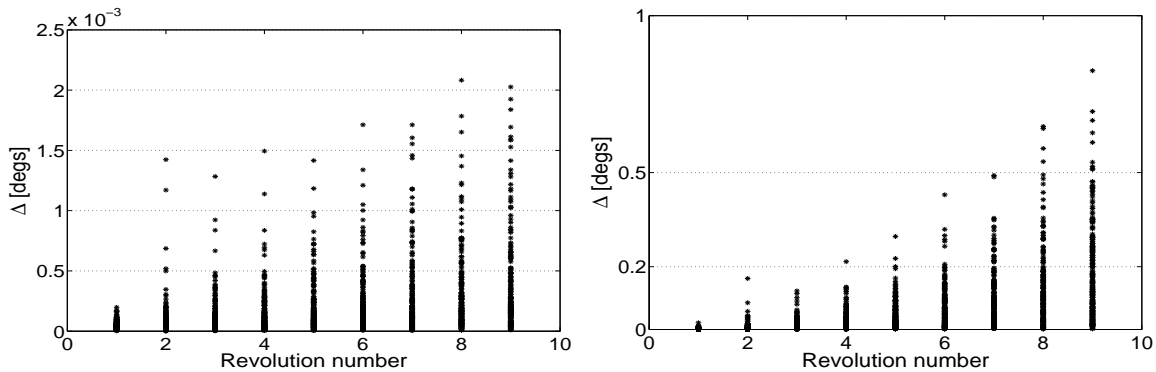


Figure 6.10: Difference Δ at the apogee between “true” and determined elliptical orbit representing the discovery track of two GTO objects with $A/M = 0.02 \text{ m}^2/\text{kg}$ (left) and $A/M = 20.48 \text{ m}^2/\text{kg}$ (right). The orbits include the discovery observations and follow-up tracks after 0.25 h, 0.5 h, 2 h, and the first apogee after 1 day. The orbit determination does not include an estimation of A/M. Each line represents the result from one of 250 simulations.

A/M, with an almost linear dependency for high A/M.

Figure 6.10 shows the differences at the apogee between the determined and the “true” orbits for $A/M = 0.02 \text{ m}^2/\text{kg}$ (left) and $A/M = 20.48 \text{ m}^2/\text{kg}$ (right). The differences are very small for $A/M = 0.02 \text{ m}^2/\text{kg}$. For $A/M = 20.48 \text{ m}^2/\text{kg}$ a strong increase of the differences is visible. To recover the objects one day after the last follow-up, a FOV larger than 1° would be needed for some of the objects.

Conclusions

The simulations have shown that accurate orbits can be determined if the A/M is well estimated, i.e., if the radiation pressure is well modeled. But it has to be noted that the reality is much more complex. Objects with a high A/M are likely to be very flat, like a piece of paper. It is further possible that these objects are tumbling. Combining the two assumptions, we conclude that the perturbations due to the solar radiation pressure depend on the rotation of the object and can change dramatically within a short time interval. This makes it much more complicated to model the orbits.

Table 6.16: Mean formal errors for the elliptical orbit determination of GTO objects with various A/M representing the discovery track and the follow-up tracks after 0.25 h, 0.5 h, 2 h, and at the first apogee after one day. The orbit determination does include an estimation of A/M.

| A/M [m ² /kg] | a [m] | e | i [°] | Ω [°] | ω [°] | rms [″] |
|--------------------------|-------------------|----------------------|----------------------|----------------------|----------------------|---------|
| 0.02 | $1.87 \cdot 10^2$ | $9.60 \cdot 10^{-6}$ | $2.21 \cdot 10^{-4}$ | $2.71 \cdot 10^{-3}$ | $3.14 \cdot 10^{-3}$ | 0.33 |
| 0.08 | $1.87 \cdot 10^2$ | $9.60 \cdot 10^{-6}$ | $2.21 \cdot 10^{-4}$ | $2.71 \cdot 10^{-3}$ | $3.14 \cdot 10^{-3}$ | 0.33 |
| 0.32 | $1.87 \cdot 10^2$ | $9.60 \cdot 10^{-6}$ | $2.21 \cdot 10^{-4}$ | $2.71 \cdot 10^{-3}$ | $3.14 \cdot 10^{-3}$ | 0.33 |
| 1.28 | $1.87 \cdot 10^2$ | $9.60 \cdot 10^{-6}$ | $2.21 \cdot 10^{-4}$ | $2.71 \cdot 10^{-3}$ | $3.14 \cdot 10^{-3}$ | 0.33 |
| 5.12 | $1.88 \cdot 10^2$ | $9.61 \cdot 10^{-6}$ | $2.21 \cdot 10^{-4}$ | $2.71 \cdot 10^{-3}$ | $3.14 \cdot 10^{-3}$ | 0.33 |
| 20.48 | $1.86 \cdot 10^2$ | $9.57 \cdot 10^{-6}$ | $2.20 \cdot 10^{-4}$ | $2.68 \cdot 10^{-3}$ | $3.10 \cdot 10^{-3}$ | 0.32 |

Some first photometric analyses of objects with high A/M have shown that the tumbling motion of these objects can be very complex ([Schildknecht *et al.*, 2005c]). This also reflects in the estimation of the A/M value. For some objects, the estimated value remains constant when adding new observations to the orbit determination. For other objects, however, the A/M value can change by up to a few percent.

6.2 Planning

Tasked observations have to be planned in order to build up and maintain a catalogue, especially to acquire “secured” orbits for the objects. The planning depends on the number of available telescopes. If only one telescope is available, it is probably not possible to observe all objects from the catalogue during one night. This depends on the size of the catalogue and on the visibility of the objects from the site. A selection of the catalogued objects has to be considered. The parameters of the selection can be the type of the object and the age and the accuracy of the catalogue orbit.

If more than one telescope is available, a larger part of the objects in the catalogue can be scheduled for observing during one night. For each object, one of these telescopes has to be selected to perform the observations. The principal selection criteria are the availability of the telescope and the visibility of the object from the site of the telescope. A telescope might not be available due to weather conditions, loss of power supply, or maintenance of the instrument. If more than one telescope meets the selection criteria, the phase angle, the range, and the elevation of the object with respect to the telescope should be optimized, too.

An orbit propagator has to be used to determine the ephemerides of the planned object for the selected telescope. It is recommended that the propagator includes the same physical models as used in the orbit determination, especially for GEO objects with high A/M and GTO objects. In addition, it should be possible to include all estimated parameters from the orbit determination into the propagation. A search algorithm may also be applied to the planning, if the object was not recovered in earlier observations. Such an algorithm should in particular include a search in along track direction.

Two observation strategies may be invoked for maintenance observations. One is to plan tasked observations for all objects in the catalogue. Another possibility is to perform surveys and to acquire all or some of the maintenance observations implicitly. This means that the same part of the population is observed every n days, where n should be below 30. A survey strategy for GEO objects was described by [Flohner *et al.*, 2005b]. Both strategies should comply with the concepts outlined in Chapter 5 and Section 6.1.

6.2.1 Maintenance Observations

The planning of the maintenance observations depends on the type of the objects. Objects with orbits, which are more difficult to model, like high A/M GEO and GTO objects, have to be observed more frequently.

GEO

We have seen in Section 5.1 that it is theoretically sufficient to observe GEO objects every 30 days to maintain their orbits. For a single station, this will not be realizable in reality for many objects due to their visibility. The visibility, i.e., mainly the return time of the objects, is a crucial parameter for the planning, especially for objects in drift orbits as most debris objects in GEO are.

For objects with large drift rates, the gap between the maintenance observations should be equal to the return time. Objects with a drift rate larger than 12.5° have a return time smaller than 30 days (s. Table 2.2). These objects are therefore observed more frequently than every 30 days.

For objects with small drift rates, however, the return times can be very long (about 280 days for a drift rate of $\pm 1.3^\circ$). The orbits of objects, which are only observed once every half-year, would of course not be very accurate. It is therefore necessary to observe these objects several times during the time period of their visibility. For visibility times longer than 60 days it is sufficient to observe the objects every 30 days. For smaller visibility times, a gap of only 15 days is recommended.

High A/M GEO

Objects with high A/M have to be observed more frequently as their orbits are difficult to model. The gap between the maintenance observations depends on the A/M. The gap has to be smaller for higher A/M. As there is not much experience with this type of GEO objects, the gap should be rather short to guarantee a recovery. Furthermore, the availability of several instruments well distributed in longitude might be mandatory to maintain the orbits of high A/M GEO objects due to the visibility.

GTO

GTO objects have to be observed more frequently than GEO objects. Furthermore, two observation tracks within about one hour should be observed as the orbit determination could be problematic with one track only. The two maintenance tracks should be observed about every 15 days. This gap may vary by one or two days due to the visibility constraints.

If the correlation procedure includes a comparison of the orbits (see below), the two series of observations within one night can be used to determine an elliptical orbit. A gap of half an hour to one hour between the two series is recommended.

6.3 Correlation

The correlation of new observations with an object from a catalogue is a critical issue. It depends on the quality of the observations and on the quality of the catalogued orbits. There are several ways to correlate

the observations with the catalogue.

In any case, a preselection of the catalogued objects is recommended in order to reduce the computation load needed for the correlation. If the catalogue contains LEO objects, they can be excluded as LEO objects appear on the frames as long streaks when observing GEO objects or GTO objects close to the apogee. Furthermore, LEO objects probably do not appear on more than one frame, depending on the FOV and the time interval between the observations.

If we accept that a few detections cannot be correlated with the catalogue then the correlation must not necessarily be performed with both, the GEO and the GTO population. Already a circular orbit determined from a short observation arc gives some indication to which population the detected object might belong. As we have shown in Section 3.1.1, the semi-major axis of the inferred circular orbit depends on the real semi-major axis and eccentricity (see Equation 3.1) and on the position within the orbit at the moment when the detection has been made. This behavior can be used to make a preselection. Detections with an inferred semi-major axis of $42\,164 \pm 2\,000$ km will be correlated with GEO and high A/M GEO objects, the other ones with GTO and high A/M GEO objects. The high A/M GEO objects have to be used anyway as the inferred orbits of these detections can look like a GEO or a GTO. Of course, also detections of GTO objects can exhibit an inferred semi-major axis that falls into the selected range. Those will be the detections that cannot be correlated. But potential follow-up observations of these detections will help to perform a correlation in a later step.

Of course, it depends on the specific requirements if such a preselection should be made.

Five correlation methods are presented in the following. Each has some advantages and disadvantages. The presented methods are:

1. Comparison of the positions,
2. Comparison of the positions and the apparent velocity vectors,
3. Comparison of the positions and the orbital elements,
4. Comparison with the error ellipsoids,
5. Comparison of the residuals from the orbit determination.

Comparison of the positions

The most simple way to correlate observations with a catalogue is to compare the positions only. Ephemerides will be determined from the orbits of the catalogued objects for the epoch of the observation and the propagated positions compared with the observed position. If the difference is smaller than a given value the correlation will be accepted. If the differences for several objects are within the given range the object with the smallest difference in the position will be selected. Each single observation is correlated separately.

The main advantage of the procedure is that an object can also be correlated if only one new observation is available. In this case, no preselection as described above can be made. But there is also a big disadvantage. Inaccurate orbital elements from the catalogue or objects with similar positions (as satellite clusters) can lead to false correlations. In the case of similar positions, it might be necessary to include one of the other methods to decide which is the correct object. Furthermore, the correlation criteria does not use any information about the accuracy of the orbits. As the error in along track is normally larger than in the other two directions, the error ellipsoid can have an elongated shape. Comparing only the

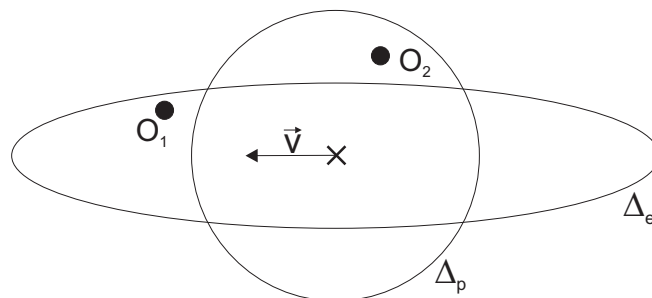


Figure 6.11: Comparison of the error ellipsoid Δ_e with observed positions O_1 and O_2 . \times is the expected position of the object and \vec{v} its velocity vector. Δ_p is the fixed search radius if the positions are compared without using the error information.

positions can therefore cause a false correlation or that the detection is not correlated although it would be the correct object. This is visualized in Figure 6.11. O_1 would not be correlated using a fixed search radius, although it could be the right object when consulting the error ellipsoid. O_2 , however, would be correlated but it is probably not the right object.

Comparison of the positions and the apparent velocity vectors

In method 1, only the single positions were compared. If more than one observation of the new detection is available, the apparent velocity vectors can also be compared. Again, ephemerides for the catalogued orbits will be determined for the epochs of the observations. The propagated positions have to be within a given range around the observed positions, as in method 1. In addition, the position differences between the first and the last observation will be compared with the corresponding differences between the propagated positions. The difference has to be smaller than a specified value.

This method should reduce the number of possible correlating objects due to the additional criteria. But the method is probably not sufficient to distinguish between satellites in a cluster.

Comparison of the positions and the orbital elements

One approach for the correlation of a newly detected object with an existing catalogue was already presented in Chapter 4. In addition to the positions, the orbital elements are also compared. The differences between the determined elements of the detection and the elements of the catalogued orbits have to be smaller than given values. Normally, not all six orbital elements have to be compared. When circular orbits were determined, it is sufficient to compare a , i , and Ω . When elliptical orbits were determined, at least the eccentricity should be additionally included. The procedure was successfully tested with detections of GEO objects.

The main disadvantage of this method is that normally only circular orbits are determined from the short observation arc of newly detected objects. If the true orbit of the detected object is highly eccentric, like for GTO objects or GEO objects with high A/M, a comparison of the orbits does not lead to a useful result. For GTO objects, this problem can be avoided if an additional follow-up track is acquired within the observation night for every detected object. An elliptical orbit can be determined from these two

tracks that should be accurate enough for a successful correlation. For high A/M GEO objects, however, also follow-up tracks might not help as the orbital elements can change very fast due to the radiation pressure (s. [Schildknecht *et al.*, 2005b], [Anselmo and Pardini, 2005], or [Liou and Weaver, 2005]). A very accurate orbit propagation of the catalogued objects is then essential.

Comparison of the positions with the error ellipsoids

Another approach is to compare the positions with the propagated error ellipsoids of each object from the catalogue. The covariance matrices are needed to determine the error ellipsoids. The object is correlated if the observed position is inside the corresponding error ellipsoid (see Figure 6.11). It is possible that this criteria is fulfilled for several objects from the catalogue. In this case, the object can be selected using method 5. As for the first method, also single observations can be correlated. If the detected track consists of more than one observation then the error ellipsoid of the velocity can be used additionally. This would also strengthen the correlation method.

The advantage of this method is, that the accuracies of the orbits from the catalogue are also taken into account. Also, no observations of the objects from the catalogue are necessary. The disadvantage, however, is that the covariance matrices of all objects in the catalogue must be available. This is often not the case for external catalogues, like the DISCOS database.

The methods described above have in common that either the orbits or the covariance matrices have to be propagated for the epoch of the observations for the objects in the catalogue, which can be very time consuming. This is especially the case for GTO objects and GEO objects with high A/M. For both, a very good model has to be used for the orbit propagation. A method that does not include ephemerides is described below.

Comparison of the residuals from the orbit determination

The most effective method is to determine orbits using the new observations together with observations of each object from the catalogue. The correlation can then be made by comparing the residuals, or the RMS, of the orbit determination. Some tests showed that the correlation is even unambiguous for satellite clusters like the Astra satellites ([Musci *et al.*, 2005a]).

The big disadvantage of this method is that the computation load will be enormous for a large catalogue. Furthermore, manual interaction may be needed as various parameters might have to be estimated for different objects. Also, the observations of every object in the catalogue have to be stored.

6.3.1 Recommendations

As we have seen, only the last method guarantees an unambiguous correlation for every object. But as the computation load is too large, the method is not very efficient. The other methods, however, might result in several objects that are possibly correlated with the detection. The solution of this problem is to use two of the described methods. One of the first four, faster methods can be used to make a preselection. In the ideal case, the method will already lead to an unambiguous correlation. If this is not the case, the orbit determination method can be applied to a small group of candidate objects resulting

after performing one of the other methods.

The selection of the methods of course depends on the information available in the catalogue. In the ideal case, observations are available for every object in the catalogue. It is then possible to determine not only the orbits, but also the covariance matrices. With all these informations, it is recommended to use method 4 to make a preselection and if necessary method 5 to make the final correlation. Observations are normally only available for objects of an internal catalogue. In external catalogues at least the covariance matrices may be included. It is then not possible to make a final correlation using method 5. Method 4 is recommended to achieve the best possible result. If neither observations nor the covariance matrices are available, like for the DISCOS database, one of the methods 2 or 3 is recommended. Which one is selected depends on the type of the determined orbit. If all six orbital elements were determined, method 3 should lead to the better result. If only circular orbits were determined, method 3 is only useful for GEO objects. Method 2 has to be used for the other objects. But as the type of the orbit cannot be identified definitely from a circular orbit it is recommended to use method 2 anyway.

The AIUB has a long experience in the correlation of detected GEO objects with objects from the DISCOS database. The method “Comparison of the positions and the orbital elements” has been used. Using this method, a large part of the detected bright objects could be correlated with one of the DISCOS objects (see Section 3.1). There are several reasons that some bright objects could not be correlated. The first is, that not all existing bright objects are included in DISCOS. The second is, that the accuracies of some orbits in DISCOS are not sufficient for a correlation. Finally, it was not possible to correlate detections of satellite clusters. In the first case, a correlation is not possible and the detected object may be added as new object in the internal catalogue. In the last two cases, none of the first four methods will lead to a correlation. The result would be no correlation or a false correlation in the case of inaccurate orbits from the catalogue, or a group of possibly correlating objects in the case of satellite clusters. If observations for the objects in the DISCOS catalogue are available, the method of orbit determination may help in both cases to perform a correlation with the right object.

As only circular orbits could be determined for most of the objects detected during the surveys performed by AIUB, no objects other than GEO objects could be correlated. The exception are a few GTO objects, which could be correlated because follow-up observations of these objects were acquired and therefore elliptical orbits could be determined.

If no follow-up observations are available, one of the methods 1, 2, or 4 can be used to make a preselection. But the first method is in general not recommended as the chance for a false correlations is higher as for the other methods. With follow-up observations, elliptical orbits can be determined. In this case, the method 3 can be very efficient. But in both cases, with or without follow-ups, method 5 might be needed to make a final correlation. It is therefore recommended to store all observations, especially when a new catalogue is built up.

The major task for the first four methods is the propagation. Either ephemerides, the orbits, or the error ellipsoids have to be propagated for the epoch of the detection. In any case, a very accurate force model is needed. As the propagation has to be performed for every object in the catalogue, it can be very time consuming. One possibility to reduce the problem with the computation time is to propagate the whole catalogue to a specific epoch for each observation night, e.g. midnight. This can be done during daytime before the observation night. A simple model can then be used to perform the propagation to the individual observation epoch. This is allowed as the propagation interval is much shorter than one revolution. Only for special objects, like objects with high A/M, an accurate model might also be needed for the propagation within the night.

Conclusions

Several methods for the correlation of newly detected objects have been presented. Every method has its disadvantages and therefore a combination of two methods is recommended. One of the methods 1-4, depending on the information available in the catalogue, should be used to make a preselection resulting in a short list of candidate objects. Of course, this preselection can already lead to an unambiguous correlation. The method of the orbit determination should be used if the result of the preselection are several candidate objects and if observations for the objects in the catalogue are available.

7. Summary and Outlook

More than 4 000 rocket launches have been recorded since the launch of Sputnik 1 on 4 October 1957, putting satellites and other man-made objects into space. About 10 000 objects are regularly tracked and catalogued by the Space Surveillance Network (SSN) of the United States Strategic Command (USSTRATCOM). Also the Russian military service is maintaining a catalogue but with only about 6 000 objects. The European DISCOS catalogue is based on the USSTRATCOM catalogue. First feasibility studies for a European Space Surveillance System have been completed in 2005. The Astronomical Institute of the University of Bern (AIUB) was contributing to these studies.

Optical instruments are used to observe objects in high altitudes, like objects in geostationary Earth orbits (GEO) and geostationary transfer orbits (GTO). The GEO region is of special interest for commercial applications as the objects have the same angular velocity as the Earth and therefore appear to remain fixed in the sky. The USSTRATCOM catalogue is limited to GEO objects larger than a meter. A GTO is used to transport satellites from a circular orbit at low altitude to the GEO region. The orbits are highly eccentric, with the perigee at low altitudes and the apogee reaching the GEO.

The AIUB has been performing search surveys for objects in GEO and GTO since 1999. The goal of these surveys is to deepen the knowledge about the space debris populations in these regions. The observations are performed with the ESA Space Debris Telescope (ESASDT) on Tenerife. More than 12 500 detections of various objects had been made until December 2004. Almost 7 000 of them could not be correlated with an object from the DISCOS catalogue. The diameter of the detected objects is larger than about 10 cm.

Only circular orbits were determined from the short observation tracks of the detections. For eccentric orbits, like GTO, this leads to inferred semi-major axes, which are different from the real semi-major axes of the orbits. The results from the surveys are therefore biased due to the assumption of circular orbits. Elliptical orbits are needed to correctly analyze the debris populations in the GEO and the GTO region from the gathered data.

One possibility to determine elliptical orbits is to search the data for multiple detections of the same object. Another solution is to perform follow-up observations of the detected objects. In both cases, the resulting longer observation arcs allow to determine all six orbital elements. A tool was developed (program CAMRES), which either searches for detections that may stem from the same object, or searches for follow-up observations of the detections. In the first case, the determined orbits of the detections are compared. The differences for selected elements have to be below given values. Unfortunately, only multiple detections of GEO objects could be identified for the performed surveys as only circular orbits were determined. The compared elements were the semi-major axis a , the inclination i , and the right ascension of ascending node Ω . The CAMRES tool, however, would be capable to compare also elliptical orbits. Follow-up observations of part of the detections were performed during the surveys. The CAMRES tool searches for objects detected on the follow-up observations. All found detections are

potential follow-ups of the progenitor detection.

Another tool was developed (program CAMCOR) to perform the final correlation for the results from the CAMRES tool. The correlation process is based on the comparison of the RMS of the residuals of the determined elliptical orbits. The input are groups of detections that are connected either by the comparison of the orbits or by the observation sequence of the night. In the first case, an elliptical orbit is determined for every combination of detections. The RMS has to be below $2''$ to accept that the detections belong to the same object. In the second case, the orbits are only determined for combinations of the progenitor detection with each of the detections from the follow-up observations.

Each monthly campaign was processed with the two tools CAMRES and CAMCOR. 1 570 detections could be correlated with other detections by comparing the orbits with CAMRES and by performing the final correlation with CAMCOR. As only circular orbits were determined, the correlated detections most likely belong to GEO objects. According to the determined circular orbits, 4 224 of the total detections seem to belong to GEO objects. By subtracting the 1 570 correlated detections from the 4 224 total GEO detections we get the maximum number of observed objects. As the monthly campaigns were processed separately and because many objects most likely have been observed during several campaigns the actual number of different objects must be smaller than the resulting 2 654. Nevertheless, the results showed that the two tools are very useful to identify multiple detections, at least of GEO objects. In a next step a whole year could be processed at once. The number of correlated detections should then get larger. But the problem is that some objects may be only detected once during each monthly campaign. It is almost impossible to determine orbits from two very short tracks with a gap of about one month between them.

The processing of potential follow-ups showed that many successful follow-ups have been performed. In 92% of the cases where at least one object had been detected on the series of follow-up frames a successful follow-up of the progenitor detection could be identified. Currently, the CAMRES tool does not search for series of follow-ups, i.e., it is not considered if a follow-up of a successful follow-up was performed. The tool should be modified to be able to identify series of follow-ups. This would allow to determine very accurate elliptical orbits.

Multiple detections can be used to determine accurate orbits and to build up a catalogue of orbits. Nevertheless, this is certainly not the most efficient way to build up and maintain a catalogue. More efficient concepts to catalogue GEO and GTO objects were therefore developed. Concepts for a narrow field of view (FOV) of 0.4° and a wide FOV of 2° were studied. Simulations were used to determine the number of the necessary observation tracks and the temporal spacing between them to generate “secured” orbits. A “secured” orbit allows to recover an object after several weeks to months. To recover an object, the error in the propagated position must be less than half of the FOV. 250 orbits for GEO and GTO were simulated. These orbits were used to simulate observations at different epochs. An error of $\sigma = 0.5''$ was assumed for the accuracy of the single observation. Orbits were determined using the simulated observations. The perturbations due to the Earth’s oblateness and the lunar and solar gravity were included in the orbit determination. Different concepts result if orbit improvement in near real time is possible or not. The cases where it is possible were discussed in detail in this work. Only the results were presented for the assumption that no real time orbit improvement is possible.

First, the concepts to acquire “secured” orbits for GEO objects were developed. For a wide FOV of 2° the discovery track and two follow-up tracks separated by one hour are sufficient to recover the objects during the following night. An additional follow-up one day after the discovery already allows to determine a “secured” orbit. For a narrow FOV of 0.4° two follow-ups during the first night are not enough. A third follow-up track three hours after the discovery is necessary to determine an orbit, which allows to recover

the object during the following night. The same concepts result when no online improvement in near real time is possible.

The situation is more complex for GTO objects. The differences of the determined orbits and the real orbits are much larger at the perigee than at the apogee. For a wide FOV of 2° two follow-up tracks, the first 0.5 hours and the second 2 hours after the discovery, allow to recover the objects at the apogee during the following night. To get “secured” orbits, another follow-up track at the apogee during the fifth night after the discovery is necessary. The concept for a narrow FOV of 0.4° is almost identical. An additional follow-up track at the beginning, 15 minutes after the discovery, is needed. The circular orbit determined for this track has to be used to acquire the second follow-up as in many cases no elliptical orbit can be determined for GTO objects from an observation arc of only 15 minutes. Other concepts result without orbit improvement in near real time. Three follow-up tracks separated by half an hour each are necessary to recover the objects during the following night with a wide FOV. Again, another follow-up during the fifth night after the discovery is needed to get “secured” orbits. For a narrow FOV a follow-up every 15 minutes until 2 hours after the discovery has to be acquired. But it is not guaranteed that this concept is successful for all objects as the errors get larger when the objects are observed further away from the apogee.

If “secured” orbits for both types of orbits, GEO and GTO, should be determined, it is recommended to implement the possibility of orbit improvement in near real time. This clearly reduces the observation time needed for follow-ups. Using a wide FOV instead of a narrow FOV will further reduce the number of needed observation tracks by one track during the first night.

The benefit of using observations from multiple sites to acquire “secured” orbits was also analyzed. Nine virtual sites were used for the simulations. The main site was assumed to be located at longitude $\lambda = 0^\circ$ and latitude $\beta = 0^\circ$. For the other sites, either the longitude or the latitude was varied from 10° to 40° . Two tracks with different time intervals between the tracks were simulated. The first track was in each case simulated to be observed at the main site, while the second track was simulated for every available site, including the main site. The results showed that a larger separation between the sites reduces the errors of the determined orbits.

For GEO objects, simultaneous observations from two sites are recommended if the separation between the sites is mainly in latitude. For a larger separation in longitude slightly better orbits result for a gap of one hour between the two tracks. For a gap longer than about three hours the result does not much depend on the site that was used to acquire the second track. The result is then dominated by the length of the observation arc. For GTO objects using observations from two sites leads to a much better improvement than for GEO objects when the observation arc is short. The results are worse for longer observation arcs than for short arcs. The reason is probably the poor distribution of the observations. But further simulations would be needed to verify this.

Simultaneous observations from three sites were also studied. The improvement of the orbital accuracy is not so large compared to two sites that it would justify to use three sites. A third site should rather be used for other tasks.

It cannot be decided from the performed analyses whether observations from one site or from two sites should be used to acquire “secured” orbits. A performance estimation for the two cases is needed to make this decision.

GEO objects have to be observed about every 30 days to maintain a catalogue. The simulations showed that accurate orbits can be determined using several tracks separated by 30 days when a good a priori orbit

is available. The observations from the acquisition of a “secured” orbit do not have to be included in the orbit improvement process. Nevertheless, it is recommended to observe the objects at different positions on their orbits as this would lead to even more accurate orbits. One problem are objects with small drift rates. Some of these objects are not visible from a single site for more than half a year. But the time period of their visibility is also very long. Frequent observations within this time allow to determine an orbit that is accurate enough to recover the object after more than half a year. Furthermore, manoeuvres were not included in the considerations above. Controlled, also called station keeping, objects have to be observed more frequently because of the manoeuvres. Station keeping objects are manoeuvred about once every two weeks. An indication that an object is controlled is a small inclination close to 0° . This fact can be used as a selection criteria for objects that should be observed every few days. There are, however, also objects with larger inclinations that are controlled in longitude only.

GTO objects have to be observed more frequently than GEO objects to maintain a catalogue. Two tracks every 15 days have to be acquired. The two tracks should be separated by 0.5 h – 1 h. Two tracks are necessary to get a better distribution of the observations within the orbits. With only one track every 15 days the orbit determination can fail.

The presented concepts are based on the assumption that only one sensor at one site is available. But the same concepts can be used if sensors from several sites contribute to the observations, which is the case for a space surveillance system. A network of sensors makes it much easier to build up and maintain a catalogue, especially when the sensor sites are well distributed in longitude. During the acquisition of a “secured” orbit, the objects will always be visible from at least one of the sites, assuming the weather conditions are good. Also the maintenance of drifting GEO objects is not anymore a problem. When they drift out of the visibility range of one site they will enter into the visibility range of another site. For GTO objects the chance is higher that the apogee is visible during nighttime from one of the sites.

The experience gained with this work and some of the tools were recently used to develop concepts to build up a catalogue of medium Earth orbits. This type of orbits are mainly used for navigation satellite systems as the U.S. Global Positioning System (GPS), the Russian GLONASS system, and the future European GALILEO system. The results will be presented by T. Flohrer from AIUB at the 36th COSPAR Scientific Assembly in Beijing, 16-23 July 2006.

The analysis of area-to-mass ratio (A/M) modeling errors showed how important it is that the A/M value can be estimated sufficiently accurate. Not only should the orbit improvement process allow to estimate a value for the A/M, but it should also be possible to introduce this value into the orbit propagation.

The correlation of newly detected objects with the catalogue is a critical issue when maintaining a catalogue. Five different methods to perform the correlation have been presented. To make an unambiguous correlation a combination of two of the described methods have to be used. One is used to make a preselection. The method of orbit determination is then used to make the final correlation. But this is only possible if observations for each object are contained in the catalogue. If this is not the case, the comparison with the error ellipsoids would lead to the best results. In this case, the covariance matrices have to be available. If neither the observations nor the covariance matrices are available the positions and the apparent velocity vectors should be compared.

The simulations presented in this work have been tested using real observations from the ESASDT, the Zimmerwald Laser and Astrometry Telescope (ZIMLAT), and the Crimean Astrophysical Observatory (CRAO). The examples showed good consistence with the simulations. Of course, a test campaign would be helpful to verify the presented concepts and if necessary to improve them.

First studies for a European Space Surveillance System have recently been presented. Such a system needs good concepts for the maintenance of the catalogued orbits. The results in this work demonstrated that the presented concepts can be used to efficiently build-up and maintain a catalogue of orbits for GEO and GTO objects. Part of the presented concepts may therefore be implemented in the processing pipeline of a future European Space Surveillance System.

A. The Program System CelMech

The program system CelMech was used to generate a major part of the results for this work. It was developed by Prof. Gerhard Beutler, head of the AIUB, and Prof. Leoš Mervart of the Technical University of Prague. The package consists of several programs for various applications, e.g., Fourier analysis, simulations of the planetary system, orbit determination and improvement, generation of ephemerides. The programs and the corresponding methods and models that are implemented in CelMech are described in detail in the two-volume work [Beutler, 2005]. A CD containing the CelMech package is attached to the mentioned books. A short version of the algorithms used for the orbit determination and improvement was published in [Beutler et al., 2003].

A short description of the two programs ORBDET and SATORB is given below. ORBDET is used for the first orbit determination and orbit improvement, whereas SATORB can be either used for orbit improvement or for the generation of ephemerides.

Both programs had to be modified to allow for an automated processing without user interaction and for a series of different objects. This was mandatory to process the large amount of data within a reasonable time.

A.1 ORBDET

The program ORBDET may be used to determine the orbits of minor planets, comets, artificial satellites, and space debris. As the program does not make use of any a priori orbital elements, a first orbit has to be determined initially. One of two different methods can be selected for the first orbit determination: a circular orbit or a general two-body orbit, formulated as a boundary value problem, may be determined.

The first method was always used in the context this work. Two observation epochs from the input series of astrometric positions have to be selected for which the circular orbit should be determined. The program performs a search over the semi-major axis a (\cong orbital radius). The search pattern starts with an initial value of $a = 6\,250$ km and ends with the final value of $a = 99\,000$ km, with a step size of 250 km. If acceptable roots for a were found, the program user has to select one of them. For artificial satellites or space debris, only one root is normally found. This is why this step could be automated for the simulations within this work.

Afterwards, an orbit improvement process including selected perturbations is invoked. Only the Earth's oblateness and the gravitational attraction exercised by the Sun and the Moon may be selected for the force model. It is then possible to include part of or all observations. If only a subset of all available observations were included, the orbit improvement process is repeated with all observations. Finally, various files are written, e.g., one containing the orbital elements and the estimated RMS.

The program ORBDET was used for all orbit determinations performed in Chapter 5.

A.2 SATORB

Three different problems may be solved with SATORB:

- Generation of ephemerides for satellites or space debris based on an initial set of osculating elements,
- Orbit determination using tabular positions for GPS, GLONASS, or LEO satellites,
- Orbit improvement using astrometric positions.

The second task is not relevant for this work and therefore not further described. A short description of the other two tasks is given in the following subsections.

A.2.1 Satellite Ephemerides

The necessary input parameters are the initial epoch, the length of the integration interval, and the initial orbital elements. For the force model, the upper limits for degree n and order m of the Earth potential can be defined, where $m \leq n$ (usually $n = m$). As for ORBDET, the gravitational attractions exercised by the Sun and the Moon can be included. But in addition, the tidal attraction and the corrections due to general relativity may be selected as well. Furthermore, a simple model for the direct radiation pressure and a drag force can be activated. If either the radiation pressure model or the drag was selected, the area-to-mass ratio and other related information have to be defined. Finally, the specifications for the integration, like the integration order and the initial step size, have to be defined. The integration is performed with a collocation method with automatic step-size control (see [Beutler, 2005]).

The principal result is a list of epochs (modified Julian date) and the corresponding osculating or mean elements $a(t)$, $e(t)$, $i(t)$, $\Omega(t)$, $\omega(t)$, and $\sigma_0(t)$. But the output needed in our context are the positions in right ascension $\alpha(t)$ and declination $\delta(t)$. The program SATORB was therefore modified to provide these positions. This modified version was used to generate the simulated observations and to determine the differences between two orbits in Chapters 5 and 6. For the former task, the option to add an error σ for the observation accuracy was implemented. A random error with zero mean and a user-specified variance σ^2 is then added to the simulated position. Note that the modifications are not included in the version delivered with the books [Beutler, 2005].

A.2.2 Orbit Improvement

The orbit determination part of the SATORB program is an orbit improvement process. A priori elements are required for this purpose. They may stem from ORBDET, SATORB from a previous orbit improvement step, or from any other orbit determination program (if the provided format of the elements file is correct).

The implemented force model was already described in Section A.2.1. The possibility to define the A/M value was used in Section 6.1.3, where the influence of A/M errors were studied.

A parameter estimation problem with initial osculating elements as unknowns has to be solved when processing astrometric positions. Consequently, six variational equations have to be solved in addition to the equations of motions. The program SATORB solves the variational equations associated with

the a priori elements, which are used as initial elements, simultaneously with the equations of motion. The variational equations associated with dynamical parameters (parameters defining the force model) are solved independently, after the solution of the equations of motion, using the method of numerical quadrature.

The following parameters may be estimated in addition to the six orbital elements with the program SATORB:

- Any combination of nine radiation pressure model parameters (constant, once per revolution: amplitude and phase) using the X-, Y-, Z- decomposition (Y: axis of solar arrays, Z: direction satellite - Sun, X: normal to Y and Z) of the perturbing forces,
- Any combination of nine empirical parameters (constant, once per revolution: amplitude and phase) using the R-, S-, W- decomposition (radial, along-track, out-of-plane) of the perturbing forces,
- Scaling parameter of the simple radiation pressure model,
- Pseudo-stochastic pulses.

Within this work, only the scaling parameter of the simple radiation pressure model was considered as unknown. This scaling parameter can be interpreted as a correction of the a priori value of the A/M. It was estimated in Section 6.1.3.

No parameters other than the orbital elements were estimated within the orbit improvement process for longer observation arcs as used in the Sections 6.1.1 and 6.1.2, except for examples of real observations.

Bibliography

Agapov, V., Z. Khutorovsky, V. Boykov, N. Sbytov, and A. Samatokhin (2003), Experience of Formation of the GEO Orbital Information Archive Based on Different Data Sources, in *Paper presented at Fifth U.S.-Russian Space Surveillance Workshop, 24-27 September 2003, Pulkovo, St. Petersburg, Russia.*

Agapov, V., V. Titenko, V. Stepanyants, J. Dick, P. Herridge, T. Schildknecht, and M. Ploner (2005), Joint RAS/PIMS/AIUB GEO Survey Results, in *Proceedings of the Forth European Conference on Space Debris, pp. 119-124, ESOC, Darmstadt, Germany, 18-20 April 2005.*

AIUB (2006), AIUB Homepage, <http://www.aiub.unibe.ch>.

Aksenov, O., O. Andreyev, V. Dicky, N. Johnson, Yu. Tretyakov, S. Veniaminov, and V. Zavaliy (2003), Dynamics of the Principal Characteristics of the US/Russian Space Objects Catalogs Since 1995 to 2002, in *Paper presented at Fifth U.S.-Russian Space Surveillance Workshop, 24-27 September 2003, Pulkovo, St. Petersburg, Russia.*

Anselmo, L., and C. Pardini (2005), Orbital Evolution of Geosynchronous Objects With High Area-to-Mass Ratios, in *Proceedings of the Forth European Conference on Space Debris, pp. 279-284, ESOC, Darmstadt, Germany, 18-20 April 2005.*

Artemis (2006), Artemis Website, <http://www.esa.int/artemislaunch/>.

Batyr, G., S. Veniaminov, V. Dicky, V. Yurasov, A. Menshikov, and Z. Khutorovsky (1993), The Current State of Russian Space Surveillance System and its Capability in Surveying Space Debris, in *Proceedings of the First European Conference on Space Debris, pp. 43-48, ESOC, Darmstadt, Germany, 5-7 April 1993.*

Beutler, G. (2005), *Methods of Celestial Mechanics*, two volumes, Springer-Verlag, Heidelberg, ISBN: 3-540-40749-9 and 3-540-40750-1.

Beutler, G., T. Schildknecht, T. Hugentobler, and W. Gurtner (2003), Orbit Determination in Satellite Geodesy, *Advances in Space Research*, 31(8), 1853–1868.

Bigalke, H.G. (1984), *Kugelgeometrie*, Otto Salle Verlag, Frankfurt am Main.

CelesTrak (2006), CelesTrak Homepage, <http://celestrak.com>.

Donath, Th., T. Michal, X. Vanwijck, B. Dugrosprez, P. Desmet, V. Martinot, T. Schildknecht, T. Flohrer, J. Laycock, C. Saunders, R. Walker, P. Ameline, and L. Leushacke (2004), *European Space Surveillance System Study*, Final Report, ESA ESOC Contract 16407/02/D/HK(SC).

- Donath, Th., T. Michal, X. Vanwijck, B. Dugrosprez, M. Menelle, T. Schildknecht, T. Flohrer, V. Martinot, J.M. Leveau, P. Ameline, C. Walker, L. Leushacke, I. Zozaya, and M. Morgenstern (2005a), *Detailed Assessment of a European Space Surveillance System*, Final Report, ESA ESOC Contract 18574/04/D/HK(SC).
- Donath, Th., T. Schildknecht, P. Brousse, J. Laycock, T. Michal, P. Ameline, and L. Leushacke (2005b), Proposal for a European Space Surveillance System, in *Proceedings of the Fourth European Conference on Space Debris*, pp. 31-38, ESOC, Darmstadt, Germany, 18-20 April 2005.
- Flohrer, T., J. Peltonen, A.J. Kramer, T. Eronen, J. Kuusela, E. Riihonen, T. Schildknecht, E. Stöveken, E. Valtonen, F. Wokke, and W. Flury (2005a), Space-Based Optical Observations of Space Debris, in *Proceedings of the Fourth European Conference on Space Debris*, pp. 165-170, ESOC, Darmstadt, Germany, 18-20 April 2005.
- Flohrer, T., T. Schildknecht, R. Musci, and E. Stöveken (2005b), Performance Estimation for GEO Space Surveillance, *Advances in Space Research*, 35(7), 1226–1235.
- Flury, W., G. Janin, R. Jehn, and H. Klinkrad (1992), Space Debris in Elliptic Orbits, in *Paper presented at 18th International Symposium on Space Technology and Science*, 17-22 May 1992, Kagoshima, Japan.
- Grigoriev, K. (2005), On the Modelling of Satellite Fragmentations in the Geostationary Ring: Spatial Motion Area, Strategy and Results of Optical Observations, in *Proceedings of the Fourth European Conference on Space Debris*, pp. 645-648, ESOC, Darmstadt, Germany, 18-20 April 2005.
- Hernández, C., and R. Jehn (2003), Classification of Geosynchronous Objects, Issue 5, ESOC, Darmstadt, Germany.
- Hoots, F.R., R.L. Roehrich, and T.W. Kelso (1980), Models for Propagation of NORAD Element Sets, *Spacetrack Report*, No. 3.
- Hugentobler, U. (1998), *Astrometry and Satellite Orbits: Theoretical Considerations and Typical Applications*, Vol. 57 of *Geodätisch-geophysikalische Arbeiten in der Schweiz*, Schweizerische Geodätische Kommission.
- IADC (2006), Inter-Agency Space Debris Coordination Committee Homepage, <http://www.iadc-online.org>.
- Johnson, N.L. (2001), Activities on Space Debris in U.S., in *Proceedings of the Third European Conference on Space Debris*, pp. 13-20, ESOC, Darmstadt, Germany, 19-21 March 2001.
- Khutorovsky, Z.N., V.F. Boikov, and A.V. Testov (2001), Monitoring of GEO Satellites, in *Proceedings of the Third European Conference on Space Debris*, pp. 117-124, ESOC, Darmstadt, Germany, 19-21 March 2001.
- Krag, H. (2003), *A Method for the Validation of Space Debris Models and for the Analysis and Planing of Radar and Optical Surveys*, Shaker, Aachen.
- Liou, J.-C., and J.K. Weaver (2004), Orbital Evolution of GEO Debris with High Area-to-Mass Ratios, *The Orbital Debris Quarterly News*, 8(3), 6–7.

- Liou, J.-C., and J.K. Weaver (2005), Orbital Dynamics of High Area-to-Mass Ratio Debris and Their Distribution in the Geosynchronous Region, in *Proceedings of the Fourth European Conference on Space Debris*, pp. 285-290, ESOC, Darmstadt, Germany, 18-20 April 2005.
- Michal, T., J.-P. Eglizeaud, and J. Bouchard (2005), GRAVES: The French Space Surveillance System, in *Proceedings of the Fourth European Conference on Space Debris*, pp. 61-66, ESOC, Darmstadt, Germany, 18-20 April 2005.
- Musci, R. (2001), *Optische Detektion von Raumschrott im geostationären Ring*, Astronomical Institute, University of Bern, diploma thesis.
- Musci, R., T. Schildknecht, and M. Ploner (2004), Orbit Improvement for GEO Objects Using Follow-up Observations, *Advances in Space Research*, 34(5), 912–916.
- Musci, R., T. Schildknecht, T. Flohrer, and G. Beutler (2005a), Concept for a Catalogue of Space Debris in GEO, in *Proceedings of the Fourth European Conference on Space Debris*, pp. 601-606, ESOC, Darmstadt, Germany, 18-20 April 2005.
- Musci, R., T. Schildknecht, M. Ploner, and G. Beutler (2005b), Orbit Improvement for GTO Objects Using Follow-up Observations, *Advances in Space Research*, 35(7), 1236–1242.
- NSSRM (2006), National Security Space Road Map, <http://www.wslfweb.org/docs/roadmap/irm/internet/spacecon/roadmap/spacecon.htm>.
- Oswald, M., H. Krag, P. Wegener, and B. Bischof (2004), Concept for an Orbital Telescope Observing the Debris Environment in GEO, *Advances in Space Research*, 34(5), 1155–1159.
- OT (2006), Observatorio del Teide, <http://www.iac.es/ot/index.html>.
- Schildknecht, T., R. Musci, M. Ploner, S. Preisig, J. de León Cruz, and H. Krag (2001), Optical Observation of Space Debris in the Geostationary Ring, in *Proceedings of the Third European Conference on Space Debris*, pp. 89-94, ESOC, Darmstadt, Germany, 19-21 March 2001.
- Schildknecht, T., R. Musci, M. Ploner, W. Flury, J. Kuusela, J. de León Cruz, and L. de Fatima Domínguez Palmero (2003), An Optical Search for Small-Size Debris in GEO and GTO, in *Proceedings of the 2003 AMOS Technical Conference*, 9-12 September 2003, Maui, Hawaii, USA.
- Schildknecht, T., R. Musci, M. Ploner, U. Hugentobler, M. Serra Ricart, J. de León Cruz, and L. de Fatima Domínguez Palmero (2004a), *Geostationary Orbit Objects Survey*, Final Report, ESA ESOC Contract 11914/96/D/IM.
- Schildknecht, T., R. Musci, M. Ploner, G. Beutler, J. Kuusela, J. de León Cruz, and L. de Fatima Domínguez Palmero (2004b), Optical Observations of Space Debris in GEO and in Highly-Eccentric Orbits, *Advances in Space Research*, 34(5), 901–911.
- Schildknecht, T., R. Musci, M. Serra Ricart, J. de León Cruz, L. de Fatima Domínguez Palmero, P. Beltrami, and K.D. Bunte (2005a), *Geostationary Transfer Orbit Survey*, Final Report, ESA ESOC Contract 12568/97/D/IM.
- Schildknecht, T., R. Musci, W. Flury, J. Kuusela, J. de León Cruz, and L. de Fatima Domínguez Palmero (2005b), Optical Observations of Space Debris in High-Altitude Orbits, in *Proceedings of the Fourth European Conference on Space Debris*, pp. 113-118, ESOC, Darmstadt, Germany, 18-20 April 2005.

- Schildknecht, T., R. Musci, W. Flury, J. Kuusela, J. de León Cruz, and L. de Fatima Domínguez Palmero (2005c), Properties of the High Area-to-Mass Ratio Space Debris Population in GEO, in *Proceedings of the 2005 AMOS Technical Conference, 5-9 September 2005, Maui, Hawaii, USA*.
- Schmidt, G.T. (ed.) (2000), Space-Based Surveillance, *Journal of Guidance, Control, and Dynamics*, 23(1), 147–190.
- Serraller, I., and R. Jehn (2005), Classification of Geosynchronous Objects, Issue 7, ESOC, Darmstadt, Germany.
- Sharma, J. (2000), Orbit Determination Applications with the Space-Based Visible Space Surveillance Sensor, *Advances in Astronomical Sciences*, 105, 275–286, Spaceflight Mechanics.
- Sharma, R.K., P. Bandyopadhyay, and V. Adimurthy (2004), Consideration of Lifetime Limitation for Spent Stages in GTO, *Advances in Space Research*, 34(5), 1227–1232.
- Siebold, K.H., and R.C. Reynolds (1995), Lifetime Reduction of a Geosynchronous Transfer Orbit With the Help of Luni-Solar Perturbations, *Advances in Space Research*, 16(11), 155–161.
- Socholina, A.S., M. Serra Ricart, R.I. Kiladze, K.V. Grigoriev, and A.N. Vershkov (1996), Catalogue of Orbits of Geostationary Satellites, Institute for Theoretical Astronomy of the Academy of Science of Russia, St. Petersburg, Russia.
- Soop, E.M. (1994), *Handbook of Geostationary Orbits*, Kluwer Academic Publishers, Dordrecht, Boston, London.
- Space-Track (2006), Space-Track Homepage, <http://www.space-track.org/perl/login.pl>.
- Stokes, G., C. von Braun, R. Sridharan, D. Harrison, and J. Sharma (1998), The Space-Based Visible Program, *MIT Lincoln Lab Journal*, 11 (2), 205–238.
- STRATCOM (2004), U.S. Strategic Command, <http://www.stratcom.mil/factsheetshtml/reentryassessment.htm>.
- Valtonen, E., J. Peltonen, E. Riihonen, T. Eronen, T. Flohrer, T. Schildknecht, E. Stöveken, F. Wokke, A.J. Kramer, and R. van Benthem (2006), *Space-Based Optical Observation of Space Debris*, Final Report, edited by T. Flohrer, ESA ESOC Contract 17140/03/D/HK(SC).
- Wokke, F., A.J. Kramer, R. van Benthem, R.B. Annes, T. Flohrer, T. Schildknecht, E. Stöveken, E. Valtonen, J. Peltonen, E. Riihonen, T. Eronen, J. Kuusela, W. Flury, and R. Jehn (2006), An Instrument Design for Space-Based Optical Observations of Space Debris, in *Paper presented at 56th Astronautical Congress, 17-21 October 2005, Fukuoka, Japan*, Paper to be published in the American Astronautical Society series 'Space Debris'.

Curriculum vitae

Name: Reto Musci
Geburtsdatum: 21. Januar 1973
Geburtsort: Dielsdorf, ZH
Heimatort: Dielsdorf, ZH
Zivilstand: ledig

1981–1986 Primarschule in Dielsdorf, ZH
1986–1993 Kantonsschule Zürcher Unterland, Bülach, ZH
Abschluss mit Matura Typus C
September–Dezember 1993 Temporärstelle bei der Zürich Leben
Februar–Mai 1994 Temporärstelle bei der Schweizerischen Volksbank
1994–1996 Studium der Biologie an der Universität Zürich
1996–2001 Studium der Astronomie an der Universität Bern
Diplomarbeit über *Optische Detektion von Raumschrott im geostationären Ring*
Abschluss als Diplom-Astronom
2001–2006 Doktorand am Astronomischen Institut der Universität Bern unter der
Leitung von PD Dr. Thomas Schildknecht

